An Analysis of Airflow Patterns in Auxiliary Ventilated Drivages

BY

Kenneth W Moloney, BEng

Thesis submitted to the University of Nottingham for the degree of Doctor of Philosophy, September 1997

TABLE OF CONTENTS

ABSTRACT

In recent years the drivage advance rates achieved within the UK coal industry have increased. In the 1980's average drivage rates were 35m per week compared to the 100/150m per week possible today. These extended rates of advance have resulted in an increase in the potential methane, dust and heat generation within the vicinity of the drivage face. In order to effectively disperse this additional pollutant load a controlled increase in air quantity is required.

Although advance rates have changed, current auxiliary ventilation practice has not. UK mining law requires that the fresh air must be delivered to within 5m of the face. This has lead to the wide spread adoption of the use of overlap auxiliary systems within mechanised drivages, since a pure forcing system set at this distance from the face would lead to excessive airborne dust. UK mining law does not at present consider on-board mounted exhaust scrubber fans to constitute an effective overlap fan within mechanised drivages. Consequently an additional overlap exhaust fan is required to be installed within such drivages.

In an attempt to determine whether working conditions could be safely and economically improved within mechanised rapid development drivages utilising an on-board mounted exhaust fan, a series of preliminary full scale gallery trials were conducted. A summary of the principal findings of these trials is presented together with an outline of a series of representative CFD simulations.

This thesis examines the accuracy of CFD simulations for auxiliary ventilated headings. This is achieved by utilising Laser Doppler Anenometry (LDA) in a scale model representative of an underground heading and a detailed underground measurement programme conducted in production headings. These measured airflow values are then compared with representative CFD simulations and conclusions drawn.

LIST OF TABLES

LIST OF FIGURES.

GLOSSARY OF NOTATION.

English Symbols

a	Speed of sound
A	Area (m^2)
b	body force per unit mass.
B	Additive constant in the law of the wall
C	Perimeter (m)
C_1, C_2	Closure Coefficients.
C_μ,	Closure Coefficients.
f	dimensionless coefficient (friction factor)
f_d	Doppler frequency
F	Force per unit area
g	gravitational constant (9.81)
h	head loss
h	Specific enthalpy
H	Total enthalpy
i j, k	Unit vectors in x, y and z directions
i_{sp}	Scattering particles current
I	amplitude
k	Kinetic energy of turbulent fluctuations per unit mass.
k	Atkinson's friction factor.
K	Scattering wavenumber.
l	Turbulent length scale; characteristic eddy size.
l_{mix}	Mixing length.
L	Characteristic length scale.
m	Mass (kg/m^3)
Ma	Mach number.
p	Instantaneous static pressure
Q	Quantity (m^3/s)
Q_g	Rate od gas emission
R	Resistance (N units ****)
R_{ij}	SGS Reynolds stress tensor.
Re	Reynolds number
S	Source term - production minus dissipation
t	time
T	Temperature; characteristic time scale
u, v, w	Instantaneous velocity components in x, y, z, directions.
u_i	Instantaneous velocity in tensor notation
u	Instantaneous velocity in vector notation
u', v',w'	Fluctuating velocity components in x, y, z directions
u_i'	Fluctuating velocity in tensor notation
u'	Fluctuating velocity in velocity notation
ui'	
U, V, W	Mean velocity components in x, y, z directions
U_i	Mean velocity in tensor notation

U	Mean velocity in vector notation
U_m	Maximum or centreline velocity
x, y, z	Rectangular Cartesian coordinates
x_i	Position vectors in tensor notation
x	Position vectors in vector notation

Greek Symbols

α_r	Alpha radiation
α, α^*	Closure Coefficients
β_r	Beta Radiation
β, β^*	Closure Coefficients
γ	Specific heat ratio (C_p/C_v)
δ	Boundary layer or shear layer thickness
δ_{ij}	Kronecker delta
$\Delta Q, \Delta x, \Delta y$	Incremental change in Q, x, y.
Δt	Timestep
ε	Dissipation rate per unit mass
ε_{ij}	Dissipation tensor
κ	Karman constant; thermal conductivity; wavenumber
λ_r	Gamma radiation
λ_i	Wavelength of incident light
μ	Molecular viscosity
μ_T	Eddy viscosity
ρ	Mass density
σ, σ^*	Closure Coefficients
$\sigma_k, \sigma_\varepsilon$	Closure Coefficients
σ_{ij}	Instantaneous total stress tensor
τ_{ij}	Reynolds stress tensor
τ_{xy}	Reynolds shear stress
$\tau_{xx}\tau_{yy}\tau_{zz}$	Normal Reynolds stress
ϕ	Dimensionless parameter, $(\nu_w/\rho u \rho^3_\tau)\ dP/dx$
ω	Specific dissipation rate; vorticity vector magnitude
ω_d	Doppler frequency

ACKNOWLEDGMENTS

The Author would like to express his sincere gratitude to the following people for their assistance during the course of this study:

- Helen for moral support and putting up with a pauper for so long.
- My family for all there support throughout my studies.
- Dr Ian Lowndes for his encouragement and direction.
- Dr Graham Hargrave for his assistance during the scale experimental work.
- Alan, Charlie and Yang for various acts of decency.
- The technical staff and in particular Bill Cully, Tony Gospel and Phil Parry for being so co-operative.

1. INTRODUCTION

1.1 HISTORY OF MINE VENTILATION

Mining is essential for a modern civilization to function efficiently. The use of minerals produced from mines are seen everywhere; various metals and minerals are used in the manufacture of cars, airplanes, household goods and computer chips. Aggregates, hard rock and industrial minerals are widely used in the construction industry. The list of materials utilised is exhaustive and without them the economies of the world would not continue to develop.

Early mining ventilation systems such as the Laurium silver mines of Greece operating in 600 BC used separate shafts to provide a circuit for ventilation. In the Roman era (23-79) Pliny describes how slaves used palm frondes to waft air along tunnels.

The discovery that coal could be used as an energy source (13th Century) lead to its use in heating. The birth of the steam engine and the railroad initiated the onset of the industrial revolution.

The industrial revolution increased the demand for coal as smelters began to produce iron in quantities never seen before. This increased demand for coal resulted in horrific working conditions for men, women and children working in the mines. Methane, coal dust explosions and roof falls were common place in the UK coal mines. The explosions were caused by; i) naked candles being carried around since it was the only means of illumination and ii) furnaces at the base of the shaft to induce the ventilation current around the mine. The explosion at Felling, Gateshead in 1812 left 92 in a fatal condition. This lead to the development of the Davy Flame safety lamp. However lack of effective legislation resulted in the continued use of candles as a source of illumination.

The first reference to mechanical ventilation was by Georgious Agricola in his book Metallica in 1556. He described the use of bellows blowing air down tunnels and wooden centrifugal fans powered by horses in German metal mines. However, the use of these fans went into decline for almost 250 years. It was not until 1827 after numerous disasters that a mine ventilating fan was re-introduced to a colliery near Paisley in Scotland. Centrifugal fans were installed in two mines in South Wales in 1849 and 1851. The latter could deliver 21m^3/s at 125 Pa. It was not until 1859 that Guibal (1814-1888) steam centrifugal fans had casing with an expanding evasse. These fans were soon used in mines all over Europe and could deliver 100m^3/s at pressures up to 1500 Pa. Today high powered axial fans are capable of passing 700m^3/s and mine ventilation practice has changed dramatically.

By the turn of the century the mines were subjected to legislative control after countless disaster enquires. In the 1920's instruments technology advances allowed ventilation surveys to be conducted to measure airflow and pressure drops for airflows for underground ventilation planning. This improved the overall ventilation system and thus the working conditions. The introduction of legislation to reduce the number of ignitions lead to a significant decrease in fatalities in underground mine. Today all electrical equipment must be intrinsically safe and the use of water sprays at mechanised districts has contributed to a safer working environment.

Analogue computers were first used to assist in ventilation planning at the University of Nottingham in the early 1950's. However, this was soon replaced by the digital computer in the 1960's. The advances in software and hardware technology since the 1960's has aided the ventilation planning team to implement a safe and efficient airflow network. The rapid development of desktop technology in the 1990's will undoubtedly assist the ventilation engineer further.

1.2 BACKGROUND

In order to improve the productivity of UK deep coal mines, there has been a move towards the implementation of high production multi-entry longwall retreat mining systems. To be competitive with oil, gas and imported coal, British coal mines must produce coal at an operating cost of under £1.30/GJ. This means that a longwall retreat face must produce a salable output between 0.75 and 1.0 million tonnes per year. To maintain such output, development rates of up to three times the face retreat rate are required (Williams, 1993). This equates to some 100 m/week.

In recent years, continuous miners have been introduced on a wide scale for drivage of in-seam gate roads. These machines use a cutting drum 3-4m wide and can excavate coal at very high rates. Peak performances of up to 650 tonnes/hour are possible to give advances per shift of some 10m. The new generation of continuous miners, which are capable of simultaneous roofbolting and cutting have a potential of 15-20m per shift, 200 m/week (Coal News, July 94; Houghton, Sept 1993)

Although advance rates have changed, current auxiliary ventilation practice has not. UK mining law requires that the fresh air must be delivered to within 5m of the face. This has lead to the wide spread adoption of the use of overlap auxiliary systems within mechanised drivages, since a pure forcing system set at this distance from the face would lead to excessive airborne dust. UK mining law does not at present consider on-board mounted exhaust scrubber fans to constitute an effective overlap fan within mechanised drivages. Consequently an additional overlap exhaust fan is required to be installed within such drivages.

Recently in the UK there has been a shift towards the use of continuous miners as production machines in room and pillar operations. This method of working precludes the use an overlap auxiliary system, due to the cyclic nature of the operation. Therefore, the forcing duct has to be set back five metres from the face. Clearly this situation is not a practical option from the perspective of dust control. Therefore, the duct is usually fitted with a diffuser and/or air is bled off further outbye. In some

cases a device called a winsock is fitted to the duct discharge. This tapers a large orifice down to a smaller outlet over a length of duct. Essentially these Winsock's are used so that the ventilation system complies with the current legislation. These laws were formulated at a time when auxiliary systems delivered 1-2m^3/s and the predominant method of working was drill and blast. The main objective of these regulations was to clear methane and blasting fumes from the face. The dust levels were of less concern since there was nobody working in the heading.

In an attempt to determine whether working conditions could be safely and economically improved by moving the forcing duct further from the face and using an on-board mounted exhaust fan, a series of preliminary full scale gallery trials were conducted by British Coal. A summary of the principal findings of these trials is presented (Chapter 5) together with an outline of a series of representative CFD simulations (chapter 7).

1.3 THE STRUCTURE OF THE INVESTIGATION

1.3.1 Overall objectives.

The overall objective of this study is to gain an understanding of the flow features and assess the accuracy of CFD predictions for an underground auxiliary ventilated tunnel. This objective will be achieved by the comparison of numerical predictions with measured value obtained from experimental data and underground field work.

1.3.2 Experimental objectives

The experimental objective of this study is to gain an understanding of the flow structure and to collect a detailed set of measurements representative of an underground heading to compare with CFD predictions. This is achieved through the use of a scale model using a flow visualisation technique and Laser Doppler

Anemometry (LDA) measurements. In parallel with these tests a number of full scale underground ventilation surveys were conduced and compared with CFD predictions.

1.3.3 Numerical simulation objectives

The objectives of the numerical simulations are to produce a representative CFD model of both the scale experimental model and each underground situation using the commercial package Fluent v4.3. Comparative analysis are then made of airflow predictions which are produced by the various turbulence models.

1.4 OUTLINE OF THESIS

Chapter two reviews the primary objectives of a mine ventilation system. The pollutants encountered in the underground environment and their potential physiological effects are reviewed along with the legal requirements of each. Environmental monitoring and control measures of these pollutants are also discussed The chapter concludes by introducing the instrumentation utilised in the underground measurement programme.

The various types of auxiliary ventilation systems employed are presented in chapter three. The type of fan, ducting and the type of machine to develop these roadways are deliberated with particular reference to the operation of continuous miners with on-board scrubber systems.

Chapter four outlines the basic design equations that are employed for mine ventilation planning. A brief introduction to the theory and application of the fluid flow equations utilised in CFD modelling technique are reviewed. The models used to simulate the turbulent activity, the algorithms for velocity-pressure coupling and the staggered grid are explored. The method utilised to achieve discretisation and solution of these equations is examined. Finally the uncertainty and reliability of these predictions are discussed.

The previous theoretical and practical research conducted in the area of tunnel ventilation and in particular the more recent application of CFD modelling is examined The main results and conclusions drawn from these studies are presented in chapter five.

The use of scale model experimentation techniques; flow visualisation using laser light and Laser Doppler Anemometry (LDA) are discussed in chapter six. The instrumentation required and the background theory of LDA is also introduced. Chapter seven reviews the CFD package employed and indicates the importance of grid sensitivity analysis in CFD analysis. The flow characteristics of jets and wall jets are covered. Finally the results from preliminary simulations of full-scale gallery tests are presented in chapter 5 and conclusions drawn from these results.

Chapter eight presents the resultant flow patterns from visualisation studies using laser light. The LDA measurements are compared with the CFD predictions for three turbulence models. The effect of altering variables, using different discretisation schemes and wall functions is explored in the latter part of chapter eight.

During this project a series of detailed ventilation surveys were conducted within drivage headings at Wistow colliery (chapter nine). Two of these heading were advance developments for retreat shortwall faces and were ventilated using a conventional auxiliary overlap system. The third heading was within a room and pillar operation. The general flow characteristics observed during these surveys are introduced and the results are compared with CFD models of each heading.

The thesis concludes with a summary of the major findings of the research work and the recommendations for further work.

1.5 WHAT IS VALIDATION?

The word validation is often used by CFD code developers to describe the process by which a code is tested against experimental results. Beard (1992) suggests that the word validation implies *"proven correct"*. However the concept of proving a model to be correct is directly contrary to scientific method. It is logically impossible for a scientific theory in general and a model in particular to be "*proven correct*". The most one can hope to achieve is to compare the numerical prediction with experimental measurements and to observe the differences. There is no number of *"good comparisons"* which may have to be taken to have proved a model to be true; comparison with theory and experiments needs to be a continual process. Thus, if a particular ventilation configuration is *validated*, it does not necessarily mean that predictions from a different configuration will predict with the same accuracy/error which ever may be the case. Consequently it is of paramount to continuously test predictions against experimental data.

Therefore a code that has been validated for a particular case, e.g. a wall jet, then it may be used to predict wall jets accurately. However if the wall jet is in a confined space as in an auxiliary ventilated tunnel the code will need validation for the refluxing part of air across the wall jet. Thus testing with experiment must be carried out in order have any confidence in the predictive capabilities of the code in question.

2. MAIN VENTILATION SYSTEMS.

2.1 INTRODUCTION.

The aim of a mine ventilation system is to provide a safe and comfortable environment in all working areas underground. This objective may be achieved through the selective application and control of an integrated ventilation and cooling system. An acceptable mine environment may be maintained, provided an adequate supply of fresh air is delivered in order to rapidly dilute, disperse and remove any airborne pollutants present. These pollutants may take the form of gases, dusts or other suspended aerosols and heat or humidity

In the UK the statutory obligation to provide and maintain a safe and comfortable underground mine environment is enshrined within mining law and other health and safety legislation. The principal legal instruments being the 1956 Mines and Quarries and Miscellaneous Mines Acts and the 1974 Health and Safety at Work Act. The corresponding underground civil tunneling standards are specified in the British Standard, BS6164.

The minimum quantifiable conditions that need to be maintained to produce a comfortable and acceptable environment, are expressed in terms of a maximum pollutant exposure level for each pollutant. These levels are specified within supplementary national statutory and/or local mine practice regulations. Maximum gas levels are often expressed in terms of Threshold Limit Values (TLV's), with maximum permissible dust and diesel particulate exposure levels being specified in mg/m^3 of ventilating air (for example EH95, HSE 1997). The interpretation of reasonable comfort and safety may vary from country to country. German mining law, for example specifies the maximum climatic conditions that are to be maintained within underground working zones, whereas within the UK it is the responsibility of the mine manger to set the acceptable levels.

The overall requirement of a ventilation system is that people must be able travel and work in an environment that is safe and provides reasonable comfort. In order to achieve

the above ventilation objectives, it is necessary to design, commission and control a suitable mine ventilation system.

A mine ventilation system normally consists of main fans(s), a network of access shafts or drifts and roadways for the air to form a flow circuit. Within this network air doors, regulators, stoppings, air crossings and booster fans control the airflow through the mine. (McPherson, 1993; Lowndes & Tuck, 1996).

UK coal mine legalisation requires that a mine should have at least two main surface fans. Both must be capable of providing adequate ventilation for the safe withdrawal of human beings in emergencies. Non coal mines may however allow for the selective siting of main mine fans underground should local conditions permit.

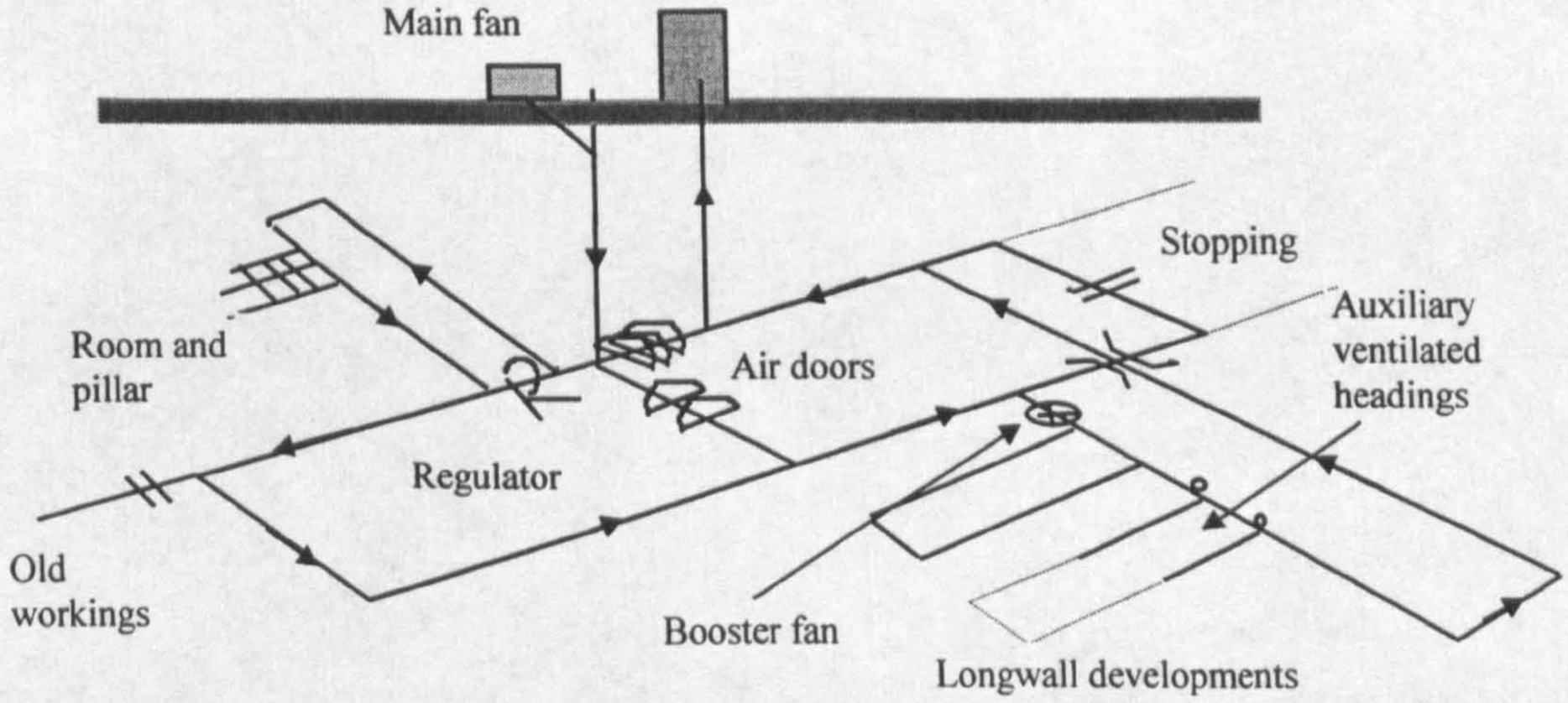

Figure 2-1 - A schematic of a typical coal mine ventilation system.

The ventilation network is designed to ensure that the workings of a mine are supplied with a sufficient quantity of fresh air. The minimum design fresh air quantity required at each working place is determined with knowledge of the potential pollutant emission rates and associated threshold limit values. The potentially polluted air is then removed through a network of designated return trunk airways to surface. Air doors may be

constructed from wood or steel. They are used to prevent the short circuiting of air through connections constructed between the main intake and return circuit.

In order to control the split of the ventilating air within the ventilation network the engineer may employ either *passive* or *active* regulation. Passive regulation requires the installation of a regulation device which can increase the resistance within one split of a ventilation circuit and hence the distribution of the ventilating air. Regulators can take the form of a set of ventilating doors through which the available flow area of an opening may be varied to regulate the flow of air. Active regulation requires the installation of booster fans that may be used to overcome the excess resistance in a particular section of a mine. It is usually located at a major split of the ventilating air. Booster fans may also be used in series with the main ventilation circuit to assist the main fan in delivering air to high resistance remote areas of a mine. Permanent and temporary stopping walls are primarily used to close off old roadways and worked out area of a mine. These may be constructed from block sets keyed into and grouted into the airway walls.

In order to design a mine ventilation system it is necessary to define the resistance and hence topology of the proposed mine ventilation circuit. It is also necessary to provide an estimate of the maximum permissible pollutant emissions that are to be expected. The pollutant emission patterns will be determined by a range of geological and mining factors. This chapter catalogues the range of pollutants that may be encountered with an underground mine.

2.2 POLLUTANTS IN THE UNDERGROUND ENVIRONMENT.

2.2.1 Introduction.

Any mine atmosphere can be considered to have three components; fresh air, combustible gases (methane, hydrogen, carbon monoxide) and excess inert gases such as nitrogen and carbon dioxide. Normally dry mine air contains 20.93% oxygen, 79.04% nitrogen, 0.03 carbon dioxide by volume. The total amount of other gases is less than 0.01% (including argon and rare gases). As fresh air travels through the workings it may become contaminated by a variety of pollutants. These include dusts, heat, humidity and the range of mine gases including methane, carbon monoxide, nitrogen oxides, and diesel

exhaust emissions. It is in this section that the sources, characteristics, potential physiological effects and threshold limits are introduced.

2.2.2 Threshold Limit Values (TLV's)

TLV's refer to those concentrations of toxic agents in the air and represent conditions to which workers may be repeatedly exposed day after day without adverse effects. There are three categories of TLV's;

i) the time-weighted average (TWA) is the average concentrations to which workers may be exposed over an eight hour shift and a 40 hour week.

ii) Short term exposure limit (STEL) is the maximum concentration for exposures up to 15 minutes. It is also recommended that such situations should not occur more than four times a day with at least 60 minutes between exposures and should not exceed the TWA.

iii) Ceiling limit (C) - The concentration that should not be exceeded at any time. (Hazardous gases underground) (Mc Pherson, 1992)

2.2.3 Gases.

2.2.3.1 Oxygen (O_2)

This is a colourless, odourless gas and is present in air at around 21% with the minimum being 19.5%. However, as the air flows through an underground mine the O_2 % will decrease. The decrease in oxygen results from respiration, the oxidation of minerals and materials brought into the mine and the release of other gases and pollutants into the mine air.

2.2.3.2 Hydrogen (H_2)

H_2 is non-toxic and is also the most explosive of all mine gases. The flammable range of H_2 is from 4-74.2% in air. It has an ignition energy of about half that required by methane and can be ignited at temperatures as low as 580 ^{0}C. Hydrogen occasionally appears as a strata gas. It is usually present at the same concentration as CO after an explosion. Dangerous accumulations of hydrogen may occur at locations where battery charging is in progress. (Located in intake air with a duct at the roof level that connects into a return airway.) It is also potentially flammable and explosive.

2.2.3.3 Carbon dioxide (CO_2)

CO_2 is more than 50% heavier than air and will, therefore tend to collect on the floors of the mine workings. CO_2 dilutes the O_2 content in the air and it also acts as a stimulant to the respiratory and central nervous system. If there is abnormal quantities of carbon dioxide and nitrogen in the mine atmosphere *blackdamp* may be present. This mixture results in a suffocating gas and tends to form along the floor of a roadway due to its high density. The TWA and STEL values are 0.5% and 3% respectively.

2.2.3.4 Carbon Monoxide (CO)

Carbon Monoxide is very toxic, colourless, odourless, and tasteless. It has similar density to air and it mixes readily into the airstream. CO is produced by the incomplete combustion of diesel fumes, fires, blasting, oxidation of coal and thermal decomposition of coal, wood and rubber. It is explosive in the range of 12.5 - 74% and it TWA and STEL limits are 0.005% and 0.04%.

2.2.3.5 Methane (CH_4)

Methane is an inert, odourless and colourless gas with a density of 0.6581 kg/m^3. It has a specific diffusion coefficient of 0.726 and hence it flows easily through a porous material. It is produced by bacterial and chemical action on organic material (e.g. formation of coal and petroleum). Methane is one of the most common strata gases

found in underground coal mines. It becomes explosive when it mixes with O_2 in certain concentrations. Figure 2.2 illustrates the explosive range of methane. This explosive mixture is referred to as "*firedamp*". This diagram was first produced as a result of the research of H.F. Coward in 1928. Methane becomes explosive when the O_2 concentration is between 14-21% and when the CH_4 concentration is between 5-15%. Thus it is important to rapidly disperse the methane and prevent the formation of an igniting source. If methane quantities exceed 1% in the general body all electric power should be isolated. If the levels exceed 2% then all the personnel should be removed immediately from the working area.

2.2.3.5.1 Methane Layering.

Methane emitted from the strata into a mine opening will often be in excess of 90% pure methane. This will in turn be diluted and at some stage will pass through the explosive range (5-15%).

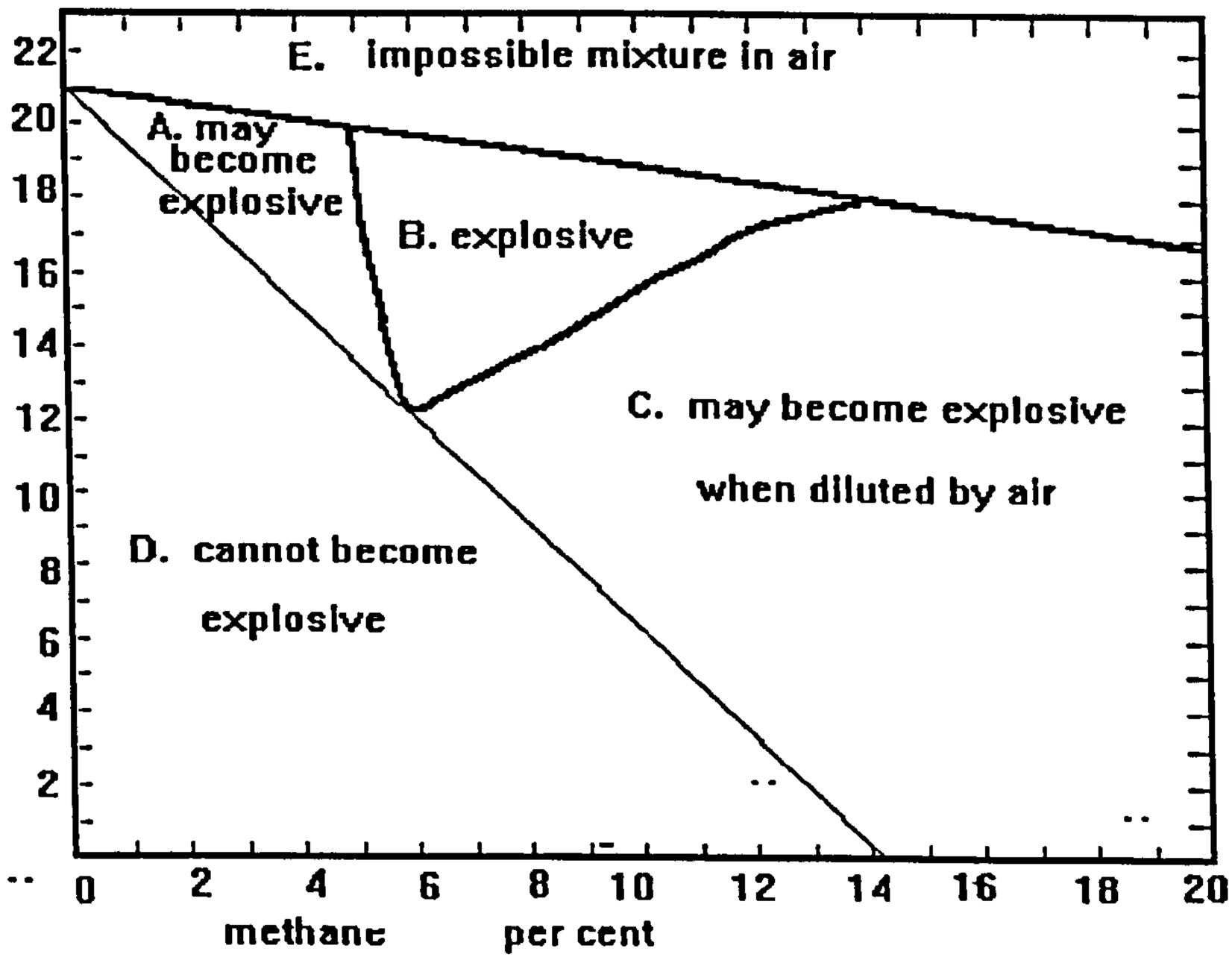

Figure 2-2- Cowards diagram (after Mcpherson, 1992)

Thus it is important to minimise the time spent in the explosive range. This is achieved by good mixing of methane and air at the points of emission. However methane may accumulate in undisturbed areas such as roof cavities or may layer along the
roof of airways of mine openings, due to the low density of methane when compared with mine air (0.554 - 1.2). In level and ascentionally ventilated airways the layer will stream along the roof in the direction of the airflow, The layer increases in thickness and decreases in concentration as it move away from the source. This methane layering extends the zones with which potential ignitions of the gas could occur. If an ignition occurs the methane layer can act as a fuse along which the flames may propagate to larger concentrations elsewhere in the mine.

Figure 2.3 illustrates methane layering in a descentionally ventilated airway. The buoyant methane layer may creep uphill close to the roof, against the direction of normal airflow. At the fringe between gas and air, viscous drag and eddy action will cause the gas-air mixture to turn in the same direction as the airflow

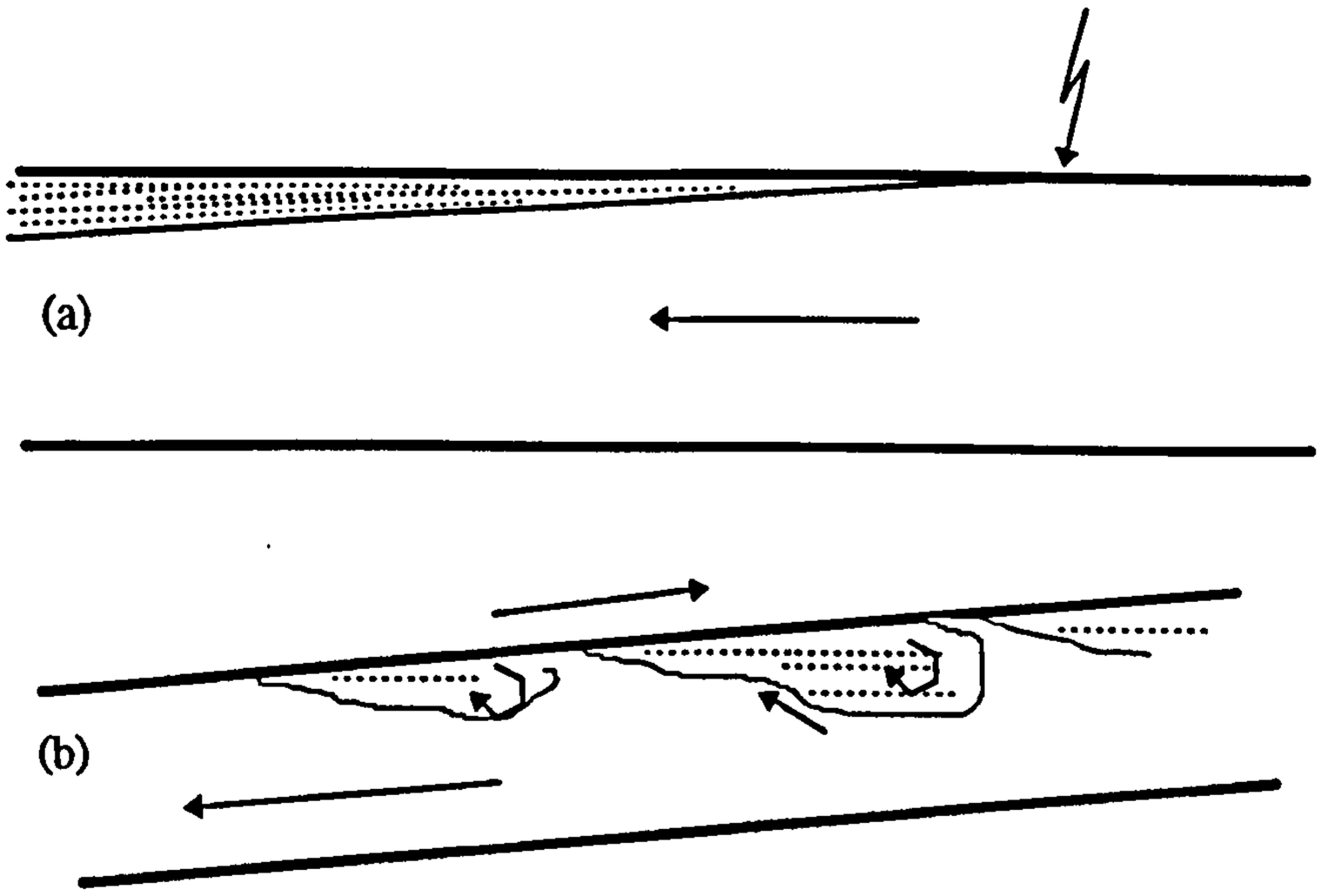

Figure 2-3 - Methane layering in underground roadways.

Thus an explosive mixture may be drawn downstream into a working area. Rough lining will promote better mixing than a smooth one. However, the effect of roughness is reasonably small (Raine, 1960). Bakke and Leach found that the characteristic behavior of a gas layer is proportional to the dimensionless group:

$$\frac{u}{(g\frac{\Delta\rho}{\rho}\frac{Q_g}{W})^{1/3}} \qquad (2.1)$$

Where $\Delta\rho/\rho$ is the difference in relative densities of the two gases (1-0.554 = 0.446 for air and methane). Using a value of g=9.81 m/s2 gives the dimensionless number of methane layers in the air to be

$$L_m = \frac{u}{(9.81 * 0.446 * Q_g W)^{1/3}}$$

$$L_m = \frac{u}{1.64}\left(\frac{W}{Q_g}\right)^{1.3} \qquad (2.2)$$

Where L = layering number

In a level airway L_m should not exceed a value of five. For an inclination of 45^0 the maximum value of L_m should be 7.8. The phenomena of methane layering that was once common place now seldom occurs due to well designed methane drainage systems.

2.2.3.6 Radon.

This is a chemically inert gas that is formed during radioactive disintegration of the Uranium series. Uranium is the most abundant element in the earth's crust. Radon emanates from ground water that has passed over radioactive minerals or from rock matrix. It has a half-life of 3.825 days and emits Alpha (α). The products of radioactive decay are solids known as radon daughters. They agglomerate with dust particles and emit α, Beta(β) and gamma (λ) radiation. The potential physiological effects are cancer of the lungs including the possibility of chronic chest disease or cancer.

2.2.3.7 Sulphur Dioxide (SO_2).

This gas is highly toxic, it has an acidic taste and it causes an intense burning sensation to the respiratory tract and eyes. It is highly soluble and forms sulphurous acid when mixed with water. Although it is colourless, white fumes may be seen as a result of oxidised vapours or traces of condensation of acidic water. SO_2 is produced by oxidation of sulphide ores and it is emitted from diesel engines. The TWA and STEL values are 2ppm and 5ppm respectively.

2.2.3.8 Oxides of Nitrogen.(NO_x)

There are three nitrogen oxides, nitric Oxide (NO), nitrous oxide (N_2O), and nitrogen dioxide (NO_2). They are found in diesel exhaust emissions and blasting fumes. NO_2 is the most toxic gas of the three. Therefore the physiological effects of this gas will be discussed. Nitrogen tetroxide (N_2O_4) is often found with NO_2 in mine openings and has a similar physiological effects. The brown fumes of nitrogen dioxide dissolve readily in water to form both nitrous (HNO_2) and nitric (HNO_3) acids. These acids cause irritation at low concentrations. At high concentrations they cause severe irritation to the eyes and respiratory tract. The TWA and STEL values are 10ppm and 15ppm respectively.

2.2.3.9 Hydrogen Sulphide.

This gas is highly toxic and is easily detected by its characteristic smell of rotten eggs. H_2S is produced by acidic action or by the effects of heating sulphide ores. It is formed when organic compounds decompose. Thus it is often found close to stagnant pools of water in underground mines. H_2S can be generated in the gob areas of coal mines. This may result in free sulphur being deposited by partial oxidation of the gas.

2.2.3.10 Dust

Mineral dusts vary widely in shape, depending on the main mineral constituents. Dust within an underground mine will consist of suspended aerosols- which may be mineral, water or oil droplets in nature. They are formed at the working faces where strata is shattered by the cutting or abrasion by machines. The sub micron particles remain suspended in the atmosphere under Brownian motion. The larger particles >10μm will settle much quicker.

Dust that can be inhaled is usually classified as: i) Inhable < 10 μm which can penetrates the upper respiratory tract, and ii)Respirable < 5 μm which penetrates the lower respiratory tract. Hence it causes the most physiological damage due to its penetration into lower respiratory tract.

The five major forms of dust classification which constitute a physiological hazard are : Toxic, Carcinogenic Dusts (diesel particulates), Fibrous Dusts (asbestos) Explosive Dusts (coal dust) and coarse dusts

The dust regulations of 1975 require maximum concentrations of 7 mg/m^3 at the coal face and not more than 3 mg/m^3 in the intake roadway.

Dust pickup and retention is influenced by air velocity. The maximum velocity considered acceptable to provide an acceptable working environment at the face is 4m/s (figure 2.4)

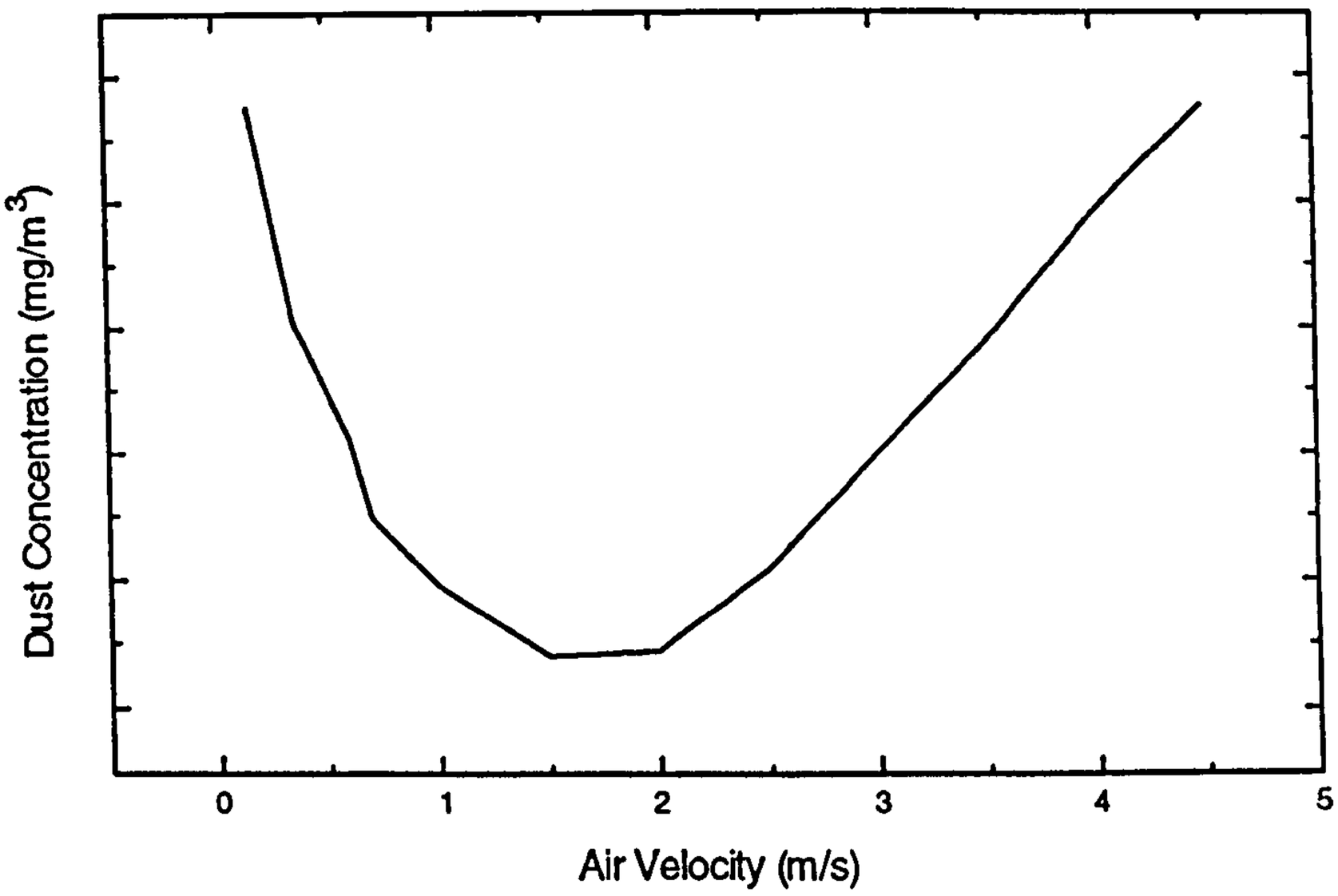

Figure 2-4 - Ideal velocities (Hall, 1956)

2.2.4 Diesel Exhaust

2.2.4.1 Exhaust Products.

Diesel fuel consists of 85-86% (by weight) carbon, 13-14% hydrogen and 0.05-0.7% sulphur. A kilogram of fuel requires 15 kg of air for complete combustion resulting in 6.4m^3 of exhaust products.(Vutukuri et al 1986) If ideal complete combustion occurred, all the carbon would combust to CO_2, all the sulfur to SO_2 and all the hydrogen to H_2O. This would then be diluted by oxygen depleted air. However, complete combustion does not occur and hence partially oxidised and uncombusted products enter the main ventilation body. Oxides of nitrogen are also produced from excess air due to high temperatures associated with the combustion process (Stewart et al, 1976). Water (H_2O) and Oxygen (O_2) are also present in exhaust emissions. (Lowndes and Moloney, 1996)

The ratio of the mass of fuel to the mass of air in the combustion chamber is represented by the Fuel to air (F:A) ratio. (Appendix 1) The value of this ratio dominated the combustion emissions characteristics. The Stoichiometric ratio is reached when the mixture contains the amount of air required to burn all of the fuel to CO_2 and water. For a typical diesel fuel this value is 0.067. The theoretical efficiency of the combustion increases as the Stoichiometric ratio is reached. However, this is not often true in practice due to imperfect fuel mixing. However if this value is exceeded then the efficiency decreases.

2.2.4.2 Constituents of diesel exhaust.

2.2.4.2.1 Hydrocarbons (HC's).

Hydrocarbons are present in small quantities. It is thought that some are toxic and may be carcinogenic. They are the result of unburned fuel in the combustion process. Aldehydes are formed from partially oxidised HC's. Their concentrations are directly related to the unburned HC fraction.(Waytulonis, 1992)

2.2.4.2.2 Diesel Particulate Matter (DPM).

Recently there has been concern over the emission of Diesel Particulate Matter (DPM). DPM is defined as the material, excluding water that is collected on a filter after dilution of the exhaust with ambient air (Waytulonis, 1992). Other terms related to DPM include smoke, particulates and soot. Smoke is defined as particles either solid or liquid (aerosols) suspended in the exhaust gases that obstruct, reflect or scatter light. The term particulates refers to the particles collected by a filter. Soot is defined as deposited DPM.

DPM contains non-volatile carbon, thousands of different adsorbed or condensed Hydrocarbons (HC's), sulphates and trace quantities of metallic compounds. DPM is almost entirely respirable, with 90% of the particles (by mass) having a diameter of less

micrometre. (Chan, L et al 1993) Since particles less than 10μm are considered respirable, (Lippman, M et al 1979) these particles can penetrate to the deepest region of the lungs. Hence, it can cause or develop respiratory diseases in humans. (Terblanche, A.P.S., 1992)

Polycyclic Aromatic Hydrocarbons (PAH) are high boiling point, combustion compounds usually containing four to seven Benzene rings. They are found in DPM and have long been suspected as the primary cause of occupational cancer. In 1972 the US committee on Biological Effects of Atmospheric Pollutants found that: an increase of one nanogram of Benzo (a) pyrene per cubic metre of urban air would signal a 5% change in lung cancer incidence (Mogan, J.P et al 1994). Many forms of PAH's have been identified from extracts of diesel emission particles. The highest concentrations of PAH identified include: Pyrene, fluoranthene, phenanthrene, methyl-phenanthrene, 2-phenylnaphthalene, benzo(j) fluoranthene, benzo-e-pyrene and many others. (Tong, H.Y et al 1984)

2.2.5 Heat

2.2.5.1 Strata-Geothermal Gradient.

The core of the Earth is a molten mass with temperature in excess of 3900 ^{0}C. Therefore as mines get deeper, temperatures increase as one get closer to the core. The temperature increase depends on the thermal conductivity of the local strata. In Northern Europe the gradient is an increase of 1^{0}C for every 30m compared to 50m/^{0}C in the Republic of South Africa (RSA). Hence the lower gradients in RSA allows mines to extract ore at greater depths.

2.2.5.2 Other heat sources.

- Autocompression - Air descending a shaft is compressed by a column of air above it by approximately 1.15 KPa/ 100m. In British mines the dry bulb temperature typically increases by 1^{0}C/100m while wet bulb temperature increases by 0.4^{0}C/100m.

- Machinery - Any work performed by machinery underground emerges as heat. The ventilation system must be capable of removing this heat, either naturally or through the use of refrigeration.

- Broken Rock - The action of breaking rock and the subsequent transportation causes the heat to spread.

- Personnel - A man working can give off 500 Watts of heat.

- Oxidation - Oxidation of wooden supports or coal may produce heat.

- Lighting - This dependent on output of the lights in Watts.

- Surface Ambient Temperature - This is not a problem in Northern Europe, however in Hot Climates it may pose a problem.

2.3 ENVIRONMENTAL MONITORING AND CONTROLS MEASURES IN VENTILATION SYSTEMS.

Prior to the introduction of electronic instruments, environmental monitoring in headings was carried out manually by competent persons. Methane measurements were taken using a flame safety lamp or later a methanometer by the district Deputy in the course of statutory inspections and at other times according to his own discretion or manager's instructions. Airflow determinations were made weekly by a competent person using appropriate measuring instruments.

Present technology enables most environmental parameters to be continuously measured with the readings displayed on an underground control box and transmitted to the surface for display, recording and processing. Parameters that can be monitored in this way include :

- methane
- carbon monoxide
- oxygen
- products of combustion
- air velocity (general body and duct)
- fan vibration
- fan temperature

Since the late 1970's British Coal has supplemented manual methane readings with continuous remote monitoring (English, 1990). By the mid and late 1980s, continuous methane and fan vibration monitors were being installed on a general basis. The monitoring of face heading ventilation systems was standardised within the North Yorkshire Area (Sykes, 1989). Each fan was equipped with a FIFFI (fan instrumentation for fault indication) vibration monitor which relayed information to the colliery control room. In a simple exhausting system, the methane detector was sited at the fan inlet to prevent more than 1.25% methane passing through the impeller. Additional methane detectors were installed if the heading was ventilated in series with another drivage or face; or if the cut section contained strata of high incendive temperature potential (ITP). Vortex-shedder type air velocity transducers were also commonly fitted at the outbye end of headings and smoke detectors installed down-wind of conveyor drives to give early indication of fire.

Prior to 1989, headings in the Nottinghamshire Area was equipped with an automatic methane monitor sited either at the entrance to the drivage in the case of main exhausting ventilation or at the intake to the fan for main forcing ventilation. These were linked with an electrical cut-off facility to isolate power to the district in the event of high methane levels.

If standard of safety and working comfort are to be maintained in the general body continuous monitoring is paramount. This is achieved through use of the MINOS system. It is used in 90% of UK collieries to provide a centralised alarm continuous

safety monitoring and control system for the entire mine . Any data monitored by the MINOS system can be passed over the network to a colliery information system (CIS) for further analysis, long term storage and for the inclusion in management reports. The data collected by other installed monitoring systems may also be sent through MINOS and hence become available in the colliery control room. The mine engineers and managers have direct access to MINOS via a PC connected to the network. The MINOS system uses standard data transmission system for use in coal mines (BS 6556). Eight separate links can be handled by a single MINOS system, and fourteen outstations may be connected to one link. (English, 1994)

2.3.1 Methane monitoring and control

This is monitored continuously at the heading face giving a visual read-out of the measured gas concentration. If the concentration exceeds the statutory limit an alarm is normally activated and an automatic shutdown of power to electrical machinery is initiated. (CEC, 1990.) Despite the development of automation, manual monitoring is still a statutory requirement and is necessary for measuring methane concentrations in such places as roof cavities. Control of methane is achieved through a combination of methane drainage, ventilation and water sprays mounted on the drum of continuous miners.

2.3.1.1 Methanometer

This is a small, hand-held device (Figure 2.5) and is used by a colliery official to make 'spot' methane determinations, either as part of a statutory inspection or as a random test. A probe can be fitted to the methanometer to enable samples to be drawn from near the roof or other places not easily accessible.

2.3.1.2 Automatic Firedamp Detector (AFD)

The AFD is a larger instrument (Figure 2.6) as it gives a continuous read-out and hence requires a larger battery than the methanometer. Carried underground at the start of each shift, it is suspended from the roof of the heading, as close as practicable to the face. A

slow flashing light (15 second intervals) indicates a safe level of methane and changes to a higher frequency (once per second) if the percentage increases beyond an alarm setting. The AFD does not record methane levels and the display must be read manually.

The pellistors of hand-held instruments are susceptible to damage and deterioration from systematic exposure to the mine atmosphere. Accordingly, they must be regularly checked and re-calibrated if necessary.

2.3.1.3 Flame safety lamp

The flame safety lamp is the oldest type of detector and is still used for testing the methane concentration in the air. The flame shows a faint blue cap when methane is present. The ratio of the height of the gas cap from the base of the flame to the overall width of the flame is used to measure the percentage of methane in the air. The conventional lamps indicate methane concentrations from 1.25 - 5%. The Garforth lamp can detect methane concentrations up to 20%.

It is also used to indicate oxygen deficiency in the air. The flame gradually reduces as the oxygen content decreases. However, if the methane concentration is very high the lamp may remain lit with an oxygen concentration as low as 13%.

2.3.1.4 Stain tubes.

These are sealed glass tubes with a chemically active compound that changes colour when a particular gas sample is sucked through it. The concentration of the gas is estimated from the length of the stain or by comparing the colour of the stain with a chart.

Figure 2-5 - An Example of a hand held Methanometer.

Figure 2-6 - An example of an Automatic Firedamp Detector (AFD.)

2.3.2 Continuous-Monitoring Transducers

Instruments for continuous methane measurement fall into two main categories: low range (0-3% or 0-5%) for monitoring levels in the general body of ventilation and high range (0-100%) for use in methane drainage ranges.

Continuous methane monitors consist of a control unit and remote detector head, or transducer. The detector head is a pellistor-based device and can be installed in the roof (inbye and outbye) and in the auxiliary ventilation duct. The signal from the detector head is transmitted to the control unit which processes the information.

Automatic monitoring instruments are constantly exposed to varying levels of methane and hence are potentially more liable to deterioration than manual devices. For instruments to meet BS6020 approval, the drift over a 2 week period must be less than 1% methane or a 8% reading, whichever is greater. Methane detectors can also be installed on the cutting machine, particularly if it is fitted with an integral exhausting fan and dust extractor (*scrubber* system). In this way, firedamp measurements can be made very close to the face, within the cutting zone. Automatic trips shut down the machine if limit levels are exceeded.

2.3.3 Dust monitoring and control.

Dust samples are normally taken in working areas monthly with a gravimetric dust sampler. Control is achieved through a combination of water sprays and scrubbers and /or filters either on-board the machine or behind the fan.

2.3.3.1 Gravimetric dust sampler.

This instrument samples dust laden air at 2.5 l/min, is portable and may be used for up to twelve hours. Dust is captured on a dust filter. The sample is analysed using ashing, X-ray diffraction, or Spectra-photometry to assess the quartz and other mineral content

2.3.3.2 MRDE dust extractor

Dust laden air is drawn into the fan where it is mixed with finely atomised water discharged from a spray. A portion of the duct is '*wetted*' at the fan impeller and along the internal surfaces of the fan case. From the fan the air/dust/water mixture passes through a rectangular extractor panel comprising of a specially designed fine wire mesh. Passage through the mesh excites the respirable dust particles so that their impact energy overcomes the surface tension bond of the water droplets and the particles become wetted. The extractor panel is continuously washed to prevent clogging. Any water/dust mixture not precipitated in the extractor panel is collected by a bank of catchment vanes sited at the downstream end of the unit. The water/dust mixture collects in the tank at the base of the unit where the dust settles as sludge. The clean water is then recirculated.

2.3.3.3 Air curtains.

Some heading machines are fitted with *'air curtain'* systems to confine the dust cloud in an area ahead of the machine operator and ensure that all dust is collected by the exhaust ventilation duct. (ECSC, 1986)

2.3.3.4 Air movers.

Air movers use either the principle that a high pressure water spray or a high pressure air jet, will entrain air and cause it to move in the direction of the spray or jet. They can be used to assist in the ventilation of the cutting element which may become masked from the general ventilation during cutting operations; either by the main body of the machine or the cutting head itself.

2.3.4 AIRFLOW MEASUREMENT AND VISUALISATION.

The high cutting rates associated with mechanised in-seam drivages can liberate large volumes of methane into the mine atmosphere. High flow rates of fresh air are required

to dilute this gas to safe levels. Interruption or reduction of the airflow into the heading can result in a swift rise in the methane concentration. For this reason it is important that intake air velocities are continuously monitored in order that any changes can be detected in time for remedial action to be taken. The first three instrument introduced are continuous monitors while the remaining produce instantaneous readings and are utilised in the underground studies (chapter 9)

2.3.4.1 Rotary Vane Type

The first continuous airflow transducers were automatic versions of the vane anemometer. early instruments used the rotation of the vane to generate an electrical output. Designs were later developed that involved no direct physical contact with the vane assembly. The BA2 sensor detects the change in capacitance caused by vanes moving past a probe fixed to the instrument body. This generates electrical impulses proportional to the speed of rotation. (CEC, 1982; Sieger, 1988.)

2.3.4.2 Vortex Shedding Type

The latest and most commonly used instrument for air velocity measurement is the vortex shedding sensor; e.g. BA5 (Figure 2.7). When an airstream passes a strut, vortices are formed behind the strut at a rate dependent on the air velocity. The vortices cause interference in an ultrasonic beam behind the strut and this beam modulation is converted into an analogue signal. This type of transducer has no moving parts, hence does not wear and is more reliable. The gate of this instrument is however susceptible to blockage due to an accumulation of both moisture and dust. Thus the transducer head requires regular cleaning to ensure that reliable and accurate readings are obtained from the transducer.

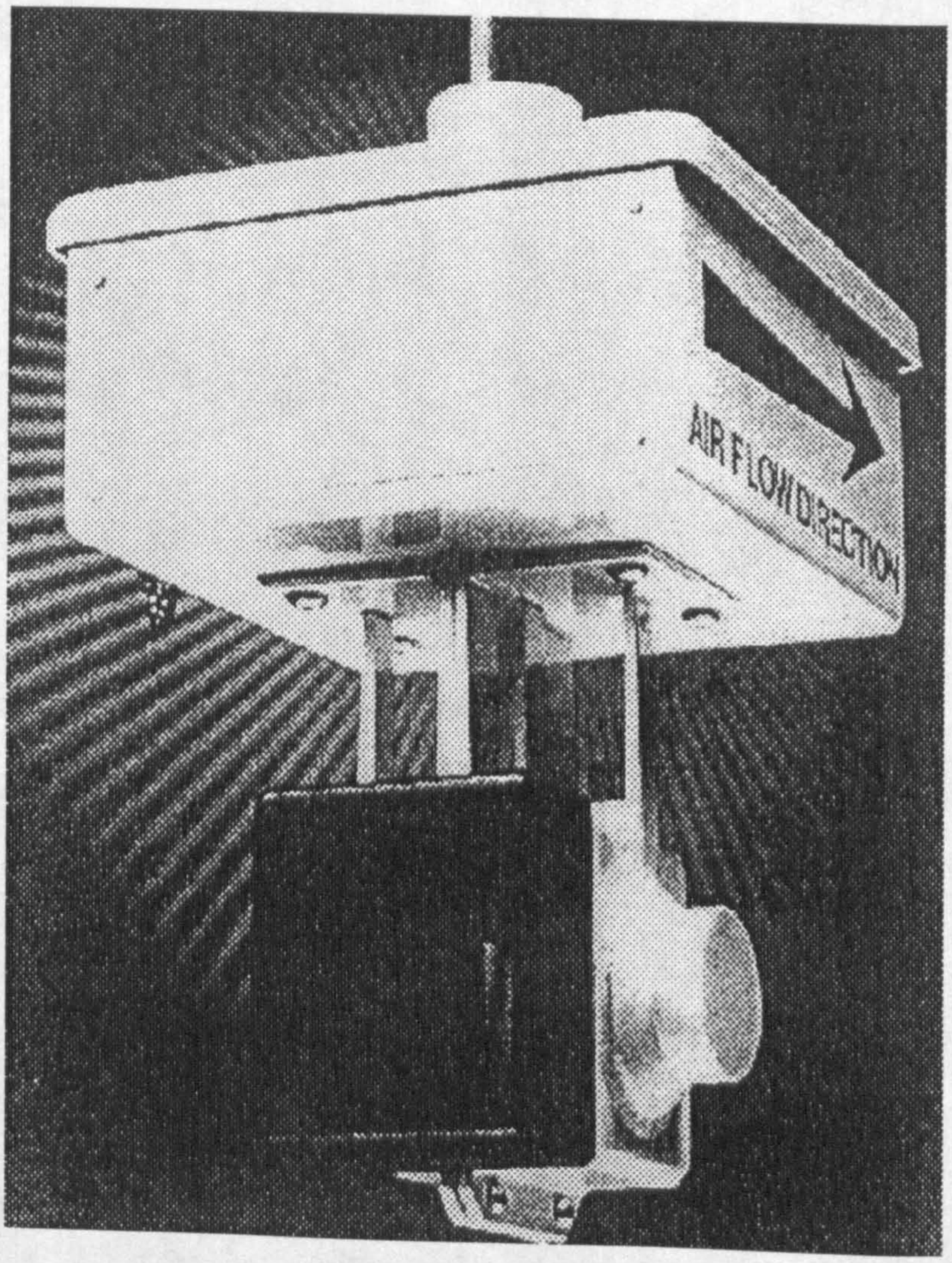

Figure 2-7 - A typical BA5 Vortex shedding anemometer

2.3.4.3 Vane Anemometers utilised.

The AM 5000 (figure 2.8) uses a digital mechanical distance indicator that can be started stopped and reset at the press of a button. The vane assembly is made from a single sheet of stainless steel and mounted on a cantilevered axle. A stainless steel band that protects the vanes from damage surrounds the instrument. The apparatus can be used to measure wind speeds from 1 to 5 m/s and is considered as a high/medium speed anemometer (Mining and minerals engineering).

The Airflow LCA 30 IS is a hand held rotating vane anemometer illustrated in figure 2.9 This instrument is capable of providing an indication on a digital liquid crystal display of the flow rate averaged over three seconds, or any period up to two minutes. The instrument can be used to measure wind speeds in the range 0.2 to 30 m/s.

2.3.4.4 Pitot static tubes.

A Pitot static tube consists of two co-axial tubes. The one that faces directly into the airstream measures the total pressure (P_t). The other tube, which is open at small holes behind the facing tube, measures the static pressure (P_s). The pitot is usually connected to a magnehelic gauge which gives a differential readout of P_t and P_s which results in P_v. The airstream velocity can be calculated for the following equation.

$$u = (2P_v/\rho)^{-1/2} \tag{3.1}$$

2.3.4.5 Smoke Tubes

These may be employed to measure airflows of low velocities. A pulse of air forced by a rubber bulb through a glass phial containing a granulated and porous medium soaked in titanium tetrachloride produces a dense white smoke. Smoke tubes are used primarily used to visualise the movement of air locally.

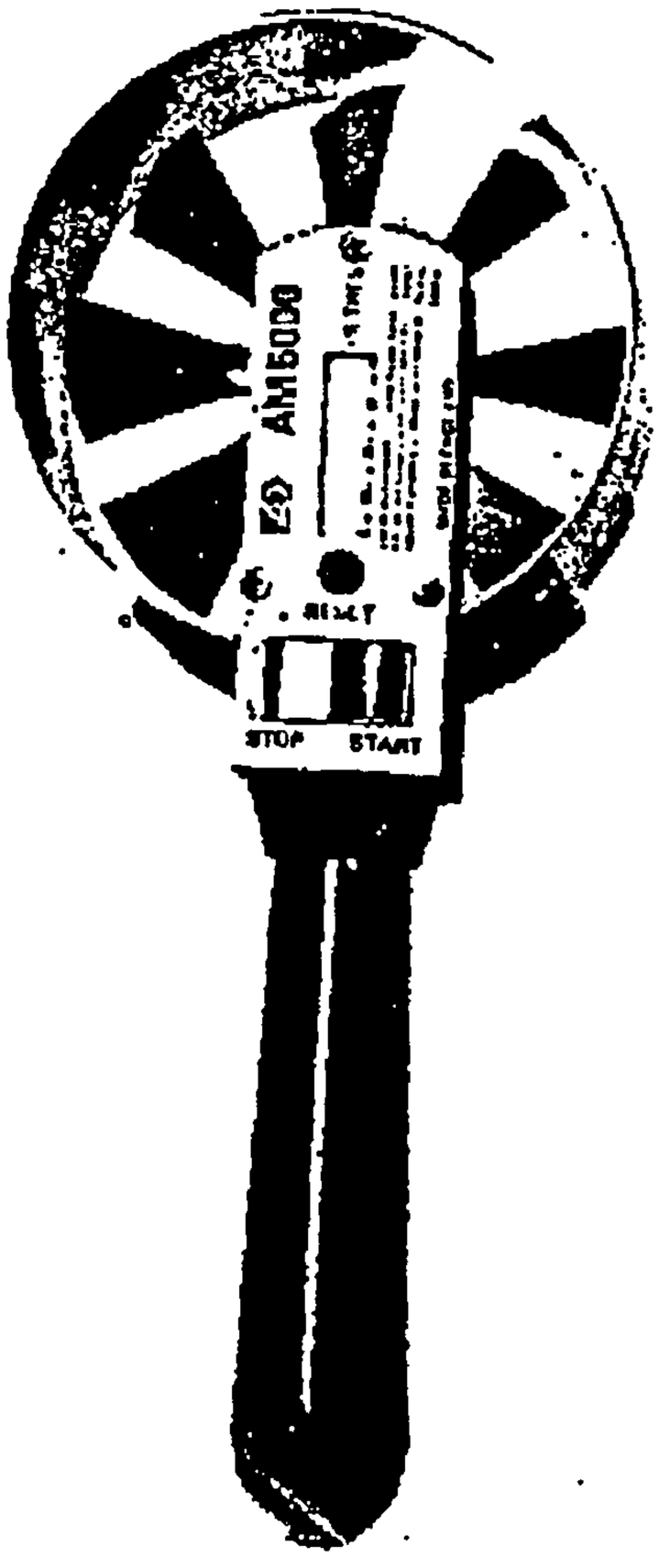

Figure 2-8 - Vane anemometer - AM 5000,

Figure 2-9 - Airflow LCA 30 IS

2.4 SUMMARY.

The aims of any Mine Ventilation System are to remove any pollutants in the underground environment. This chapter has reviewed the pollutants present, the methods and instrumentation to measure methane and airflow quantities in an underground mine.

The following Chapter introduces tunnel drivage methods and the system employed to ventilate them.

3. TUNNEL DRIVAGE SYSTEMS AND THEIR VENTILATION

3.1 INTRODUCTION

Auxiliary ventilation is the term used to describe the method of ventilating unconnecting openings. The auxiliary system employed should in no way affect the flow of air in the main ventilation system. It normally comprises of a fan(s) and ducting or brattice. In metal mine and construction work compressed air may be sufficient to ventilate these openings. The objective of the auxiliary ventilation system in soft rock mining is to adequatly ventilate the face area while the machine is cutting. It is well known that the highest gas emmissions occur when virgin coal is being cut. Therfore, it is important to ventilate the cutting zone well to prevent the occurance of frictional ignitions without raising dust levels beyond the statutory limits. The following section will introduce the various systems employed to maintain the best possible conditions at the heading face.

3.2 TYPES OF HEADING

3.2.1 Conventional Drill and Blast

In this method holes are drilled in the heading face, the pattern of which depending on the type of strata. The holes are filled with explosives and then blasted. The debris is then removed in an operation known as "mucking out". The method has the advantage that it can produce any shape of roadway. However, it usually requires more support than other methods due to damage caused by the blast. The method is the slowest of the drivage methods due to the cyclic nature of the operation.

3.2.2 Tunnel Boring.

Full face tunnel boring machines (TBM's) have been in common use in Civil Engineering for many years. Constant development and improvement in the tools utilised have resulted in machines that are capable of advancing large diameter openings in strong igneous and metamorphic formations. Advance rates of 213 metres per week (moderate utilisation) have been obtained mines in the USA (Forrester, 1995)

TBM excavation is a continuous process, with cutting, mucking and support installation proceeding concurrently. This method is limited by the fact that it can only produce circular section roadways and its high capital cost. This means that it used primarily in long drivages usually in excess of 3500 metres. TBM's were used to develop main access drifts averaging 81m/wk for 4800m at Gascoigne wood mine in the Selby complex. (Forrester, 1995)

3.2.3 Roadheaders

This type of machine was developed in the coal mining industry in the 1960's. Today it has a wide range of applications in other forms of mining and Civil Engineering work. In coal mines they are used to develop main roadways. They are more flexible than TBM's in that they are not limited to a circular cut. They also have a lower capital cost when compared to TBM's. The advance rates depend on type of strata, area of face and the percentage of time spent cutting.

3.2.4 Continuous Mining Production Headings.

This machine is crawler mounted and is similar to the roadheader except it has a wider drum-type head for mainly in-seam applications. They are very successful versatile machines predominately used in room and pillar and shortwall operations. In the UK they are used for longwall gate roads also. Advance rates of 100 metres per week are typical when using this technique. The new generation of continuous miner can similtaneously mine and rockbolt thus increasing the time spent cutting. Hard rock continuous miners are currently being developed for use underground.

3.3 AUXILIARY VENTILATION PRACTICE IN HEADINGS.

The objective of the ventilation of a development heading is to replace the contaminated air at the face with fresh air. This is achieved through the use of fans and ducting/brattice or jet fans

3.3.1 Line Brattice

It is common in United States coal mines to ventilate multi-entry drivages by coarsing air around the face ends using line brattices pinned to the roof and floor (McPherson, 1993). This system is also used in Australia (Aziz et al, 1993) and South Africa (De Kock & Smith, 1988). The brattice is hung loosely at the crosscuts to allow the passage of the equipment.

At present in the UK, auxiliary fans and duct must be used to ventilate headings. British Coal Production Instruction PI/1956/18 states that:

1, *Brattice shall not be used in roadways as a means of diverting or regulating air currents, nor in place of doors to prevent short-circuiting of air, except:*

2, *a) in bord and pillar workings;*

b) for hurdle sheets and in fast ends;

c) for the construction of frame doors in unsettled ground;

d) in emergencies.

The method suffers from a number of disadvantages which would preclude its general use in Britain.

a) The large cross-sectional area of a forcing air channel formed by brattice results in a low air velocity that may be inadequate to prevent methane layering.

b) In the United States and Australia, where the coal has about twice the strength of UK coals, pillar widths of some 10m are adequate at the typical mining depths of 200m. In Britain, where workings are up to 900m in depth, the minimum required pillar size is 50m. This means that the length of headings in multi-entry developments is much greater.

The inevitable leakage associated with brattice would prevent sufficient air quantities reaching the face of the heading.

c) Brattice may easily be dislodged or damaged by the movement of equipment.

d) In the system above, potentially contaminated air is used to ventilate all headings except the first. Where methane and dust production is high, this is dangerous. The brattice can be arranged such that only a proportion of the intake air is diverted into a heading. Hence, each heading within a multi-entry section can receive some fresh air. However, it is difficult to control the auxiliary ventilation quantities obtained in this manner.

d) Line brattice ventilation channels offer a high resistance to airflow compared to a full-width heading. This high resistance at the most inbye areas of a mine ventilation system forces more air to be lost at all leakage points throughout the entire network (McPherson, 1993).

3.3.2 Auxiliary ventilation systems employed

3.3.2.1 Simple Forcing/exhaust.

A fan situated outside the heading blows fresh air through a single duct to the face. (Figure 3.1). The air delivered to the face is highly turbulent and is moving relatively fast, therefore any accumulation of gases are swept away. However, the law states that; *"air must be delivered to within 5m of the face"*. Thus this system alone is not practical because excessive dust will become airborne.

In the exhausting system (Figure 3.2) contaminated air from the face of the heading is drawn through the duct and exhausted into the main return airflow. Air entering a heading with the exhausting system does so across a much larger cross-section and hence is slow moving.

Tunnelling operations frequently use a forcing/exhaust exchange method where the ventilation can be altered. This system is generally used where shot firing is utilised. It is never used where flammable gases are present.

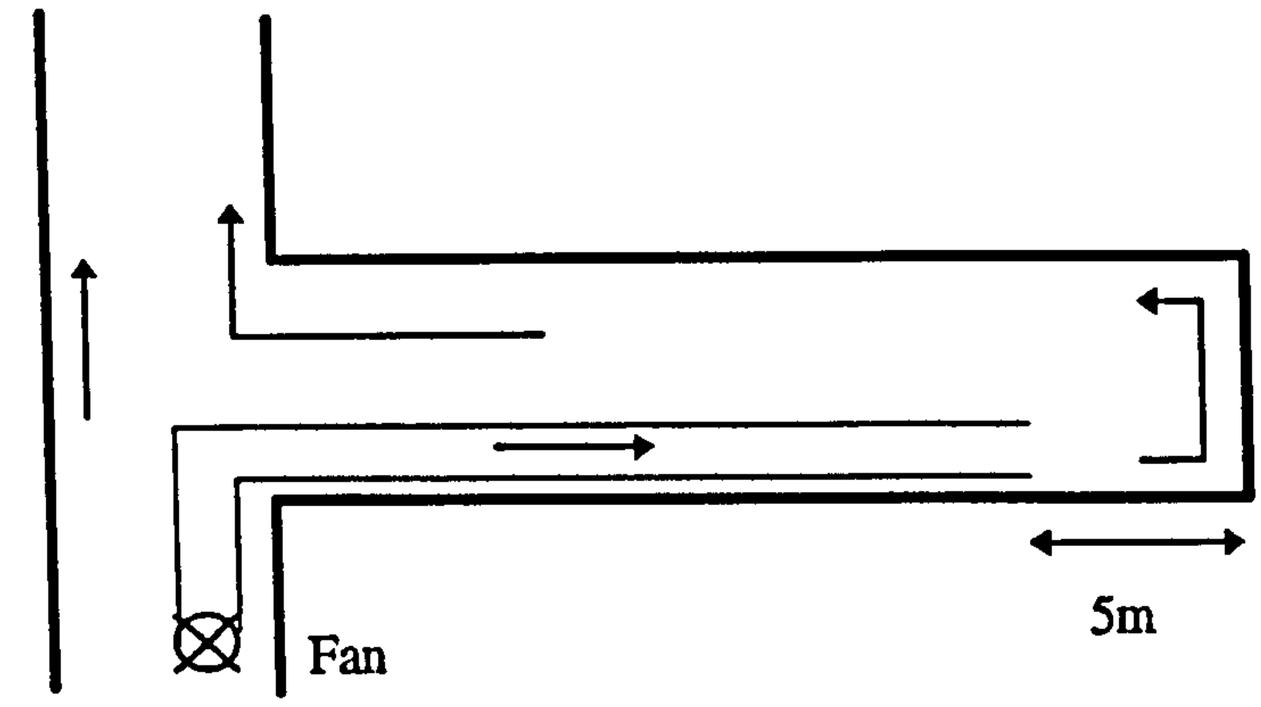

Figure 3-1 - Simple Forcing system.

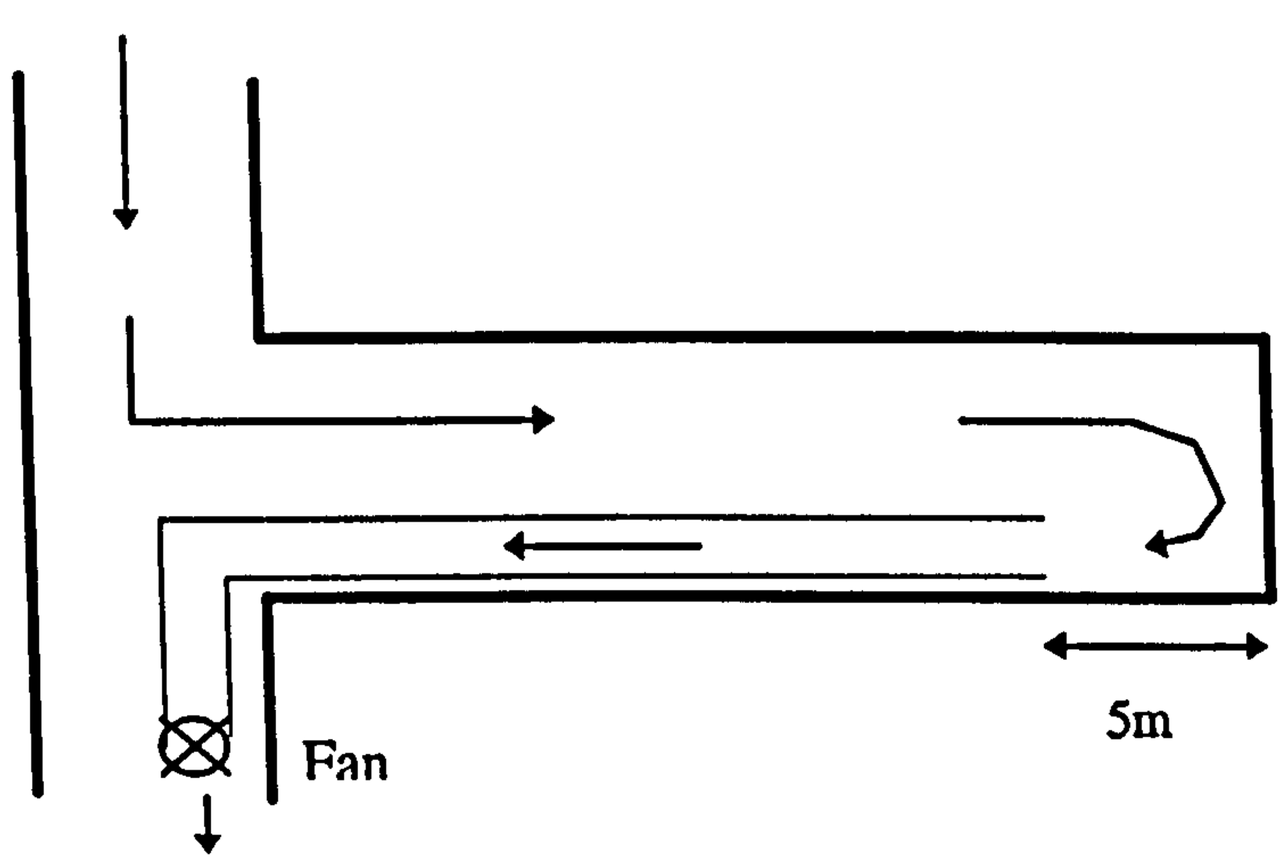

Figure 3-2 -Simple Exhaust system

3.3.2.2 Overlap systems

Overlap auxiliary ventilation systems utilise a second fan and a short length of duct at the inbye end of the heading. A forcing with exhaust overlap (Figure 3.3) consists of a main forcing system with a secondary exhausting installation. An exhaust with forcing overlap

is the opposite arrangement and is used primarily in tunnelling operations (Tagaki, 1978). These systems were developed to combine the advantages of forcing and exhausting ventilation to best effect in particular mining situations.

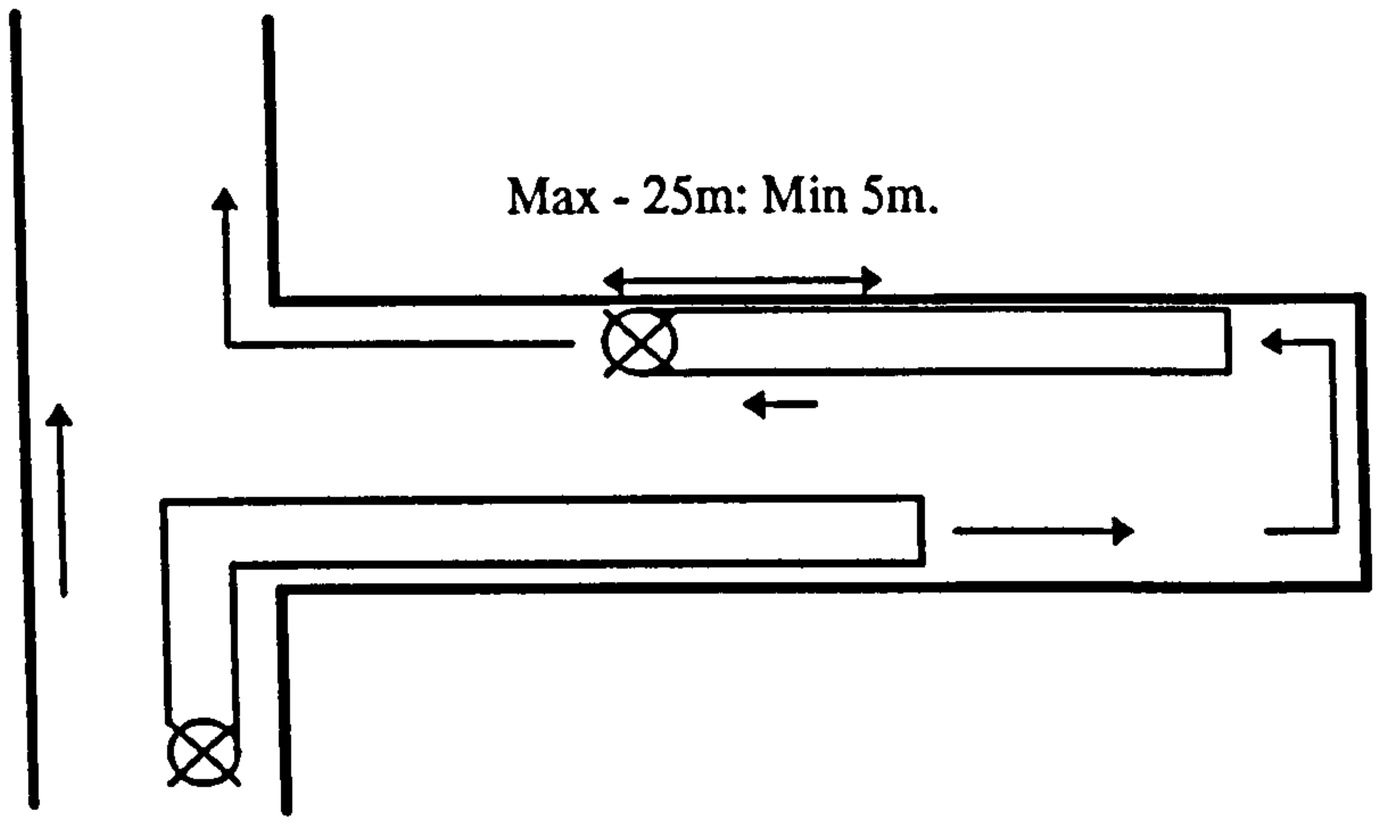

Figure 3-3 - Normal Overlap System.

In UK mechanised drivages the forcing with exhaust arrangement is by far the most common of the two overlap systems (Sykes, 1989; Browning & Warwick, 1993). The jet from the forcing duct scours the face of firedamp although the effect is reduced by the need to either fit a diffuser to the outlet or to keep the discharge end some 15m from the face to avoid dust pick-up and dispersion. The inlet of the exhaust overlap is maintained within 5m of the face to remove airborne dust and a collector or filter cleans the air before it is discharged into the general body. Within the overlap area between the discharge of the forcing duct and the exhaust fan there is a reduced airflow, depending on the quantity in each duct. For this reason, the length of the overlap should be minimised, but according to conventional practice, no less than 5m to prevent significant recirculation.

3.3.3 Types of fans utilised.

3.3.3.1 In-line Axial Flow fan

This fan has the motor mounted within the airstream (figure 3.4) behind the impeller. The fan has an efficiency of between 45-50%. It also emits higher noise levels when compared to radial flow fans due to the higher blade speeds. The impellers of the fan are exposed to contaminants due to its design. Therefore they need regular maintenance.

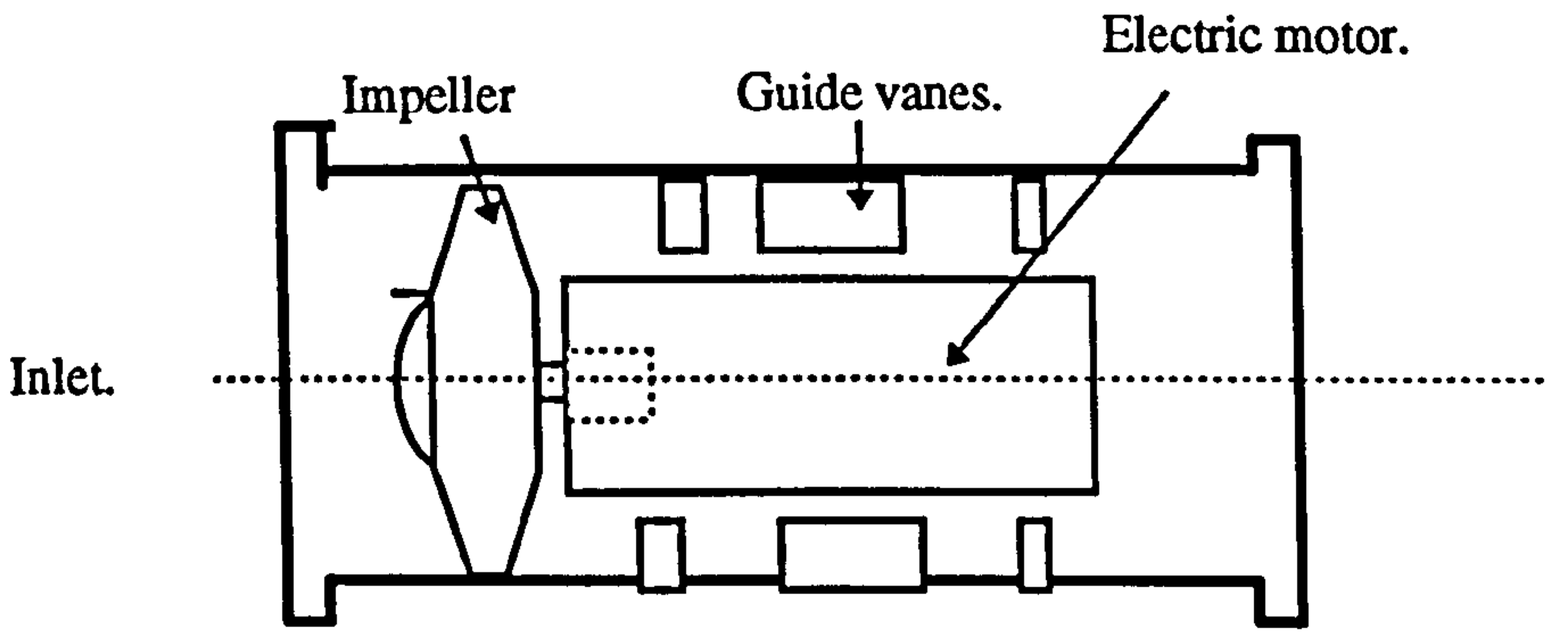

Figure 3-4 - In line axial flow fan.

3.3.3.2 Bifurcated Axial Flow Fan.

The bifurcated fan casing is split in an aerodynamic shape and the motor is out of the airflow (Figure 3.5). Hence they are suitable for exhausting systems. This type of fan has an efficiency of between 40-50%. The basic axial fan is not commonly used in British coal mines because it is; undesirable that an electric motor should be located in a potentially polluted airstream.

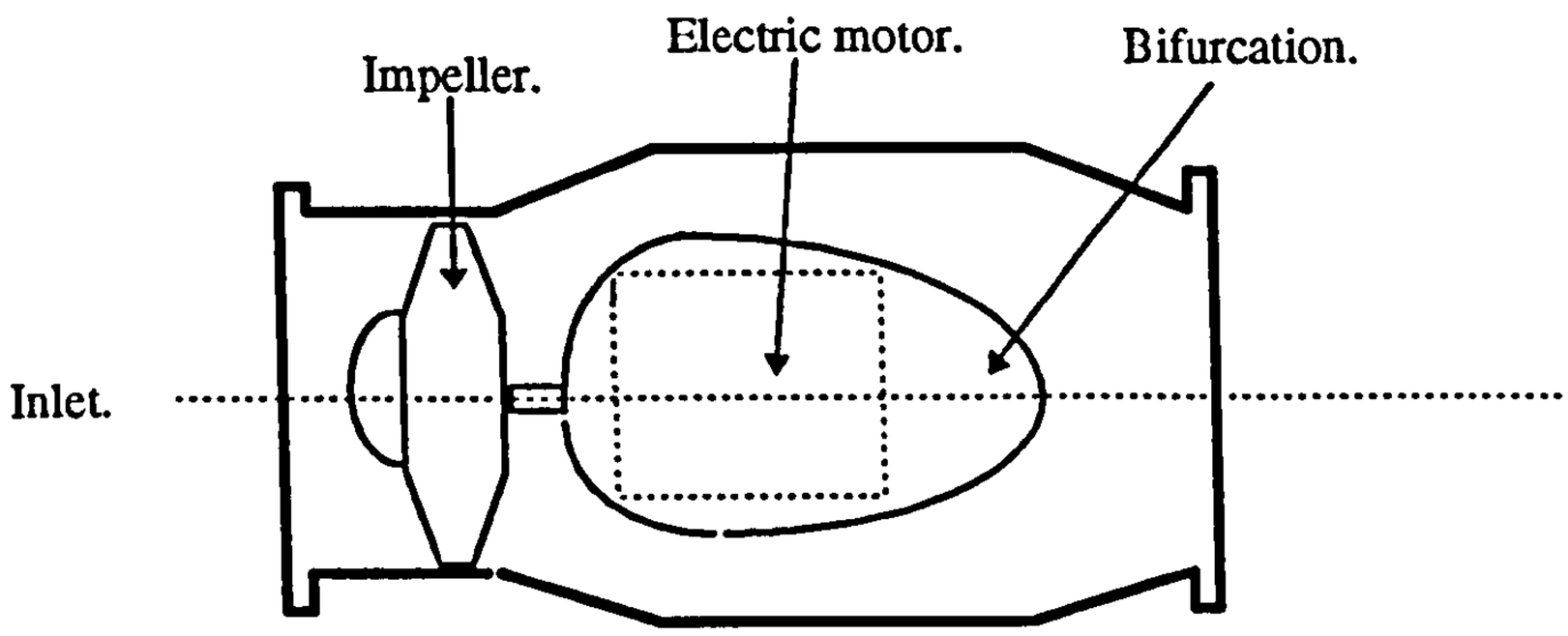

Figure 3-5 - Bifurcated In-line axial flow fan.

3.3.3.3 In-line Radial Flow Fans.

Air enters the eye of the impeller and is turned through 90° within the impeller. Guide vanes in the casing then turn the air back through 90° to flow through a bifurcated casing. The motor is mounted outside the airstream (Figure 3.6) The centrifugal impeller of the radial flow fan produces a fan characteristic which has a high pressure curve relative to the same size and power of axial fan (Cluett, 1987).

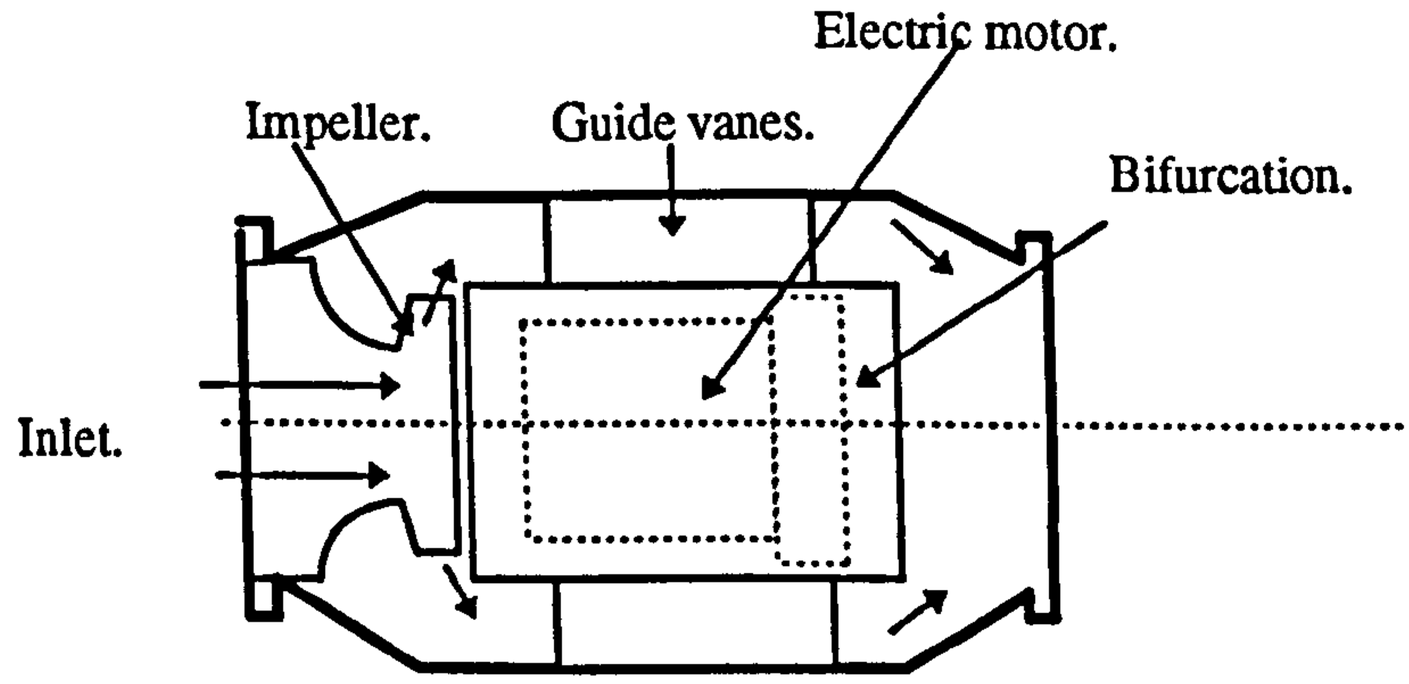

Figure 3-6 - In - line radial flow fan.

3.3.4 Fan arrangements

Auxiliary fans can be used alone or in various combinations to achieve specific objectives. The basic arrangements are introduced.

3.3.4.1 Single fan

This is the simplest arrangement and is utilised extensively in UK coalmines.

3.3.4.2 Fans in series

This system is used in long drivages when a single fan is unable to deliver the desired quantity to the heading face. This increases the pressure considerably without increasing the air quantity by the same proportion. When using this system identical fans should be employed. If they are not utilised the net effect upon the volume delivered relates to the duct characteristics (Barker & Highton, 1981)

3.3.4.3 Fans in Parallel.

If fans in series are unable to increase the volume delivered to a heading face with the same pressure, then a parallel fan arrangement may be employed. (Ramani, 1992 p1078)

3.3.4.4 Jet Fans

Investigation has been carried out in South Africa on the use of ductless fans to ventilate multi-entry headings (De Kock & Smith, 1988; Meetz & Meyer, 1993). As with line brattice, the method is only suitable when the maximum distance of the face from the last cross-cut is relatively short; less than 30m. Generally in Britain, somewhat larger pillar sizes are required for stability.

Trials have been carried out using two types of fan, the Vortex fan and the Jet fan (Meetz & Meyer, 1993). The Vortex fan uses an impeller design adapted from those used in vertical take-off aircraft. They create a vortex column of air that is maintained up to 30m from the fan discharge. A Jet fan is a standard axial flow fan fitted with outlet reduction pieces that increase the velocity pressure at the discharge to increase the air penetration distance and enhance air entrainment.

Tests were carried out in headings to determine the optimum position for the fan and the maximum distance at which the discharge penetration would provide satisfactory face ventilation. Airflow patterns were determined using SF_6 tracer gas. The airflow velocity

through the last through road (LTR), direction right to left, was also varied. Both types of fan had a rating of 4 kW.

a) Vortex fan.

With the fan sited at the entrance to the heading, the best position was found to be on the left hand side. This gave a penetration distance of 25m with 30% recirculation at an air velocity in the LTR of 1.4 m/s.

Siting the fan where there is cleaner air, in the LTR, the optimum location was at the right-hand side. Penetration depth was 23m with recirculation of 20% at an LTR air velocity of 1.2 m/s.

b) Jet Fan.

Results with the jet fan were similar. Penetration of the air jet was less than that produced by the Vortex fan and less air was entrained. Investigations have also been carried out in South Africa with ductless fans positioned within the heading itself (De Kock & Smith, 1988). Under South African regulations, electric fans cannot be used in such circumstances so a hydraulically-driven system was developed. It was based on the Vertol Airjet design, a specialised vortex generating fan which produces a long discharge throw. Tests conducted in a 6.5m wide heading showed that the face could be adequately ventilated with the fan at a distance of 21m.

3.3.5 Ducting utilised.

There are four main types of ducting for auxiliary ventilation.

3.3.5.1 Non-Reinforced Flexible Ducting

This type is fabricated from heavy grade PVC with a semi-rigid ring at each end. It is available in various lengths which are coupled by inserting the end-ring of the up-stream (outbye) section into the mouth of the down-stream (inbye) section. The joint is secured with a either a buff type (male/female) coupling or flexible coupling band incorporating two wires. This type of duct can only be used with a forcing systems as it relies on a positive internal pressure to hold it open.

3.3.5.2 Reinforced Flexible Ducting

This type of duct is fabricated from PVC with steel spirals along the duct. These provide stiffening whilst still allowing the duct to be closed down like a concertina for transportation.

3.3.5.3 Rigid Ducting

This type is fabricated from either steel or glass-reinforced plastic (GRP). In UK coalmines GRP is preferred because steel ducting is expensive, heavy and slow to install (HSE, 1978).

3.4 AIR LEAKAGE IN AUXILIARY VENTILATION SYSTEMS

In practice all ducts leak, the quantity of which depends on the quality of installation. There are three methods available for analysis for leaky ducts; i) mathematical analysis - with a uniformly distributed leakage, ii) ventilation network analysis and iii) treatment of air as a series-parallel combination of airflows along the duct through leakage paths.

3.4.1 Mathematical analysis

Many researchers have developed mathematical equations to calculate the volume increase ratio (Q1/Q2) and the pressure increase ratio (P1/P2). (Browning, 1983; Vutukuri, 1983) Vutukuri, 1993 assessed the accuracy of these and other equations. The resistance and leakage constants used in these equations are based on work conducted in the 1960's by MRDE. Fan and duct pressure and flow measurements were carried out at a fixed pressure of 1kPa. A simple Fortran program (Appendix 2) was also written to calculate the leakage using Brownings equations because of their superior accuracy (Vutukuri, 1993).

3.4.2 Ventilation Network Analysis

This method assumes a number of discrete leakage paths, enabling treatment as a ventilation network. Thus a ventilation network package can be used to analyse the leakage.

3.5 USE OF CONTINUOUS MINERS (CM'S)

3.5.1 Introduction

Continuous miners have been used in room and pillar operations as production machines in the US for some time. In the UK they have primarily been used to develop retreat longwall faces. They have been used for this purpose because of their ability to develop roadways rapidly. Recently they have found use in room and pillar operations in the UK because in some areas caving of the strata is not desireable.

Remotely controlled Continuous Miners (CM's) have the ability to cut up to 12m in advance. However this method can not be utilised because the law states that the air must be supplied to within five metres of the face. This rule was introduced when quantities supplied were up to eight time less than today and conventional methods were used to produce coal.

To achieve these extended cuts one must provide adequate ventilation to the face. This may be achieved by using a combination of forcing ventilation and a machine mounted scrubber exhausting the air away from the face. However, the UK inspector does not consider the scrubber fan to be an adequate exhaust fan. Thus a conventional overlap system is used in longwall development roadways with the exhaust duct mounted on the machine and therby keeping the duct within the statutory limits. In room and pillar operations use of overlap systems is not possible due to the nature of the operation. i.e. the machine cuts one roadway and roof bolting conducted in the other, then they swap;

thus the CM is not idle for long periods. Research conducted into scrubber system and their ventilation is reviewed in chapter 5.

3.5.2 Overlap using a Cassette system at Welbeck Colliery.

The heading ventilation system including the duct cassette, which was employed at Welbeck Colliery, is illustrated in Figure 3.7. All equipment except for the inbye exhaust duct sections are mounted on the conveyor receiving section. A combination of two 5" rams and the tractive power of the continuous miner advance the unit.

The inbye forcing duct section is of rectangular steel section with a circular-section adapter at the outbye end where the connection with the flatlay is made. As the assembly is advanced, flatlay is fed from the back (outbye end) of the cassette. A spare cassette is stored and may be swung into position using an hydraulic crane. The length of rectangular-section exhaust duct inbye of the main assembly is suspended from monorail. Each assembly can be re-handled for installation on the left or right-hand of a roadway. (Yates et al, 1996)

3.5.2.1 Machine-Mounted Exhaust Overlap (Dust Scrubber)

Welbeck Colliery uses a continuous miner, the BJD 1038 HHS, which is equipped with a dust scrubber (Yates, et al 1996). The fan is an electric centrifugal model with the motor sited outside the fan casing. It is capable of passing a nominal quantity of 4.5m^3/s. The fan is located at the back left hand corner of the miner with the exhaust inlets sited underneath the jib at the front corners of the machine body (Figure 3.8). When the machine is cutting, the inlets are 2.5m from the face, drawing air from beneath the drum. Due to the resistance of the ducting across the front of the miner, the right-hand inlet draws only approximately half the air quantity of the left-hand inlet. A wet dust extractor unit powered by an electrical centrifugal fan forms an integral part of the machine.

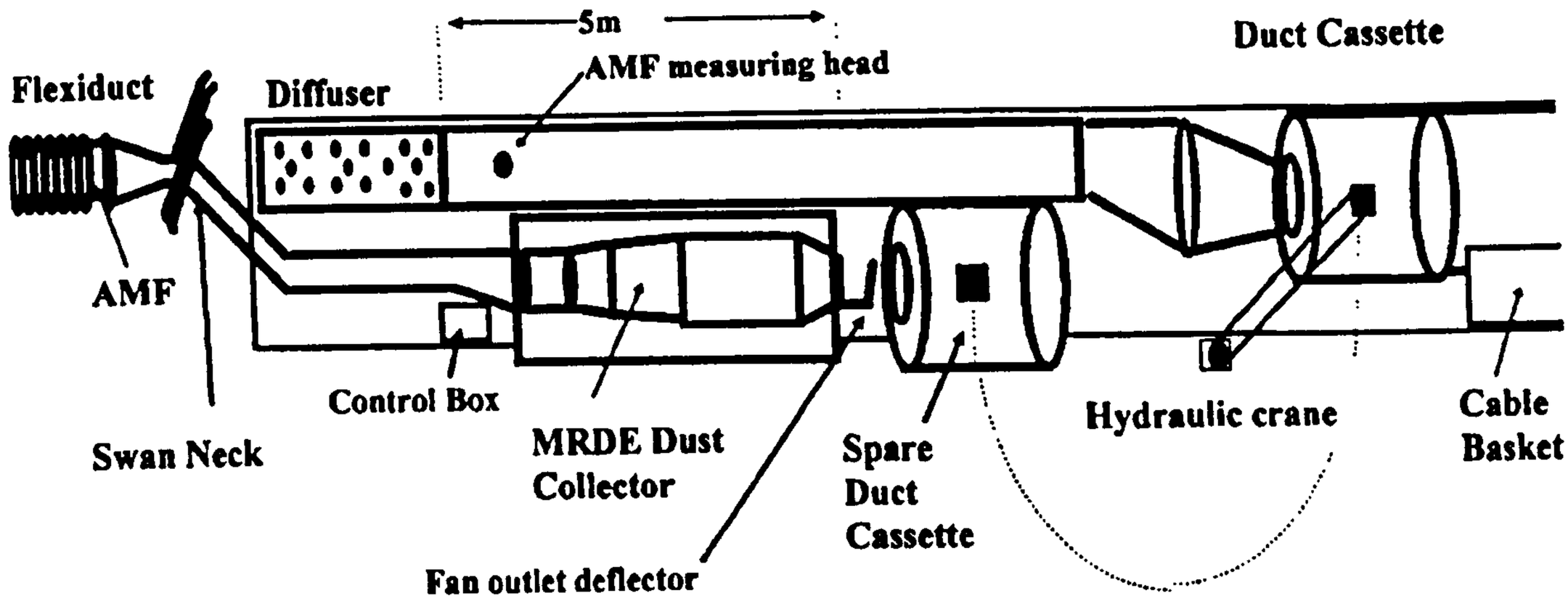

Figure 3-7 - Plan View of the Mk 4 Auxiliary ventilation system employed at Welbeck Colliery.

3.6 SUMMARY.

This chapter has reviewed the various techniques used to develop and ventilate tunnels. The current use of continuous miners in UK coal mines has also been discussed.

The general equations used for mine ventilation calculations are reviewed in the following chapter. The governing equations of fluid flow are introduced and the methods utilised to obtain closure are also discussed.

Figure 3-8 - Continuous miner with on-board scrubber.

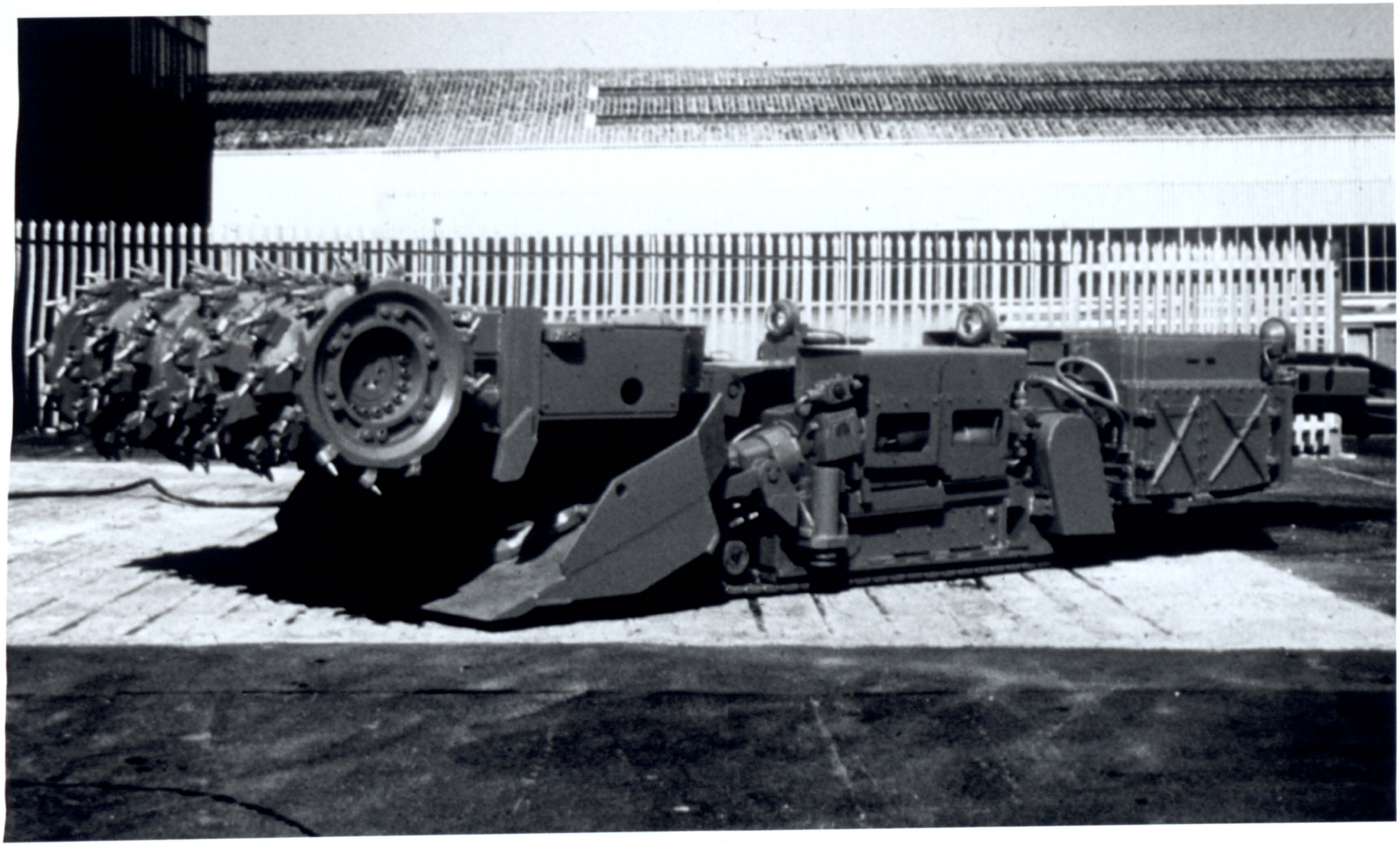

4. MECHANICS OF FLUID FLOW.

4.1 INTRODUCTION

Fluid mechanics is concerned with the statics and dynamics of liquids and gases. The analysis of the behaviour of fluids is based upon the fundamental laws: the conservation of mass-energy and force-momentum equations. This chapter reviews general fluid mechanics and terminology used by practicing mine ventilation engineers.

An introduction to Computational Fluid Dynamics (CFD) is also reviewed. This section introduces the governing equations in three dimensions. The techniques employed to obtain a solution from these equations is analysed. Finally the uncertainty and reliability of CFD simulations are covered.

4.2 FUNDAMENTALS OF FLUID FLOW

4.2.1 Definition of a Fluid.

A fluid is defined as a *substance that deforms continuously when subjected to a shear stress*. In other words the molecules that make up the fluid are free to move relative to each other. It offers no lasting resistance to the displacement, however great of one layer over another. This means that when the fluid is at rest, no shear force can exist in it. A solid on the other hand can resist a shear force while at rest.

Fluids may be divided into liquids and gases. The former are practically incompressible and posses a definite size but they take the shape of the containing vessel. Whereas gases are readily compressible and they adopt both size and the shape of the containing vessel. If a gas is free to expand it will do so indefinitely.

4.2.2 Conservation of Mass.

When a fluid is in motion, mass can neither be created or destroyed. If one considers a steady flow in a fixed volume this law can be expressed as;

$$\text{Mass flow in} = \text{Mass flow out} = \text{Constant}$$

or

$$\rho_1 A_1 U_1 = \rho_2 A_2 U_2 \tag{4.1}$$

4.2.3 Conservation of Momentum.

Newton's second law of motion states that the rate of change of momentum of a body is equal to the force acting on it. i.e.

$$F = ma \tag{4.2}$$

where F = force acting on a body of mass m traveling at a velocity a. (Providing m remains constant)

If pressures p_1 and p_2 act on the two opposite faces of a control volume as illustrated in Figure 4.1 the corresponding forces are p_1yz and p_2yz. In addition to these surface forces the fluid element may be subjected to body forces. If b is the body force per unit mass a and ρ the density then;

$$F = p_1 yz - p_2 yz + b\rho xyz \tag{4.3}$$

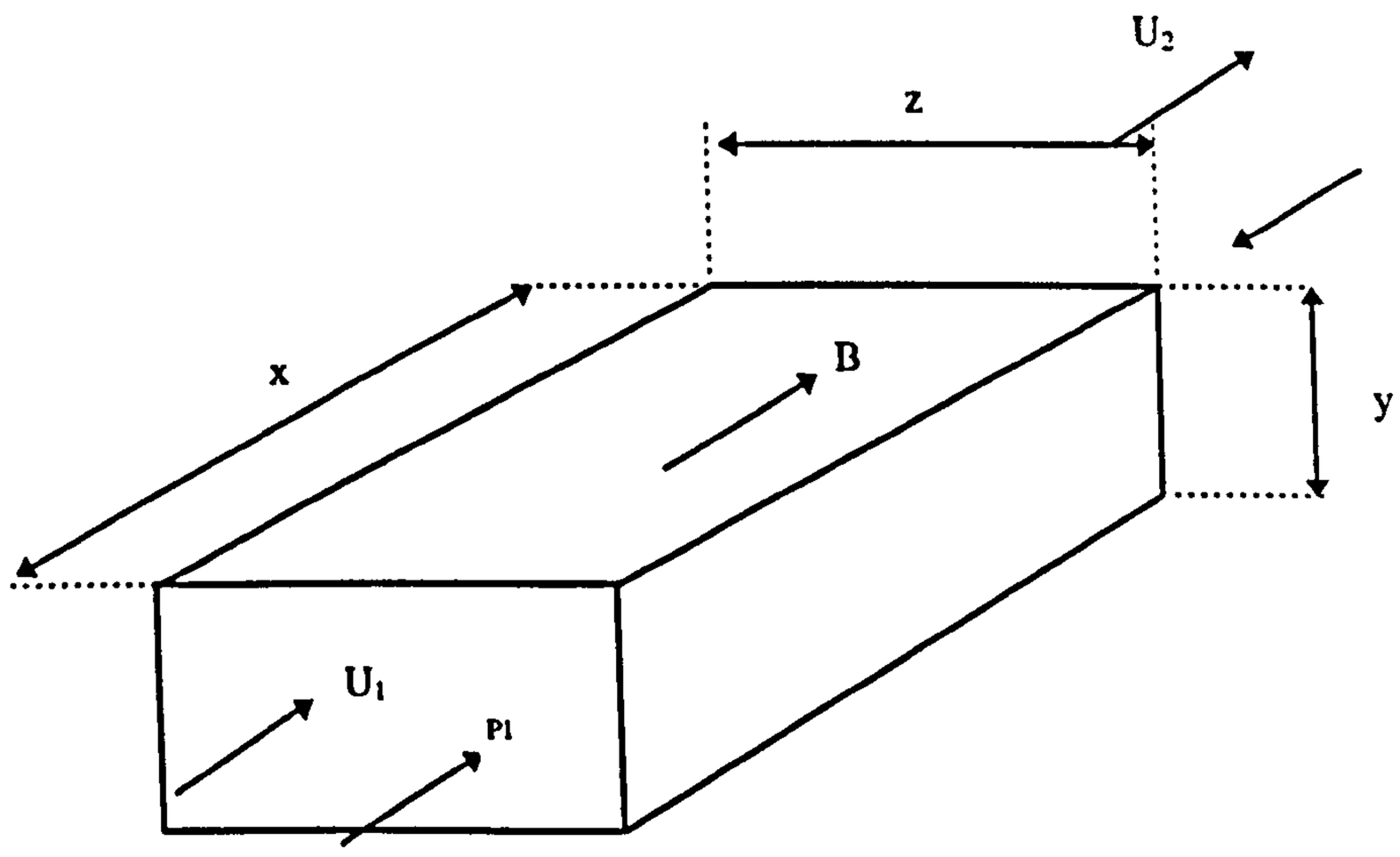

Figure 4-1 Flow through a fixed control volume.

The mass of the fluid element is ρ xyz and if x is a very small distance then

$$a = \frac{u_2 - u_1}{t}$$

where t the time taken to travel across the fluid element. Equation 4.3 can be written as;

$$(P_2 - P_1)yz + b\rho xyz = m\frac{u_2 - u_1}{t} \tag{4.4}$$

The average velocity across the fluid element can be written as $\frac{u_2 + u_2}{2} = \frac{x}{t}$ and

equation 4.4 becomes:

$$P_1 - P_2 + b\rho x = \rho\left(\frac{u_2^2 - u_1^2}{2}\right) \tag{4.5}$$

This equation is known as the momentum equation or Euler's Equation (x-direction only). If the x-direction is taken as being vertical such that P_1 and u_1 are at a height H_1 and p_2 and u_2 at a height H_2. The force B per unit mass is now due to gravitation. Therefore the weight per unit mass is B = -g . Thus, since the weight is directed downwards equation 4.5 now becomes:

$$P_1 + \rho\frac{u_1^2}{2} + g\rho Z_1 = P_2 + \rho\frac{u_2^2}{2} + \rho g Z_2 \tag{4.6}$$

This is Bernoulli's equation for the ideal incompressible fluid in terms of pressure. As a fluid moves along any opening, Bernoulli's equation allows one to see the relationships between the different variables. This equation only applies to an ideal fluid.

4.3 GENERAL PROPERTIES AND TERMS UTILISED IN FLUID MECHANICS.

4.3.1 Static, Total and Velocity Pressures.

Pressure is defined as the force applied to a known area. Static pressures act in all directions regardless of the direction of flow. The open end of the U-tube manometer measures the atmospheric pressure while the end in the pipe measures the static pressure. (Figure 4.2 (a)) The total pressure is defined as the total pressure of the oncoming fluid stream. Figure 4.2 (b) illustrates the total pressure is measured. Figure 4.2 (c) measures static and total pressures. Thus the velocity pressure is be calculated using the equation:

$$P_v = P_t - P_s \tag{4.7}$$

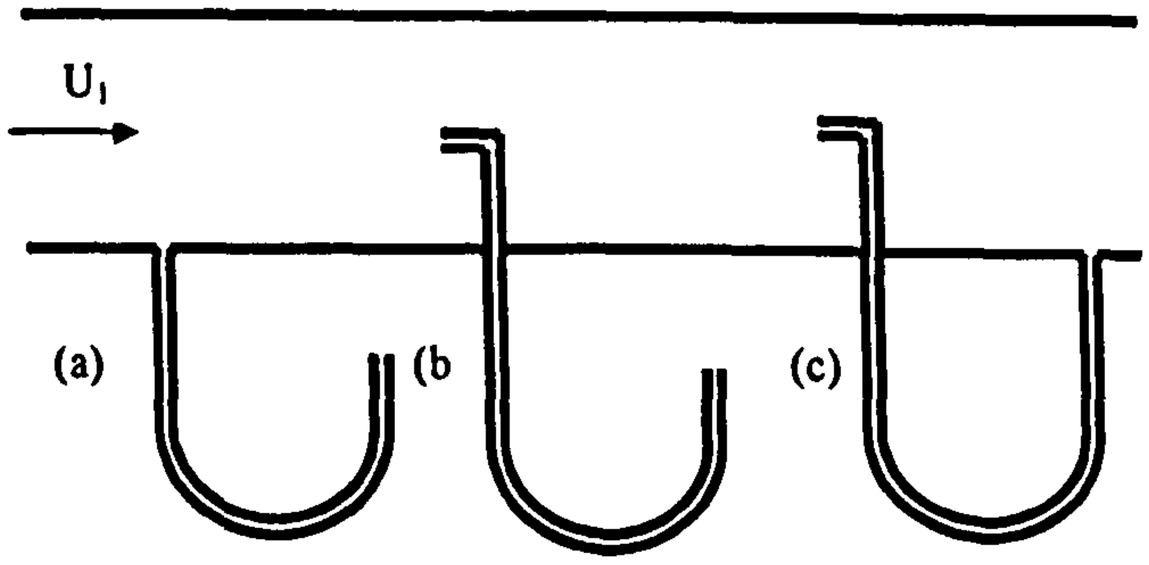

Figure 4-2 (a) static, (b) total, and (c) velocity pressures

4.3.2 Viscosity.

Viscosity is the resistance a fluid has to shear forces acting upon it. This varies for different fluids. The equation for viscosity is:

$$\mu = \tau \, {du}/{dy} \, \text{Ns/m}^2 \tag{4.8}$$

where μ= Coefficient of dynamic viscosity, $du/dy = L/L_t = t$ (seconds), $\tau = F/A$.

A **Newtonian fluid** is a fluid which obeys Newton's law of viscous flow. i.e. μ is constant with respect to the rate of shear du/dy for a given temperature and pressure.

The effect of viscosity is such that fluid particles immediately adjacent to a solid surface do not move with respect to that surface. This is known as the **no-slip condition**.

An **ideal fluid** is a fluid that has zero viscosity. This concept is useful in the solution of many complex fluid flow problems.

The effects of shear resistance's in many real fluids are small. Thus Bernoulli's equation is reasonably accurate for most practical cases concerning the relationship between pressure and velocity changes in a fluid. The Navier-Stokes equations allow for viscous forces and are the governing equations used in CFD packages and will be introduced later. In a general way, Bernoulli's equation may be modified to account for losses due to internal friction by adding the total pressure losses to the downstream side of the equation as follows:

$$P_1 + \frac{\rho_1 + u_1^2}{2} + g\rho_1 Z_1 = P_2 + \frac{\rho_2 u_2^2}{2} + g\rho_2 Z_2 + P_l \qquad (4.9)$$

Where P_l is the loss in total pressure between P_1 and P_2.

4.3.3 Density

Density is symbolized by ρ, this is defined as the mass per unit volume (kg/m^3).

4.3.4 Laminar and turbulent flow.

Consider a fluid flowing in the pipe (Figure 4.3). In section A the fluid is moving smoothly along streamlines, layers or laminae, parallel the axis of a pipe. This is called

laminar flow. In section B the flow has been disturbed by a bend in the pipe. The fluid flow in this region is mixing in a random fashion and is said to be turbulent.

Professor Osbourne Reynolds used a dimensionless ratio of 'inertial forces' to viscous forces to classify laminar and turbulent flows. He derived the following formula:

$$R_e = \frac{\rho u L}{\mu} \qquad (4.10)$$

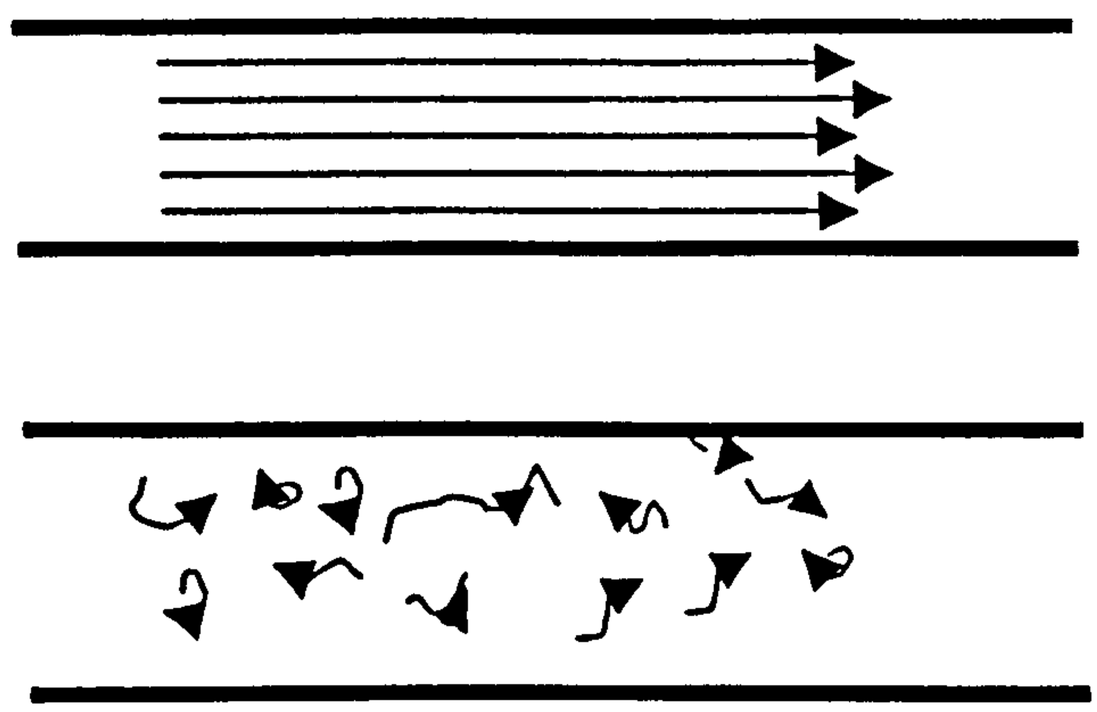

Figure 4-3 Example of Laminar and turbulent flow.

** In underground ventilation L is normally taken to be the hydraulic mean diameter of and airway. (D)

Reynolds showed that fluid flow with a Reynolds number less than 2000 is laminar and values in excess of 2500-3000 is said to be fully turbulent.

4.3.5 Frictional losses in laminar flow.

J.L.M Poiseuille (1799-1869) studied the flow of blood in capillary tubes. From his work he derived and equation (4.11) for the frictional losses in laminar flow.

$$P_L = \frac{8\mu\mu_m}{\rho R^2} L \qquad (4.11)$$

Where μ_m= mean viscosity

The frictional losses (P_L) for laminar flow can now be added to equation 4.9 (Bernoulli's equation):

$$\frac{u_1^2 - u_2^2}{2} + (Z_1 - Z_2)g + \frac{P_1 - P_2}{\rho} = \frac{8\mu\mu_m}{\rho R^2}\frac{J}{kg} \qquad (4.12)$$

4.3.6 Frictional losses in turbulent flow.

Antoine de Chezy (1749-1798) developed an equation (4.13) for channel flow that he used for water distribution in Paris.

$$u = C\sqrt{\frac{A}{per}\frac{h}{L}} m/s \qquad (4.13)$$

Where $C = \sqrt{2g/f}$ $m^{1/2}/s$, f = dimensionless coefficient.

Henri Darcy (1803-1888) adapted Chezy's work to the case of circular pipes and ducts containing fluids. The Area (A) was changed to $\pi d^2/4$ per πd and the fall in elevation (h) became the head loss. Equation 4.13 becomes;

$$u^2 = \frac{2g}{f}\frac{\pi d^2}{4}\frac{1}{\pi d}\frac{h}{L} \tag{4.13}$$

or

$$h = \frac{4fLu^2}{2gd} \text{ metres of fluid.}$$

This is known as the Chezy-Darcy equation. The head loss h can be converted to frictional pressure drop because p=ρgh. The equation becomes;

$$p = \frac{4fL}{d}\frac{\rho u^2}{2} Pa \tag{4.14}$$

Now this equation can be converted to a frictional work term and hence can be put into Bernoulli's equation.

$$P_L = \frac{P}{\rho}\frac{4fL}{d}\frac{u^2}{2} J/kg \tag{4.15}$$

Now Bernoulli's equation for frictional and turbulent flow becomes;

$$\frac{u_1^2 - u_2^2}{2} + (Z_1 - Z_2)g + \frac{P_1 - P_2}{\rho} = \frac{4fL^2}{d}\frac{u^2}{2} J/kg \tag{4.16}$$

4.3.7 Coefficient Of Friction.

There have been many equations developed to calculate the friction factor of pipes. The most widely used method to determine the friction factor is the **Moody Chart.** In underground ventilation problems, changes in density are ignored in most cases. Most airflows that are encountered in underground ventilation are turbulent. The exception being in large openings where the flow is usually laminar. The mining fraternity uses equations proposed by J.J. Atkinson in 1854. Although the equations already presented are more precise and can be used for underground ventilation planning problems. The equations proposed by Atkinson simplify the process thus saving many manhours.

Atkinson utilised the Chezy-Darcy relationship of the form expressed in equation 4.14

$$p = \frac{4fL}{d}\frac{\rho v^2}{2} Pa \qquad (4.17)$$

When Atkinson conducted his work, the friction factor (f) was a true constant for any given airway. Another assumption was that the density (ρ) was constant. Thus Atkinson could assume that;

$$k = \frac{f\rho}{2} kg / m^3 \qquad (4.18)$$

giving;

$$P = \frac{kcL}{A} u^2 \text{ Pa} \qquad (4.19)$$

This is known as Atkinson's equation and may be written in terms of airflow;

$$P = \frac{kcL}{A^3} Q^2 \text{ Pa} \qquad (4.20)$$

Atkinson's resistance of an airway is;

$$R = \frac{kcL}{A^3} Q^3 \text{ Pa} \tag{4.21}$$

Now we can put R into equation 4.20 giving;

$$P = RQ^2 \text{ Pa} \tag{4.22}$$

This equation is known as the square law. The parameter R or Resistance governs the amount of airflow (Q) that will pass when subjected to a certain pressure (P).

4.3.8 Continuum.

Normally there are two ways of approaching problems in fluid mechanics. i) Microscopic approach to individual molecular motion and the ii) Macroscopic approach describes the behavior mathematically by examining the motion of small volumes of fluid which contain a large number of molecules. In other words the effect of many molecules is averaged and this is considered a continuous medium or a continuum.

4.4 INTRODUCTION TO COMPUTATIONAL FLUID DYNAMICS (CFD) THEORY.

4.4.1 Introduction to CFD

Three fundamental principals govern the physical aspects of any fluid flow: Newton's second law; mass flow conservation and energy conservation. These fundamental principles can be expressed in terms of a set of partial differential equations known as the governing equations of fluid flow. Computational Fluid Dynamics (CFD) is a technique for determining a numerical solution for these governing equations.

Experimental fluid dynamics has played an important role in validating and delineating the limits of the various approximations to the governing equations. The wind tunnel, as an example, provides an effective means of simulating real flows. Traditionally this has provided a cost-effective alternative to full scale measurement. However, in the design of equipment that depends critically on the flow behavior of a fluid, full scale measurement as part of the design process is economically impractical. This situation has led to an increasing interest in the development of a CFD based *numerical wind tunnel.*

The steady improvement in the processing speed of computers and the available memory size since the 1950s has led to the emergence of computational fluid dynamics. This branch of fluid dynamics complements experimental and theoretical fluid dynamics by providing an alternative cost-effective means of simulating real flows. As such it offers an alternative means of testing theoretical predictions for a wide range of conditions not readily available on an experimental basis.

In the previous section the mass and momentum equation were introduced in general terms. In this section they will be introduced along with the energy, Navier-Stokes and integrated transport equations in Cartesian (x, y, z) co-ordinates (for full derivation refer to text). If one considers a fluid element with sides δx, δy *and* δz, *a* centre point (x, y, z) the changes in mass, momentum and energy due to fluid flow across its boundaries and action due to sources inside the element result in the fluid flow equations presented below. Fluid properties are functions of space and time expressed as $\rho(x,y,z,t)$,

p(x,y,z,t), T(x,y,z,t) and u(x,y,z,t). In the following equations the dependence on space and time are not explicitly written. i.e. density at a point (x,y,z) at time t is expressed as ρ and the x-derivative of pressure p at (x,y,z) at time t by $\partial p / \partial x$.

4.4.2 Mass Conservation

In words the mass conservation is;

Rate of increase	=	Net rate of flow of mass into fluid element.

after re-arranging yields;

$$\frac{\partial \rho}{\partial t} + \frac{\partial (\rho u)}{\partial x} + \frac{\partial (\rho v)}{\partial y} + \frac{\partial (\rho w)}{\partial w} = 0 \qquad (4.23)$$

or written in vector notation;

$$\frac{\partial \rho}{\partial t} + div(\rho u) = 0 \qquad (4.24)$$

Equation 4.23 is the unsteady, three dimensional continuity equation at a particular point in a compressible fluid. The first term on the left is rate of change of density. The other three terms describe the net mass flow out of the element and is known as the convective term.

4.4.3 Momentum Equation In Three Dimensions.

Newton's second law states that;

Rate of increase of momentum of fluid particle	=	Sum of forces on fluid particle

The following equation is for the x-component of the momentum equation only. The term on the left is rate of increase per unit volume. The first three terms on the right are force per unit volume due to viscous forces and the last term is due to sources (body forces).

$$\rho\frac{Du}{Dt} = \frac{\partial(-p+\tau_{xx})}{\partial x} + \frac{\partial \tau_{yx}}{\partial y} + \frac{\partial \tau_{zx}}{\partial z} + S_m \qquad (4.25)$$

4.4.4 Energy Equation In Three Dimensions.

The energy equation is derived for the first law of thermodynamics and is defined by;

Rate of increase of energy of fluid particle.	=	Net rate of heat added to fluid particle.	+	Net rate of work done on fluid particle.

The energy equation only needs to be solved with other equations when heat transfer is considered. It is not examined in any of these simulations therefore a full description of the equation and its derivation can be found in Versteeg & Malalsekera (1995).

4.4.5 Navier-Stokes Equation for a Newtonian Fluid.

The governing equations also contain unknown viscous stress component τ_{ij}. In many flow problems these stresses can be expressed as functions of the local deformation rate (strain rate). In 3-D flows this local deformation rate consists of linear and volumetric deformation rate. The rate of linear deformation has nine components in 3-d and is denoted by e_{ij}. Three are linear elongating and six are shearing deformation components. Substitution of these stresses into the momentum equation yields the Naviar- Stokes equation in three dimensions and re-arranging yields;

x- component;

$$\rho\frac{Du}{Dt} = -\frac{\partial p}{\partial x} + div(\mu\, grad\, u) + S_{Mx} \qquad (4.26)$$

4.4.6 General Transport Equations.

The transport equations are a common differential form for all the flow equations. If a general variable ϕ is introduced and using previous equations the following equation in conservative form results;

$$\frac{\partial(\rho\,\phi)}{\partial t} + div(\rho\,\phi\,u) = div(\Gamma\ grad\,\phi) + S_\phi \qquad (4.27)$$

In words:

Rate of increase of ϕ of element	+	Net rate of flow of ϕ out of element	=	Rate of increase of ϕ due to diffusion	+	Rate of increase of ϕdue to sources

Integrating 4.27 produces the most useful form for the development of the finite volume method and for a steady state problem yields;

$$\int_A n.(\rho\,\phi\,u)dA = \int_A n.(\Gamma\ grad\,\phi)dA + \int_{CV} S_\phi dV \qquad (4.28)$$

4.4.7 Turbulence Models

Modeling of turbulent flow requires appropriate modeling procedures to describe the effects of turbulent fluctuations of scalar quantities and velocities on the basic conservation equations. (4.23-25). The conservation equation utilised for turbulent flow are obtained from the laminar form of the equations using a time averaging procedure called Reynolds averaging.

Reynolds averaging of the scalar conservation equation over a sufficiently large time period yields:

$$\frac{\partial}{\partial t}(\overline{\rho}\ \overline{\phi})+\frac{\partial}{\partial x_i}(\overline{\rho}\ \overline{u_i}\overline{\phi})=-\frac{\partial}{\partial x_i}(\overline{\rho}\ \overline{u'}\overline{\phi})+\overline{D_\circ}+\overline{S} \qquad (4.29)$$

Where:

ϕConserved scalar quantity($\phi = \overline{\phi}+\phi'$).

Time averaged value $\overline{\phi}=\frac{1}{\Delta t}\int_t^{t+\Delta t}\phi\, dt$ (Reynolds Equation)

Turbulent Fluctuations $\overline{\phi'}=0$,

D = Diffusion, S = Source.

Reynolds averaging of the momentum equation or substitution of the equations in figure 4.4 into the Naviar-Stokes equation and time averaging (neglecting the overbar on mean velocity) yields:

$$\frac{\partial}{\partial t}(\rho\ u_i)+\frac{\partial}{\partial x_j}(\rho\ u_iu_j)=\frac{\partial}{\partial x_j}(\mu\left[\frac{\partial u_i}{\partial x_j}+\frac{\partial u_j}{\partial x_i}\right]-\left(\frac{2}{3}\mu\frac{\partial u_l}{\partial x_l}\right)\ )$$
$$-\frac{\partial u_i}{\partial x_i}+\rho\ g_i+F_i+\frac{\partial}{\partial x_j}(\rho\ \overline{u_i'u_j'}) \qquad (4.30)$$

$u_i = u_{avei} + u_i'$

$p = p_{ave} + p'$

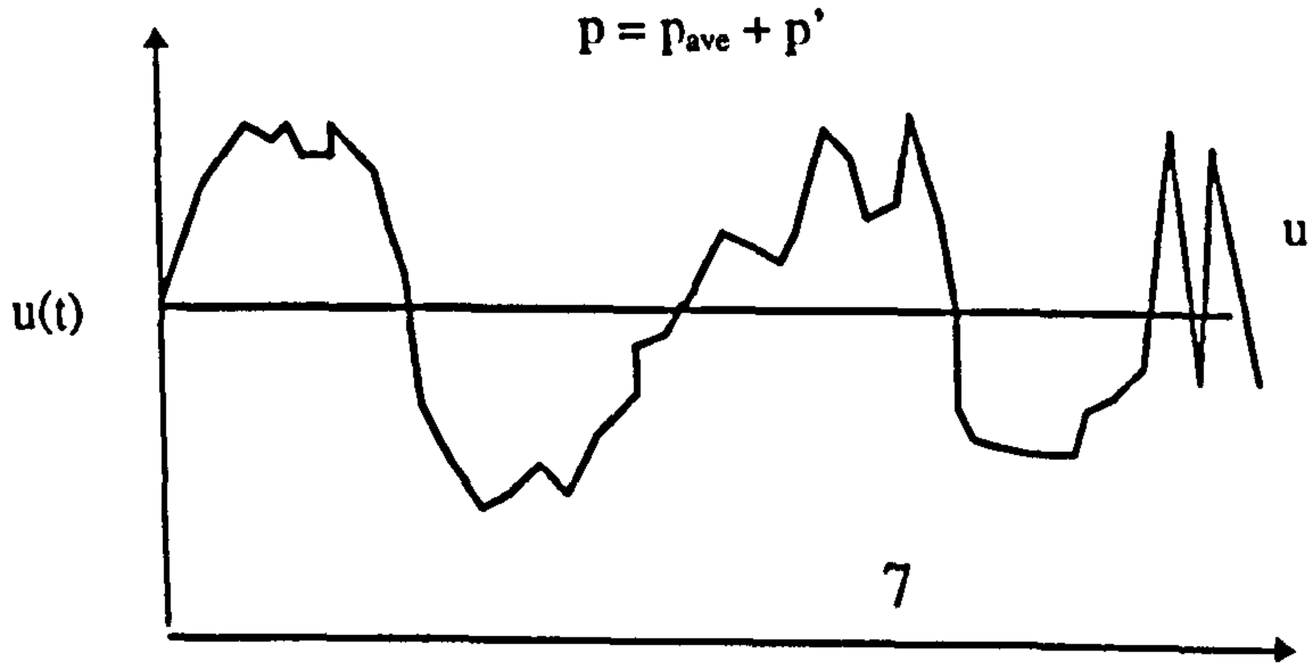

Figure 4-4 Typical turbulent activity.

The Reynolds stresses $\rho \overline{u_i' u_j'}$ are predicted using turbulence models. The models used in Fluent are the standard k-ε, k-ε RNG and the differential Reynolds Stress Model (RSM). Other turbulence models used in other CFD packages is discussed in more detail in the literature (Versteeg & Malalasekera) include; the Zero equation model, Algerbraic stress and large eddy simulations.

4.4.7.1 k-ε Model

4.4.7.1.1 Boussineqs Hypothesis Describing The Reynolds Stresses.

The k-ε model is an eddy-viscosity model in which the Reynolds stresses are assumed to be proportional to the mean velocity gradients. The turbulent viscosity (μ_t) being the constant of proportionality. This assumption is known as Boussinesq hypothesis (second term on the right) and produces this equation for the Reynolds stresses.

$$\rho \overline{u_i'} \overline{u_j'} = \rho \frac{2}{3} k \delta_{ij} - \mu_t \left(\frac{\partial u_i}{\partial x_j} + \frac{\partial u_j}{\partial x_i} \right) + \frac{2}{3} \mu_t \frac{\partial u_l}{\partial x_l} \delta_{ij} \qquad (4.31)$$

where k is the turbulent kinetic energy $k = \frac{1}{2} \sum_i \overline{u_i'}^2$

It is assumed that the turbulent viscosity is proportional to the product of a turbulent velocity scale and a length scale. These are obtained from k, the turbulent kinetic energy and ε the dissipation rate of k. The velocity scale is $\sqrt{k}$ and the length scale is taken to be $\frac{\sqrt{k^3}}{\varepsilon}$. Hence, μ_t for the k-ε model is:

$$\mu_t = \rho C_\mu \frac{k^2}{\varepsilon} \qquad (4.32)$$

Where Cμ is an empirically derived constant of proportionality. (Default in Fluent is 0.09)

The turbulent viscosity - $\mu_t \sim \rho \upsilon \iota$, Turbulent velocity scale is $\upsilon = k^{1/2}$, Turbulent length scale $\iota = k^{3/2}/\varepsilon$.

4.4.7.1.2 Transport Equations For k and ε

The values of k and ε required in equation 4.32 obtained by solution of the conservation equations:

$$\frac{\partial}{\partial t}(pk)+\frac{\partial}{\partial x_i}(\rho u_i k)=\frac{\partial}{\partial x_i}\left(\frac{\mu_t}{\sigma_k}\frac{\partial k}{\partial x_i}\right)+\rho(P-\varepsilon) \qquad (4.33)$$

and

$$\frac{\partial}{\partial t}(p\varepsilon)+\frac{\partial}{\partial x_i}(\rho u_i \varepsilon)=\frac{\partial}{\partial x_i}\left(\frac{\mu_t}{\sigma_\varepsilon}\frac{\partial \varepsilon}{\partial x_i}\right)+\rho\frac{\varepsilon}{k}(C_1 P-C_2\varepsilon) \qquad (4.34)$$

The main assumption made in the k-ε model are that turbulence in homogenous, high reynolds stresses are present, there is a gradient type diffusion and the dissipation is related to k and length scale l_r as $\varepsilon=u^{3/2}$.

4.4.7.2 Reynolds Stress Model (RSM)

The limitations of the k-ε model is that μ_t is isotropic. i.e. velocity and length scales are the same in all directions. The RSM model computes the individual Reynolds stresses in the transport equations and is sometime called a second order closure model. This requires the solution of seven modelled transport equations, six of which are Reynolds stresses and one for ε.

$$\frac{\partial\,\overline{u}_i'\overline{u}_j'}{\partial t}+u_k\frac{\partial\,\overline{u}_i'\overline{u}_j'}{\partial x_k}=\frac{\partial}{\partial x}=\frac{\partial}{\partial x_k}\left(\frac{\nu_t}{\sigma_k}\frac{\partial\,\overline{u}_i'\overline{u}_j'}{\partial x_k}\right)+P_{ij}+\Phi_{ij}-\varepsilon_{ij}+R_{ij}+S_{ij}+D_{ij} \qquad (4.35)$$

Where; P_{ij} is the stress production rate, Φ_{ij} is a source/sink due to pressure/strain correlation, ε_{ij} is the viscous dissipation, R_{ij} is the rotational term, and S_{ij} and D_{ij} are curvature related terms that arise when the equations are written in cylindrical co-ordinates.

This model is computationally intensive but is though to model flows with rotation or high strain rates better than the standard k-ε model.

4.4.7.3 RNG K-ε Model.

The RNG based model uses a similar framework to the k-ε model but contains an additional rapid strain term. It has been derived using mathematical techniques called the Renormalisation Group (RG) theory. The method differs from the standard k - ε method in the following ways: i) the constants and functions are derived from theory and not from empiricism and ii) new terms appear in the dissipation rate transport equation including a rate of strain term. Therefore, it is thought to model flow with separation and curvature with a superior degree of accuracy. The transport equations for k and ε in the RNG model are;

$$\frac{\partial k}{\partial t} + u_i \frac{\partial k}{\partial x_i} = \nu S^2 - \varepsilon + \frac{\partial}{\partial x_i} \alpha \nu_t \frac{\partial k}{\partial x_i} \tag{4.36}$$

$$\frac{\partial \varepsilon}{\partial t} + u_i \frac{\partial \varepsilon}{\partial x_i} = C_{1\varepsilon} \frac{\varepsilon}{k} \nu_t S^2 - C_{2\varepsilon} \frac{\varepsilon}{k} - R + \frac{\partial}{\partial x_i} \alpha \nu_t \frac{\partial \varepsilon}{\partial x_i} \tag{4.37}$$

where;

α is the inverse Prandtl number (1.39) for turbulent transport, R is the rate of strain, $S = 2S_{ij}$, S_{ij} is the modulus of the rate of strain tensor, $C_{1\varepsilon} = 1.42$, $C_{2\varepsilon} = 1.68$. (Fluent user guide pg 19-28)

4.4.7.4 Boundary Conditions Required.

In order to model a given situation boundary conditions must be set. These include inlet, outlet and walls. At the Inlet turbulence parameters must be input for k and ε so the transport equation can be solved. In this series of simulations k and ε are calculated from the characteristic length and turbulence intensity. Where $k= 3/2(u')^2$ and $\varepsilon=C_\mu(0.09)^{3/4}\ k^{3/2}/\iota(o.07L)$ The outlet boundary condition is one which values for all variables are extrapolated from the interior cells adjacent to the flow. The outlet condition corresponds to fully developed flow conditions.

4.4.7.5 Treatment of flow near walls.

Owing to a solid boundary the flow behavior and turbulent structure are considerably different from free turbulent flows. In the flow away from the wall there is usually a substantial region of inertia-dominated flow. Inside this region a thin layer exist in which the viscous effects are important. Closer to the walls the flow is influenced by viscous effects and does not depend on the free stream parameters. The mean velocity only depends on the distance y from the wall, fluid density and viscosity and the wall shear stress τ_w. Solution of the momentum equations in the near wall region require a description of the near-wall pressure gradient and shear stress. CFD packages use empirical wall functions to estimate the effect of the wall on the turbulent flow. This approach eliminates the need to fully resolve all regions of a turbulent boundary layer. This allows less grid points to be set close to the wall thus providing a great saving in the CPU time to solve the equations for turbulent flows. Fluent 4.3 uses the standard wall function and the non-equilibrium wall function. (Fluent 4.3 users manual, 1995)

4.4.8 Discretisation Procedures.

The solution of the finite difference equations introduced requires; i) calculation of the pressure stored at the control volume faces, ii) calculation to determine the face fluxes and iii) interpolation to relate face values of the unknowns (u and ϕ) to the stored values at the control volume centres.

In order to avoid oscillating pressure or velocity fields interpolation is required to determine unknown values at the face. Hence the face fluxes are obtained such that velocities obey an averaged momentum balance and pressures obtained such that the velocities stored at cell centres obey the mass balance. This interpolation is achieved using;

- Power Law Scheme(Patankar, 1980)
- Quadratic upstream interpolation for convective kinetics (Quick).
- Blended second order upwind/central differencing scheme.

4.4.8.1 Power Law Scheme

This is the default scheme used by Fluent, it interpolates the face value ϕ, using the exact solution to a one-dimensional convective diffusion equation. This scheme has proved useful in practical flow problems (Versteeg & Malalsekera, 1995).

4.4.8.2 Higher Order Differencing Schemes.

The QUICK and the blended second order upwind/central differencing schemes compute unknown face values based on stored at two adjacent cell centres and on a third cell centre at an additional upstream point. They provide greater accuracy but tend to be numerically unstable.

4.4.9 Pressure-Velocity Coupling Algorithms.

The continuity and momentum equations provide four equations for solution of four unknown's u_1, u_2, u_3, and p. Simultaneous solution of these equations would seem the obvious choice. However, this is computationally intensive, thus the equations are solved iteratively. In this solution process, an equation describing the update of pressure is required. This is not explicitly available via the mass and momentum balances. The SIMPLE family algorithms use the relationship between velocity and pressure correction to recast the continuity equation in terms of a pressure correction calculation.

4.4.9.1 Staggered Grid

The finite volume method starts with the discretisation of the flow domain and the relevant transport equations. If the velocities and scalars (pressure, temperature) are both defined at the nodes of an ordinary control volume a highly non-uniform pressure field can act like a uniform field in the discretised momentum equation. Therefore, if the velocities are represented at scalar grid nodes the influence of pressure is not represented correctly, thus a staggered grid is utilised. The scalar variables are calculated at ordinary nodes while the velocity is calculated on a staggered grid centred around the cell faces. The staggering of the grid avoids unrealistic behaviour of discretised momentum equations of spatial oscillating pressure fields. A further advantage is that it generates velocities at exactly the location where they are required, therefore interpolation is not necessary.

4.4.9.2 Semi-Implicit Method For Pressure-Linked Equation's (SIMPLE).

Essentially the method is a guess and correct for calculation of pressure on a staggered grid. Figure 4.5 illustrates the steps in the SIMPLE algorithm.

SIMPLEC (SIMPLER-consistent) algorithm (Van Doormal and Raithby, 1984). This follows the same steps as the SIMPLE algorithm. The main difference is SIMPLEC omits insignificant terms in the velocity correction equations. This method cuts down on computational time but in certain flows it become unstable.

4.4.10 Solution of the Discretised Equations.

The methods of discretising the finite difference equations has been introduced. The discreisation process results in a system of linear algebraic equations. There are two families of solution techniques; direct methods and iterative methods. The former involves solution of a vast amount of data and hence is computationally intensive. Therefore, iterative methods are utilised because they are more economical than direct methods. Fluent utilises the line-by-line method that simultaneously solves the equations along the Sweep Direction and marches in the Marching direction in order to visit all grid points (figure 4.6)

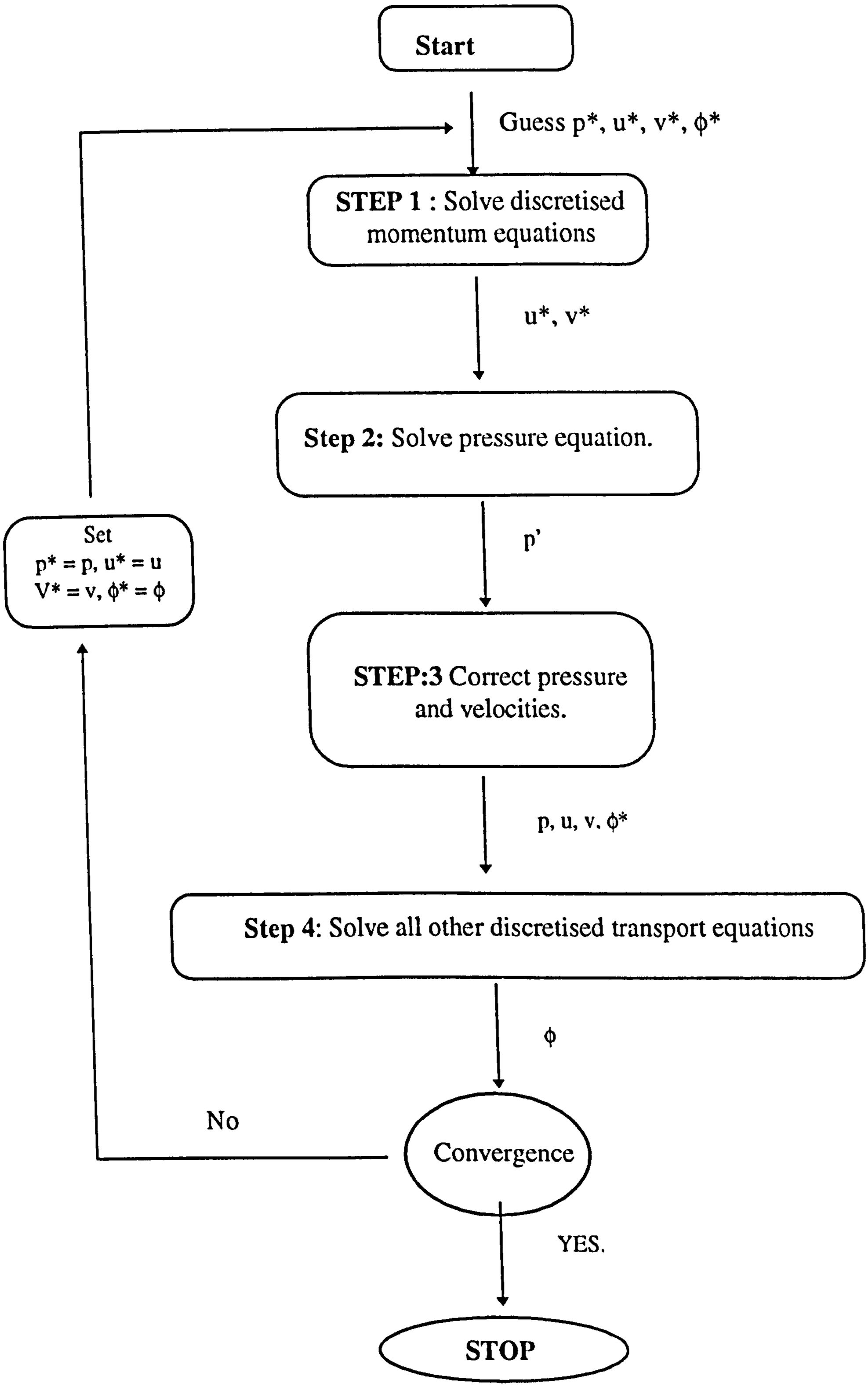

Figure 4-5 The SIMPLE algorithm.

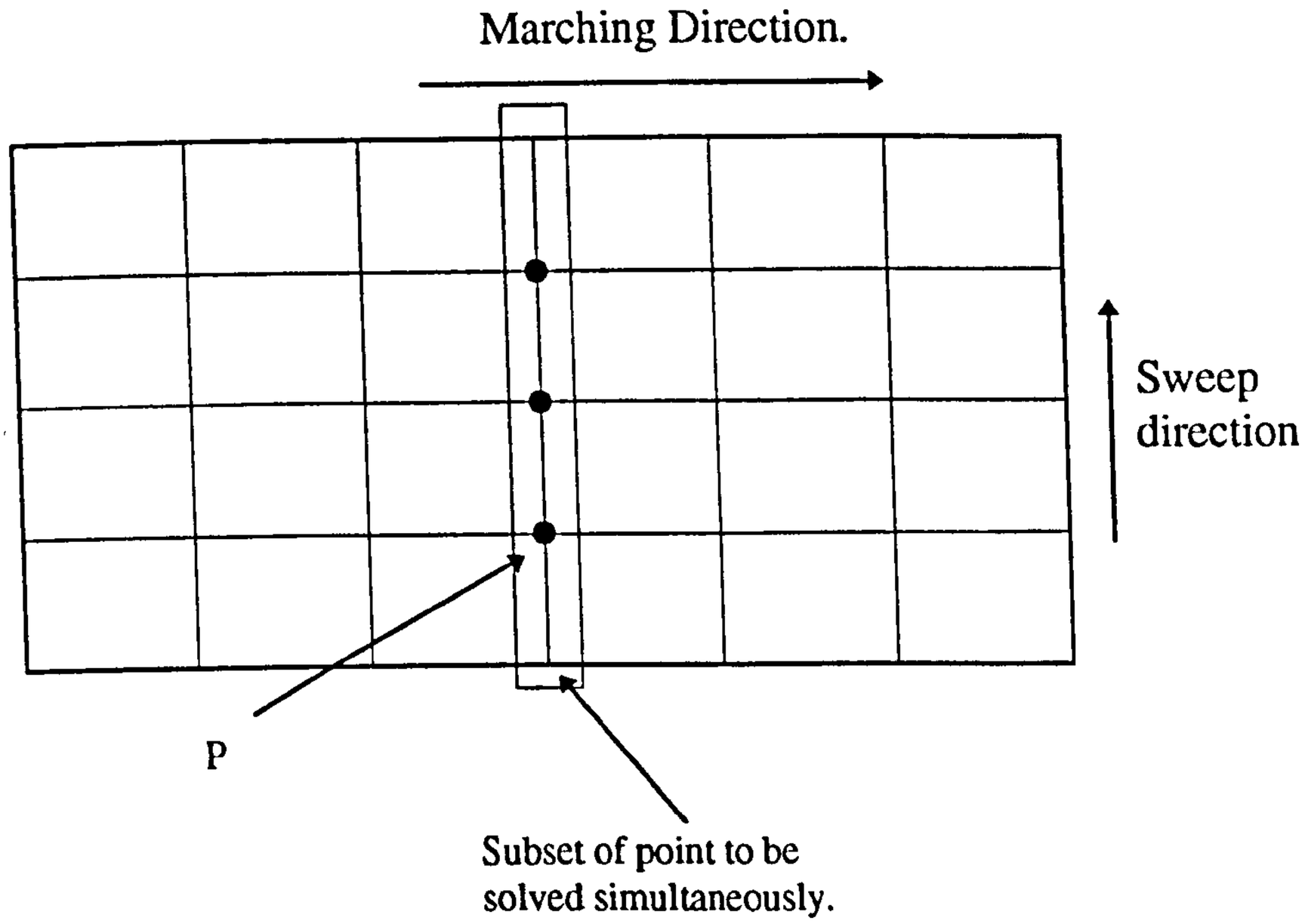

Figure 4-6 Example of solving grid

The algebraic equations along each line to be solved for any variable ϕ at a point P may be written as :

$$A_p \phi_p = \Sigma_{NB} A_{NB} \phi_{NB} + S_\phi$$

Where the subscript NB denotes neighbour values, the coefficients A_p and A_{NB} contain connective and diffusive coefficients, and S_ϕ is the source of ϕ in the control volume surrounding the point P.

4.4.11 Summary of process involved in each iteration

1) The u, v, and w momentum equations are solved using current values for pressure, in order to update the velocity field.

2) The velocities obtained in step one may not satisfy the mass continuity equation locally. Consequently a Poisson-type equation is derived from the continuity equation and the linearised momentum equations. The pressure correction equation is then solved to obtain the necessary corrections to the pressure and velocity fields such that continuity is achieved.

3) The k and ε equations for turbulent flow are then solved using the updated velocity field.

4) Any additional equations such as enthalpy, species are solved using the previous updated values of the other variables.

5) The fluid properties are updated.

6) A check for convergence is made.

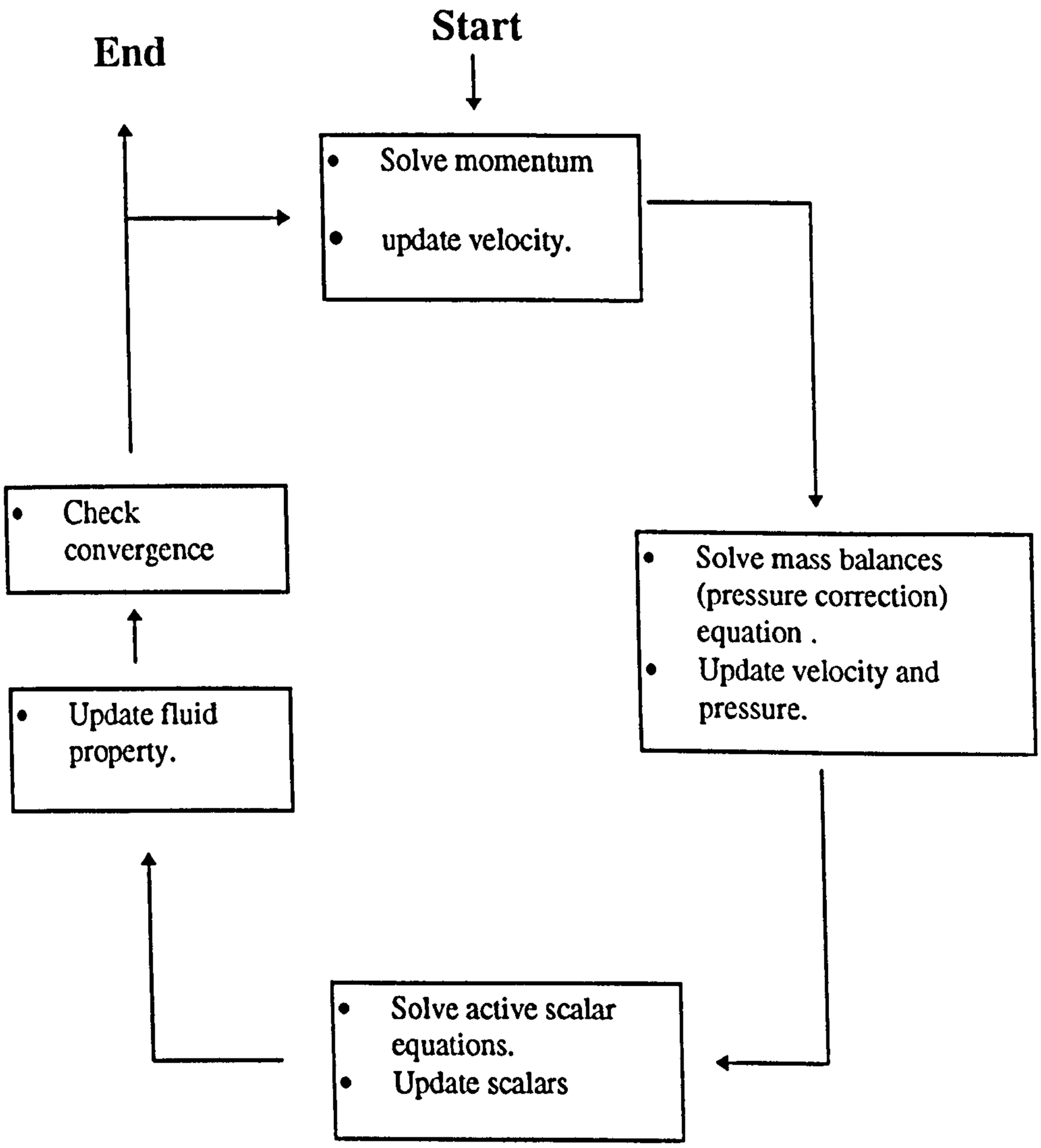

Figure 4-7 Overview of the solution procedure.

4.4.12 Uncertainty in CFD analysis.

It is necessary to consider uncertainties and the possible errors that may occur in a CFD simulation. Mehta (1991) concerned with the uncertainties of using CFD to simulate the performance of a space plane identified the following areas and possible errors in CFD analysis.

i) Computational - includes the non-physical effects of simulation using a computer. These are introduced by the method used to solve the equations of motion. Significant errors may be introduced by the discretisation of the differential equations, which describe the fluid flow.

ii) Fluid dynamics - This may include modelling of individual physical processes that govern fluid flow. Uncertainties are introduced for the following reasons: Insufficient understanding of the flow phenomena, inaccurate values of parameter within the model or inappropriate simplification of models. Lack of experimental confirmation of the validity of the model.

iii) Human factors - mistakes or lack of knowledge about the physics of the flow phenomena.

4.4.13 Reliability of CFD simulations.

CFD can and in some cases produces totally inaccurate predictions. CFD developers tend to see the possibilities that their code offers, while the sceptics cite plenty of examples of CFD models that have produced completely different predictions from experimental measurements. The fact that CFD can churn out pretty pictures has lead to some skeptics referring CFD as an art rather than a science. This can be true if the user lacks experience and knowledge of the code, its pitfalls and the flow phenomena in question. (Ferziger, 1993) In the right hand CFD can be a very powerful tool in the design process.

4.5 SUMMARY.

The general equations used for mine ventilation calculations have been introduced. The governing equations of fluid flow and the attempt by the turbulence models to simulate the turbulent fluctuations were discussed. The algorithms used to interpolate the integrated governing equations (discretised equations) between neighboring cells have also been reviewed. Finally the method used to solve this set algebraic equations has been covered.

The following chapter reviews previous research conducted in the area of auxiliary ventilation.

5. PREVIOUS RESEARCH

5.1 INTRODUCTION

Scale modelling has been used in mine ventilation studies in the UK since 1926 when Cooke modelled airway resistance using a scale model. In 1937 Millar and Bryan modelled the effect of stationary locomotive cars in airways. In 1952 Sales and Hinsley also used models to study the effect of timber supports on the frictional coefficient.

As the process of extracting coal moved away from traditional method to mechanisation, scale modelling of the airflow around faces and headings was the only means of confirming the ventilation regimes suitable for these new mining methods. The use of roadheaders and the advent of continuous miners has lead to concerns regarding the efficiency of conventional auxiliary ventilation systems to adequately ventilating the face area. Consequently, there has been a lot of research conducted into this area. Striving to improve conditions at the face, machine mounted scrubbers were introduced in the USA on high production continuous miners in the early eighties. This lead to research to determine the effectiveness of scrubbers controlling the dust levels in headings. With the demand for cheaper coal and the pressure on the local industry to compete. The industry must access the coal seam more efficiently. This has lead to the investigation of alternate auxiliary systems to reduce downtime.

5.2 PREVIOUS RESEARCH IN AUXILIARY VENTILATED HEADINGS

Shuttleworth (1963) conducted scale model tests in water and underground tests to visualise the behaviour of airflow in auxiliary ventilated headings. The model was constructed to 1:24 scale and represented an arched section roadway of 3.65m high, 4.572m wide and 29m long. It was found that the forward penetration of the jet was 16-17 metres with the remaining of the heading being ventilated by turbulent dispersion. When the duct was placed closer than 9m from the face the re-entrainment behind the duct is more pronounced. The penetration of the jet decreases from 16.45m to 11.8 as the duct is moved from the wall to the centre of the roadway. The main characteristics of the flow remained the same regardless of duct size and quantity delivered, however it

was noted that jet re-entrainment decreased with an increase in duct size. It should be noted that when these test were conducted quantities of $2m^3/s$ being delivered to the face were common.

In 1978 Tagaki, reviewed research conducted into the area of auxiliary ventilated tunnels in Japan. He reported that research using a scale model of a tunnel (Re = 38,000) demonstrated that the jet from the auxiliary duct penetrated 6.67De when placed asymmetrically in the tunnel (with smooth walls) compared with 5.56 De when placed in the centre of the roadway. (Where De = 4 * Area/perimeter).

In Germany, Graumann, (1978) found that; as one moves away from the outlet of the duct the velocity in a free jet decreases while the volume flow in the jet increases. Thus demonstrating that the jet draws air into the jet through entrainment. He also demonstrated that high velocities and insufficient distances did not cause excessive dust from the face but by too great a volume flow over too large a distance.

Wesley, (1984) also conducted extensive research into auxiliary ventilation of arched roadways through use of a 2:1 scale model. He found that the penetration of the jet was $4.5\ (A)^{-1/2}$ with this value increasing to $8\ (A)^{-1/2}$ in mechanised headings with machines channelling flow to the face (Where A is the roadway area).

Gilles (1982) carried out basic scale model tests to demonstrate that dust scrubber system mounted on the machine improve the underground-working environment. The study found that a scrubber system assists airflow at the face, which leads to improved working conditions. He also demonstrated that if the brattice distance from the face exceeded 21 metres that excessive recirculation takes place for gassy mines. He concluded that 12-15 metres supplying $4m^3/s$ provided the best working conditions.

Tests carried out by Volkwein et al (1985) have shown that a suitable machine-mounted scrubber system can adequately ventilate the face at brattice setbacks of up to 15m. No deterioration in ventilation performance was observed as brattice setbacks were increased from 7.5m to 15m. The scrubber system effectively controlled face methane

levels at larger setbacks, although respirable dust levels increased as much as 33% at the operator's cab at setbacks greater that 7.5m.

Jayaraman et al (1989) developed a compact, high pressure scrubber system for a CM. Full scale model and underground trials demonstrated that the dust concentrations around the operator and return were reduced by more than 50%.

Samanta et al (1993) carried out full scale tests to determine potential dispersion patterns and the transport of dust at the continuous miner face, using various ventilation arrangements. Gas was released and pollutant patterns plotted. They found that: (1) When scrubber flow rates decreased, the peak concentration of dust increased. (2) Lower dust capture levels were recorded at higher water spray pressures, (3) Recirculation occurs when the forcing quantity exceeds scrubber exhaust quantity.

Goodman and Taylor (1993) proposed a method to determine the fraction of the air recirculated from the scrubber exhaust toward the face and the fraction of the gas captured by the scrubber. The tests found that: (1) Recirculation values were reduced by placing a 9.14m length of tubing on the scrubber exhaust. However this also resulted in decreased scrubber capture. This is due to greater resistance from the additional tubing being added and hence a lower quantity being drawn through. (2) Increased curtain setback distance led to increased scrubber capture levels. i.e. reduced levels of turbulence.

There has been extensive research in the USA and the UK into the control of dust using water sprays mounted on the CM's, Roadheaders and supply of airflow. (Ruggieri et al, 1985; Jankowski et al 1987; Tanius, 1987; Gong and Jankowski, 1991; Wang et al, 1991; Campbell and Dupree, 1991; ECSC, 1992; Lowndes et al 1994).

5.2.1 *Full Scale Gallery trials conducted at Swadlincote*

The trials were conducted at the Swadlincote test facility and carried out in a fabricated 5.0m x 3.2m x 35m rectangular cross section gallery (Lowndes et al, 1994). In order to visualise the airflow patterns smoke was released from a smoke generator at various positions within the heading. The resulting traces were captured by video.

5.2.1.1 Simple exhaust arrangement

In this test the duct was placed 3.5 metres from the face, exhausting a quantity of 4.5 m^3/s. This ventilation arrangement resulted in the creation of a dead zone in the bottom right hand corner of the face of the gallery and along the gallery floor (Figure 5.1).

This experiment was then repeated with the machine at the face of the gallery with no sprays operational. In this case the dead air zone extended further back into the gallery

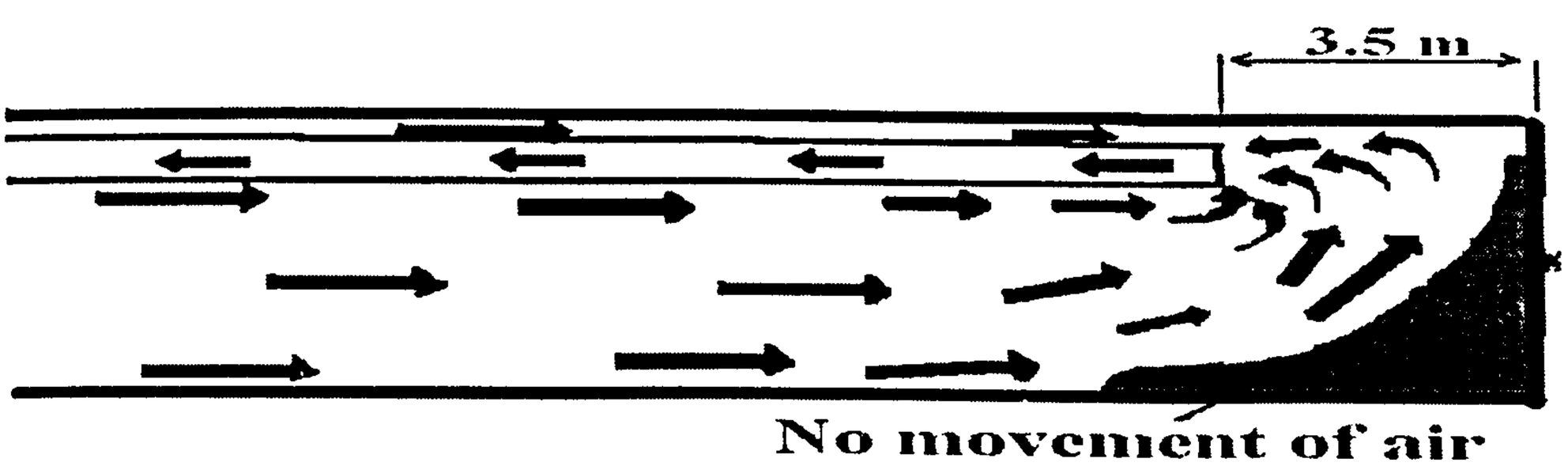

Figure 5-1 - Flow patterns with exhaust duct at 3.5 metres from the face.

However, when this experiment was repeated with all the Ignition Prevention sprays working this dead air zone was eliminated.

5.2.1.2 Simple forcing systems.

The forcing duct delivered 6.0 m^3/s and was located for three successive tests at distances of 5, 15 and 25 metres from the face (Figure 5.2-5.4). For each test smoke was released at the face of the gallery in advance of the forcing fan being switched on.

In all of the three tests secondary entrained flows caused by a venturi effect were observed at or near the duct discharge.

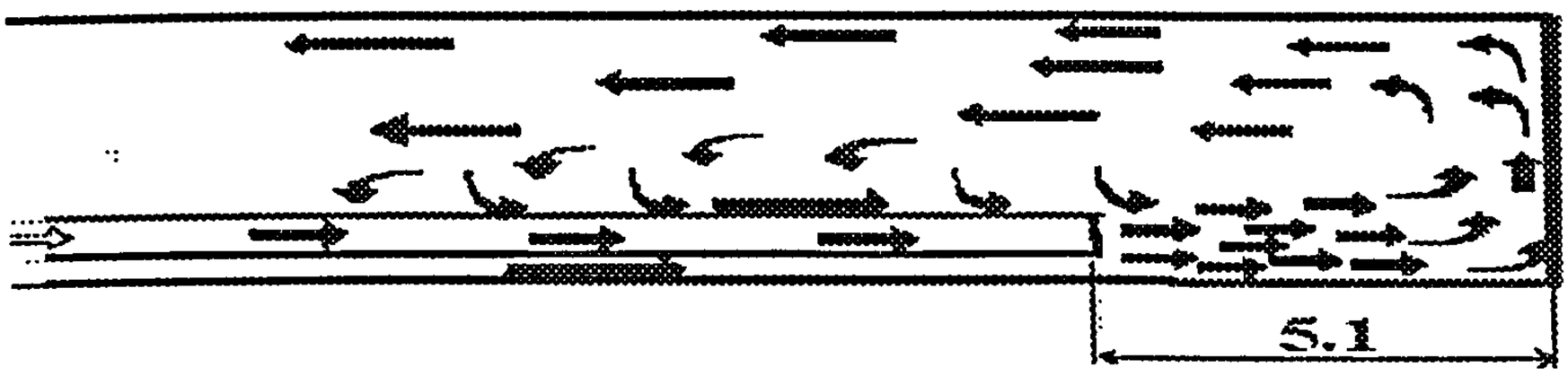

Figure 5-2 - Flow patterns with forcing duct at 5 metres from the face.

5.2.1.3 Simple forcing ventilation system with machine and scrubber.

A further series of experiments were performed in order to determine the minimum workable distance for the forcing duct to be located from the face, without adversely affecting the dust control (with the scrubber operational). At twenty metres the system was effective. When the duct was placed 15m from the face, the smoke swept past the scrubber inlet. This smoke was pushed passed the machine and rejoined the main body of air flowing outbye. When the duct was placed 5 metres from the face, visibility was greatly reduced such that the operator was unable to see the cutting head.

5.2.1.4 Additional trials

In the previous set of trials it was established that when the duct was moved closer than 15m from the face, dust was pushed past the scrubber inlets. To combat this, a diffuser was fitted to the end of the forcing duct. Test showed that the furthest point at which the face was effectively ventilated was 11m. If the diffuser is placed further back, the forcing air loses its momentum before reaching the face. When the diffuser is placed closer than 8m from the face, the scrubber system was unable to collect the air returning from the face due to excessive turbulence. (Figure 5.5)

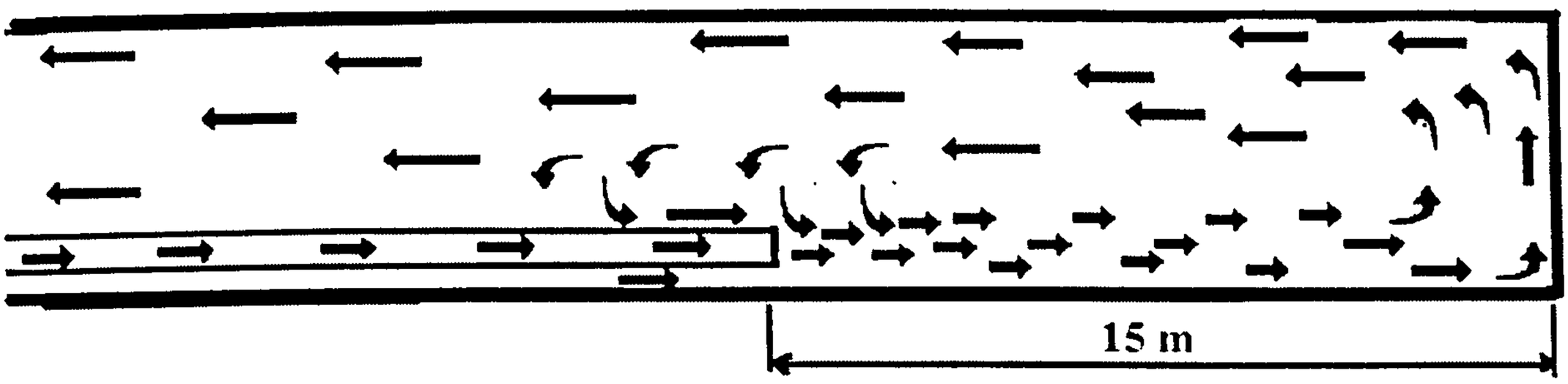

Figure 5-3 - Flow patterns with duct 15 metres from the face.

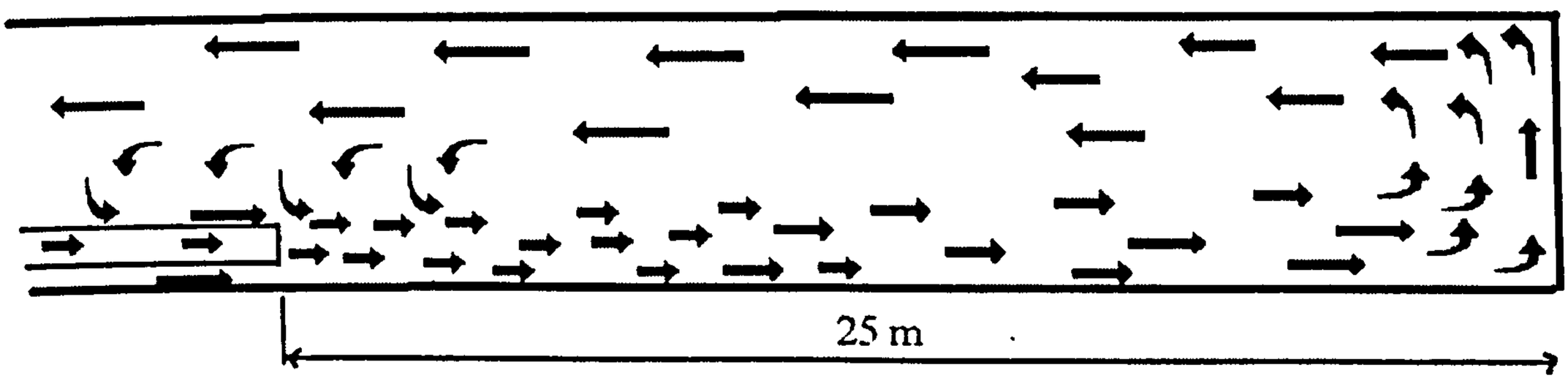

Figure 5-4 -Flow patterns with duct 25 metres from the face.

Figure 5-5 -Flow patterns with diffuser fitted and scrubber operational.

5.3 USE OF CFD IN TUNNELS AND MINING OPERATIONS

There has been extensive research into the area of fire in tunnels and rooms using experiment and CFD. Van de Leur et al modelled fires in corridors using a 2d approach with the standard k-ε model. In 1988 the commercial computer code FLOW 3D was used by the Health and Safety Executive (HSE) to investigate the King's Cross underground station fire. It successfully predicted the gross aerodynamic behaviour and they suggested a possible mechanism for the rapid spread of the fire (Fennell, 1988).

Further work by HSE by Bettis et al (1994) concluded:

> *"The CFD model predicted the main qualitative aspects of the experiment, but was less accurate quantitatively. The CFD results in this case erred in a way that would reduce safety margins."*

Apte et al (1991) investigated the effects of different ventilation rates and on fires in a tunnel representing a mine roadway. Ventilation velocities were between 0.5 - 2 m/s. They found that the simulation results obtained agree qualitatively with experimental measurements. Other researchers into this area include Galea and Markalos (1987), Brandal and Berrgman (1983) Most researchers in the area of tunnel fires have demonstrated that CFD predictions compare well with experimental measurement but Woodburn (1996) points out that there was no sensitivity analysis conducted on various parameters.

It has also been used to study the behaviour of smoke from fires in a UK mining tunnel.(Lea, 1994) This study concluded that CFD simulations of a mine fire although producing a slight overestimation are in broad agreement with network based models. It has also been used extensively in vehicular tunnels to simulate the effects of the critical velocities on fires and analysis of the subsequent backlayering (M^{C}Kinney et al, 1994; Brunner et al, 1995).

Nakayama et al (1993) used a 3d unsteady turbulent flow code using the SIMPLER algorithm and a finite difference code to simulate auxiliary ventilated headings. Figure 5.6 illustrated the results obtained in the wall jet and compared with theory and previous results. They concluded that; "the results of the simple heading face model showed a basic flow structure and similarity to a wall jet".

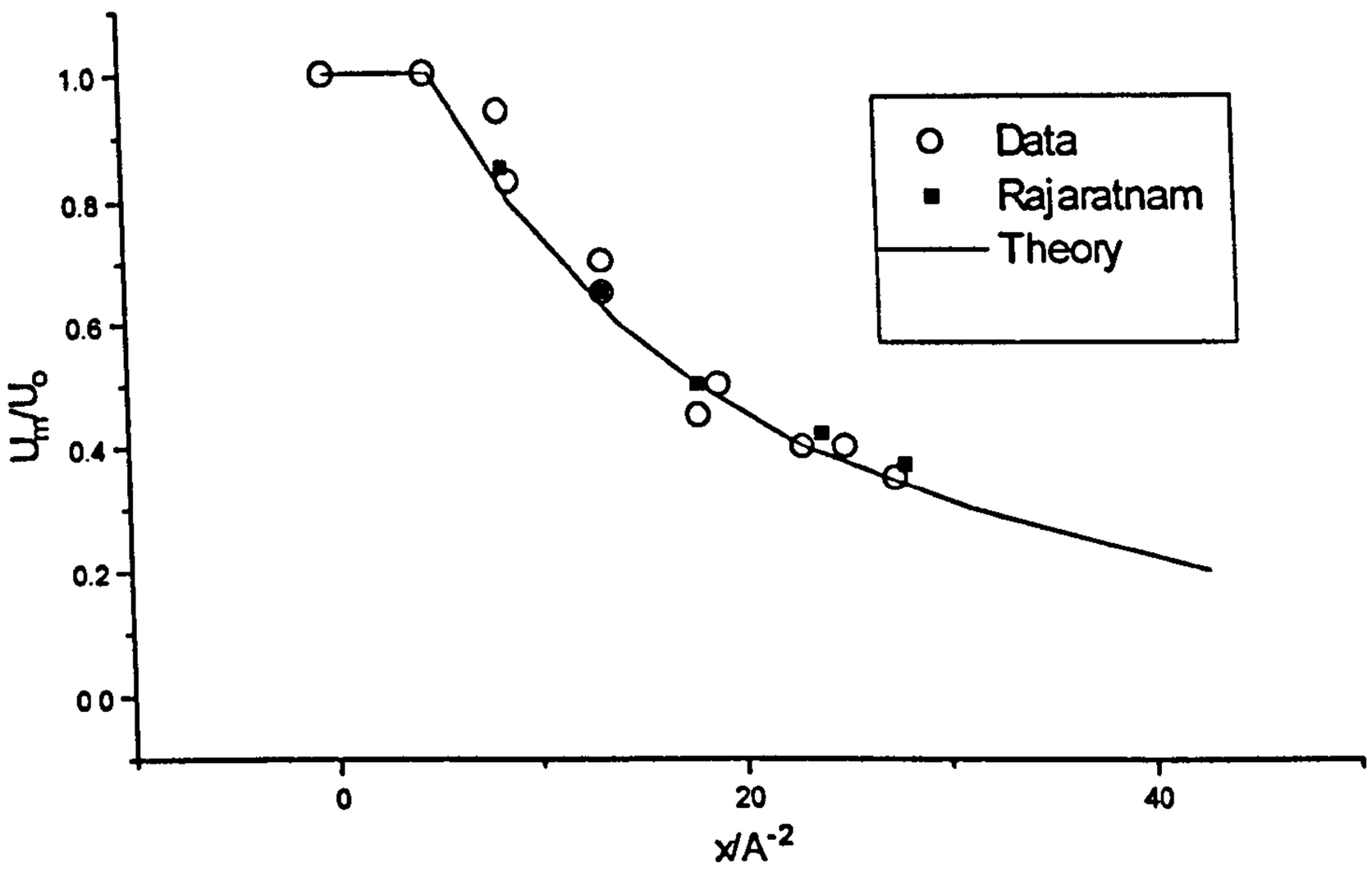

Figure 5-6 -Comparison of previous wall jet data with CFD predictions and theory (After Nakayama et al 1993).

Computational Fluid Dynamics has been employed in Australia and the UK to assess its suitability in the development of effective gas and dust control measures for faces and headings. (Aziz et al, 1993; Moloney et al, 1996)

In South Africa the technique has been used over a four-year period to simulate the operation of continuous miners in development headings which employ on-board scrubber fans. The results showed good correlation between measured and predicted results. (Oberholzer and Meyer 1995; Sullivan et al, 1993) In the UK the behaviour of

diesel exhaust emissions from the tailpipe of underground vehicles have been modelled successfully. (Morton 1993) Ren, 1996 used CFD to model methane dispersion across the goaf and a longwall coal face.

Recently Uchino, & Inoue (1997) used an actual mine sized gallery, and a scale model to validate a CFD code developed in Japan. The heading dimensions were 2.8 * 2.4 metres arched section delivering $1m^3/s$ and a 3-D ultrasonic probe for measuring air velocities. They concluded that CFD showed good overall predictions although the exhaust model predictions were not so accurate. They also demonstrated that the CFD model predicted gas dispersion quite well.

The use of free standing Jet fans in mining have become a recent area of research due to their potential applications. (Mutama and Hall 1995; Konduri et al 1997). This has led to some researchers using 2-D CFD models to predict the penetration of the ventilating jet and to estimate the potential recirculation quantities.

Wala et al (1997) studied the flow across the main airway in an attempt reduce energy costs with particular reference to the transition zone between the upcast shaft and the fan ductwork. The research work concluded that there was a favourable correlation between the experimental work performed and the resulting CFD predictions.

5.4 CONCLUSIONS

Independent research has concluded that a forcing duct being placed at a distance of 15m or greater may adequately ventilate a drivage. Volkwein et al (1985), Shuttleworth (1963) and Lowndes et al (1994) specified a particular optimum distance from the face for the case in question. Tagaki (1978) and Wesely (1984) expressed the penetration depth as a dimensionless value. When typical values for roadway areas are substituted into these equations similar ventilating jet penetration depths are predicted.

CFD researchers have concluded that CFD can model the general flow characteristics fairly accurately. However, many workers have not published data in graph form or conducted a detailed sensitivity analysis to substantiate their conclusions. This is particularly evident in mining research publications to date and thus CFD predictions presented thus far demands further detailed analysis.

6. SCALE MODEL EXPERIMENTS

6.1 INTRODUCTION.

The previous chapter has reviewed the use of scale models in mine ventilation. However, model testing occurs in practically all areas of engineering. Wind tunnel tests are conducted on cars, aircraft and ship. Models are constructed to simulate piston movement in engines. The list of applications is endless.

This chapter introduces the theory behind the construction of a perspex scale model. This was used to study the flow patterns that are produced by auxiliary ventilation systems within rapid development drivages. The experimental techniques and apparatus utilised to obtain the flow characteristics and pointwise velocity measurements are also reviewed.

6.1.1 Similarity.

There are two types of similarity: geometric and dynamic. The following section defines similarity and how it was applied to our scale model.

6.1.1.1 Geometical similarity.

This is achieved when all body dimensions in all three co-ordinates have the same linear-scale ratio. This exists when the model and prototype have the same length scale ratio, time scale ratio and force scale ratio. Similarity is assured if the Reynolds number are the same. If a free surface is evident the Re, Fr and We numbers must be the same. For compressible flows the Ma number must be the same.

6.1.1.2 Dynamic similarity

The definition of dynamic similarity is: "*forces which act on corresponding masses in the model and prototype shall be the same ratio throughout the area of the flow modelled*".

The drawback of small scale experiments is that scaling to give data for full scale scenarios is complicated by the many phenomena present. (Drysdale, 1985) Which are dependent on the dimensionless group where one parameter dominates the flow. Thus in order to achieve dynamic similarity the Re number must be identical. This is very difficult to achieve in air. Cooling and pressurising the air will reduces the length scale but not significantly to achieve similarity. Therefore Reynolds scaling is commonly violated in aerodynamic testing and extrapolation is required. (Figure 6.1)

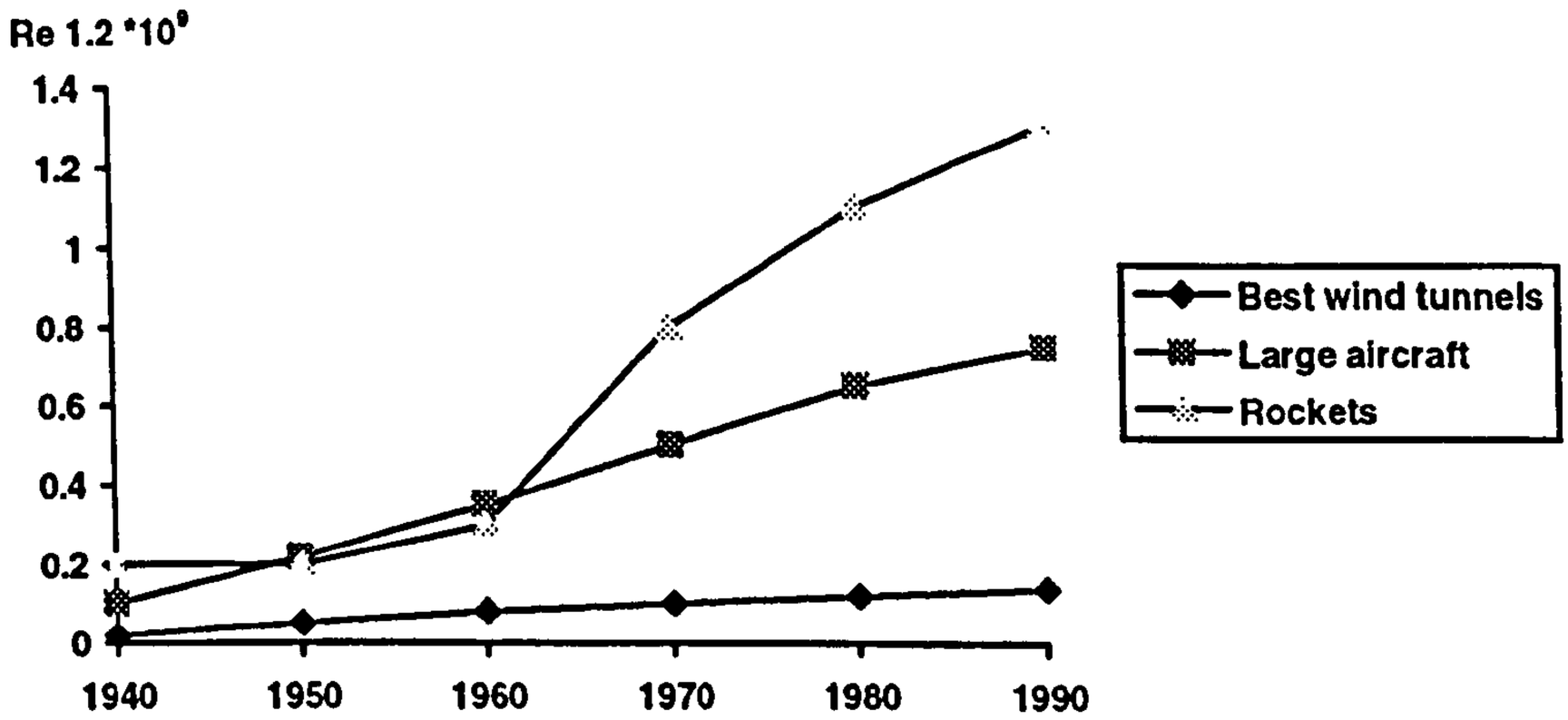

Figure 6-1 - Example of where Dynamic similarity is violated. (after White, 1986)

6.2 MODEL CONSTRUCTION

The 1/10 th scale model was constructed with a wooden base, 6mm perspex at the side walls and top while the perspex at the front is 20mm thick. The model dimensions are 450mm*320mm*3000mm representing a 30m of a 4.5 * 3.2 underground roadway. The ventilation duct is suspended (Figure 6.2) from the roof using clips and bolts.

The model can be adapted to simulate various primary forcing, exhausting and overlap configurations. For the overlap arrangement the inlet to the exhaust duct is set 350mm (3.5m) from the face. The outlet to the force duct may be positioned at varying

distances from the face. An overlap distance equivalent to 7-9 metres must be maintained between the outlets of the force and the exhaust ducts.

Geometric similarity was achieved by scaling a typical UK heading using a 1/10th scale. However, dynamic similarity is difficult to achieve using air. In order to produce the same Reynolds number (**Re** - 420,000) the exit velocity would have to be 62 m/s. The maximum **Re** number achieved for the forcing arrangement was 120,000 and 48,000 for the overlap arrangement. Appendix three summarises the construction of the venturi meter.

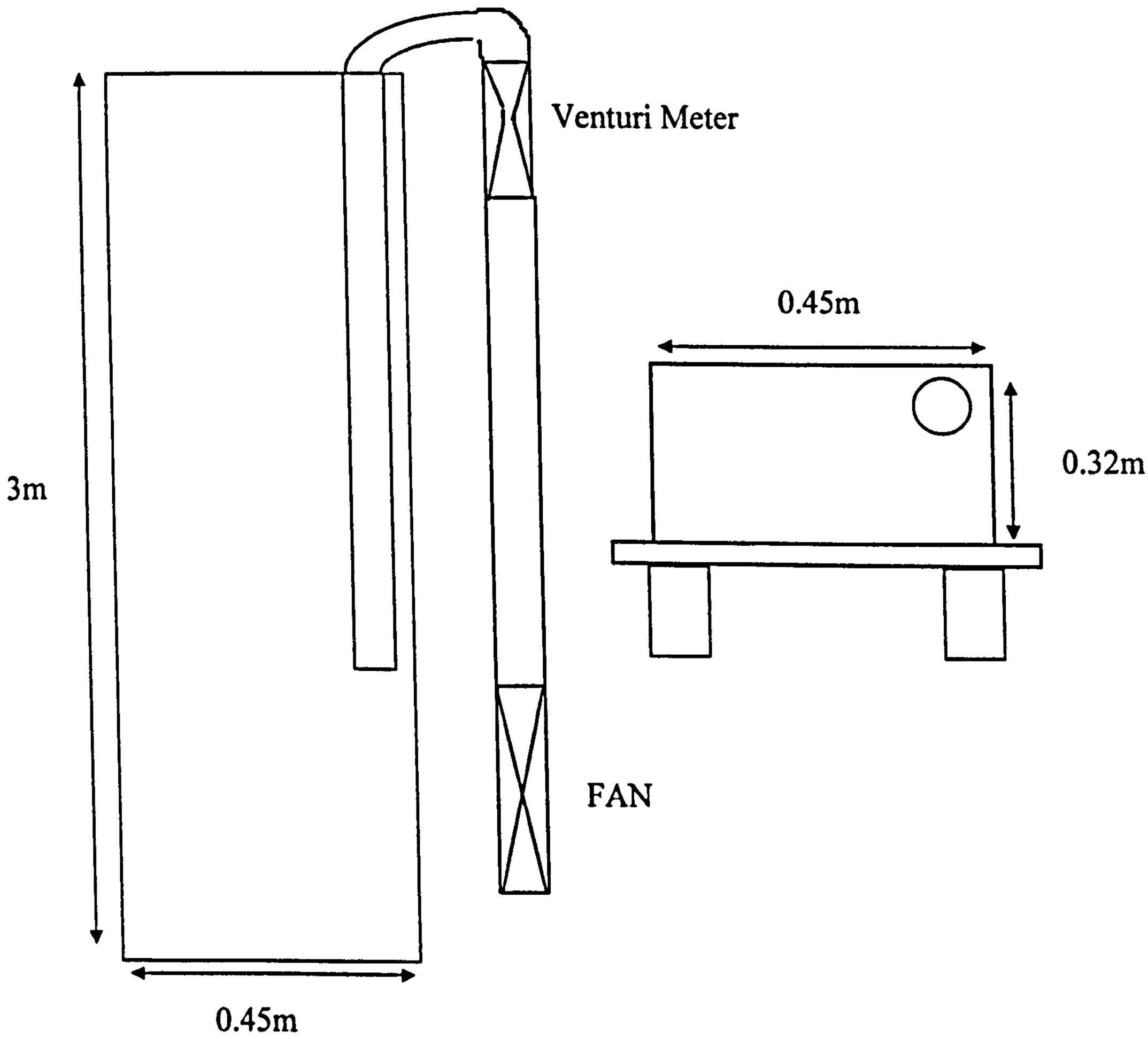

Figure 6-2 - Schematic of model illustrating dimensions.

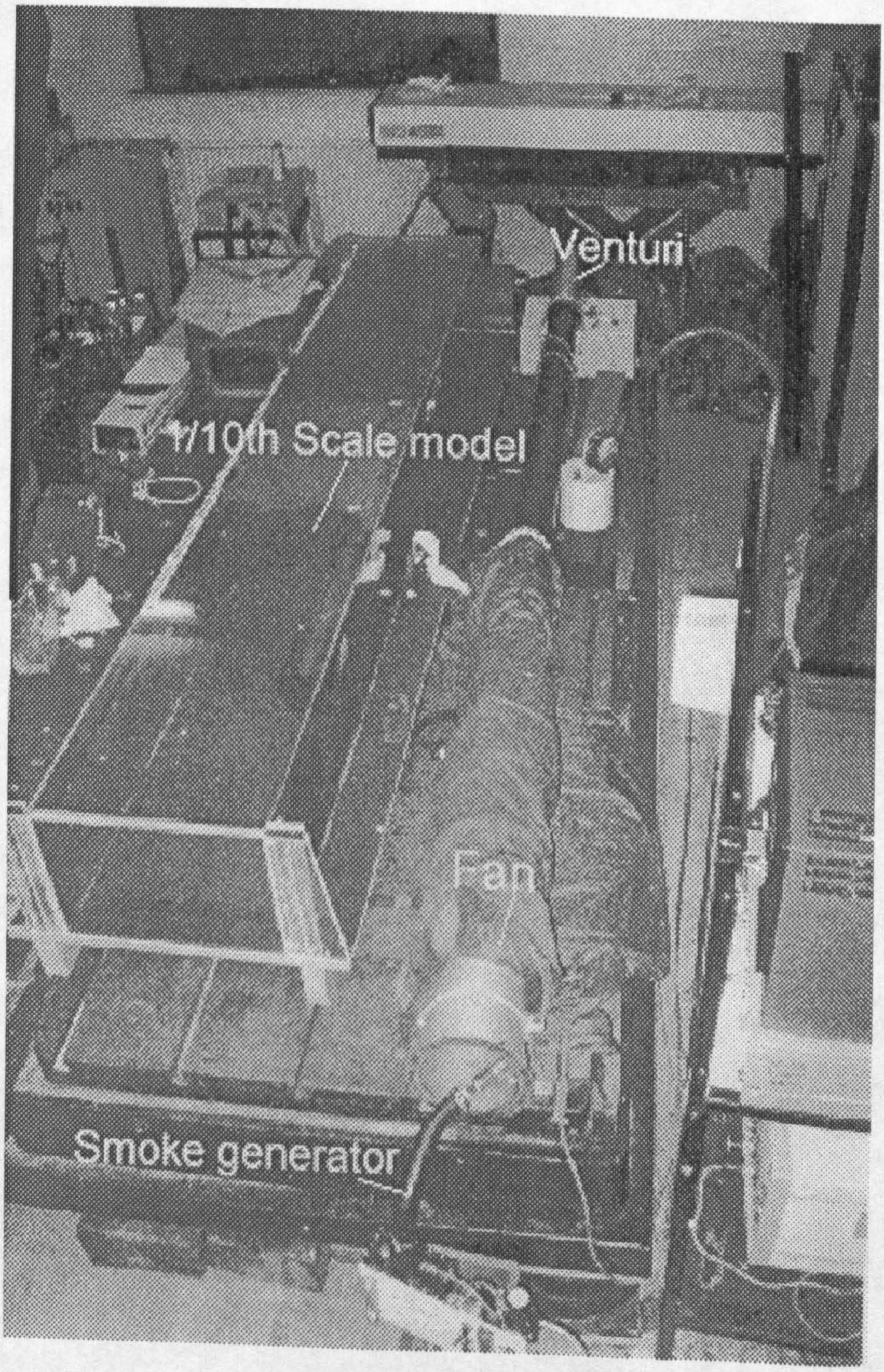

Figure 6-3 -Picture illustrating model, fan and other fittings

6.3 TECHNIQUES UTILISED

6.3.1 Laser Sheet Flow Visualisation and Digital Image Processing.

Flow visualisation is a technique that is widely used to develop an understanding of the structure of a flow field. It is often the first tool, which is used to study a flow field and allows the definition of regions of interest that may be studied using more complex measurement devices. Flow visualisation may be achieved by the simple addition of a tracer to the flow. Smoke produced by the combustion of oil is often employed as a tracer for the study of gaseous flows. The tracer is illuminated by a strong light such as a laser to allow photographic or video recordings to be made of the resultant flow patterns. With complex, three-dimensional flow fields this often produces unsatisfactory flow images as it is often difficult to see through the outer envelope of the flow field to visualise the regions of interest.

The flow visualisation studies used laser sheet illumination in order to isolate two-dimensional planes (figure 6.4) within the complex three-dimensional flow. The arrangement used for this study employed an Oxford lasers 10 Watt Copper Vapour Laser (CVL) as the illumination source (figure 6.5). A combination of a 1500mm focal length spherical lens and a 300mm focal length cylindrical lens was used to generate a laser sheet, which was 500mm wide, and 4mm thick at the test section. To visualise the flowfield the inlet air was seeded using a vaporising oil smoke generator. The seeding was pulsed into the driving air fan at a rate of approximately 2 Hz. At the test section, this pulsing provided a contrast between the unseeded and seeded air prevented complete clouding of the test section.

In order to provide rapid access to flow visualisation images and allow the extraction of quantitative data the images were recorded digitally. A solid state CCD camera with a resolution of up to 1000 * 1000 pixels provides image records to video tape or directly to computer memory. Using such high-resolution digital images it is possible to extract information about the size and shape of objects and to measure the light intensity. By mixing flow fields the intensity of light scattered by the flow tracer can be directly related to the tracer concentration. These flows can then be analysed using a SVHS video. This system has the ability to view seventy-five frames a second.

Figure 6-4 - Illumination of a two-dimensional plane within the flow field

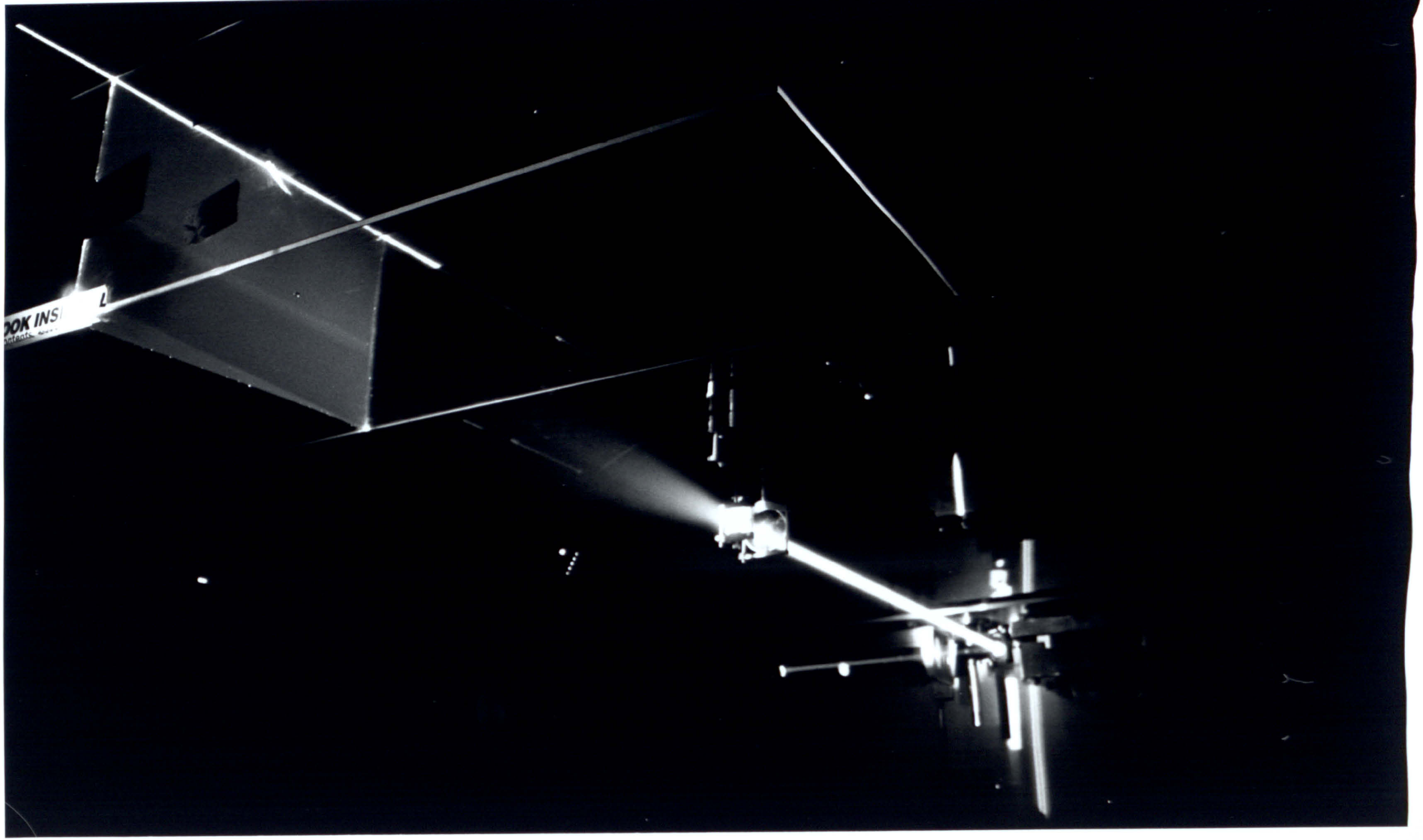

Figure 6-5 - Oxford laser 10 Watt copper vapour laser

6.3.2 Laser Doppler Velocimetry (LDV)

6.3.2.1 Introduction

Experimental fluid mechanics has, for many years, made use of mechanical measuring probes to obtain information on fluid velocity. Total-pressure probes in conjunction with static pressure probes, have provided the principle means of measuring mean velocity. Instruments such as hot-wire anemometer have been utilised for the recording of instantaneous velocity. Mechanical probes have the disadvantage of obstructing the flow at the measuring point. Laser Doppler Velocimetry (LDV) or Laser Doppler Anemometry (LDA) is a technique which allows the non-intrusive measurement of flow velocity. The method was develpoed 25 years ago and relies on the fact that when two beams of laser light are crossed an interference pattern is generated at the intersection region. As micron sized particles, added to the flow as flow tracers, pass through the intersection region they scatter light that is modulated by the interference pattern at a frequency that is dependant on the particle velocity. (Durst et al, 1981)

6.3.2.2 LDV - Theory

The technique is based on the Doppler shift. The best way to describe the doppler shift is to consider an example. As a train, blowing its horn, approaches at constant speed, the sound of the horn will be slightly higher pitch. As the train passes by, the pitch lowers. If the train were not moving, the sound would be of a pitch somewhere between the higher one and the lower. This is known as the frequency shift.

The scattering particles, seeding (smoke) in this case generate a Doppler Current:

$$i_{sp}(t) = I(x_p)CosK.x_p \qquad \text{(Eqn 6.1)}$$

x_p is the position of particle.

I_x is the position dependent intensity, determined by illumination of the measuring volume and the optics.

K = scattering wavenumber vector.

The position of the particle can be related to its initial position a and its velocity history u_{sp} (a,t) by:

$$x = a + \int_0 u_{sp}(at_1)dt_1 \qquad \text{(Eqn 6.2)}$$

The scattering wavenumber vector K can be defined as the vector difference in the wavenumbers of the incident and scattered light. Thus (figure 6.6) k_1 and k_2 are the two beams differing by an angle θ, then

$$K = k_1 - k_2 \qquad \text{(Eqn 6.3)}$$

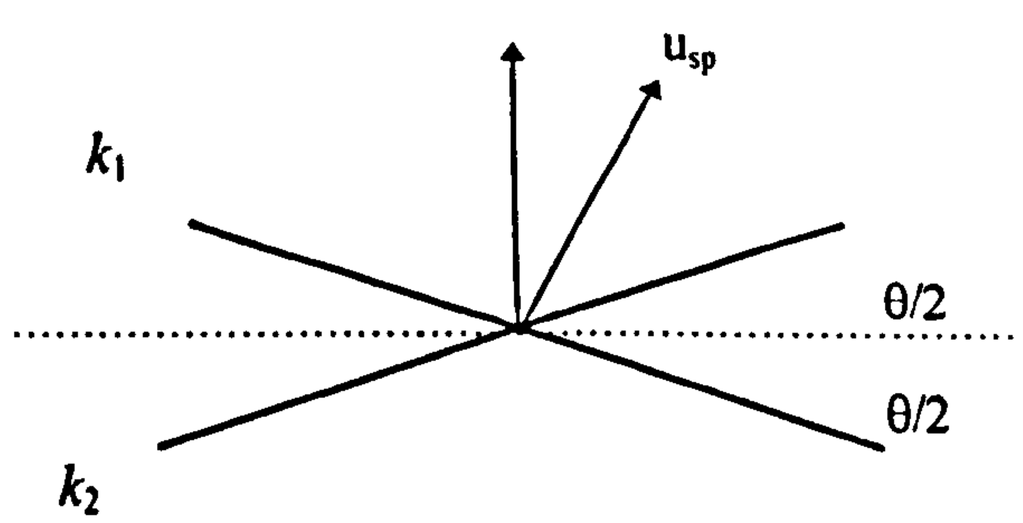

Figure 6-6 - Illustration of scattering geometry.

The product $K.x_p$ selects the component of the velocity colinear with the scattering wavenumber, say u_{sp} , Thus equation 6.1 becomes:

$$i_{sp}(t) = I(x_p)Cos[K_a + K\int_0 u_{sp}(at_1)dt_1 \qquad \text{(Eqn 6.4)}$$

assuming constant velocity across the scattering volume,

The Doppler current due to a single particle consists of; amplitude I that varies with the spatially varying intensity of the measuring volume, a phase Ka determined by the particle's position at some arbitrary origin in time and a Doppler frequency:

$$\omega_d = Ku_{sp} = \frac{2\pi}{\lambda_i} u_{sp} Sin(\theta/2) \qquad \text{(Eqn 6.6)}$$

$$\text{or } f_d = \frac{Sin\theta/2}{\lambda_i} u_{sp} \qquad \text{(Eqn 6.7)}$$

Where λ_i = Wavelength of incident light.

The amplitude I is generally close to Gaussian as illustrated in figure 6.7

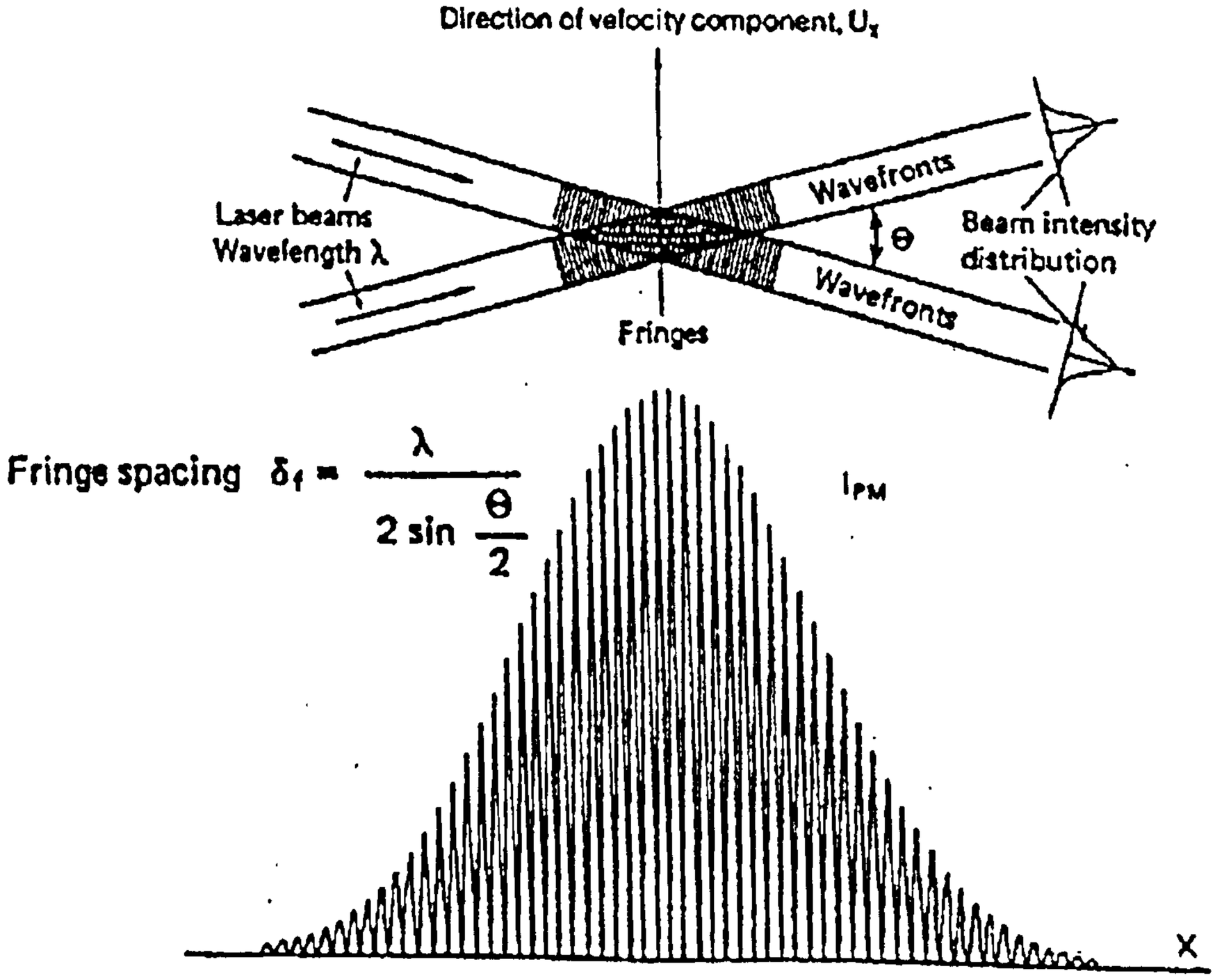

Figure 6-7 - Typical Doppler signal from a single particle.

Therefore if the frequency of the doppler burst can be determined then the particle velocity can also be resolved. There are numerous ways in which this can be achieved. First of all the Doppler burst is amplified and the rising part of the envelope is utilised to start the clock. (Figure 6.8 Illustrates the operation of typical burst processor) After a fixed number of cycles the clock is stopped. Since the number of cycles (or fringes crossed) is known the frequency of the burst can be determined and hence the velocity can be calculated.

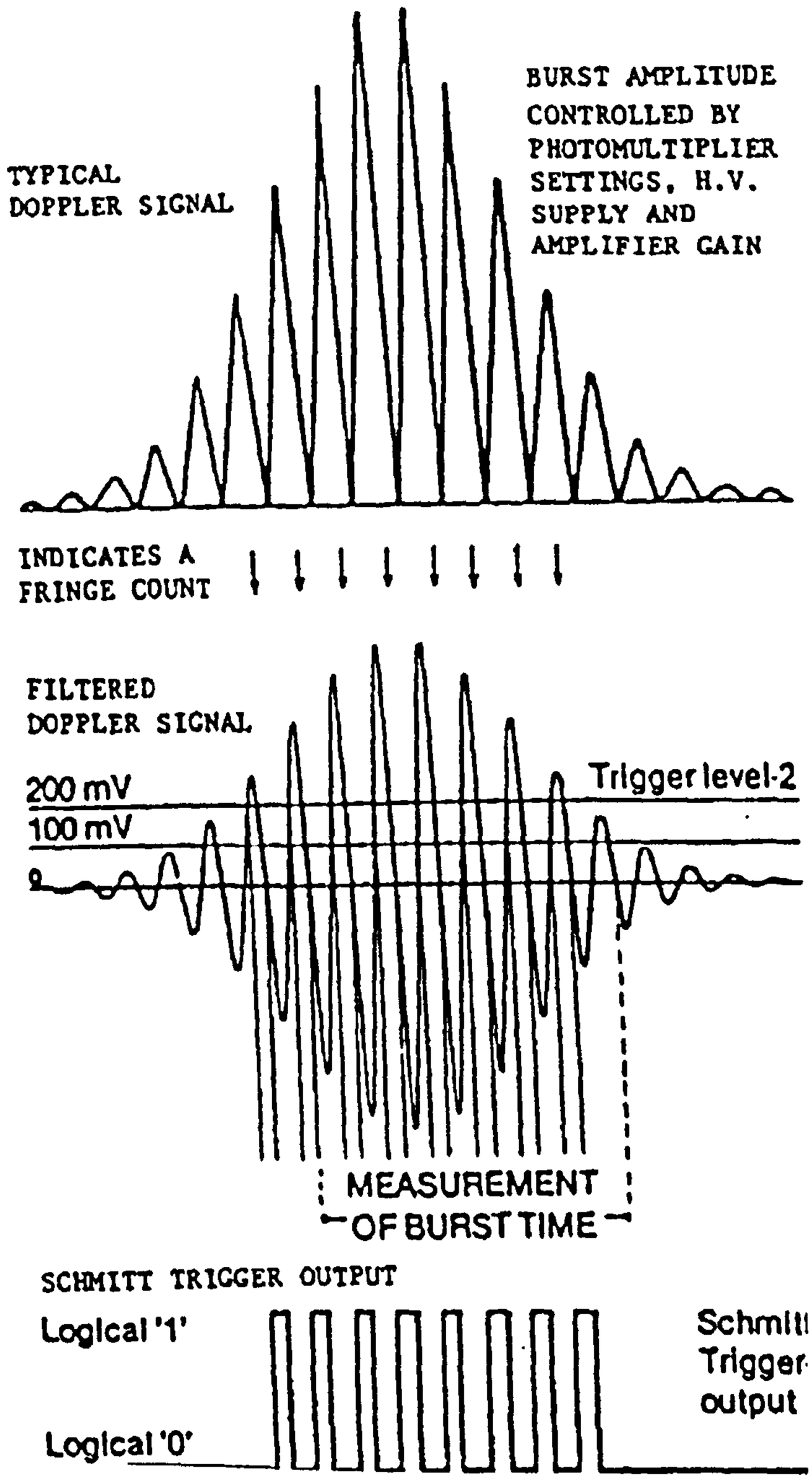

Figure 6-8 - Typical operation of burst processor.

6.3.3 Equipment utilised

The LDV system (figure 6-9) used was a commercially available Dantec two-component system. The arrangement used a Coherent 5W argon ion laser (figure 6-10) launched into a Dantec Colour separator which provided 40MHz frequency shift and coupling to the fibre optic cables. The measurement head was an 85mm diameter unit which was operated with 60mm beam separation and 600mm focal length optics (figure 6-11). This arrangement allowed the LDV measurement head to remain external to the model test section. The system used two colours of light (514.5nm and 488nm) from the laser to form two measurement control volumes by focusing the beams to an intersection at the point of interest in the flow. (figure 6-12) This allows the simultaneous measurement of two components of velocity. The light scattered by the particles in the flow was collected by the focusing lens. It is then transmitted by fibre optic cable to photomultipliers and a signal analyser(figure 6-13). This is to determine the modulation frequency and thereby the particle velocity.

The Doppler signal analysis was provided by two enhanced BSA processors. For the LDV measurement seeding was provided by a TSI six jet atomiser injecting micron sized olive oil droplets directly into the inlet of main air fan. At each measurement location approximately 30,000 data samples were collected over an averaging period of 60 seconds. This arrangement allows the recording of two components of velocity at a point in the flow at a rate of up to 100k samples per second.

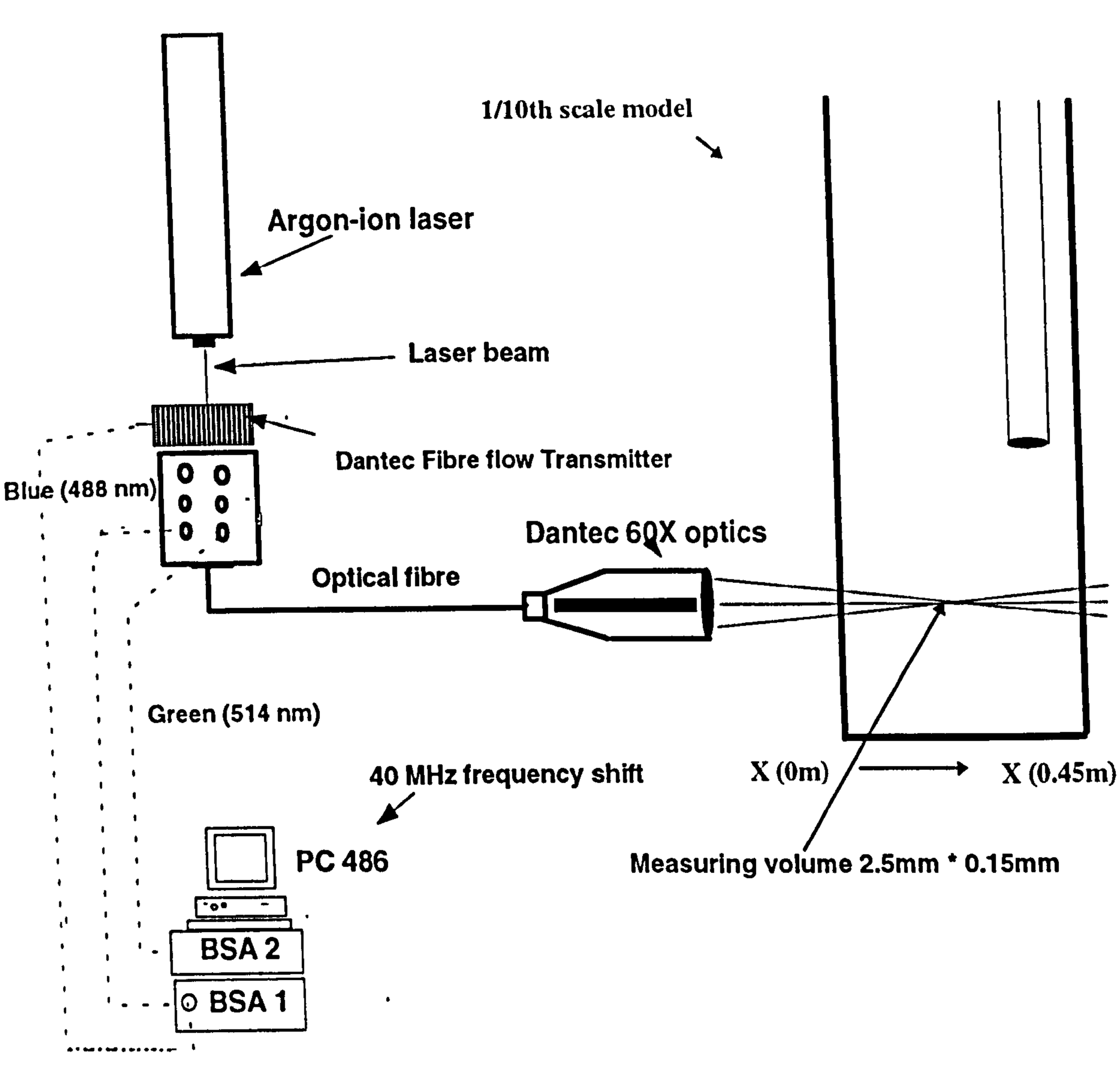

Figure 6-9 - Two-component LDA, showing back-scatter optical system and signal processing equipment.

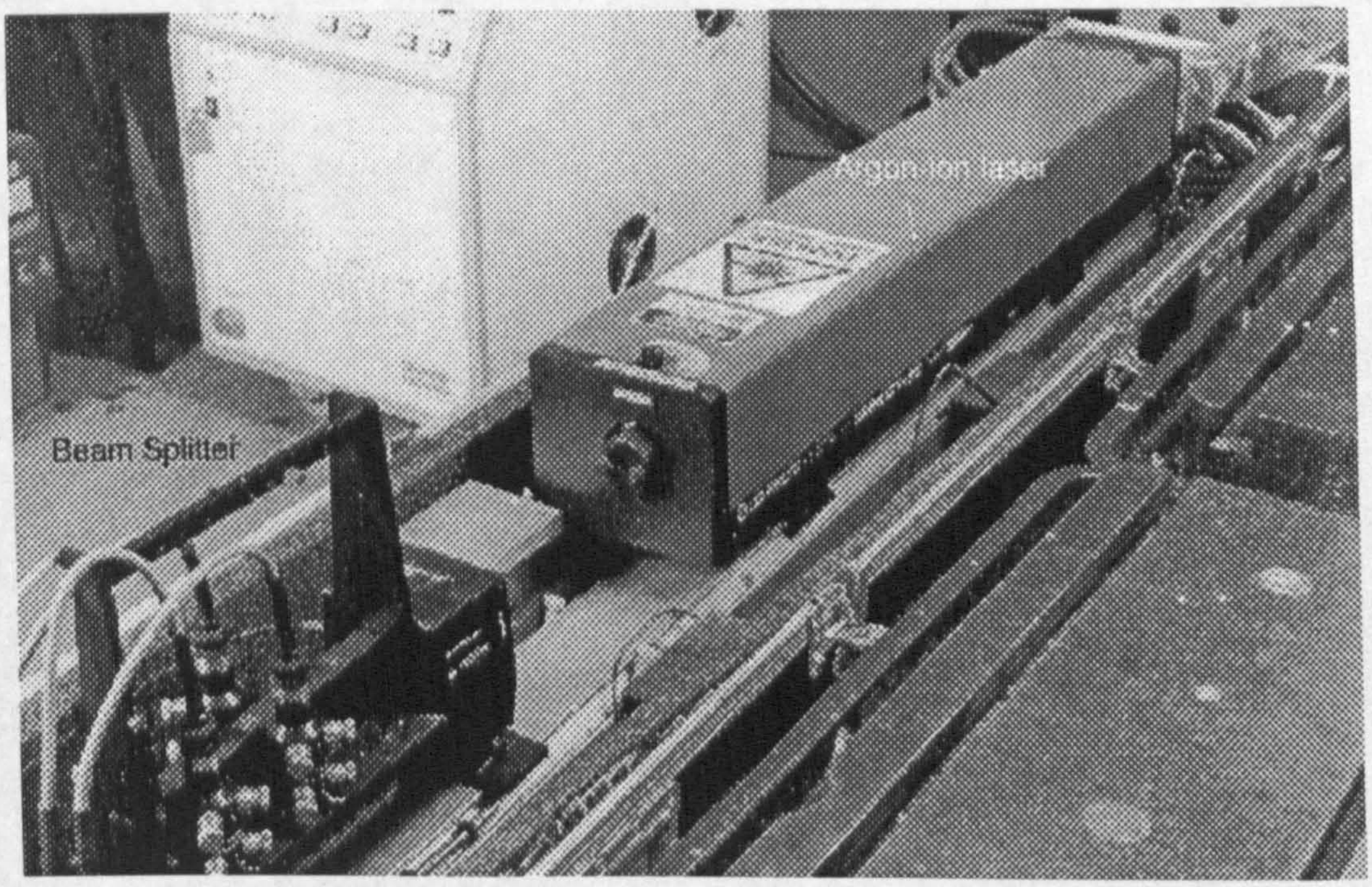

Figure 6-10 - Argon ion laser

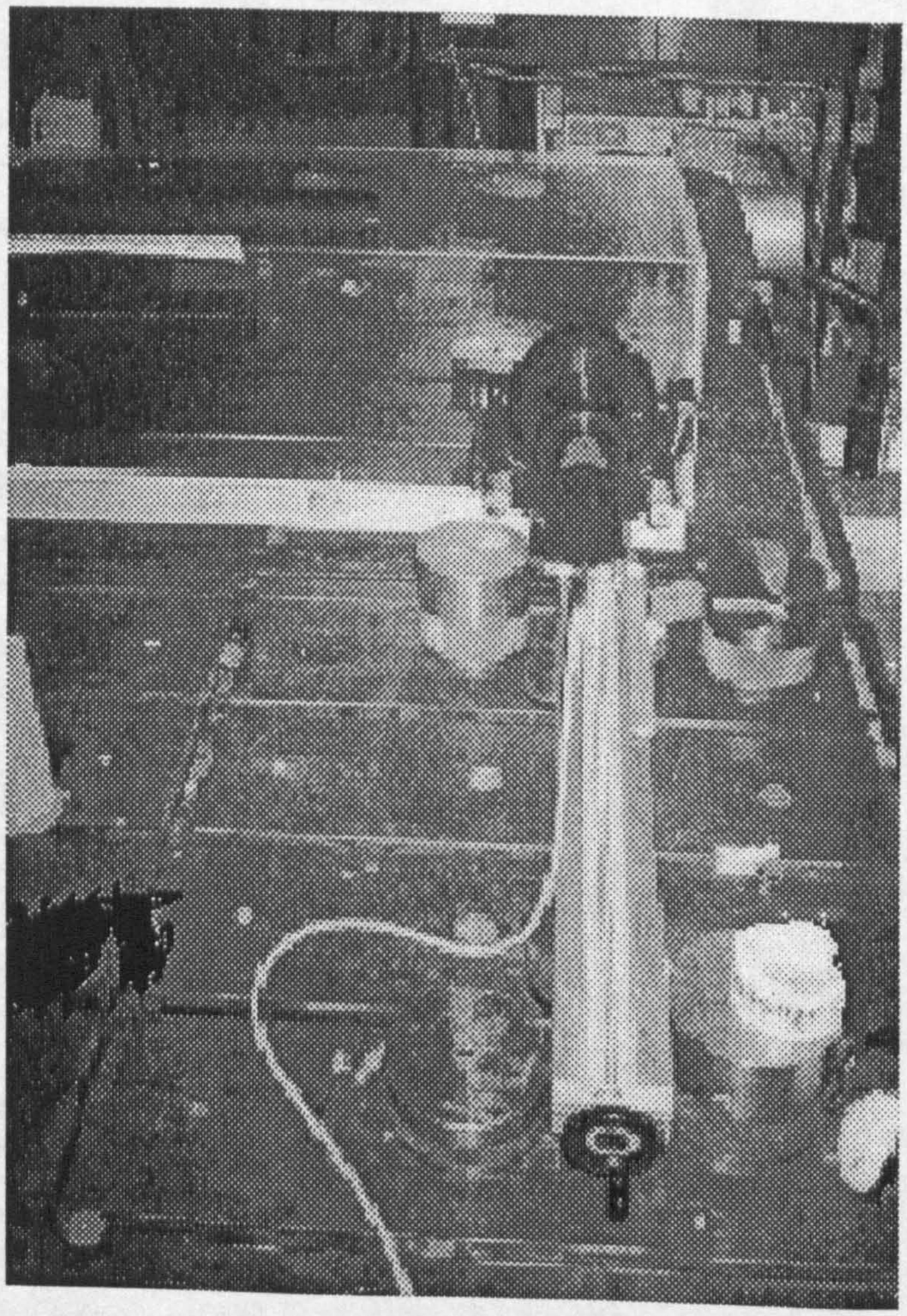

Figure 6-11 - LDV measurement head

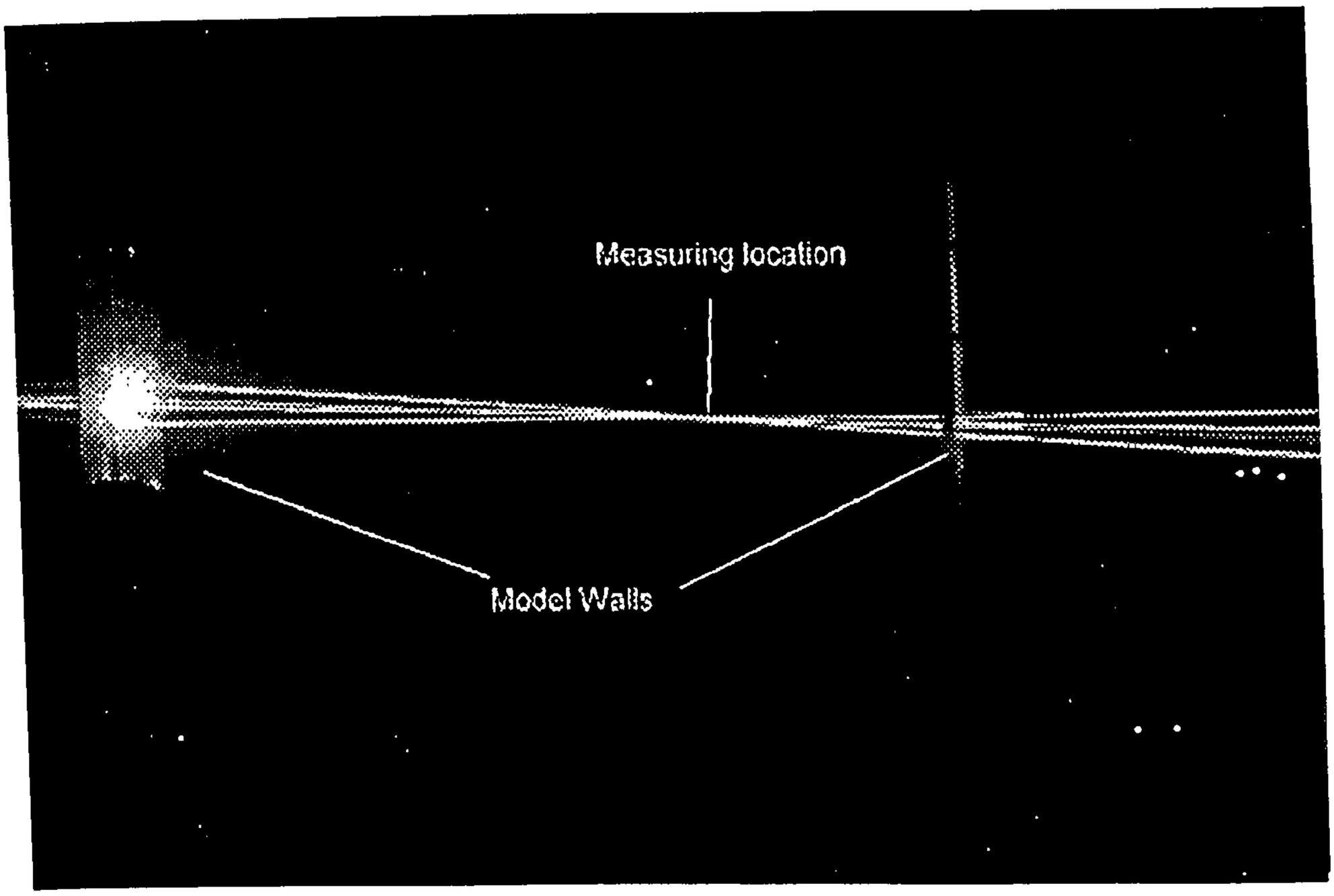

Figure 6-12 - Laser beams intersecting at a measuring point in the flow field

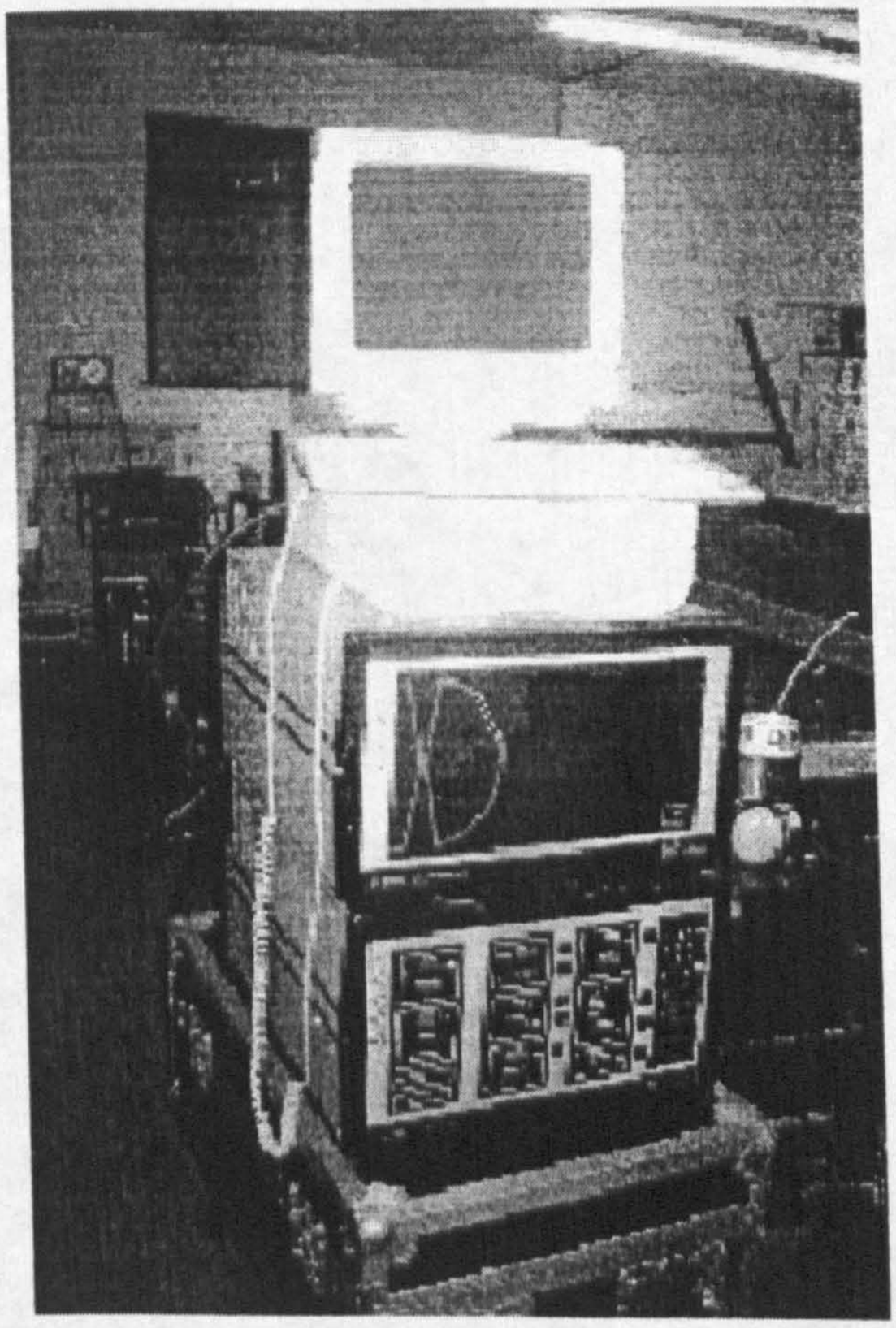

Figure 6-13 - Burst Spectrum Analyser.

6.4 SUMMARY

Similarity and its importance have been discussed. The construction of the scale model and the techniques employed to obtain qualitative (flow visualisation) and quantitative (LDA) have also been introduced in this chapter.

The following chapter discusses the physics of the flow problem, the importance of grid quality and some preliminary CFD simulations are presented.

7. AN INTRODUCTION TO PRACTICAL CFD UTILISATION

7.1 INTRODUCTION.

The use of CFD modelling by the engineering community has increased dramatically in recent times. This rise in interest and use has resulted in the improvement of the predictive capabilities of codes, reductions in the cost of computer hardware, and the inflation in the costs to perform experiments and maintain facilities. There are many commercial CFD codes currently available to the user including, Fluent, Flow 3D (CFX), Pheonics and Star CD. Freitas, 1995 summarised a comparison of various codes and their ability to model selected benchmarks. The author concluded that all the codes produced acceptable results when modelling laminar flow. However, all the vendors failed to conduct a grid sensitivity analysis and they showed little insight into the solution process. The turbulent benchmark employed taxed the numerices and turbulence models of the codes. They also had difficulty in accurately modelling flow regimes travelling at angles of 45-degrees and greater in the 180-degree pipe.

Fluent v4.3 and v4.4 was utilised to perform the simulations during the project. The code is split into three distinct packages: i) pre-processor to set up the geometry, grid density and spacing, ii) main CFD numerical processor which solves the governing equations, and iii) a post processor that presents the predictions in a numerical and graphical environment.

This chapter introduces the physics of the flow problem studied. The application of CFD is illustrated by presenting model predictions and comparing them with full-scale gallery trials. A discussion on the topic of sensitivity of the grid size on CFD models is also introduced.

7.2 GEOMESH

This is the pre-processor for Fluent CFD solvers. It is essential for creating triangular grids as used in Fluent UNS and is divided into three distinctive packages:

i) DDN: This is essentially a Computer Aided Design (CAD) package and is utilised to construct complex geometries for a given situation.

ii) P-Cube: This package creates control volumes that form a grid. In order to create a grid the geometry is split into blocks. The node density, boundary conditions are then specified before the mesh is created. The following example describes how the blocks are split so that when analysed in fluent they are all linked together in the subsequent calculation process.

- A block is created around the tunnel drivage that defines the outer boundary of the flow regime. (Figure 7.1) The block is then split at the end of the duct, and around the auxiliary ducting. The edges can then be mapped to the cylinder using the appropriate tracking tool.

- In order to optimise the grid density, P-cube allows the spacing of the elemental nodes to be non-uniform. Hence critical areas of flow can be modelled more effectively using less computational time on areas of known flow behaviour. The inlet, outlet, walls are specified and the grid created.

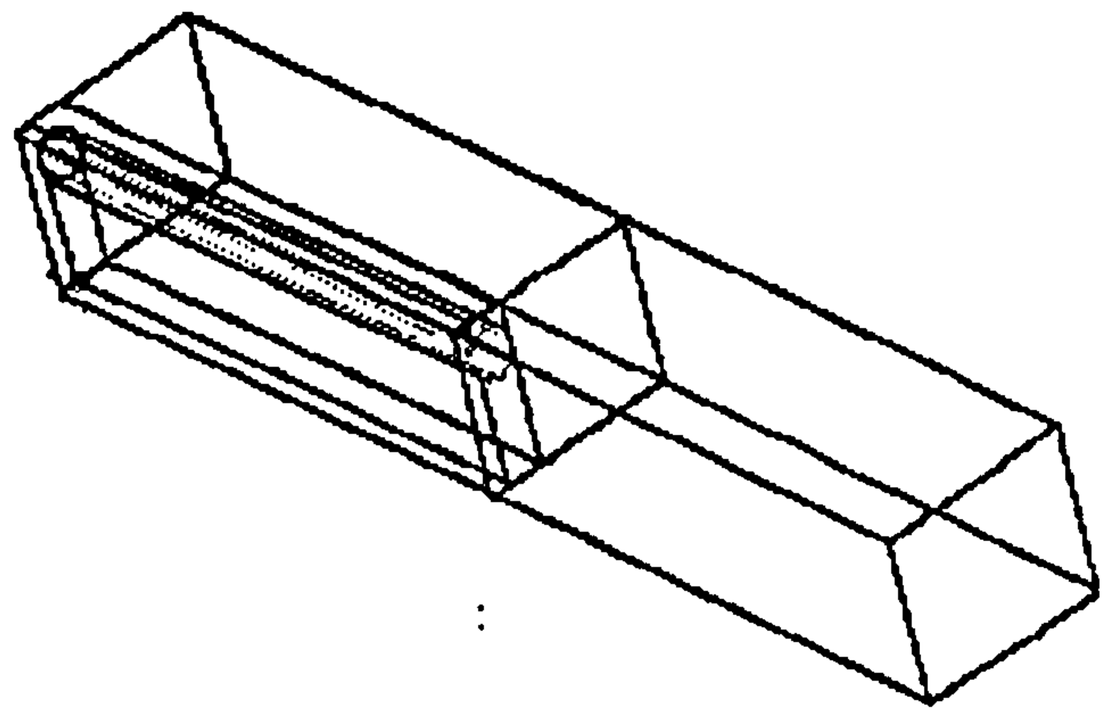

Figure 7-1 - Example of Grid generation in P-cube.

iii) Leo - This package allows the user to visualise the grid and thus analyse its quality using diagnostic tools. These include skewness, aspect ratio, and adjacent cell size ratio. If the grid is highly skewed or the aspect ratio is large the solution will not converge and will probably diverge. Therefore it is important that the quality of the grid is optimised before processing commences (For a definition of terms refer to Appendix 4).

7.3 FLUENT ™ .

Fluent is a general CFD package that solves the governing equations of fluid dynamics by a finite-volume formulation. This method integrates these equations over all of the control volumes in the solution domain. The resulting integral equations are then converted into a system of algebraic equations using discretisation. This involves using a variety of finite-difference-type approximations for the terms in the integrated equations representing the flow process. The final solution is achieved by an iterative method. A grid file may be imported into Fluent from Geomesh together with the appropriate boundary conditions such as inlet velocity and wall roughness (Calculation procedure detailed in Appendix 5). Fluent version 4.4 allows a roughness height to be specified. The fluid properties such as density, viscosity and pressure are also specified. Once a solution has converged (i.e. the algebraic sum of the residual errors is less than a prescribed value) the data file may be analysed. The results may be graphically presented through a number of forms that includes the use of velocity/pressure vector or contours. These displays may be specified in any plane and the scaling of the velocity vectors can be exaggerated for effect.

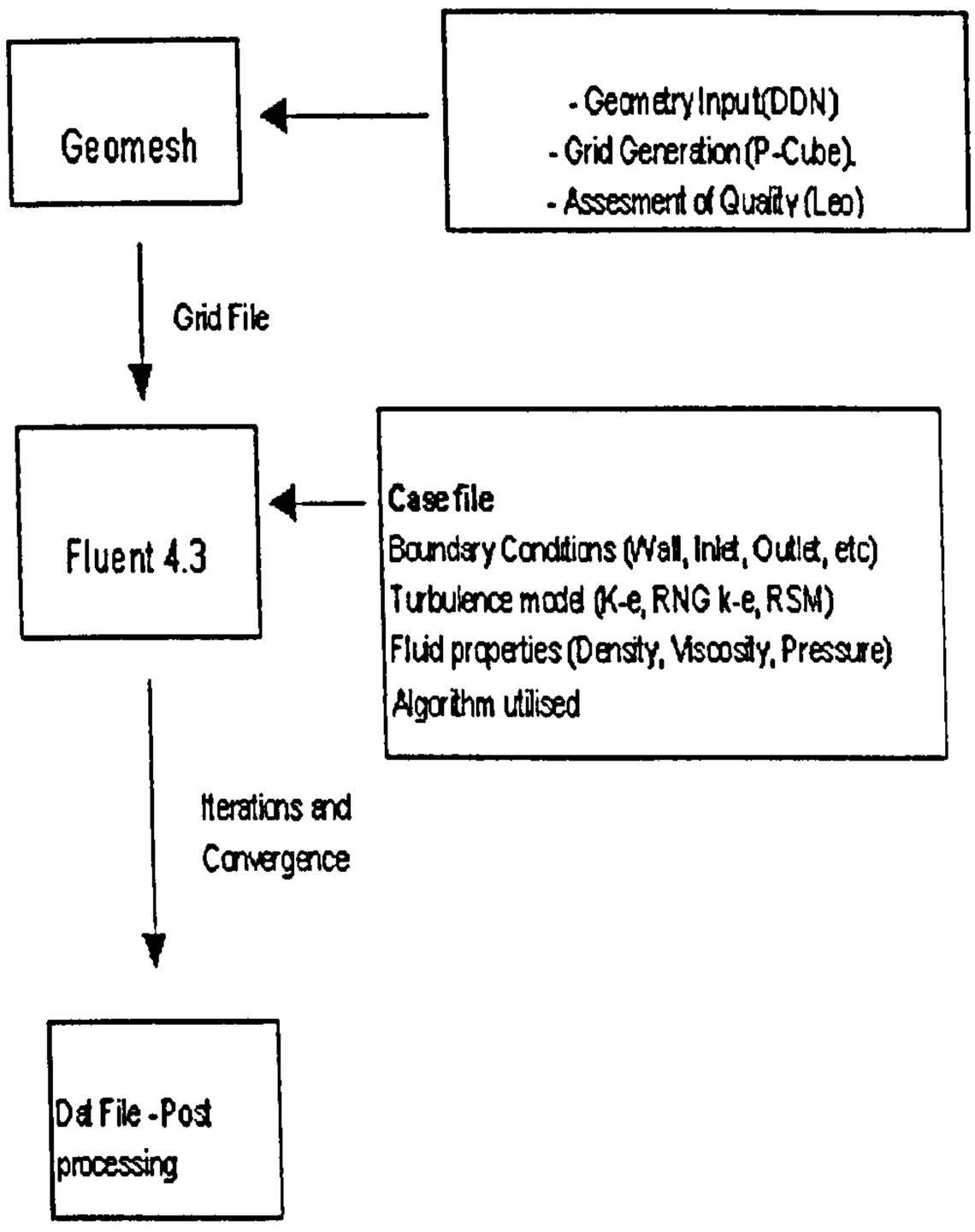

Figure 7-2- Summary of program structure.

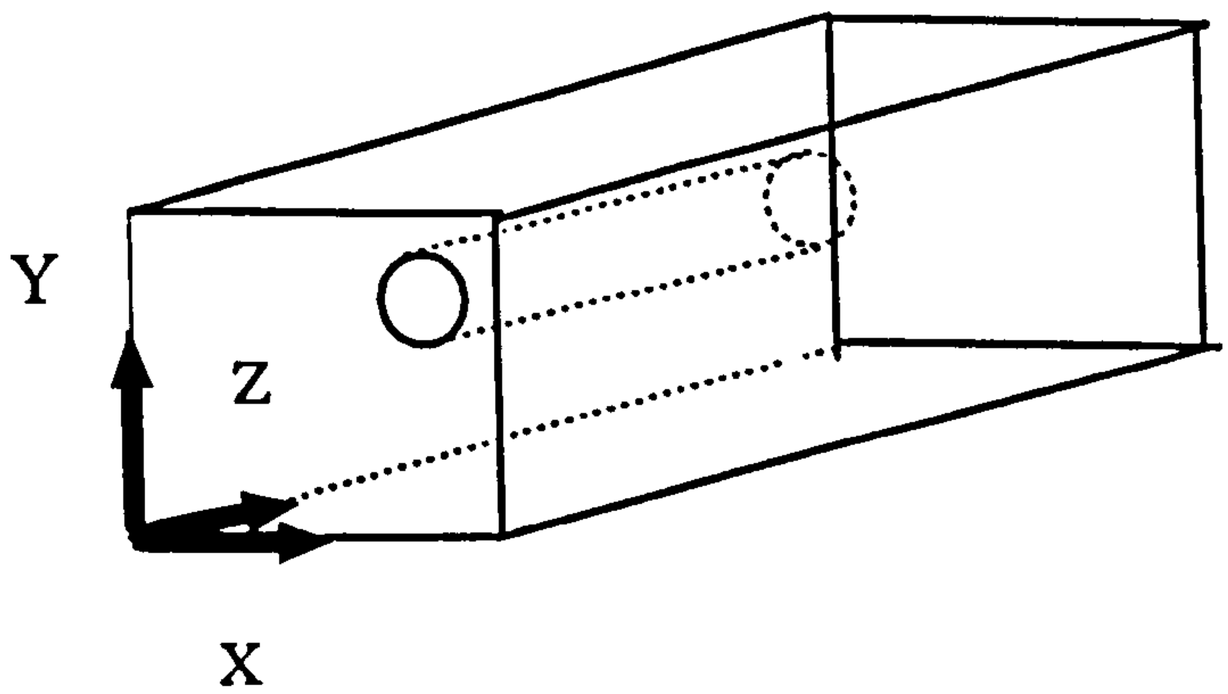

Figure 7-3 - Co-ordinate system employed for experiments.

7.4 GRID SENSITIVITY ANALYSIS.

7.4.1 Introduction

In order to obtain a meaningful CFD simulation and eliminate some computational uncertainty (Metha, 1991; Freitas 1995; Versteeg and Malalasekara, 1996) it is important to demonstrate that the flow solutions obtained from a particular model are independent of the size of the grid used. It has been known that exactly the same problem with different grid densities to produce totally contrary predictions. Therefore it is essential that sensitivity analysis be performed over a range of computational grid sizes.

7.4.2 Methodology

For this study a representative tunnel drivage currently used by UK coal producers was chosen. This drivage has a cross sectional area of 4.5m wide and 3.5m high. The duct positioned 10m from the face delivering $6m^3/s$ of fresh air. Four grid sizes were constructed which had 14, 37, 63, 82 thousand (k) cells each. The process of building a grid is a continual trial and error process. The initial grid is normally designed so that the mesh is denser in particular areas where the flow features are of interest. Consequently there are more nodal points in the area of the jet development and adjacent to the walls of this model.

Once a suitable grid has been identified and the solution of the governing equations converges, the resultant data is analysed. In areas where steep flow or pressure gradients occur more grid points are added. This process continues until all extraneous flow features are resolved and the resultant flow features resembled the actual flow characteristics of the problem. The density of this grid was then increased and the resultant predictions compared with each other.

The k-ε RNG and the RSM turbulence models were applied with the SIMPLE algorithm utilised for the pressure/velocity coupling.

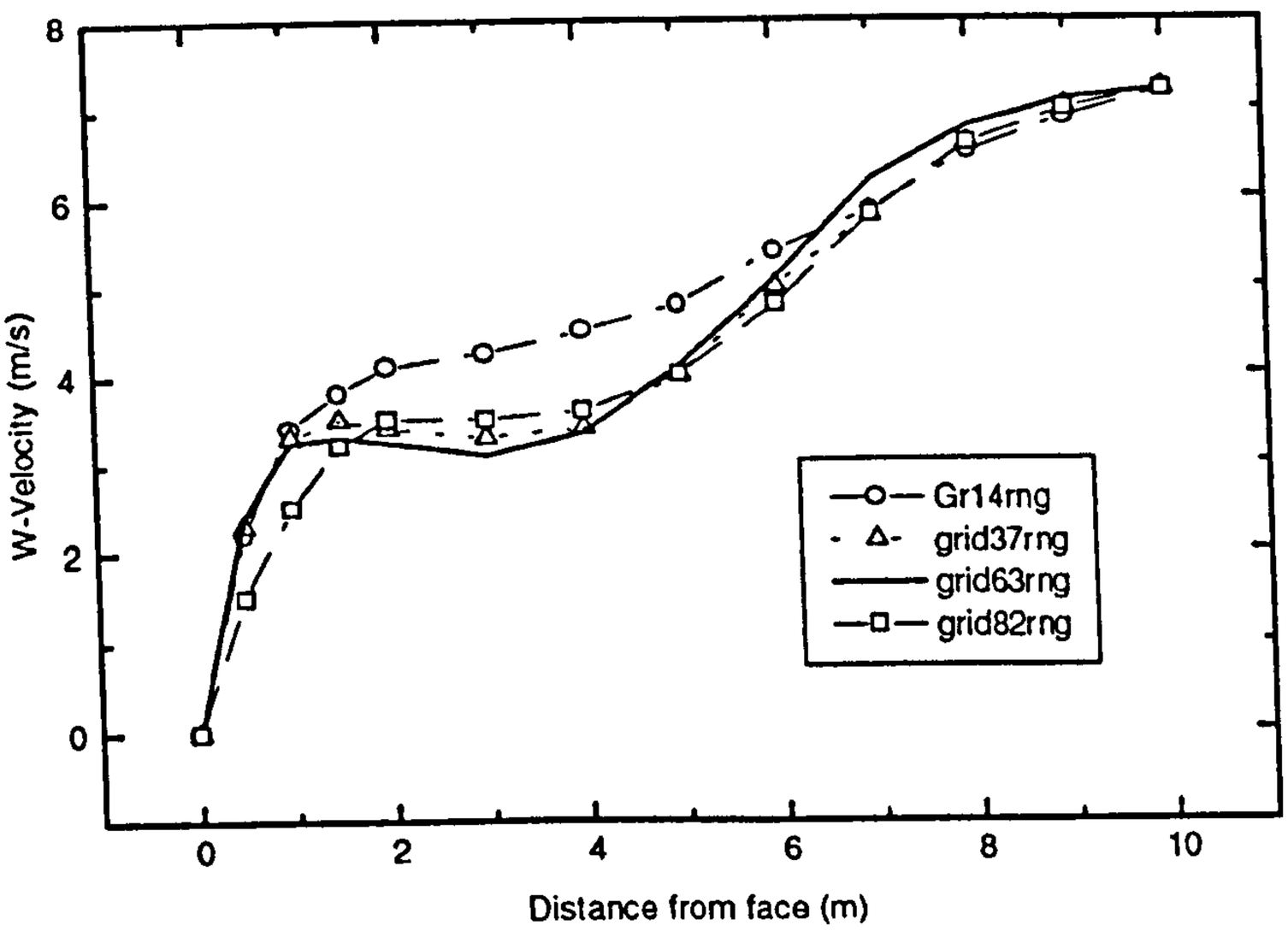

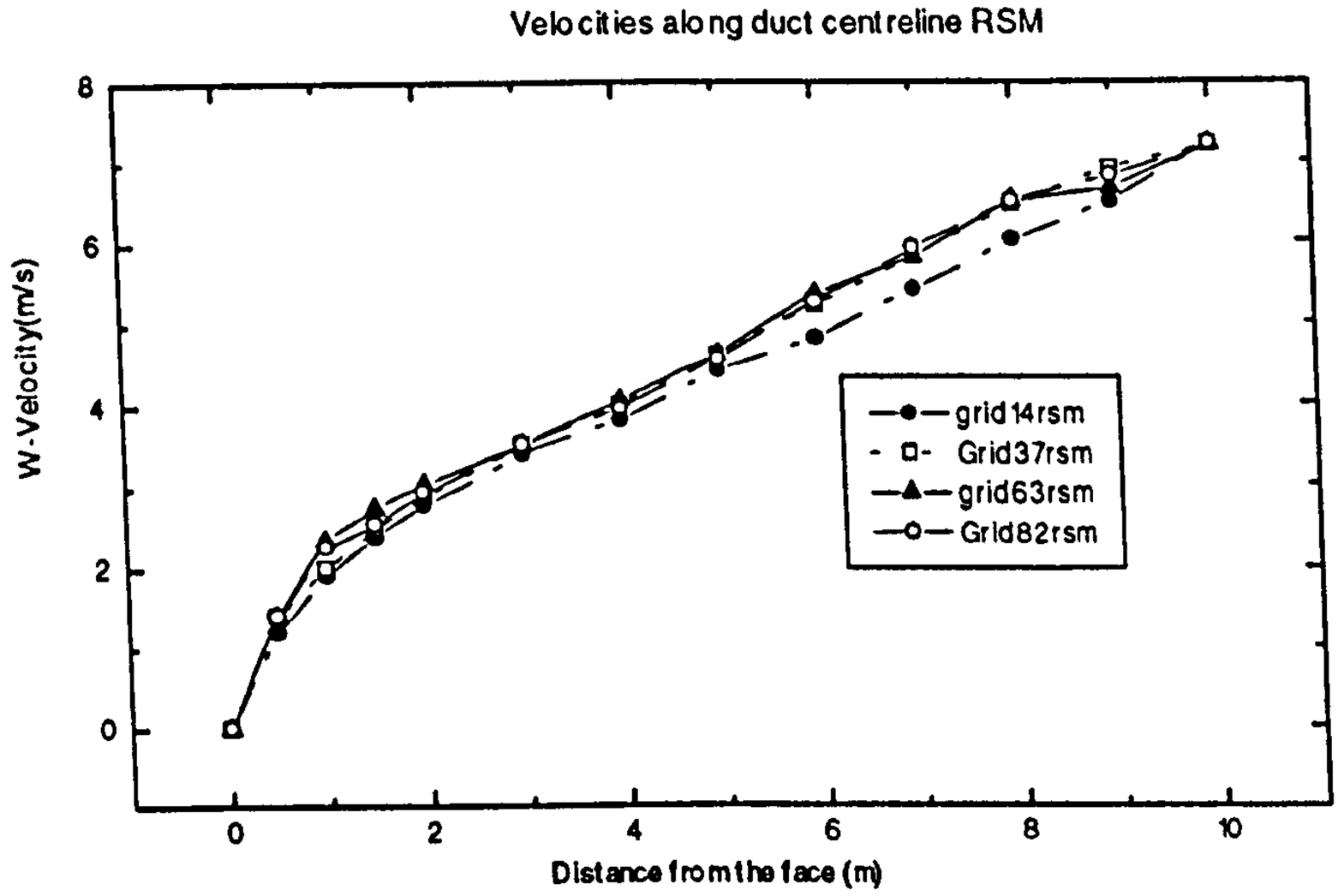

Figure 7-4 W - velocities along duct centreline from duct discharge to face with RNG (top) and RSM (bottom) turbulence models.

7.4.3 Discussion

An analysis of the graphs illustrated in figure 7-4 indicate that the grid with 14k cells does not predict the velocities as accurately when compared with predictions obtained using the other sized grids. The RSM model shows a better correlation than the RNG model but it is still not satisfactory. Therefore the grid with 14k cell was discarded in further analysis. Figures 7-6 & 7-7 illustrate the predictions obtained for a traverse in the X-direction. All the grid sizes show a reasonable correlation, with the 63k and 82k grids giving the closest predictions.

A larger grid (120k) was constructed and the results were compared with those obtained for the other grid densities. This increase in grid density made no difference to the overall predictions. Therefore it was not used due to operational issues.

Chasse (1993) used similar grid densities and geometries to model fires in tunnels. He also demonstrated that by increasing the grid density made little difference. Therefore, from this and the above argument it was decide to use the 63k and 83k grids for further analysis since increasing the grid density showed no appreciable gains in accuracy. This simple example illustrates the need to obtain a grid independent solution to ensure that the predictions obtained from the model are consistent.

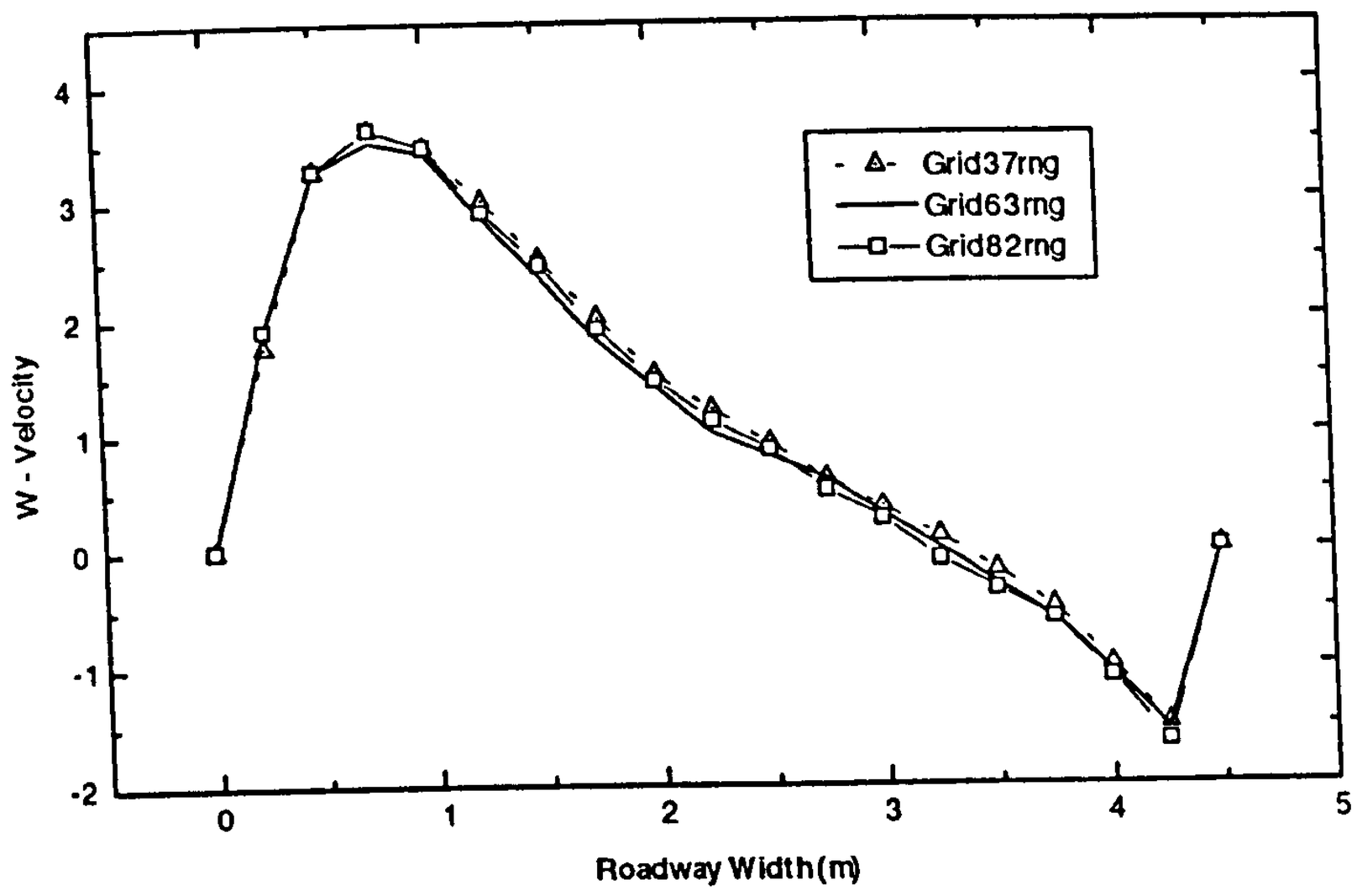

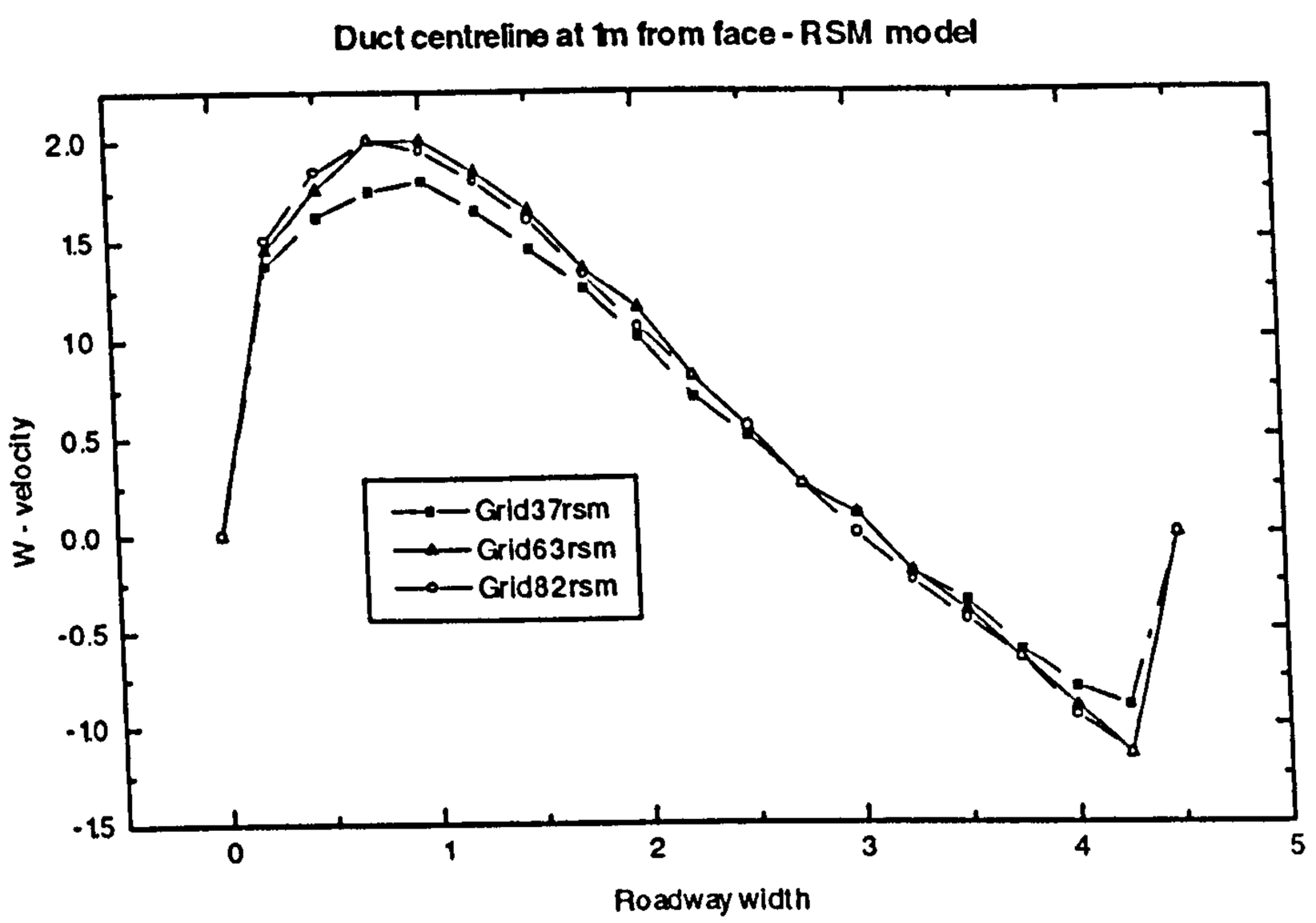

Figure 7-5 - W - Velocities - X traverse 1m from the face along duct centreline RNG (top) and RSM (bottom)

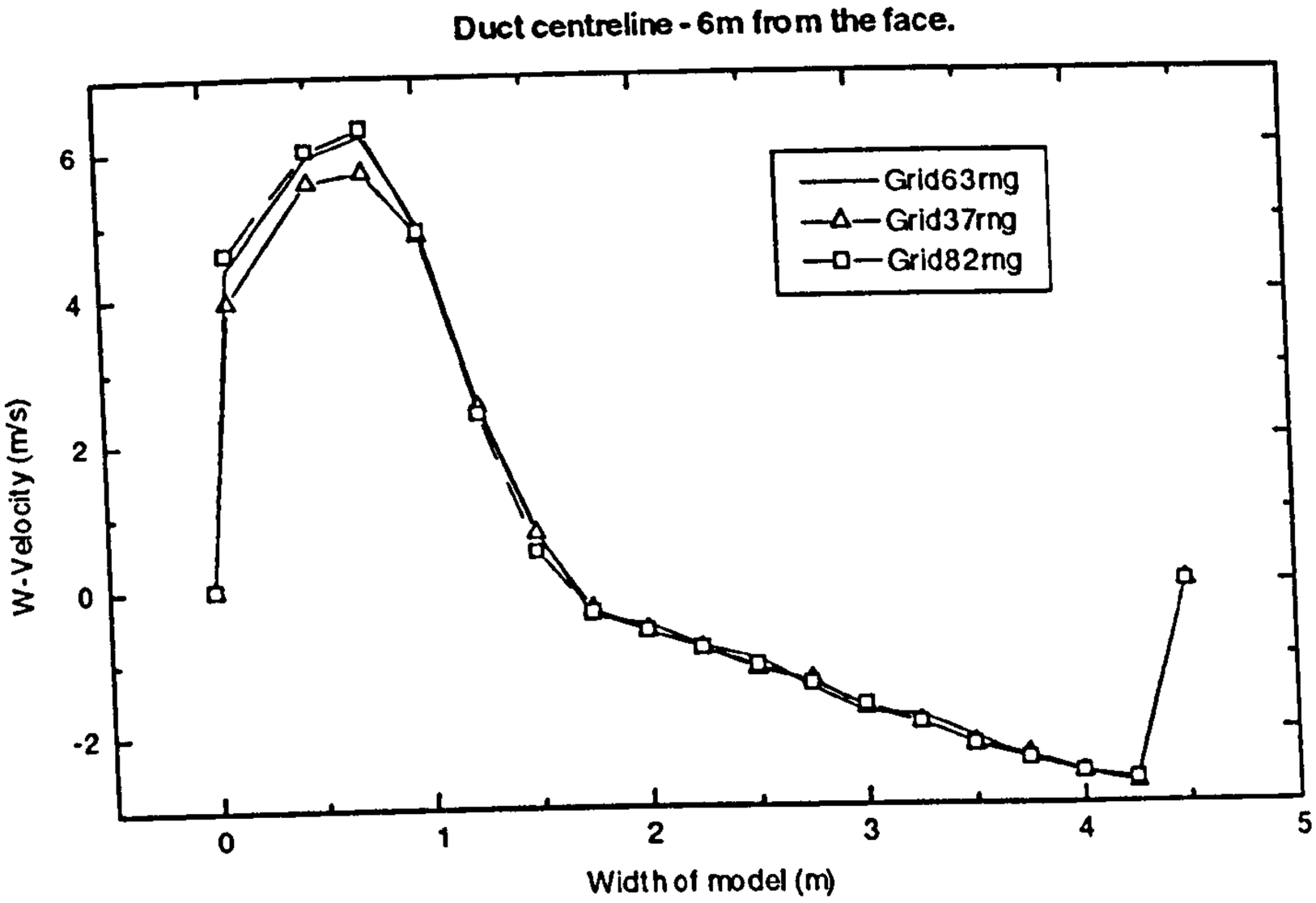

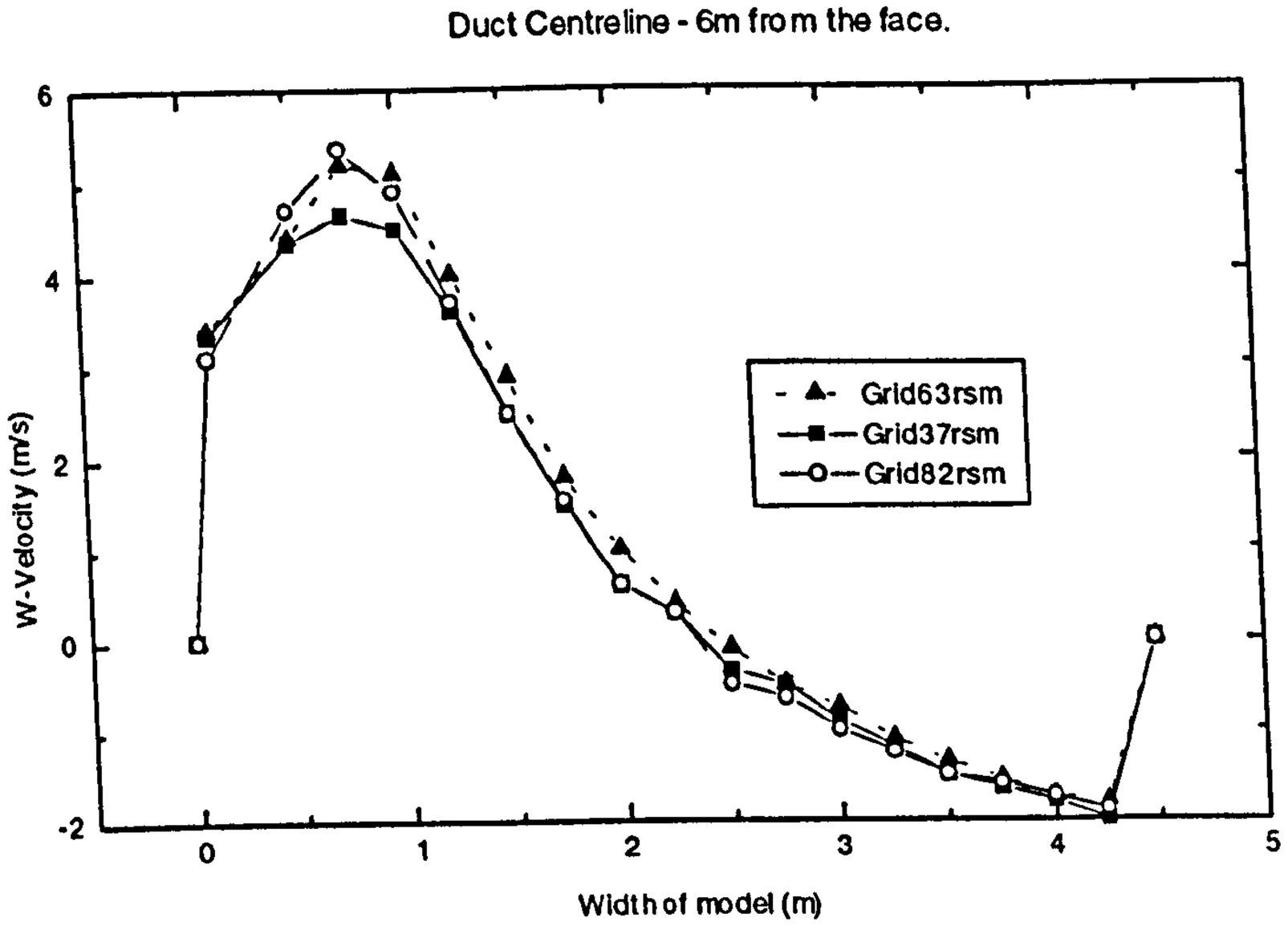

Figure 7-6 - W - Velocities - X - traverse 6m from face along duct centreline with RNG(top) and RSM (bottom).

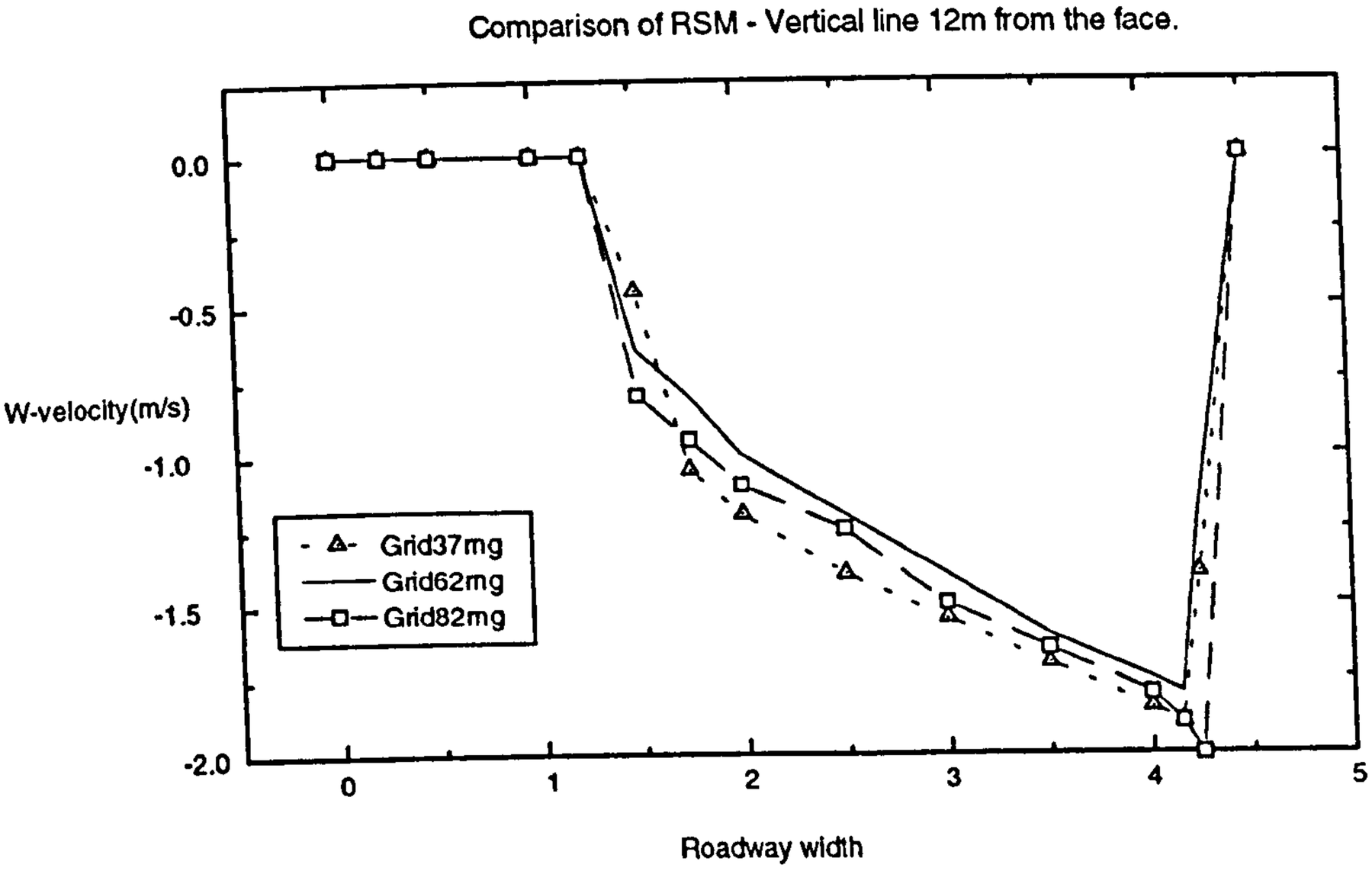

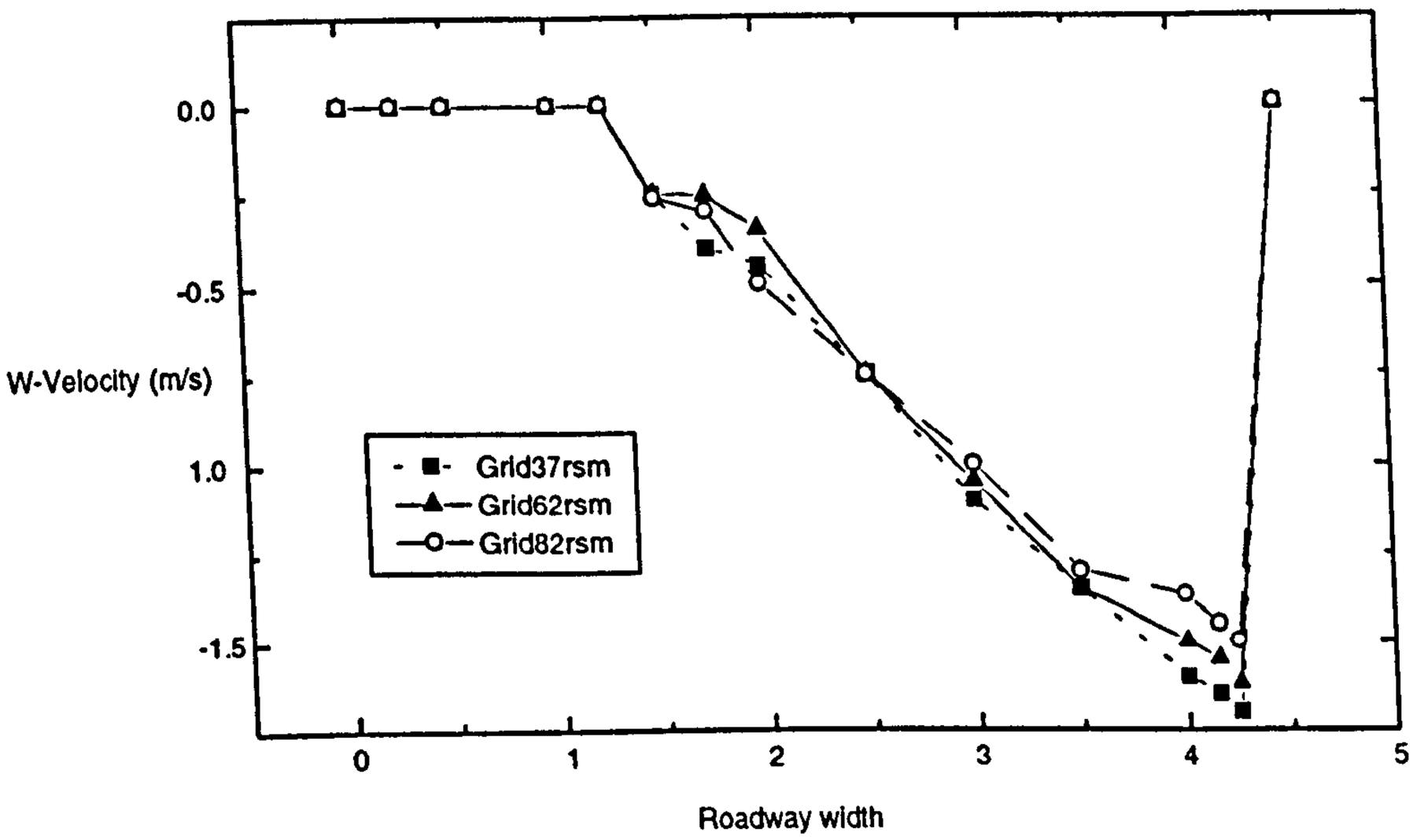

Figure 7-7 - W - Velocities - X traverse 12m from the face along duct centreline RNG(top) and RSM(bottom).

7.4.4 Conclusions

It has been demonstrated that in order to have any confidence in the simulation one must conduct a sensitivity analysis on the grid. It is also a requirement of the American Society of Mechanical Engineers (ASME) that a solution produced from a single grid density would not be acceptable for publication in their journal. It should be noted that a grid independent solution may be achieved and it may not replicate the true physics characteristics of the flow. This is due to the limitations in the physical models within the code, specifically the turbulence models.

Following these initial series of studies it was observed that the RSM turbulence model produces more consistent predictions for grids of smaller densities. Thus if one is severely limited by the number of cells this model may provide the best choice.

7.5 CHARACTERISTICS OF THE FLOWS ENCOUNTERED.

7.5.1 Free jet in space

The theoretical behaviour of a free jet is illustrated in Figure 7-8. It shows the development of the velocity distribution of a turbulent isothermal free jet. Air is discharged from the nozzle (d) at a constant velocity Um, into an unconstrained space. The stationary air around the vicinity of the jet is entrained so that the jet widens at an angle 2 α. In the central core of the a jet of length x_0, immediately downstream of the nozzle, the velocity U_m remains equal to the discharge velocity U_m. The core diameter decreases linearly from the nozzle. The length of this core (x_0) depends on the degree of turbulence in the jet. Typically, X_0 would be 5-8 nozzle diameters for non-rotational flow. The local centre-line velocity $U_{0(x)}$ decreases from the end of the jet core.

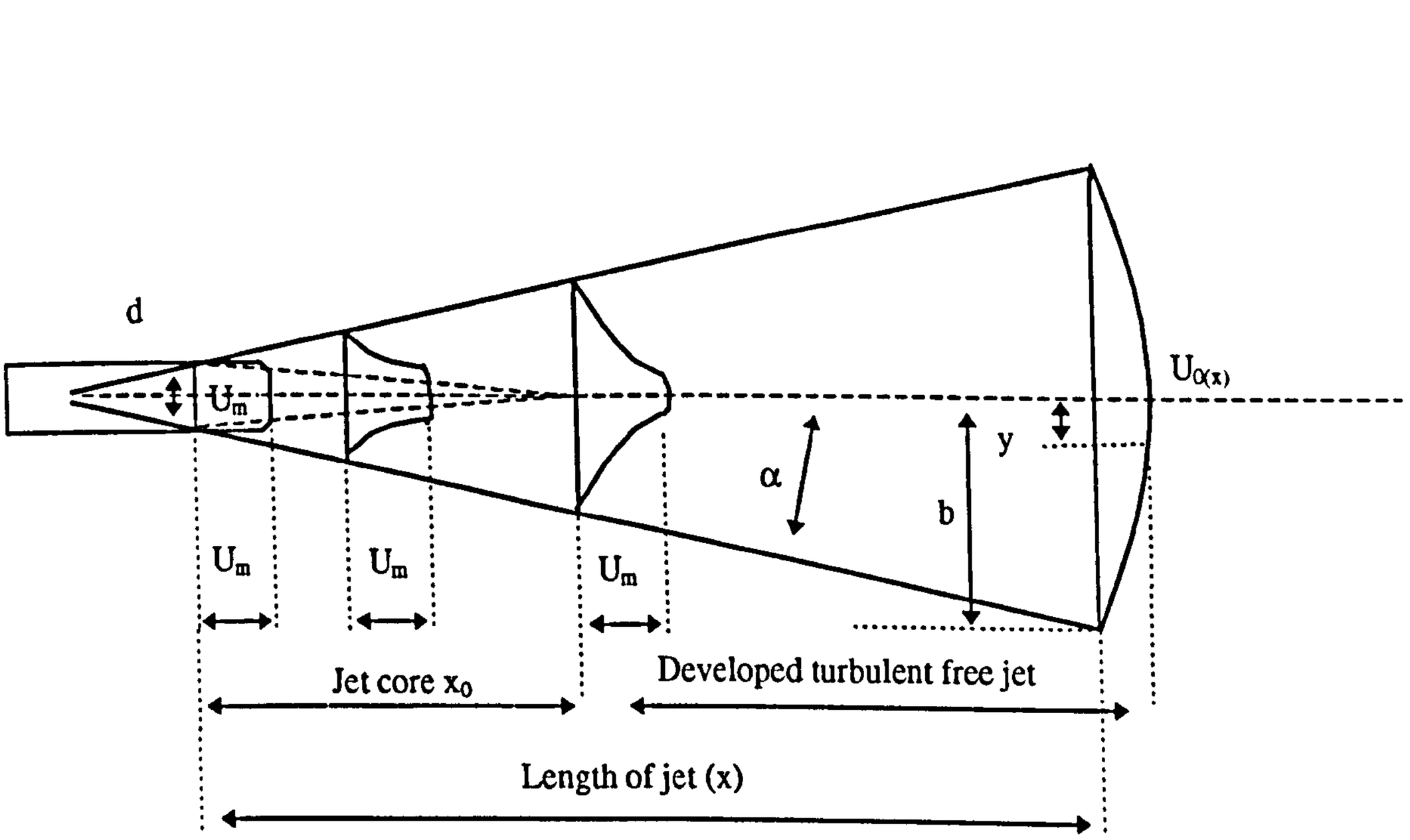

Figure 7-8 - Turbulent round free jet.

The velocity distribution profiles are bell-shaped and they are similar from one turbulent jet to another (Abramovich, 1963).

7.5.2 Wall Jets in tunnels.

The term wall jet was introduced by Glauert (1956) to describe the flow that develops when a jet consisting of a fluid similar to that of its surroundings impinges on a plane surface and spreads out over its surface. Wall jets can be recognised as an example of the interaction between free jets and boundary layer types of flows. There has been much research on the study of two-dimensional jets (Glauert, 1956; Abramovich, 1963). The first published work on three dimensional wall jets investigated jets discharging from a rectangular orifice of various sizes. Rajaratnam & Pani (1974) studied a variety of nozzle shapes including circular, rectangular, elliptical, triangular and square. Where most research concentrated on jets adjacent to the wall Davies and Winarto (1980) considered a circular duct offset from a wall. They found as the orifice is moved closer to the wall the penetration of the jet is increased.

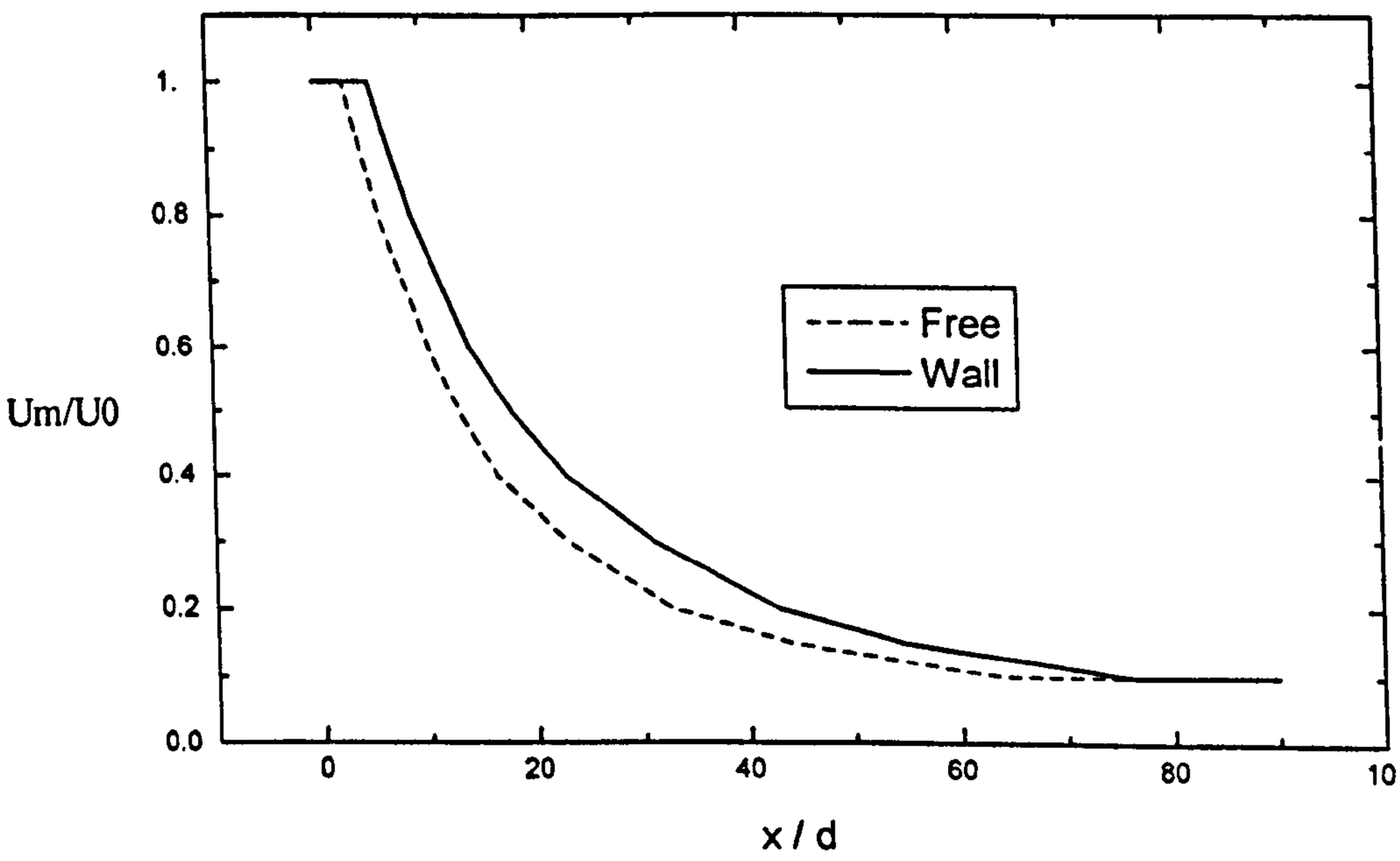

Figure 7-9 - Comparison of a wall jet and a free jet.

In a tunnel one also has to consider the effect of the walls and the returning air attempting to exit the roadway. The distance between the duct discharge and the region of flow reversal is known as the penetration depth of the jet. The penetration of a jet depends on the mixing number , $m=d/x_0$ and therefore the turbulence rather than the cross-sectional area ratio $(d/D)^2$. Applying this concept of a mixing number to a typical auxiliary ventilated tunnel the penetration of a concentric jet is estimated to be three times the hydraulic diameter. If the turbulence is increased, the mixing zone and therefore the penetration of the jet decreases (Wesley, 1984).

Many tunnel operations have the auxiliary duct placed asymmetrically. Therefore, the friction of the wall and roof decelerate the jet, thus entrainment only occurs on two sides. The degree of turbulence is reduced and the penetration increases to 4.5 - 5 times the hydraulic diameter.

7.6 PRELIMINARY STUDIES AND FLOW FEATURES.

7.6.1 Methodology

A preliminary series of CFD models were constructed in an attempt to simulate the flow patterns observed during full scale gallery trials summarised in chapter five. The gallery was modelled using a grid containing 63 thousand cells. The k-ε RNG turbulence model (TM) and the SIMPLE algorithm were employed. The fluid density was set to 1.2 kg/m^3 and the viscosity set at $1.79 * 10^{-05}$ Ns/m^2. A one-metre diameter duct delivered $6m^3/s$ of fresh air with setback distances of 5, 15 and 25 metres. The results obtained from these models are presented and discussed below.

7.6.2 Results

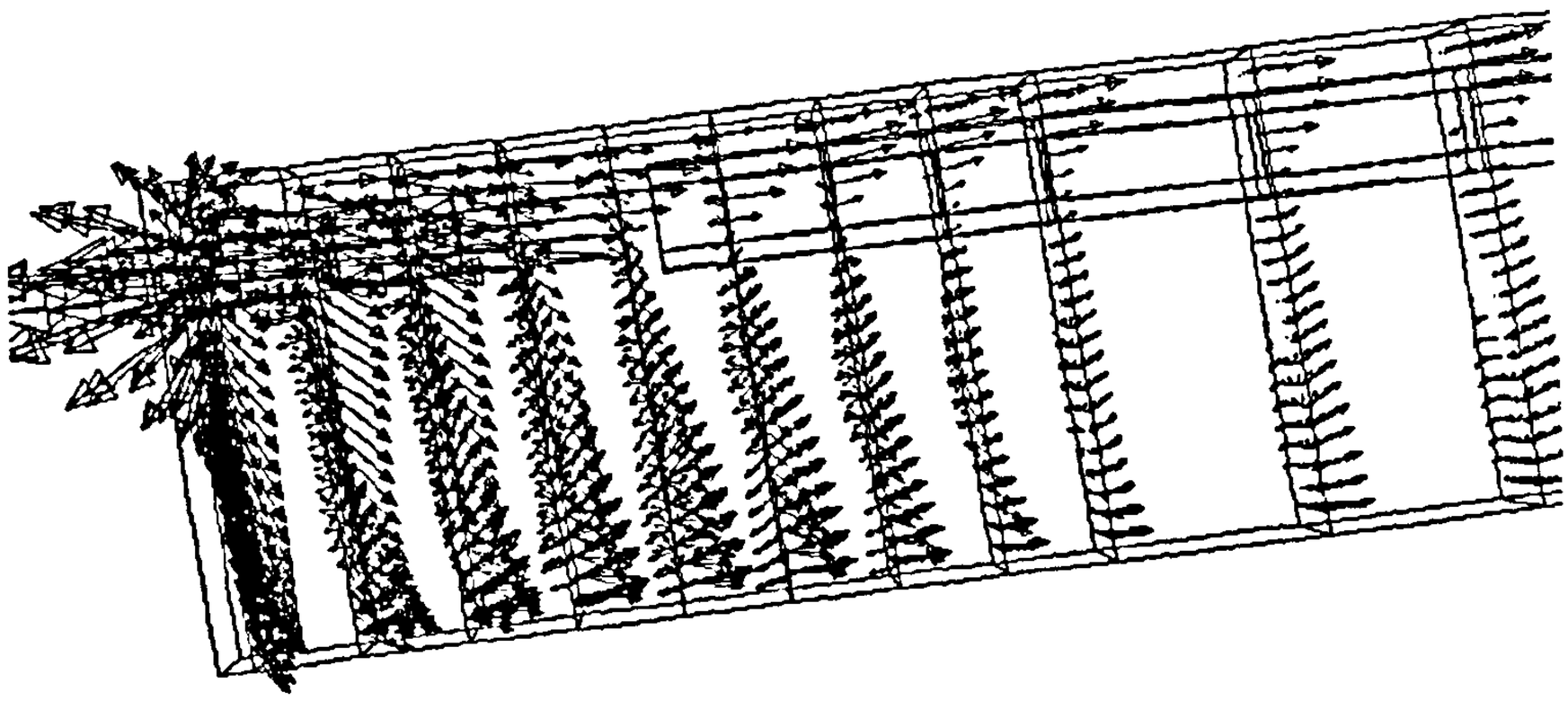

Figure 7-10 - Force duct at 5m From face.

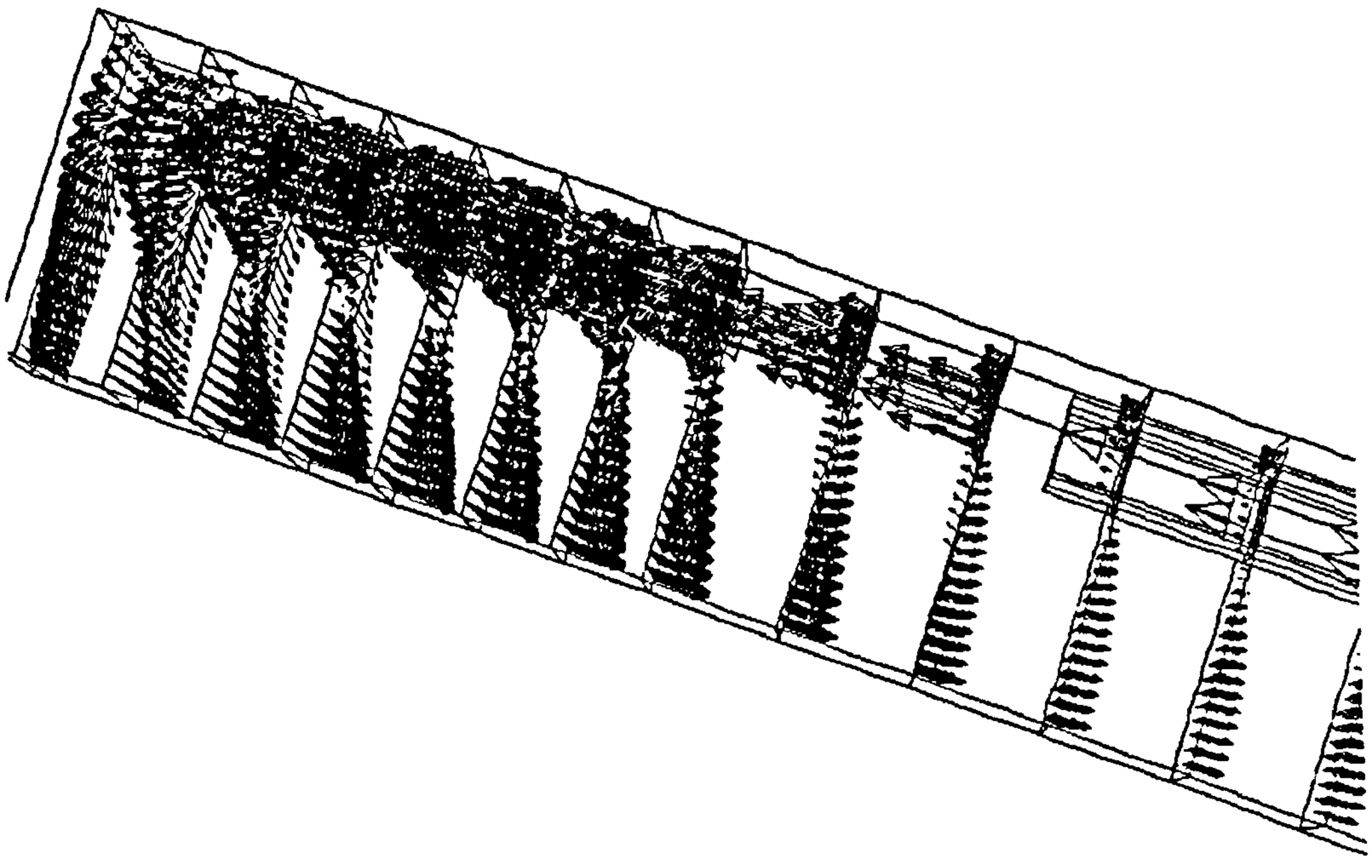

Figure 7-11 - CFD simulation with forcing duct at 15 metres from the face

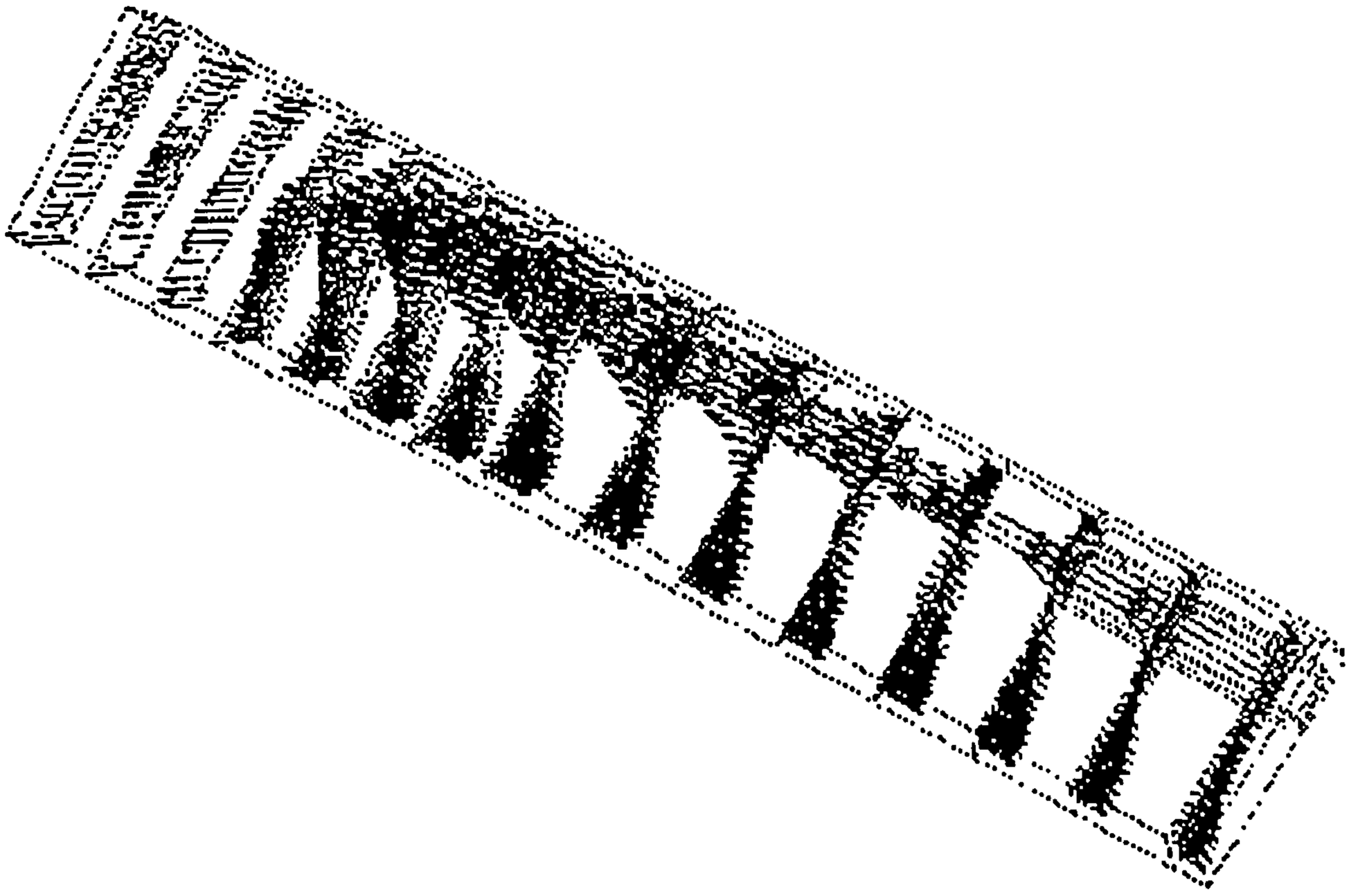

Figure 7-12 -CFD simulation of forcing duct at 25m.

7.6.3 Discussion

The general characteristics of the flow observed in the gallery have been produced by this series of models. These simulations were able to replicate the entrainment of air that had been observed both adjacent to the forcing jet and behind the duct outlet. This entrainment is caused by the venturi effect that creates a low-pressure zone behind the jet outlet. The models also confirmed that placing a forcing jet at 5m from the face causes excessive turbulence, which in turn causes much dust to become airborne. Dust may pose a health and safety hazard. Therfore, in practice it is necessary to bleed off some of the air and/or use a diffuser to maintain dust standards.

Care must be taken when choosing the setback distance of the duct outlet from the drivage face. This is to allow the forcing jet to retain sufficient momentum to allow it to effectively ventilate the face of the heading and prevent any build up of methane.

7.6.4 Conclusions

The basic CFD models have predicted the general flow characteristics qualitatively. However, in order to have confidence in the model predictions one must evaluate the quantitative accuracy of the values obtained. To obtain quantitative data a series of scale model tests using laser light and Laser Doppler Anemometry (LDA) were conducted. These results of these preliminary experiments are described in the following chapters.

8. COMPARISON OF EXPERIMENTAL DATA WITH CFD PREDICTIONS.

8.1 INTRODUCTION.

Chapter six described the construction of the scale model, introduced the measurement techniques employed and the theory behind the experimental work. Chapter seven discussed the problems associated with the use of practical CFD modelling of real flow systems. The importance of grid independence has also been highlighted.

This chapter provides a description of the experiment methodology employed. It will also present a comparison of the data obtained from the experimental studies with CFD models. The results of the flow visualisation studies are compared with CFD predictions by employing velocity vector and contour plots. The experimental LDA measurements are graphically compared with CFD predictions of the flow produced by three turbulence models.

8.2 CFD MODEL PARAMETERS.

It has been demonstrated in chapter seven that in order to obtain a consistent and meaningful solution one must obtain a grid independent solution. From these initial studies it was concluded that a grid containing 82 thousand cells spaced in a non-uniform manner (body fitted) is the most efficient grid spacing. Therefore, such a grid spacing was used for the comparison with the experimental study. The Power law discretisation scheme was used for the solution of the governing equations. The SIMPLE algorithm was utilised for the pressure-velocity coupling. The flow regime produced by three different turbulence models were compared with those obtained from the LDA experimental results. The three models employed were the standard k-ε, k-ε RNG and the RSM turbulence models. The standard wall function was used for treatment of near-wall effects. The air density was set to 1.2 kg/m^3 and the viscosity 1.79 * 10-5 N-s m^2 with the ambient inlet pressure being set at 101.3 Pa.

8.3 FLOW VISUALISATION.

8.3.1 Flow visualisation methodology.

The copper vapour laser used to produce the laser beam was set up in the desired position. The sheet of light is created through use of a mirror to deflect the light beam through two optical lenses that spread the laser to produce the sheet of light. The model auxiliary fan is switched on to full power which realised a Reynolds number of 120,000. The lights were switched off and the smoke pulsed into the model from a smoke generator at the fan inlet. Video recordings were then taken of the resultant airflow patterns.

The same series of visualisation studies were repeated for a Re of 75,000. This is to determine whether the airflows produced Reynolds number independence. A series of horizontal slices (duct centre and floor) were illuminated by the sheet of light and recorded on video (figure 8.1 & 8.2 illustrate the location of the slices). A similar series of vertical slices were illuminated and recorded at distances of 45mm, 510mm, 920mm, 1085mm, and 1800mm from the face (figure 8.6-8.11)

8.3.2 Post processing

Video analysis was conducted utilising a Super VHS Video recorder which has the ability to look at seventy five frames per second. The main flow patterns were initially identified from an analysis of the video tapes. Reynolds number independence of the experimental results was tested by a comparison of the flow regimes produced by the 75k and 120k experiments. There appeared to be no apparent difference between the flows produced by the two tests. Therefore, it was assumed that Reynolds number independence was achieved. The main flow patterns were then sketched onto W-velocity vector plots (figures 8-1, 8-2) and contour plots (figures 8-6 - 8-11) obtained from the CFD predictions. Four specific flow features of interest were captured and identified using image analysis equipment. They included: the Coanda effect, eddies breaking away from the jet (figure 8-3), a dead zone in the top corner (figure 8-4) and finally the venturi effect (figure 8-5).

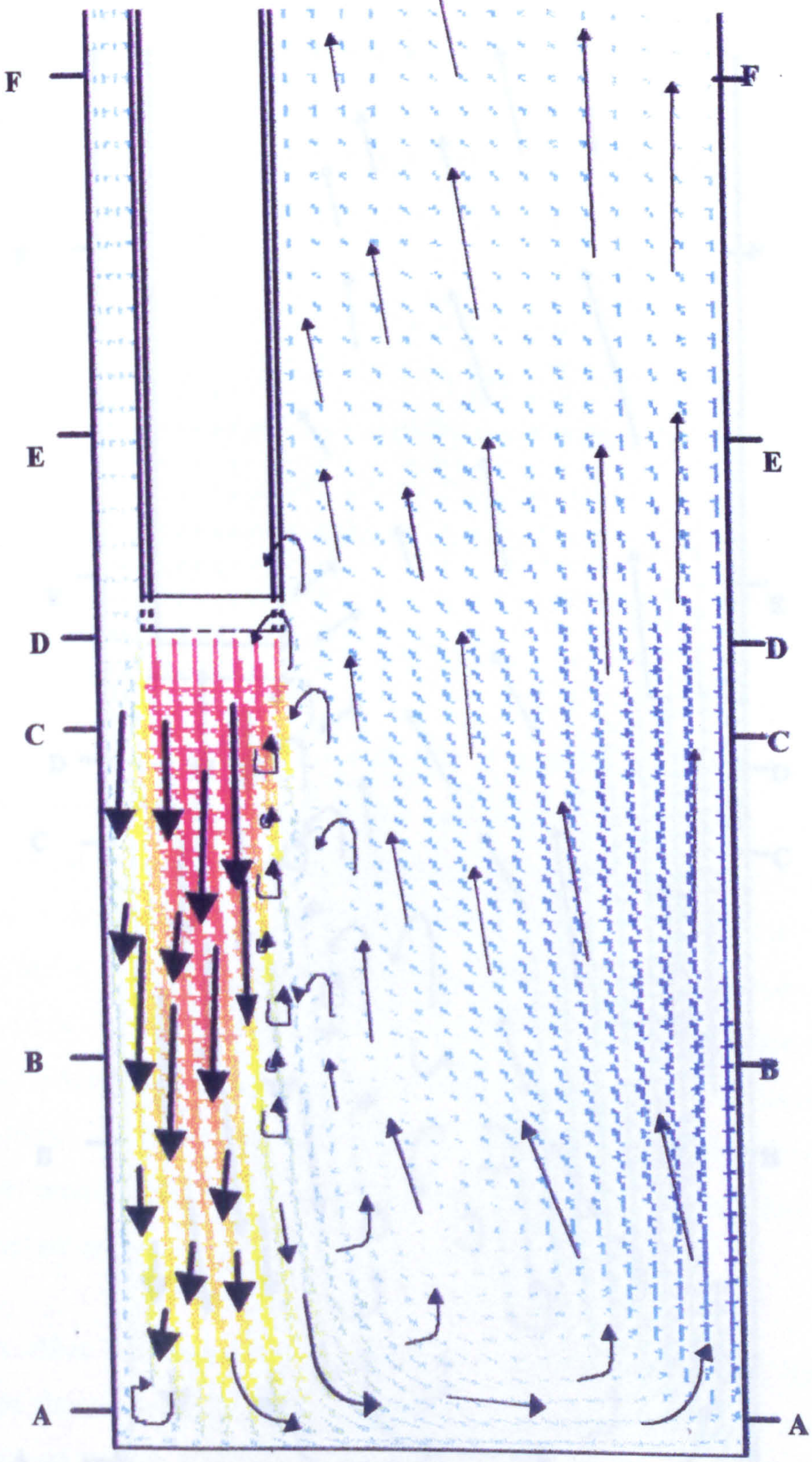

Figure 8-1 - Horizontal slice through centre of duct.

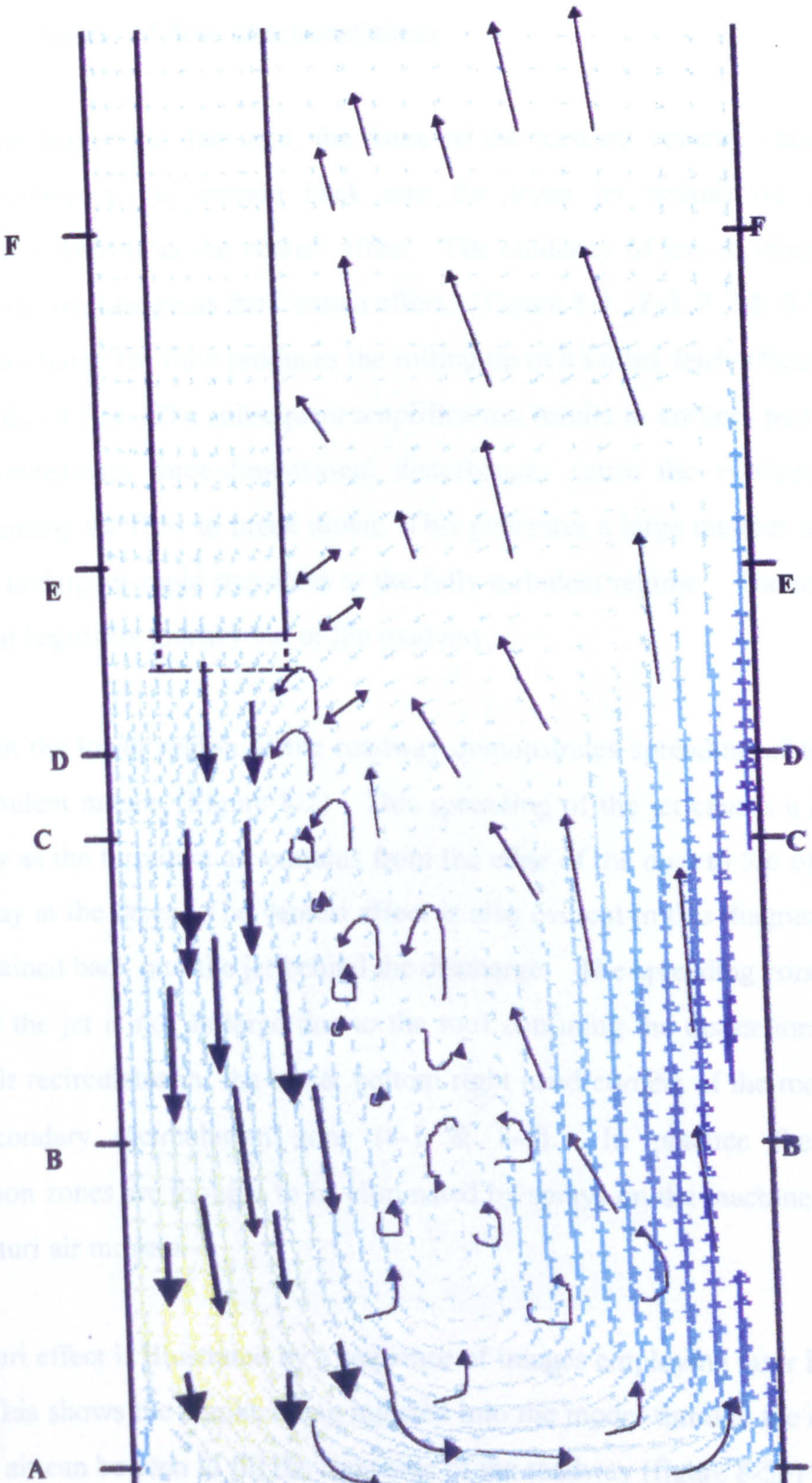

Figure 8-2 Horizontal Slice 90 mm from the floor.

8.3.3 Discussion of results

8.3.3.1 Description of flow characteristics.

As the air jet leaves the duct exit, the force of the forward velocity causes the slow moving returning air to entrain back into the main jet behind the duct. This phenomenon is known as the venturi effect. The tendency of jets to cling to adjacent walls is commonly known as the Coanda effect. (Figure 8-1, 8-3, 8-7 & 8-9) As the jet leaves the discharge the flow produces the rolling up of a vortex fairly (figure 8-1 and 8-3) close to the orifice. The subsequent amplification results in vortices pairing. A short distance downstream three-dimensional disturbances cause the vortices to become distorted causing the flow to break down. This generates a large number of small scale eddies and undergoes rapid transition to the fully turbulent regime. The jet then scours the face and begins its journey out of the roadway.

The slice in the lower region of the roadway demonstrates spreading of the jet and its highly turbulent nature. (Figure 8-2) This spreading of the jet causes a large zone of uncertainty as the turbulent air entrains from the edge of the duct to 5/6 of the width of the roadway at the face. The venturi effect is also evident in this diagram with the air being entrained back into the jet behind the discharge. The spreading zone in the upper portion of the jet is not as large due to the roof confining the dispersion rate. At the face the air recirculates in the top & bottom right hand corners of the model to form a small secondary recirculation zone (8-1 & 8-4). In practice these secondary recirculation zones are thought to be eliminated by sprays on the machines and in some cases venturi air movers.

The venturi effect is illustrated by a sequence of images employing laser light (figure 8-5 a-c). This shows the smoke being injected into the model through the duct (figure 8-5a). The air can be seen to fill the right side of the roadway (figure 8-5b) and then drifts towards the duct. The air is then entrained underneath the duct back into the jet (figure 8-5c).

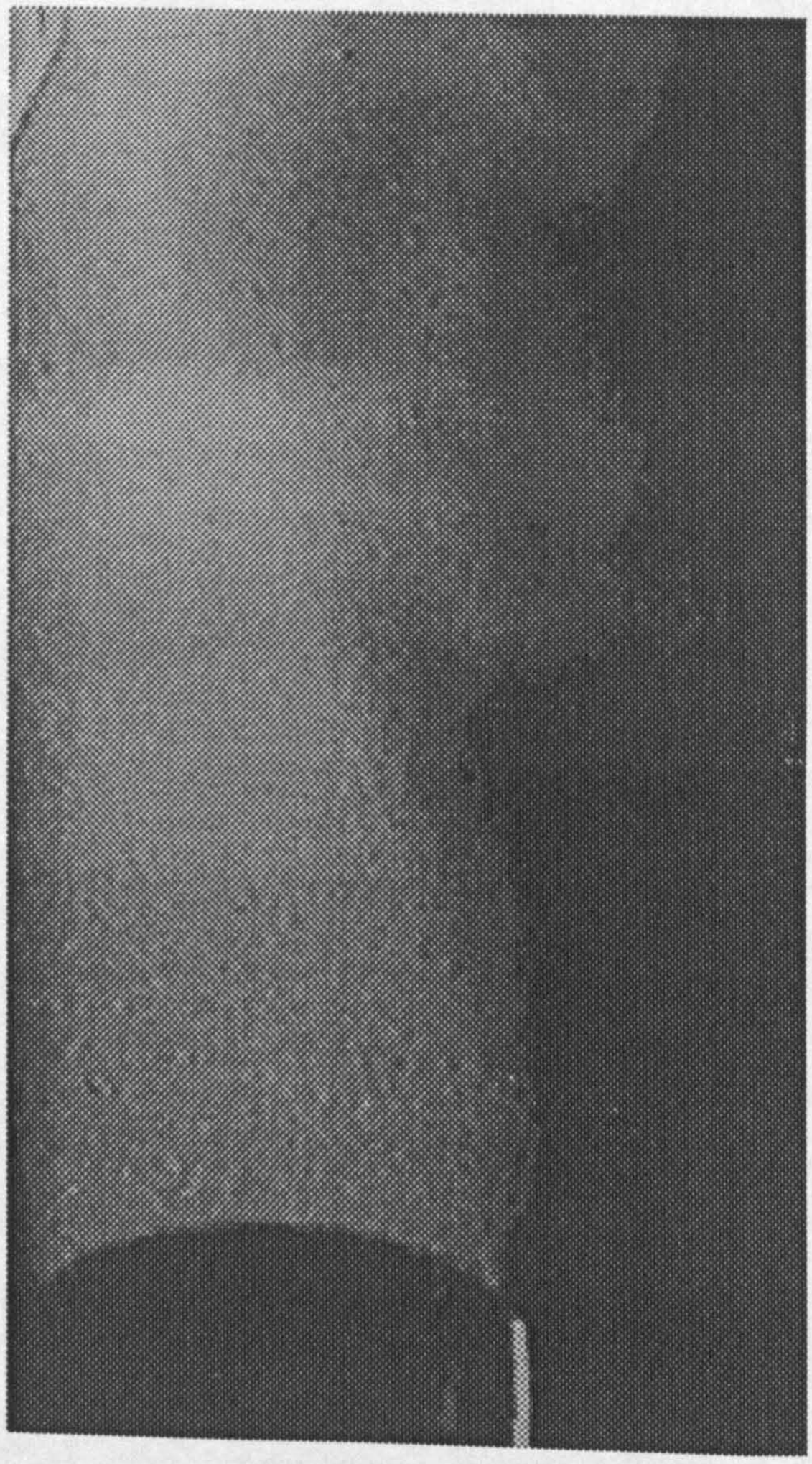

Figure 8-3 Eddies breaking away from the Jet

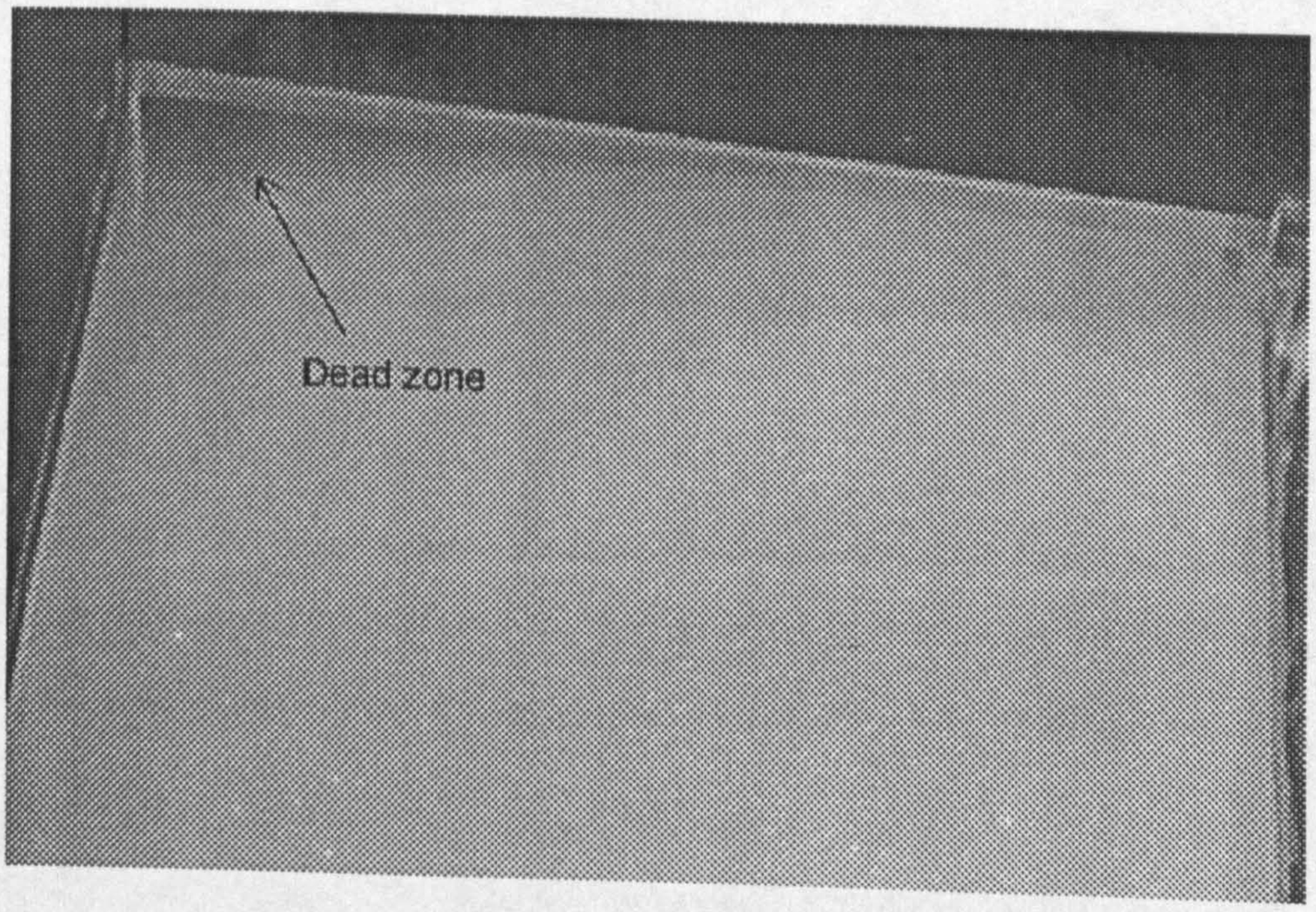

Figure 8-4 - Dead zone in top left corner of the model.

Figure 8-5 - Sequence illustrating the venturi effect.

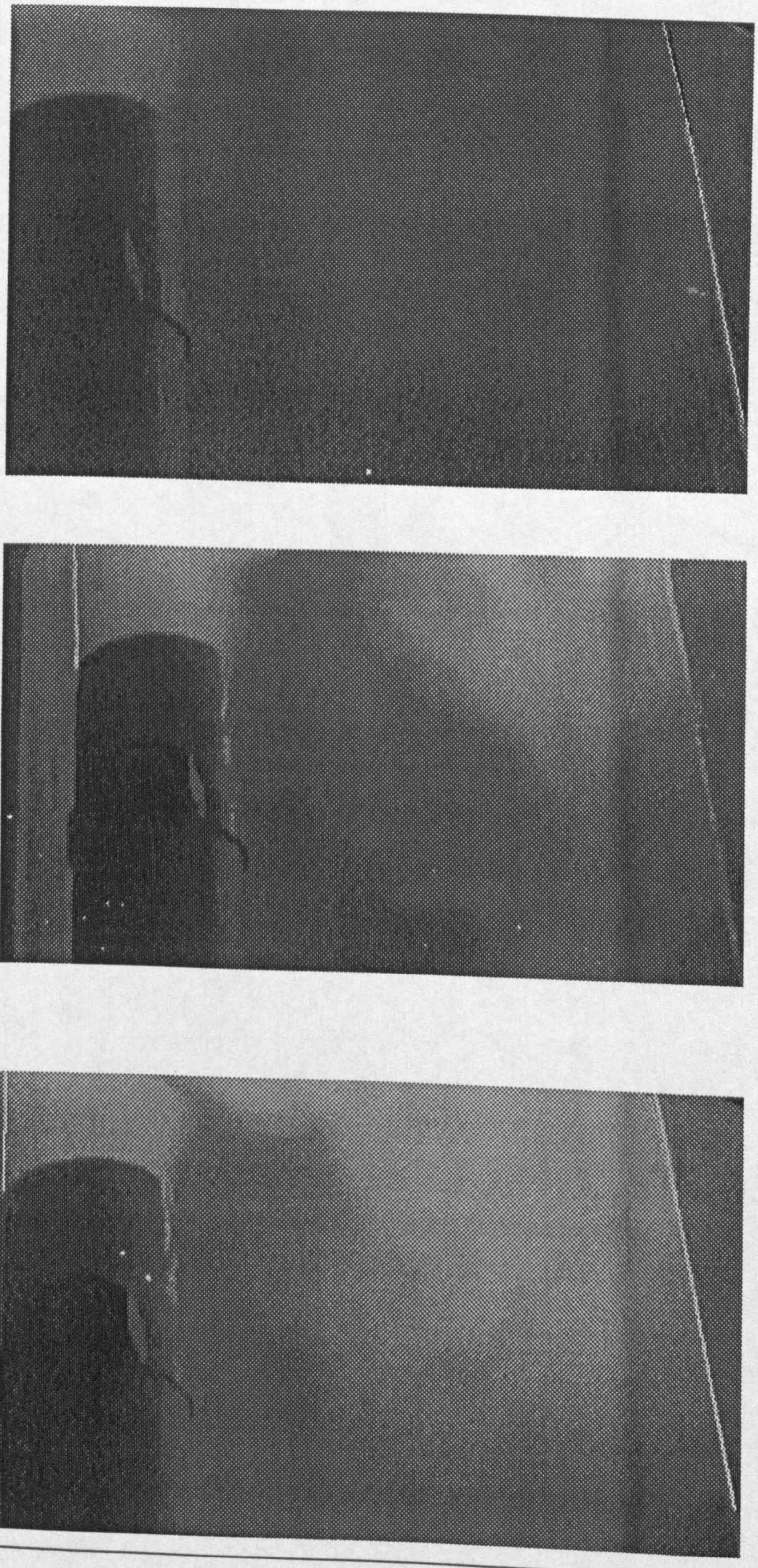

The vertical slice A-A (figures 8-6) illustrates the scouring of the face with the tendency of the jet to stick to the wall. At this stage the returning air occupies around 20% of the roadway area. As the air moves oubye it fills more of the roadway and interacts with the jet which increases the turbulence. This is particularly evident in the lower region of the model. The oscillating nature of the flow is clearly demonstrated in figures 8-6 to 8-11. As the jet leaves the duct it scours the face and the returning air interacts with the jet as it leaves the roadway.

Section F-F or 1890 mm from the face illustrates the air occupying all of the roadway (figure 8-11) as it leaves.

8.3.3.2 Prediction Vs experiment.

The CFD prediction replicates the general flow very well from the discharge to the face. This is illustrated in figures 8-1, 8-2, 8-6, 8-7, 8-8. The flow is highly time dependent and oscillating between positive and negative values in some regions of the flow. The CFD simulation produces an average which in most cases is close to zero but in reality this value oscillates frantically. The small recirculation zone illustrated in figures 8-1 & 8-4 and the jet entrainment (figure 8-5) are also predicted by the CFD model.

The region behind the duct does not prognosticate the flow so accurately. The entraintment region in the lower region of the roadway is slightly over predicted (figure 8-9 & 8-10). However the model does illustrate that the majority of air leaves via the top right corner of the roadway. The oscillating air around the duct is also predicted by the CFD simulation (figure 8-10). Again it should be noted that the oscillating nature of the air makes zero difficult for the model to anticipate.

Symbols

● Air leaving Roadway (negative velocity)

..... Region where air starts to reverse

■ Air entering roadway (positive velocity)

⟷ Flow Oscillating

Jet Clinging to wall

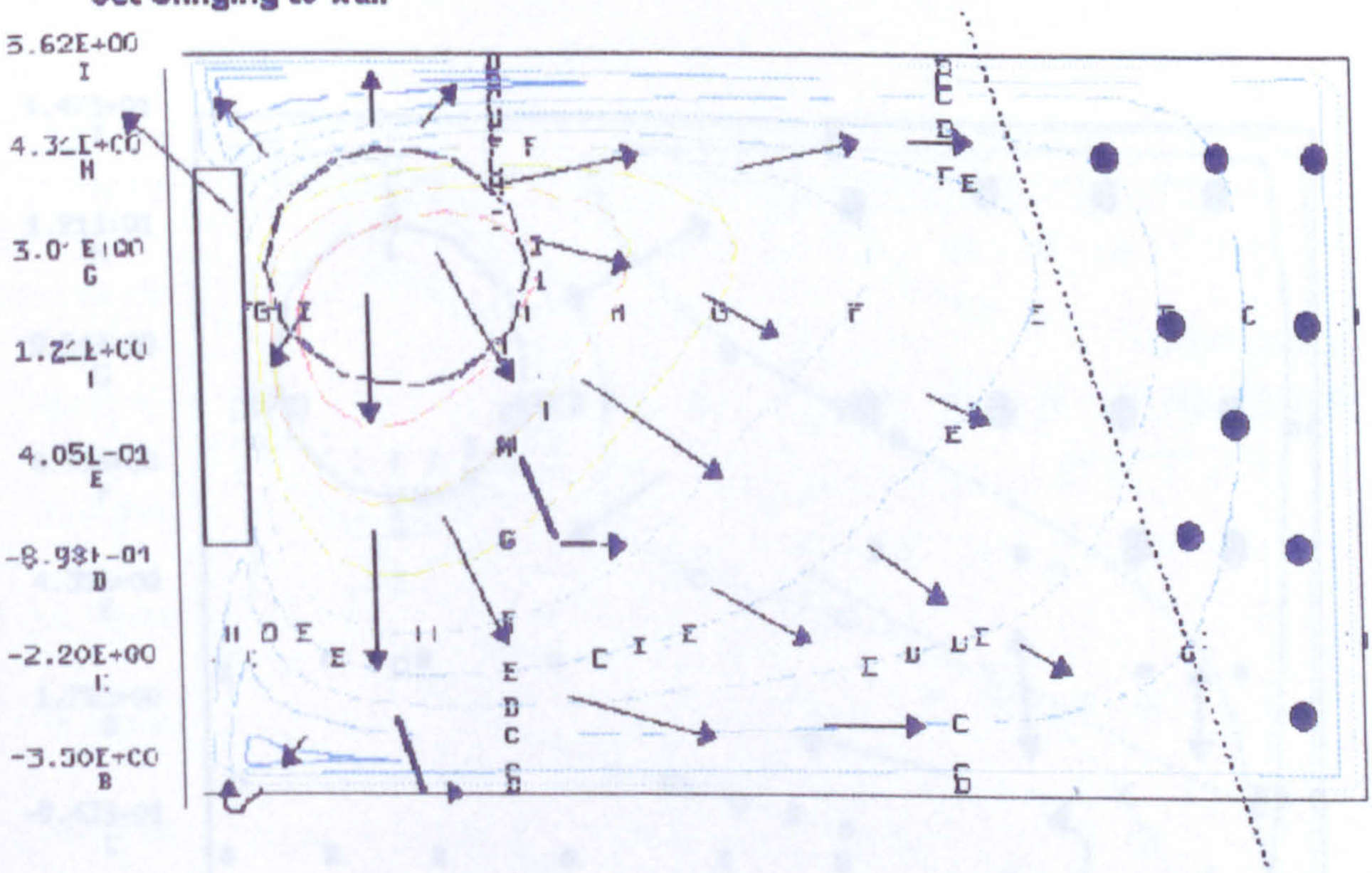

Figure 8-6 Section AA - 45 mm from the face.

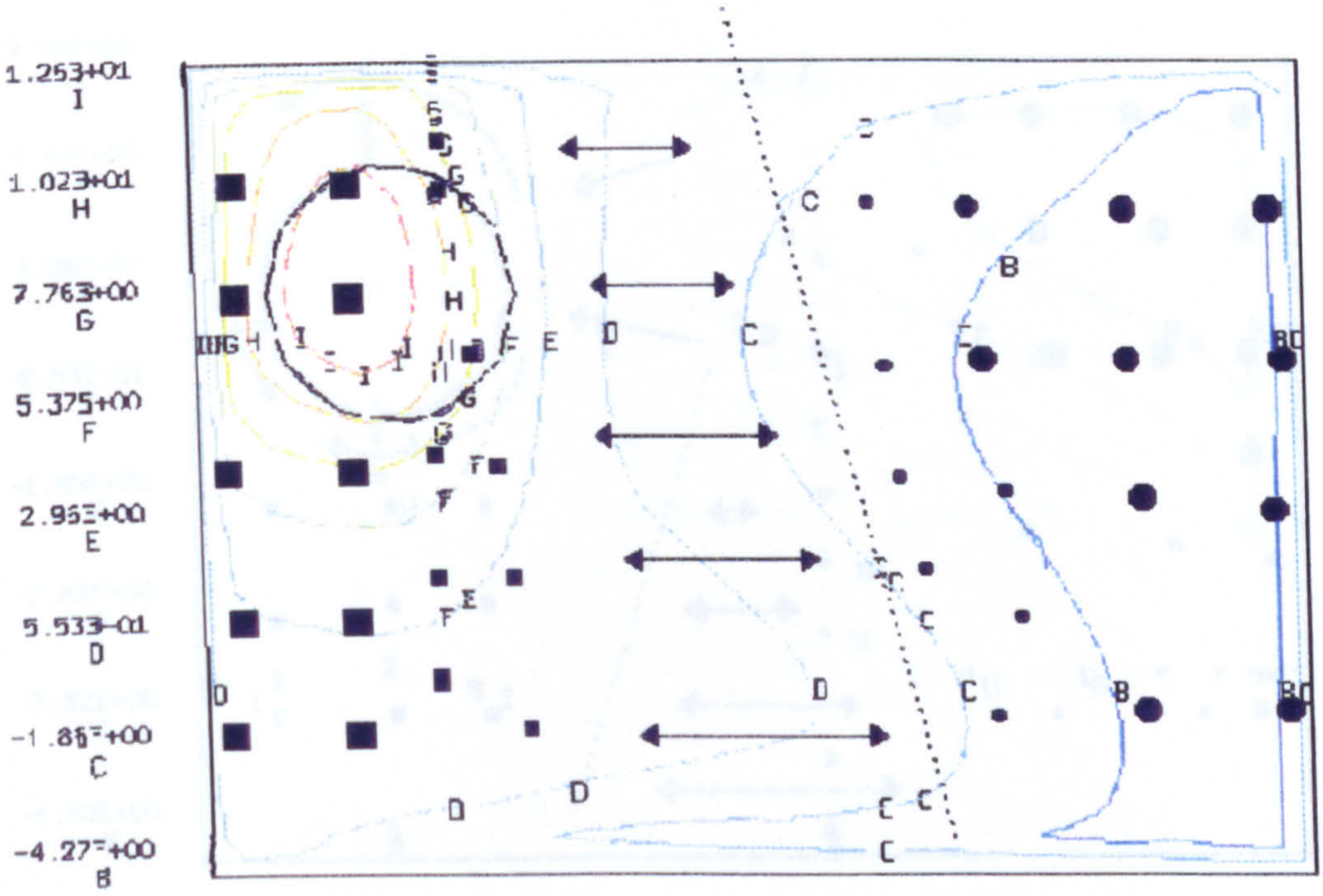

Figure 8-7 Section BB - 510 mm from the face.

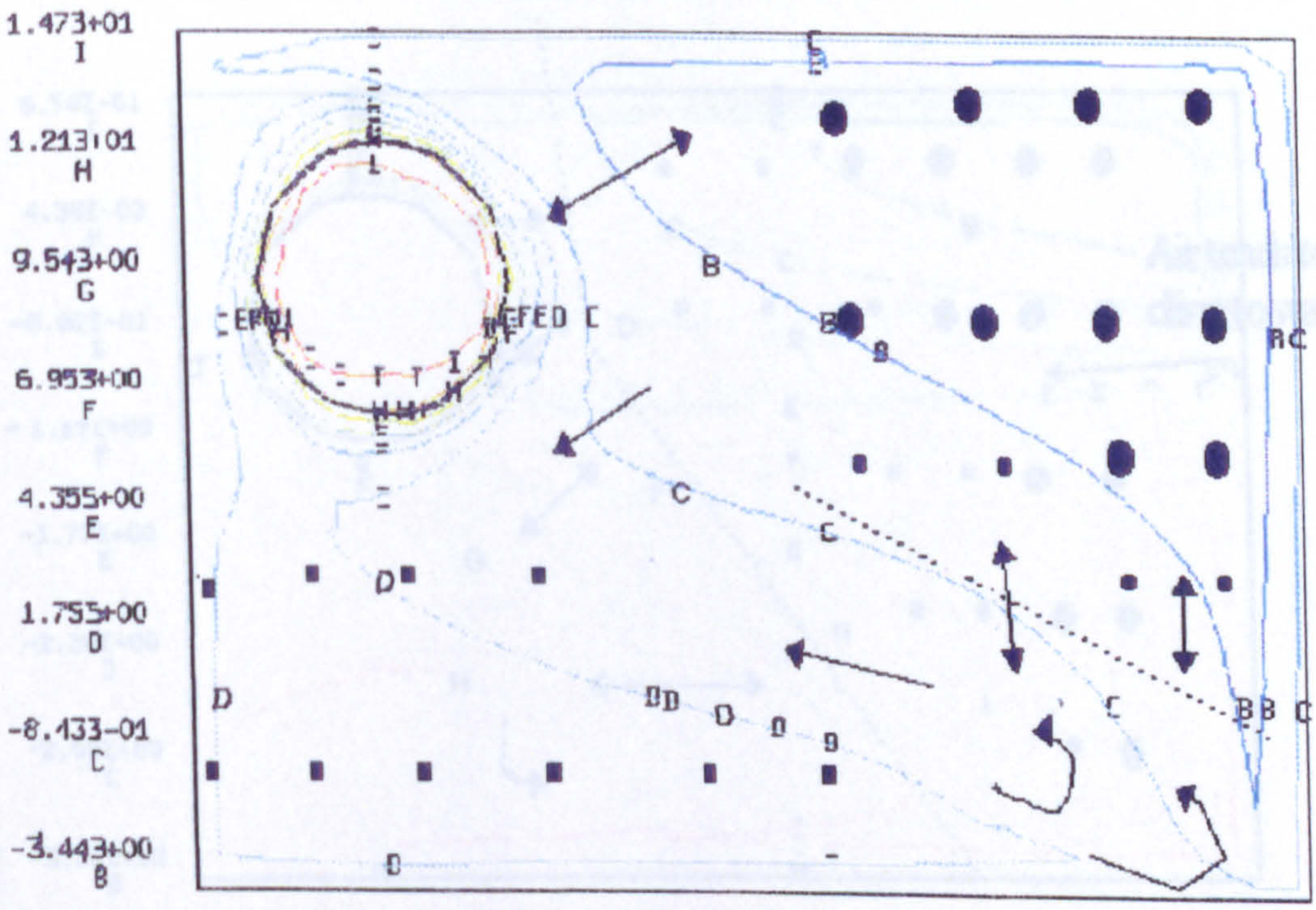

Figure 8-8 Section cc - 910 mm from the face

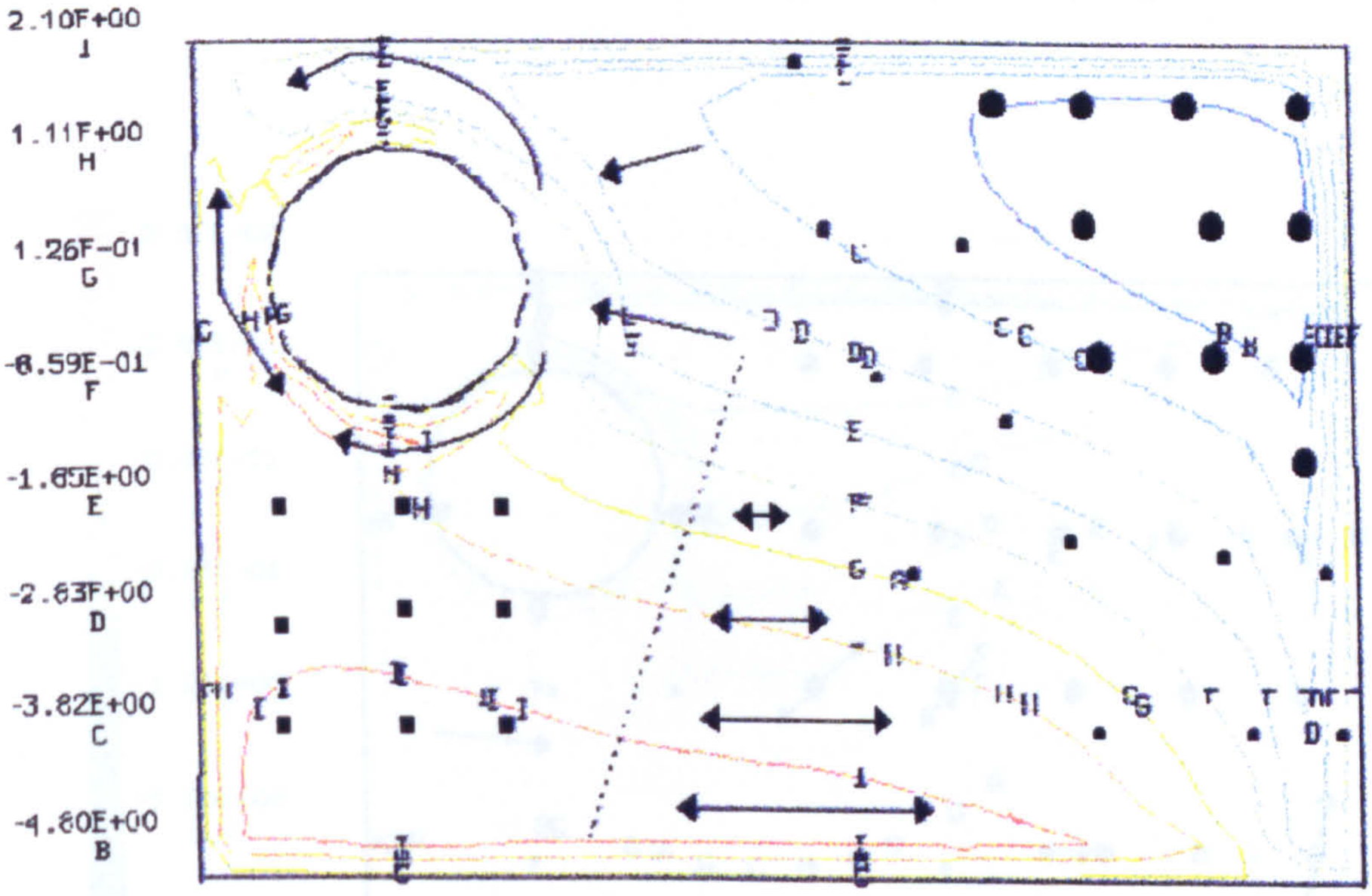

Figure 8-9 Section DD 1360 mm from the face

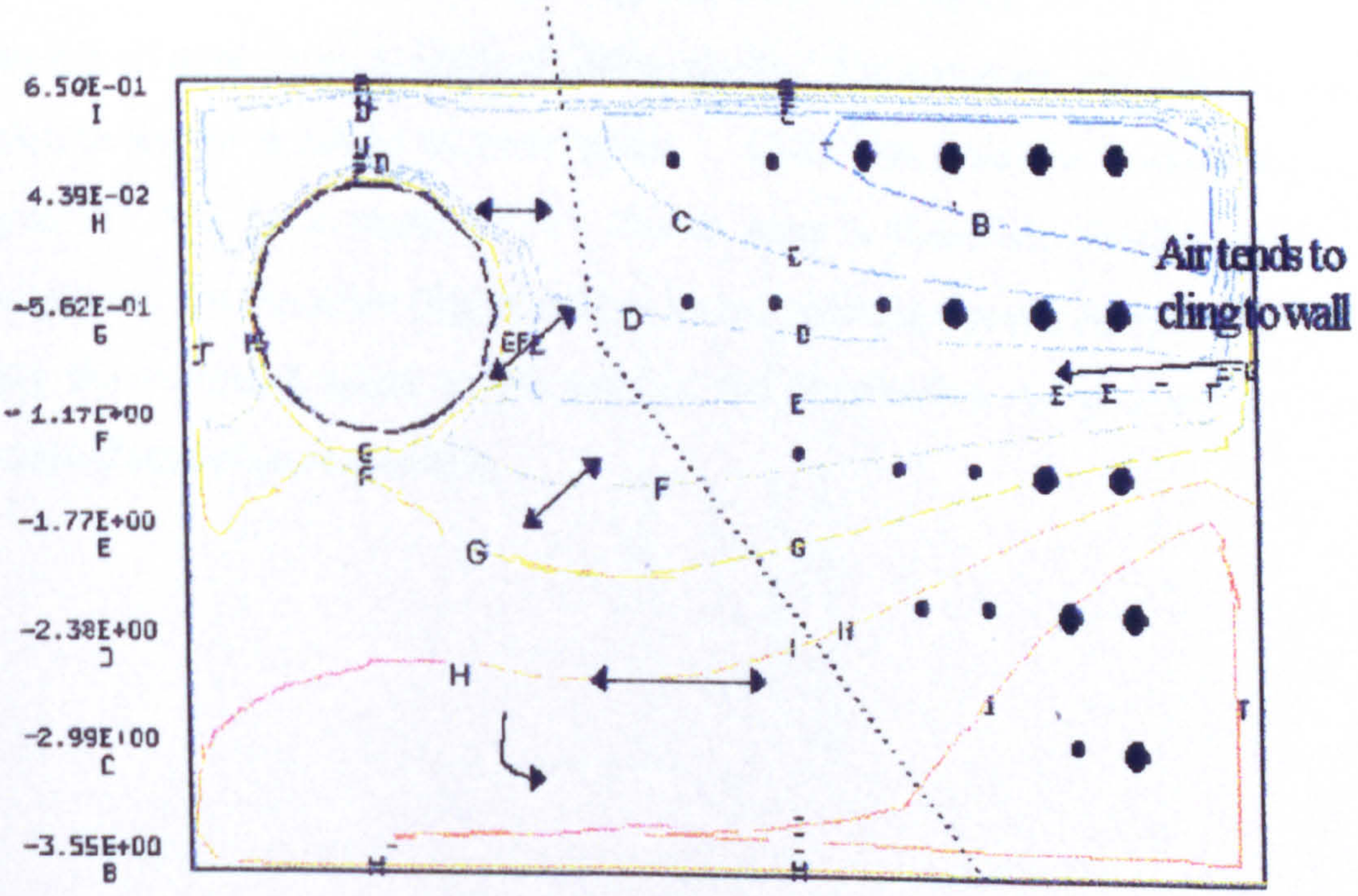

Figure 8-10 Section EE - 1360 mm from the face.

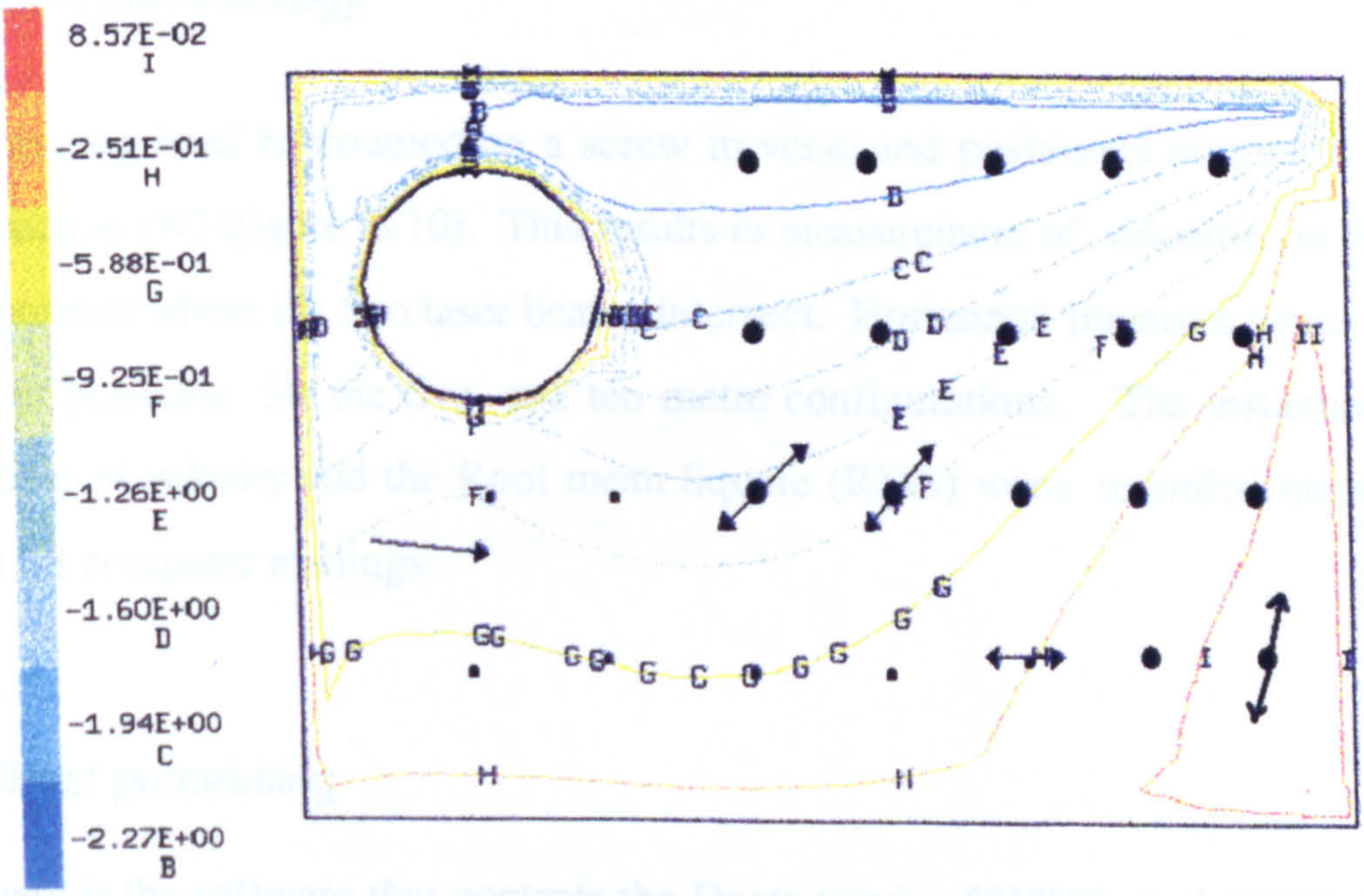

Figure 8-11 Section FF. - 890 mm behind discharge.

8.4 LASER DOPPLER ANEMOMETRY (LDA)STUDIES

8.4.1 LDA methodology

The measuring head is mounted on a screw traverse and positioned normal to the main flow direction (W) (figure 6.10). This results in measurement of velocities in the W and V components where the two laser beams intersect. Horizontal traverses were taken in a variety of positions for the five and ten metre configurations. The instantaneous W-component of velocity and the Root mean Square (RMS) were recorded manually as a backup for computer readings.

8.4.2 Post processing

Burstware is the software that controls the Dantec series 57HOO and 56600 traversing system and hence completely automates the flow field mapping. Statistical analysis (Fast Fourier Transforms, FFT) is conducted on the data obtained at a single traverse position to eliminate any erroneous readings (Appendix 6). The instant reading produced by the software are based on an average of 100 readings. The software actually obtains 20,000 measurements for a single traverse point. Once the data has undergone statistical analysis the data at a single point should have a Gaussian distribution. If the distribution is not Gaussian (figure 6.7) in nature then the spread (noise) is eliminated by cutting the abnormal values at the ends of the distribution to produce as close to a Gaussian distribution as possible

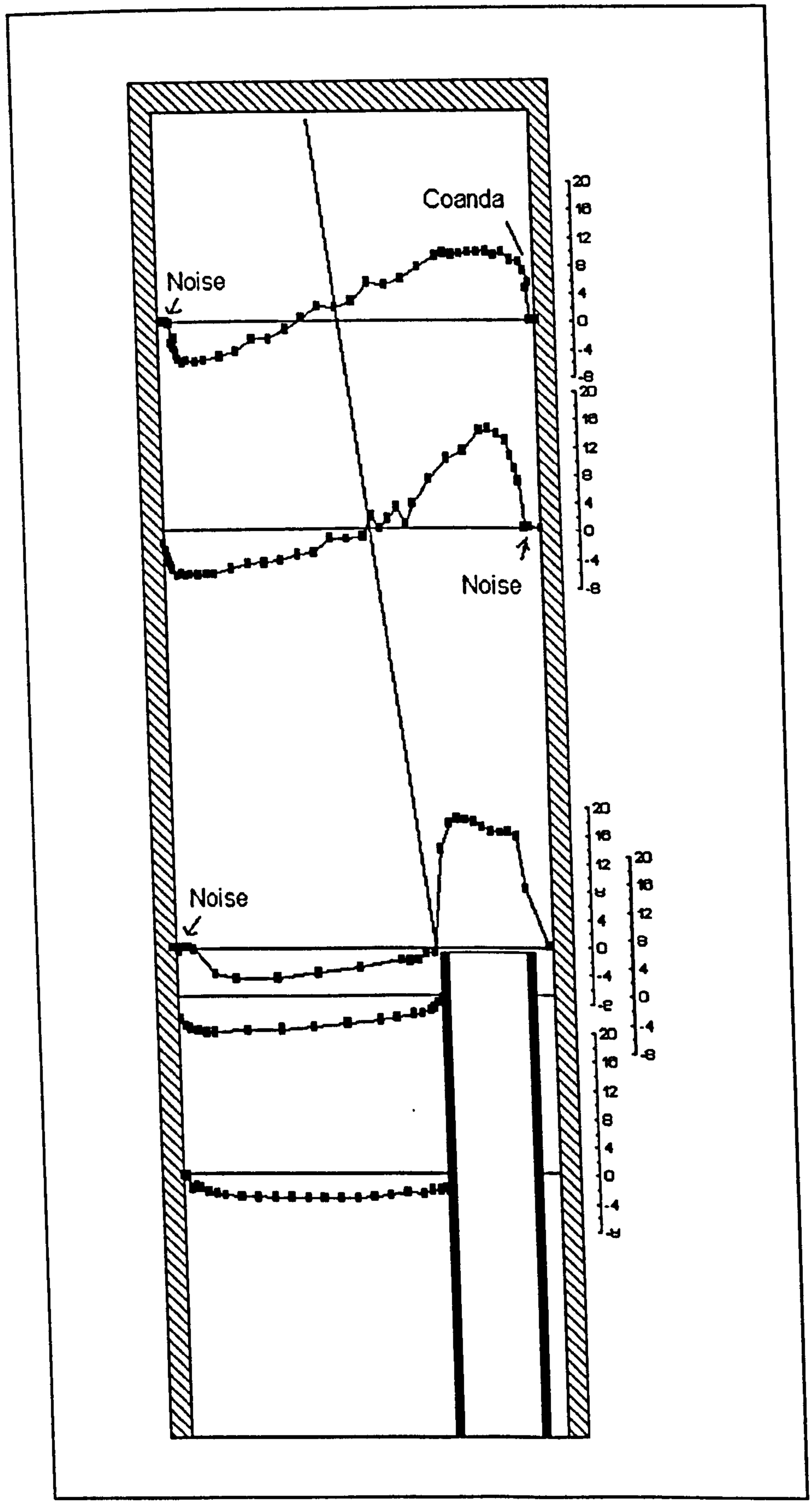

Figure 8-12 Profile of Velocities from LDA results - Duct centre.

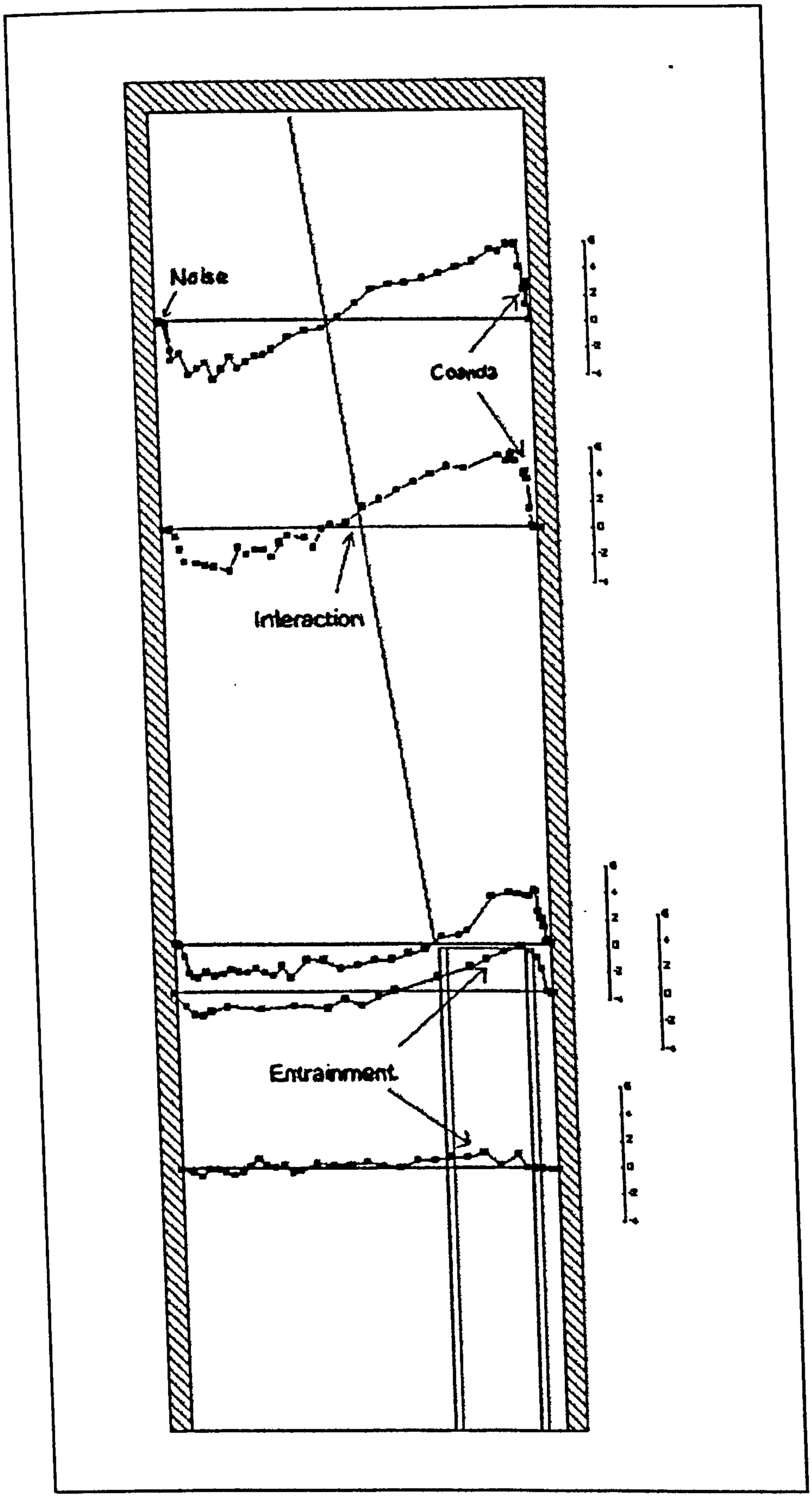

Figure 8-13 Profile of Velocities from LDA results - 82 mm from floor

8.4.2.1 *Discussion of 10 m configuration results*

Figures 8-12 and 8-13 illustrate the measurements obtained from the LDA study. The results are plotted on an outline of the scale model roadway with W-velocity represented by the scale (m/s) at the side. The jet can be seen to leave the duct outlet and propagate into the dead-end.

Both figures illustrate a number of points: 1) the interaction between the jet and the returning air. 2) the Coanda effect, 3) the entrainment of air underneath the duct (Venturi) and 4) possible sources of noise.

Three turbulence models were compared with LDA results and Table 8-1 summaries the merits of each. Generally the turbulence models predict the jet region for W-velocities quite well (figure 8-14, 8-16, 8-18, 8-24, 8-26, 8-28) with the k-ε RNG faring the best. Most of the predictions in this area agree to within 20% with some going as close as 5% in some areas.

At first glance the V-velocity[1] plots (figure 8-15, 8-17, 8-19, 8-21, 8-23, 8-25, 8-27, 8-29, and 8-31) appear to be very poor predictions. However, it should be noted that the variance in this area was very large. Figure 8-15 illustrates this with error bars of RMS on the actual measurements. The turbulence intensity in some areas was as high as 300%. During the experiment these high turbulence intensities were noticed. Thus in an attempt to demonstrate the excessive turbulence, some of these measurement were repeated three times over a period of two minutes. The resultant values varied by as much as 40% between each successive measurement. Hence the CFD model has a difficult task to accurately predict measurements with such high turbulence intensity.

[1] Standard k-ε model not illustrated because it did not model the flow any better than models presented.

The LDA measurement points marked on figure 8-14 demonstrate entrainment around the duct. The tendency for the air to cling to the walls is illustrated in figure 8-15, 8-17 with the negative V-velocity values indicating a bias toward the lower portion of the drivage and a positive value a bias to the roof.

The LDA measurements (figure 8-16) appear to be off-line. This may be due to a movement or a misalignment of the measuring head. Another possible source of error for *stray* measuring points may be due to laser power fading during the measuring process. It should be noted that most of these rouge measurement points have been eliminated during processing.

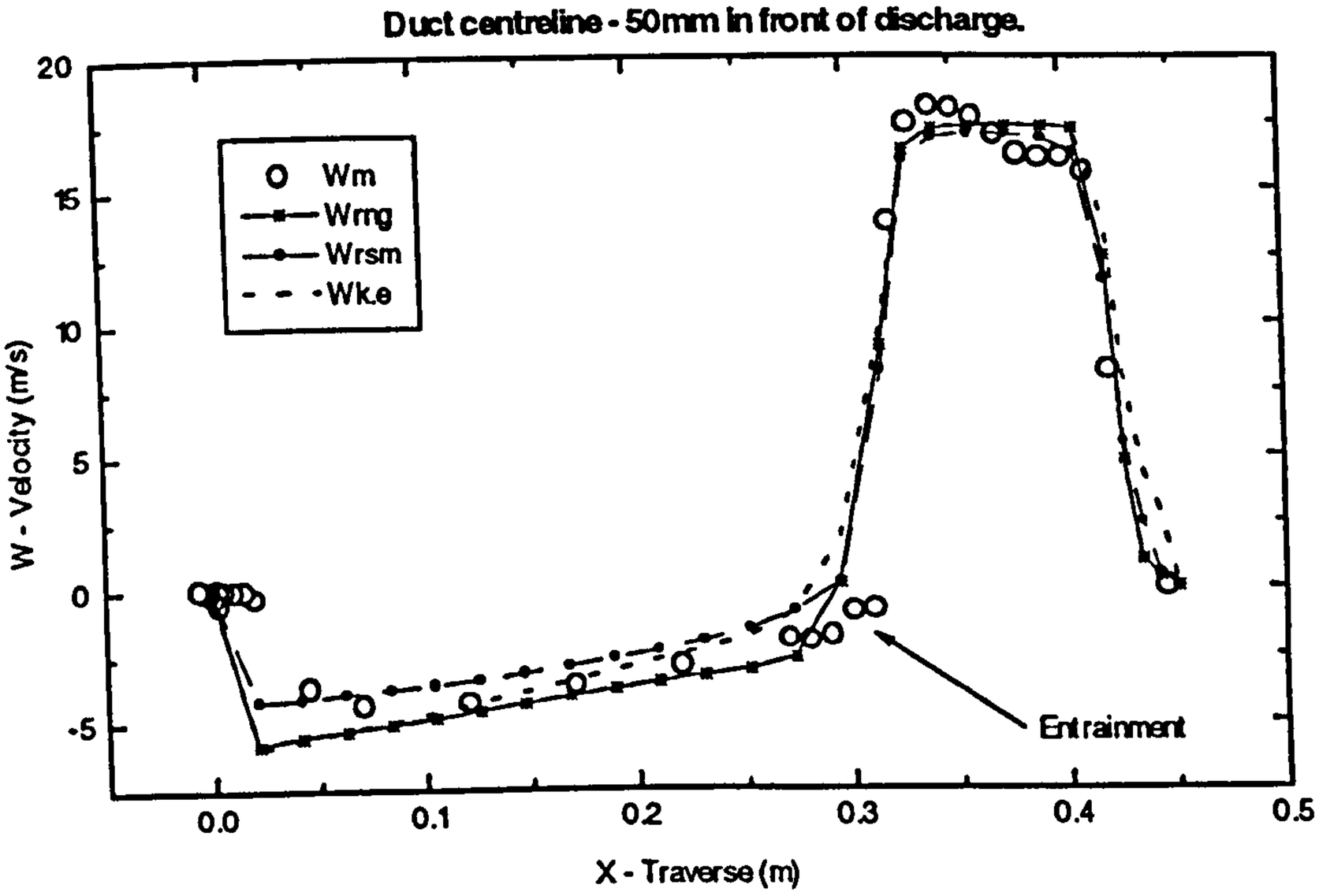

Figure 8-14 Duct Centre at 50 mm from the discharge (W - velocity)

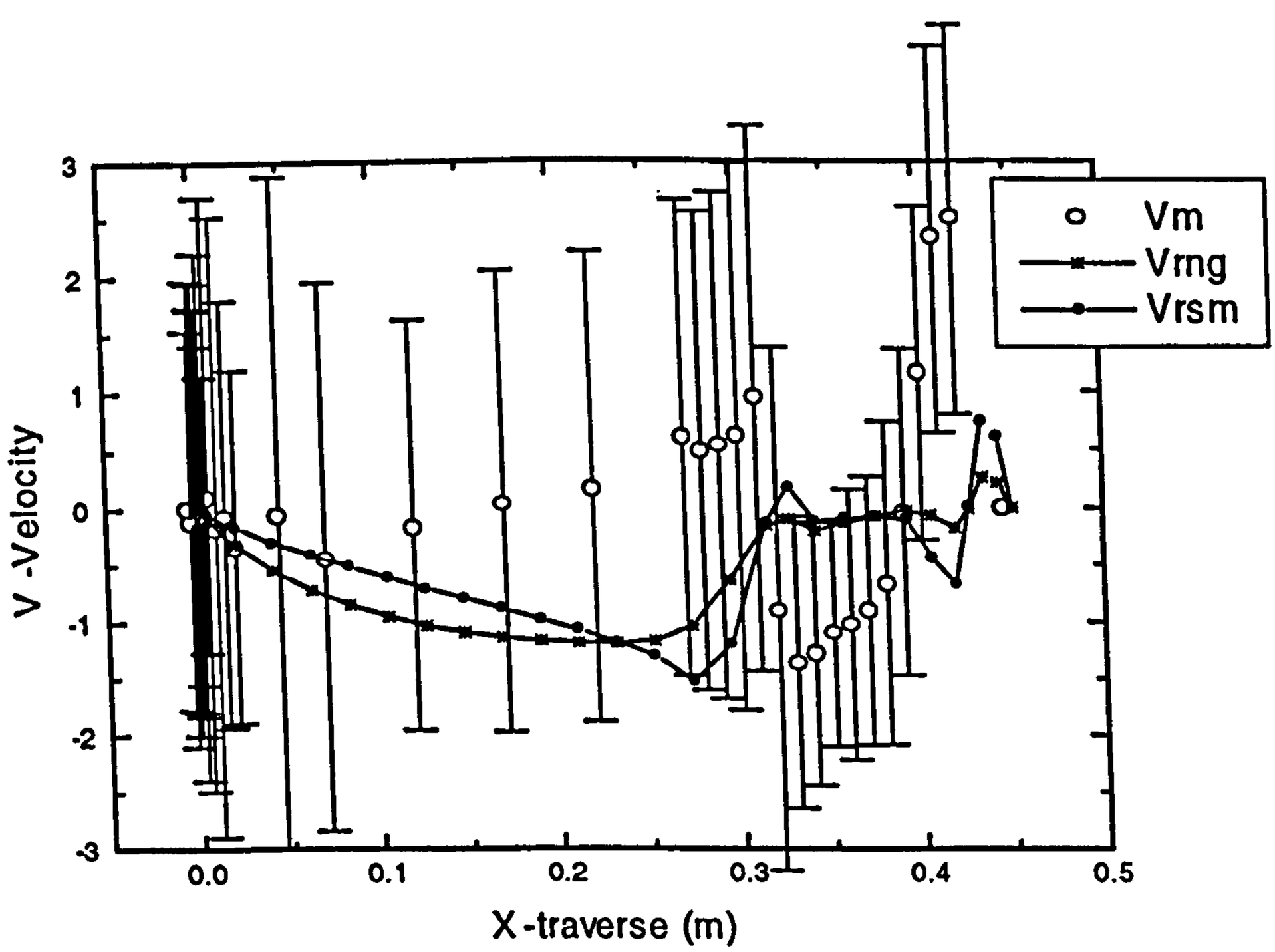

Figure 8 -15 Duct Centre at 50 mm from the discharge (V - velocity)

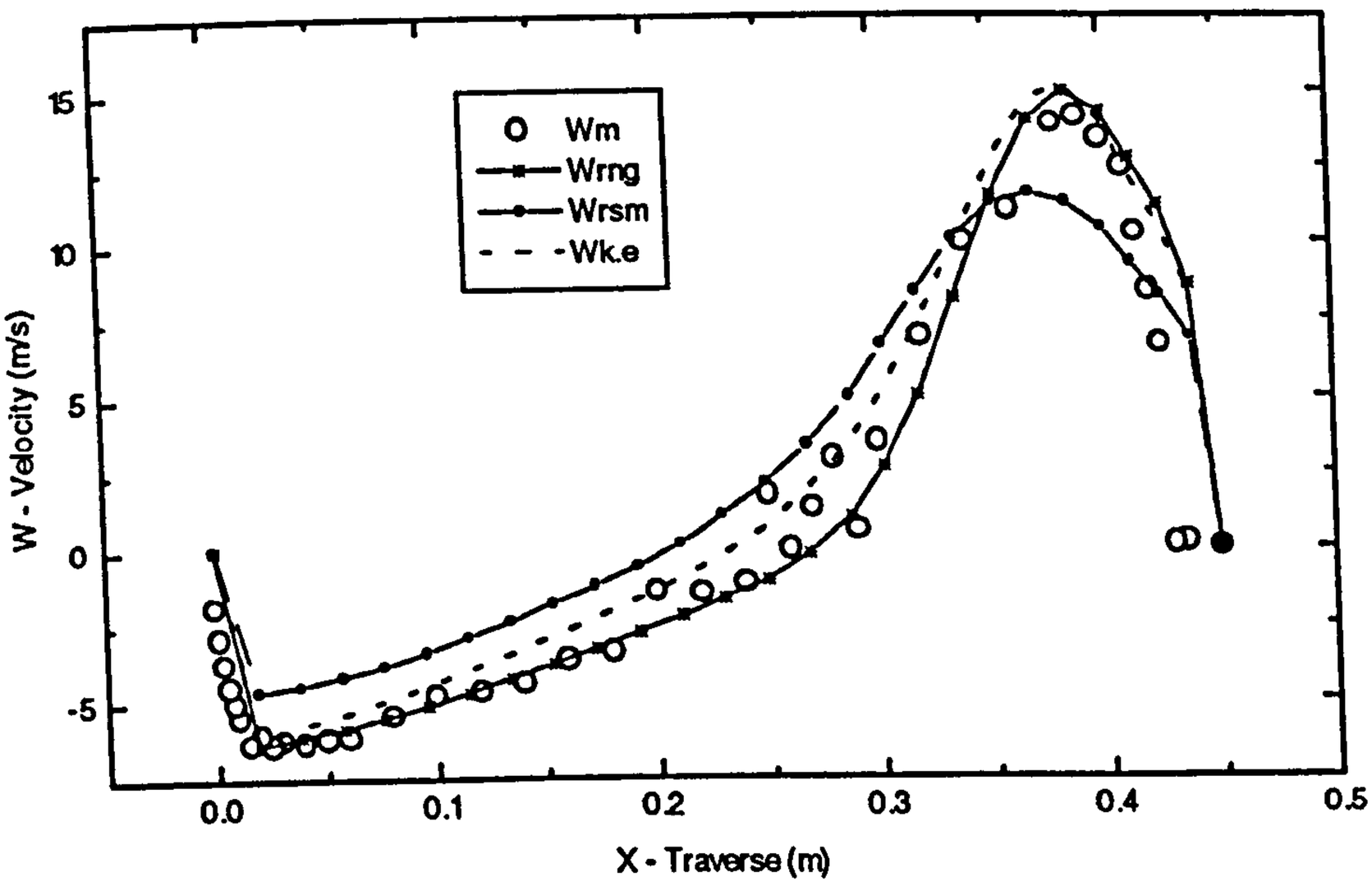

Figure 8-16 Duct Centre at 500 mm from the discharge (W - velocity)

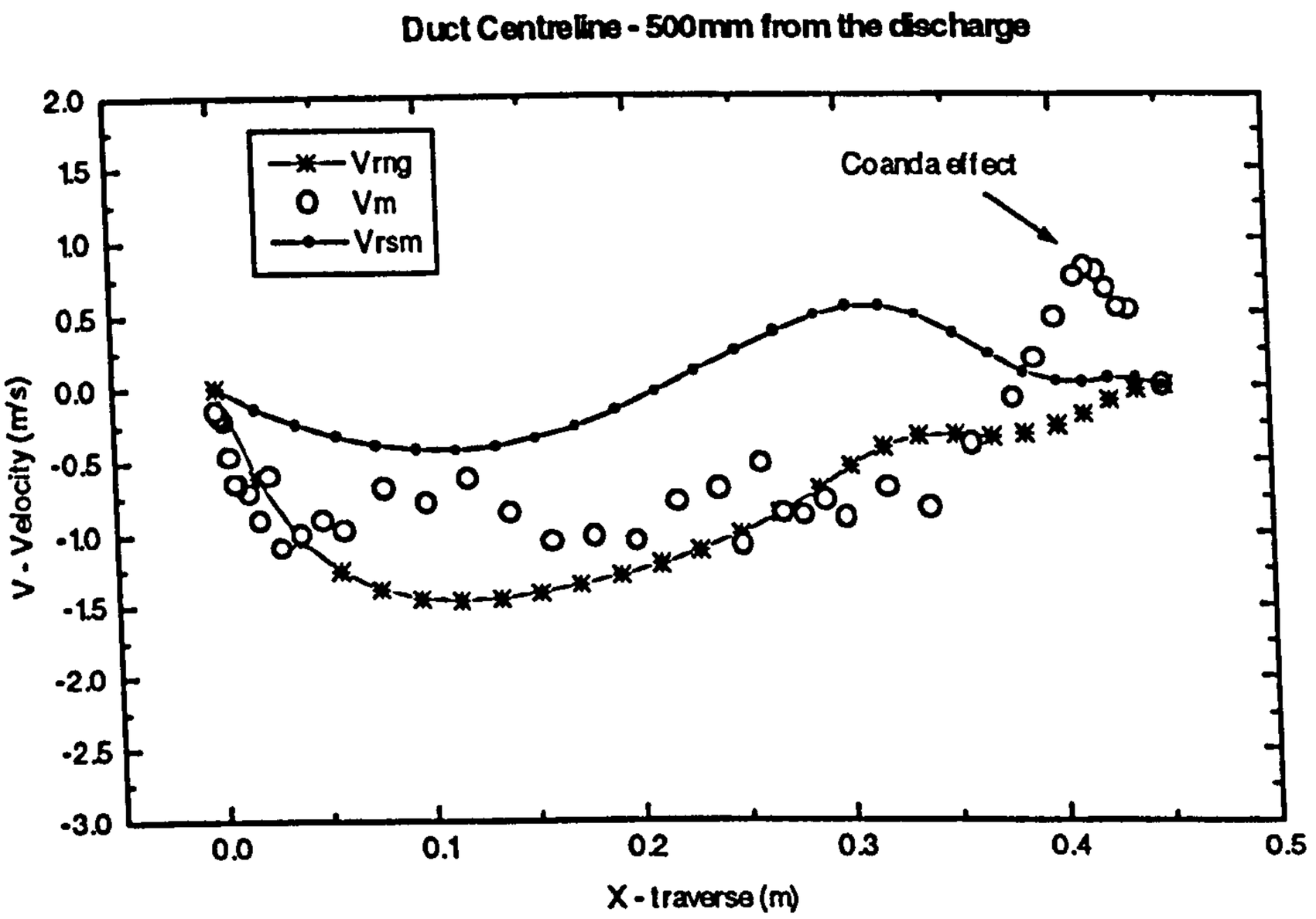

Figure 8-17 Duct Centre at 500 mm from the discharge (V - velocity)

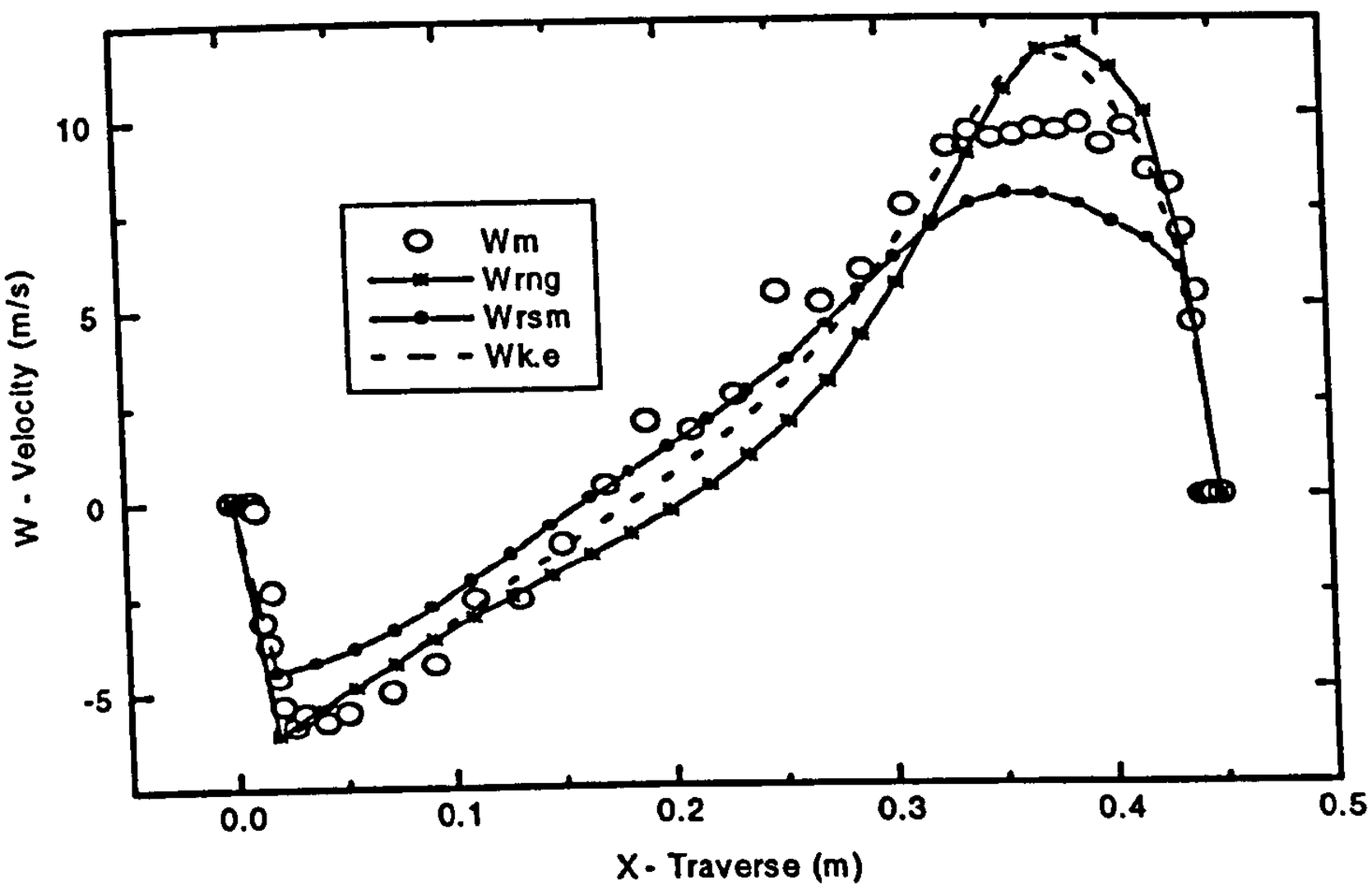

Figure 8-18 Duct Centre at 750 mm from discharge (W - velocity).

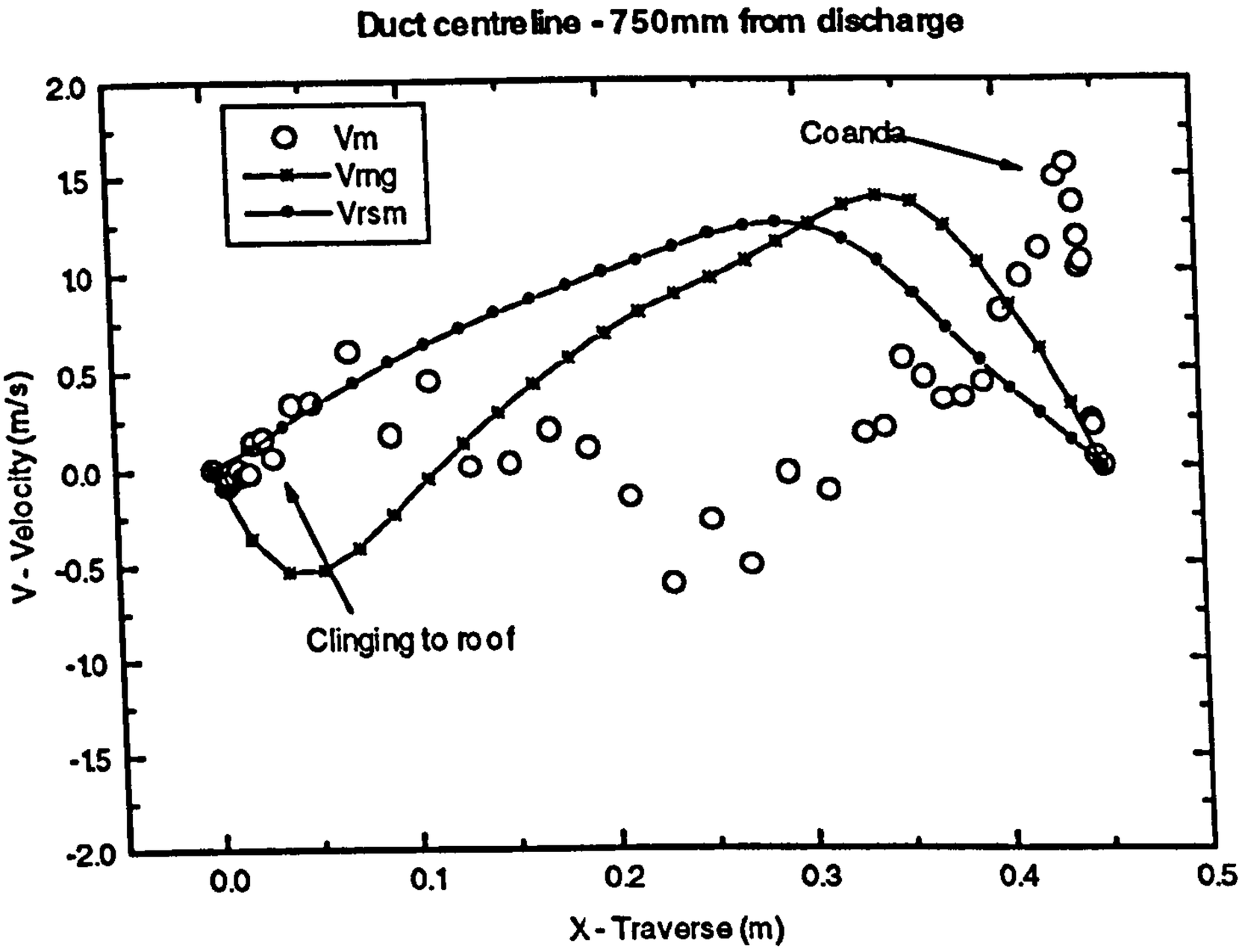

Figure 8-19 Duct Centre at 750 mm from discharge (V-velocity).

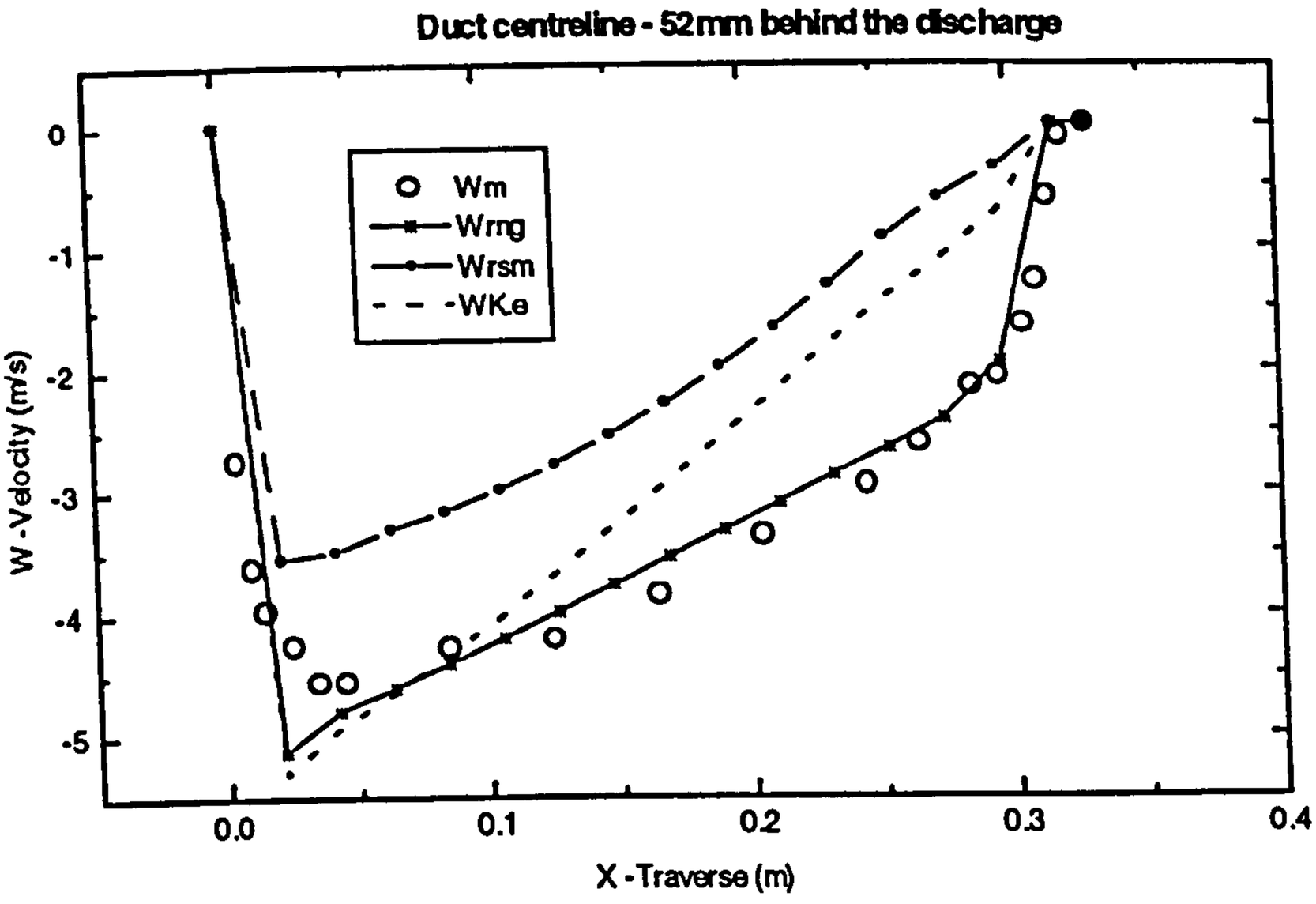

Figure 8-20 Duct Centre at 52 mm behind the duct discharge (W - velocity)

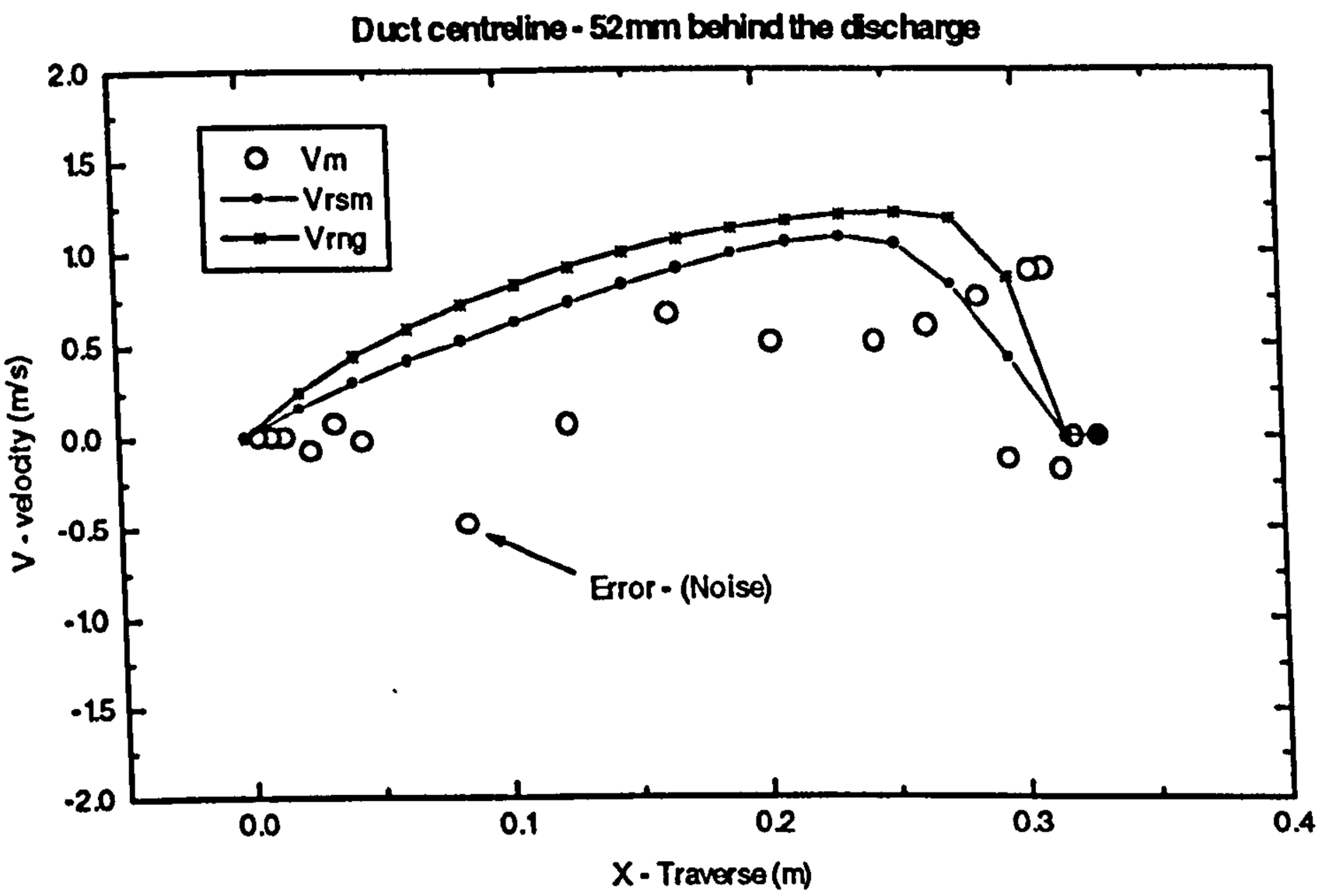

Figure 8-21 Duct Centre at 52 mm behind the duct discharge (V - velocity)

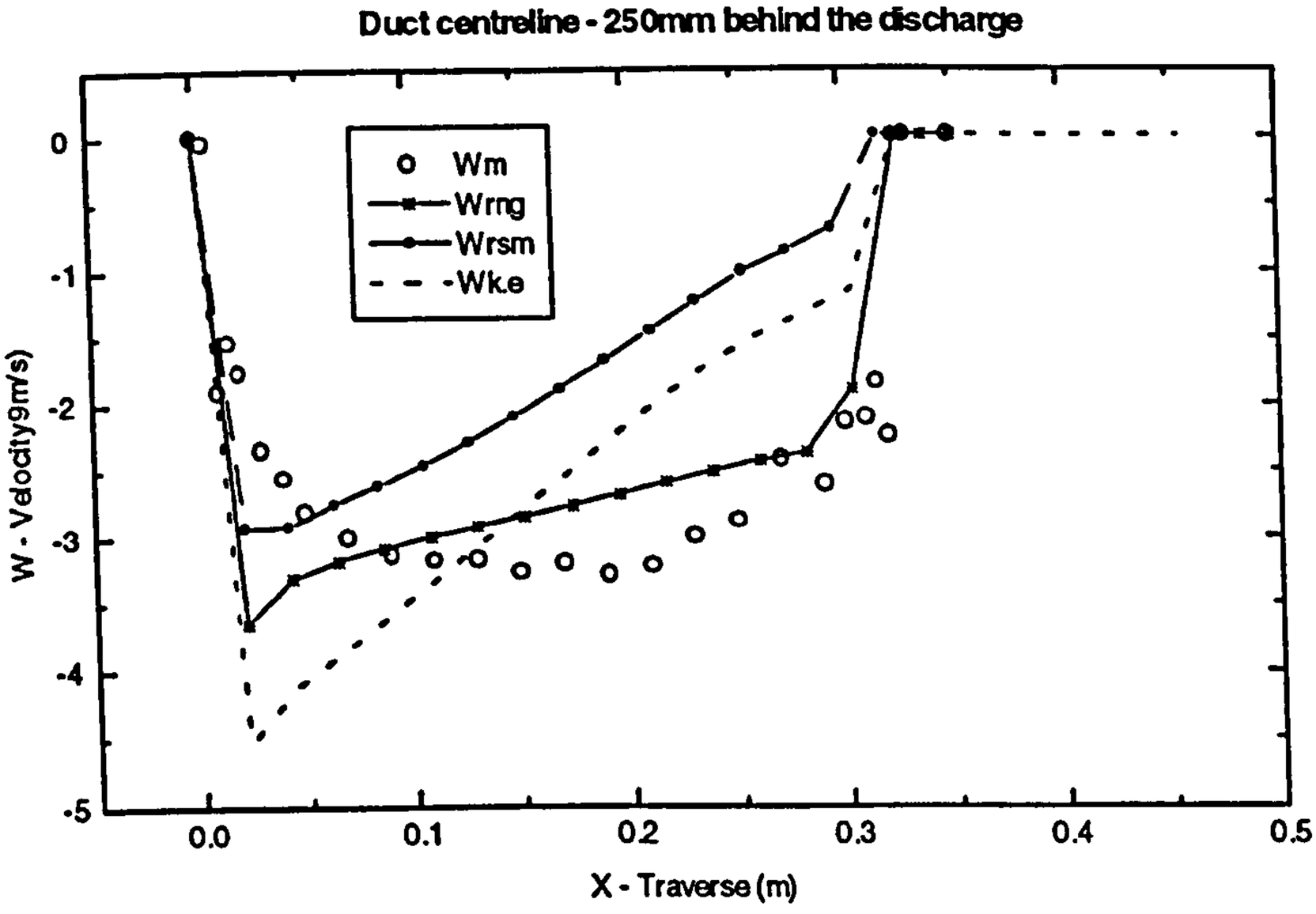

Figure 8-22 Duct Centre at 250 mm behind the discharge (W- velocity)

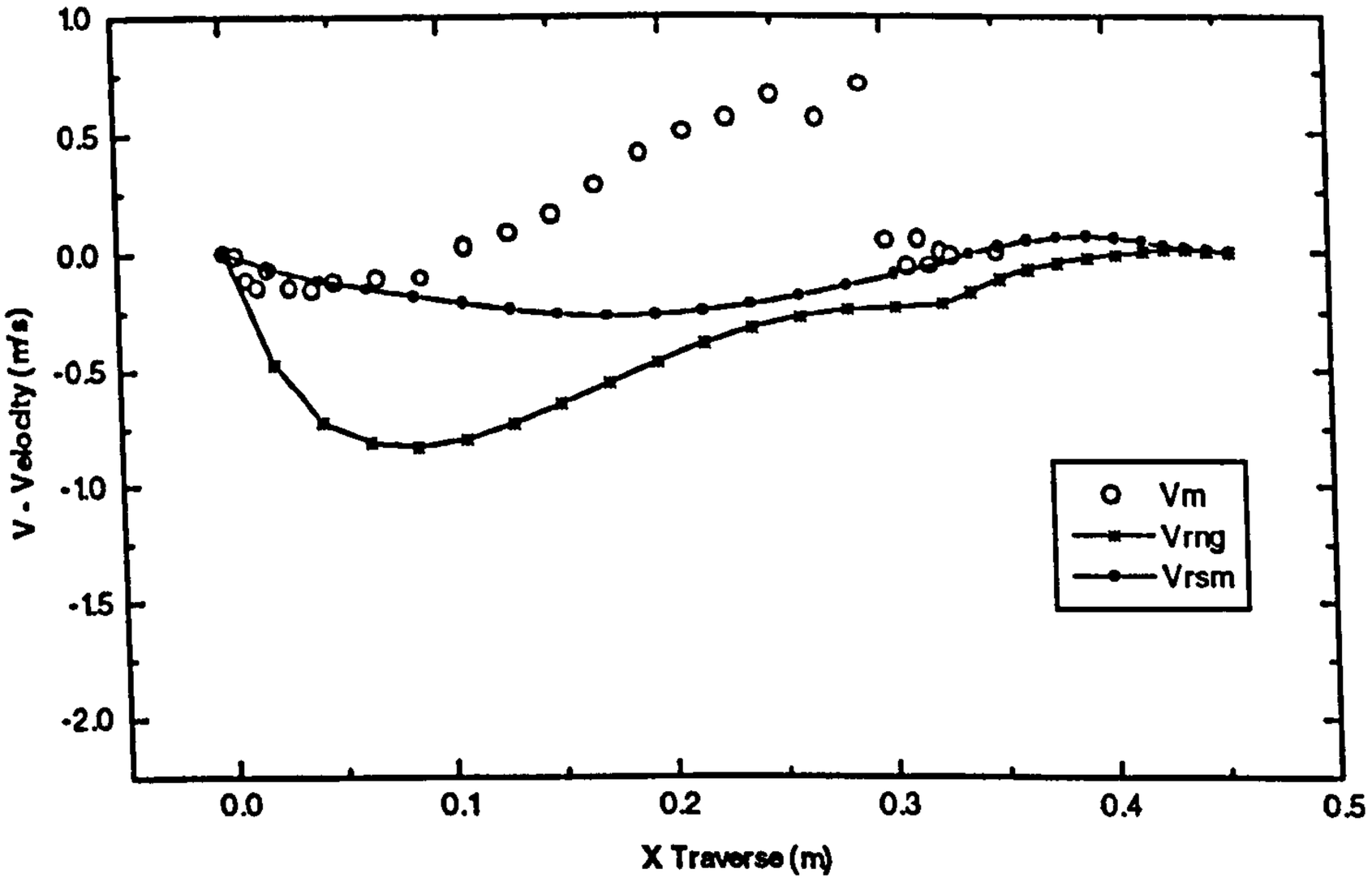

Figure 8 -23 Duct Centre at 250 mm behind the discharge (V- velocity)

Predictions for the area behind the duct (figure 8-20, 8-22) do not match the measurements as well as the flow in the jet region. The gradients seem to be a little too steep on the left side. This may be due to inadequate grid spacing near the wall.

The simple k-ε predicts the flow well in some areas. However, due to the fact that this model assumes homogenous turbulence, it can not be considered to model accurately in three dimensions.

In general the k-ε RNG turbulence model predicts the flow in the upper portion of the roadway better than the other models. Whereas the RSM model predictions for the lower region produces a superior degree of accuracy. Overall the RNG produces better results when compared with the other models. All the models in Figure 8-22 indicate that the air leaves the left side of the roadway where the experiments suggest that the air tends to drift to the right. This is probably due to the fact that CFD has difficulty in picking up turbulent structures that predominantly travel at 45^0 or greater. (Freitas, 1995). This may be due to three factors, i) the Power law differencing scheme is susceptible to numerical diffusion effects. These effects are predominant when the flow is aligned at 45 degrees to the grid lines and when there are significant gradients in the direction normal to the flow. ii) the grid spacing close to the wall may not be have an adequate resolution to eliminate the steep gradient. iii) the wall function.

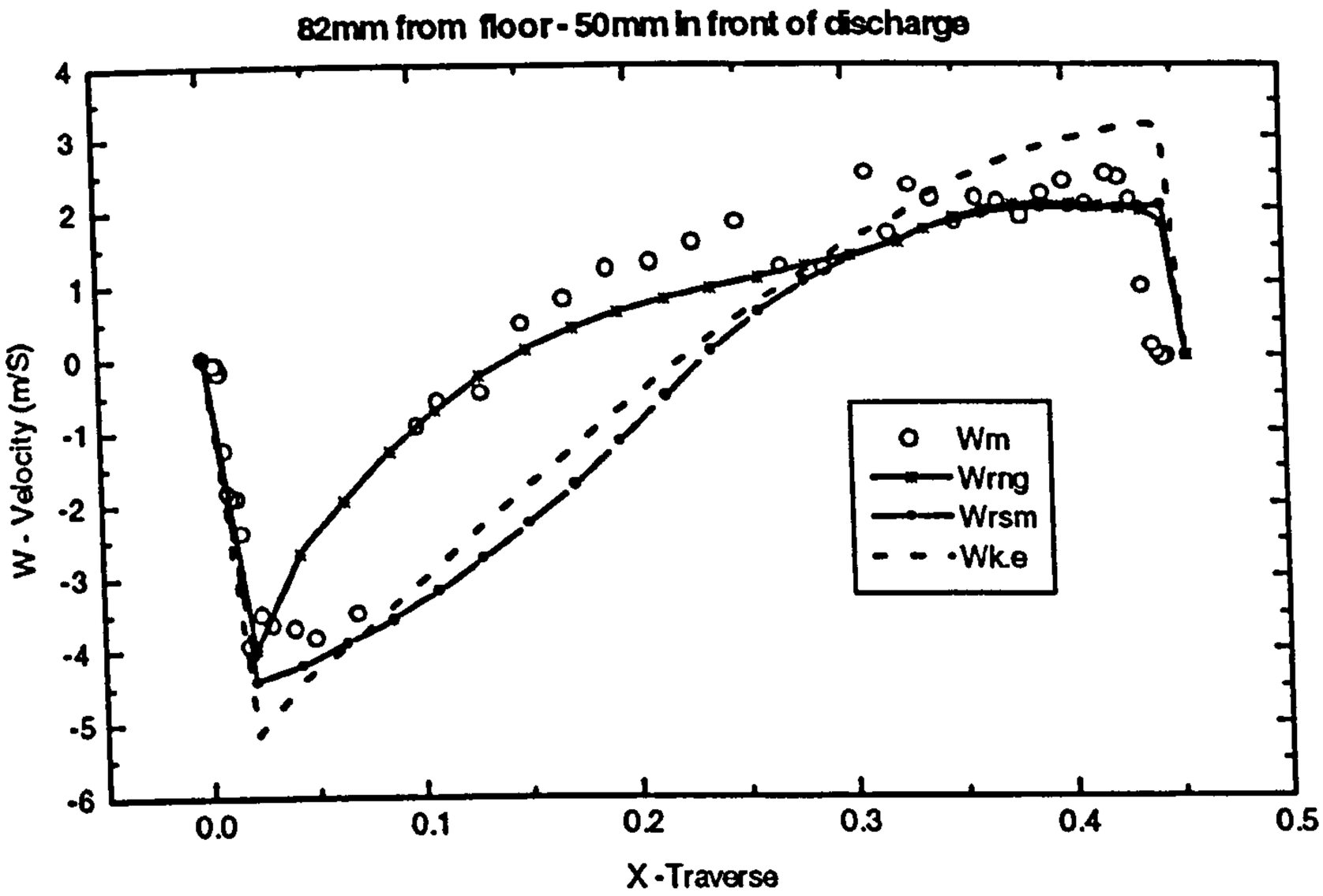

Figure 8-24 82 mm from the floor and 50 mm from discharge (W-velocity)

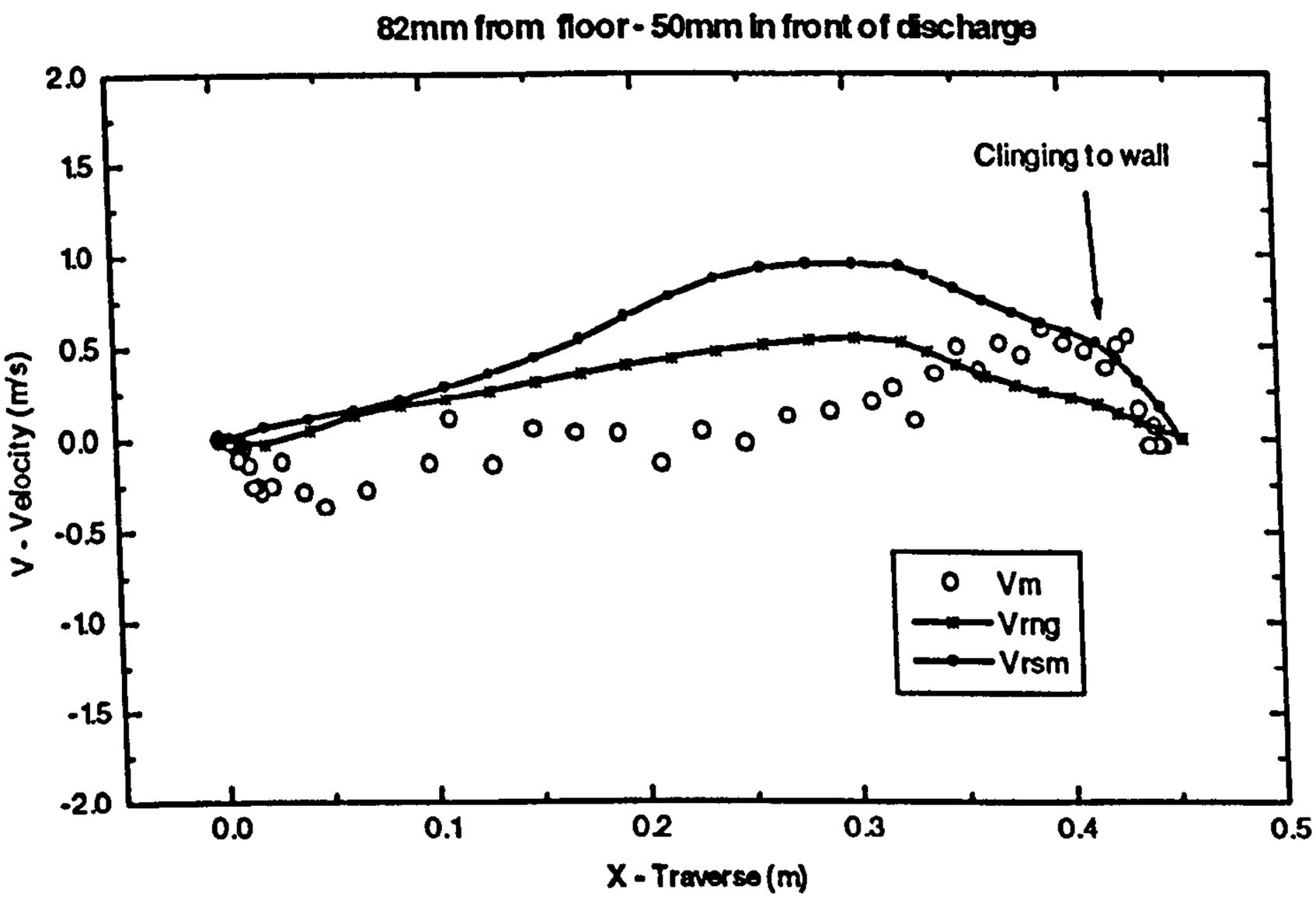

Figure 8-25 82 mm from the floor and 50 mm from discharge (V-velocity)

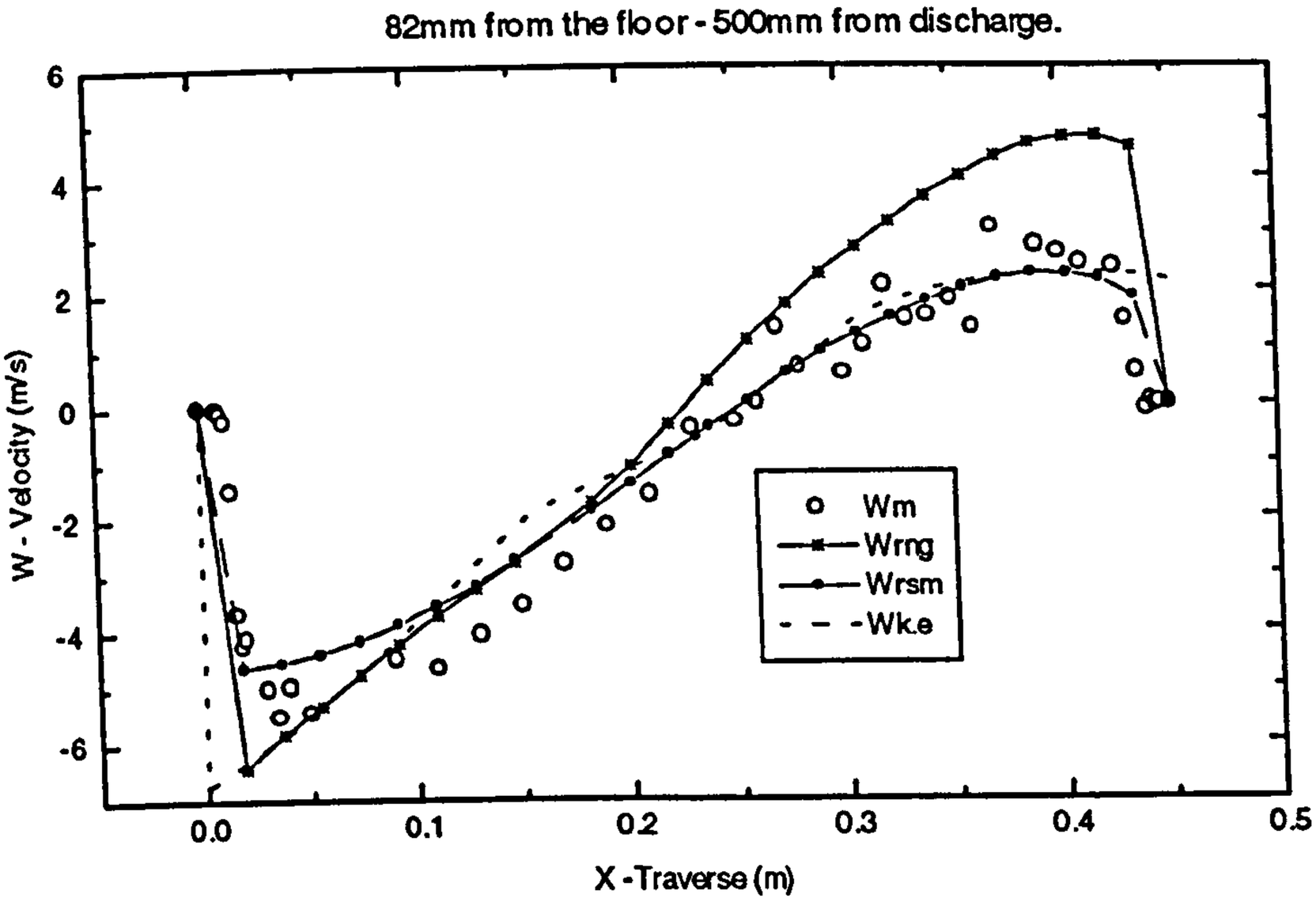

Figure 8-26 82 mm from the floor and 500 mm from discharge (W-velocity)

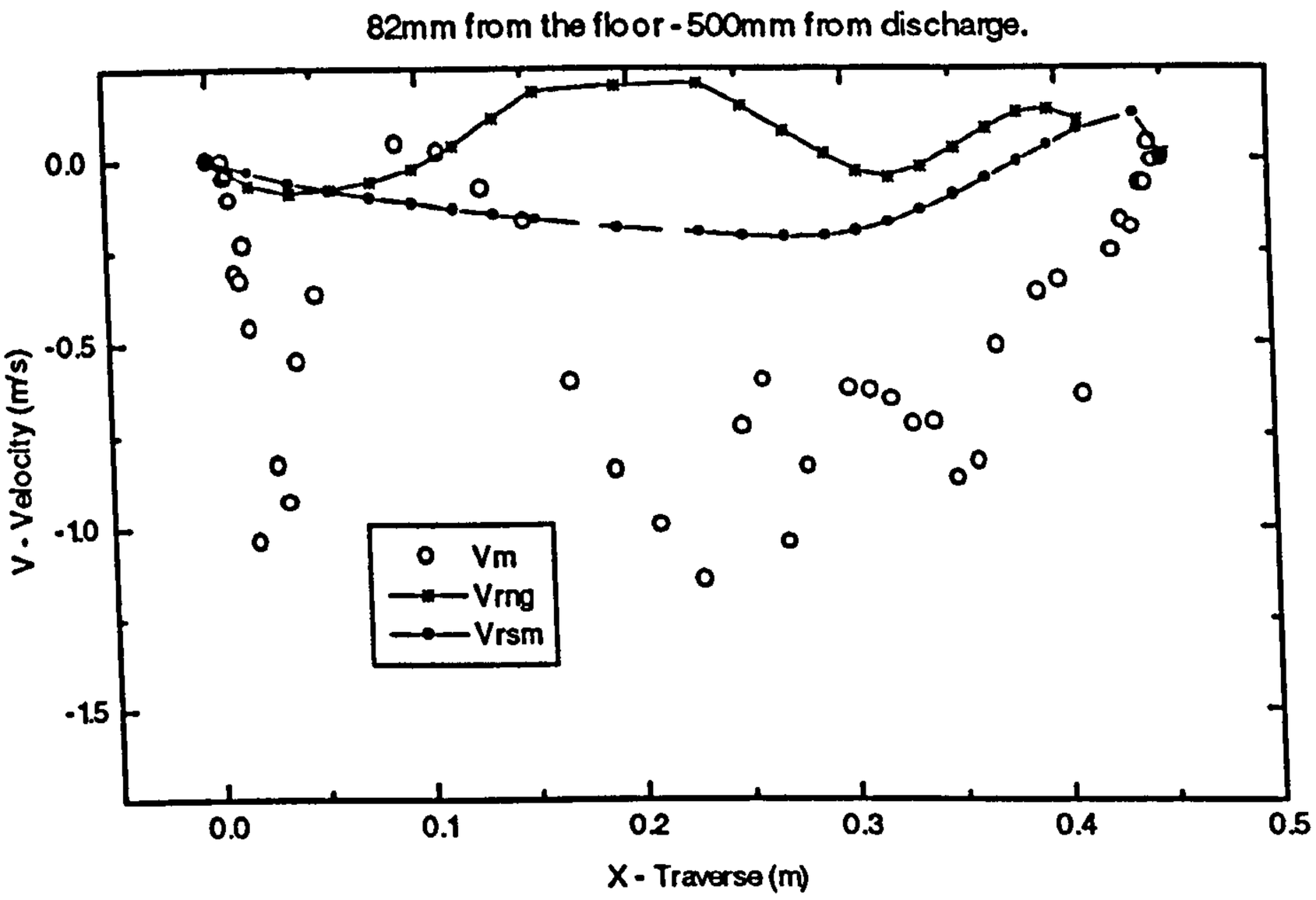

Figure 8-27 82 mm from the floor and 500 mm from discharge (V-velocity)

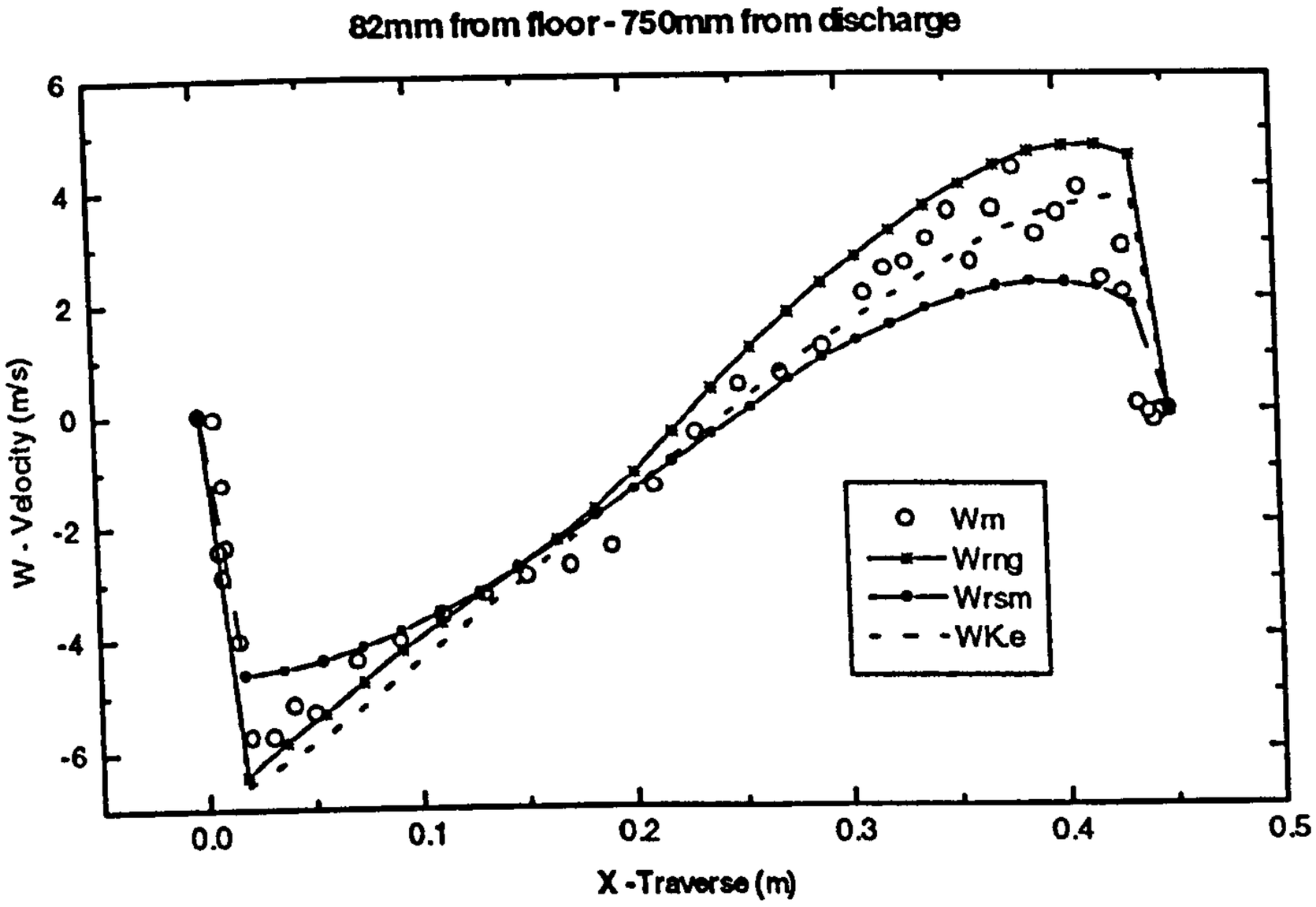

Figure 8-28 82 mm from the floor and 750 mm from discharge (W-velocity)

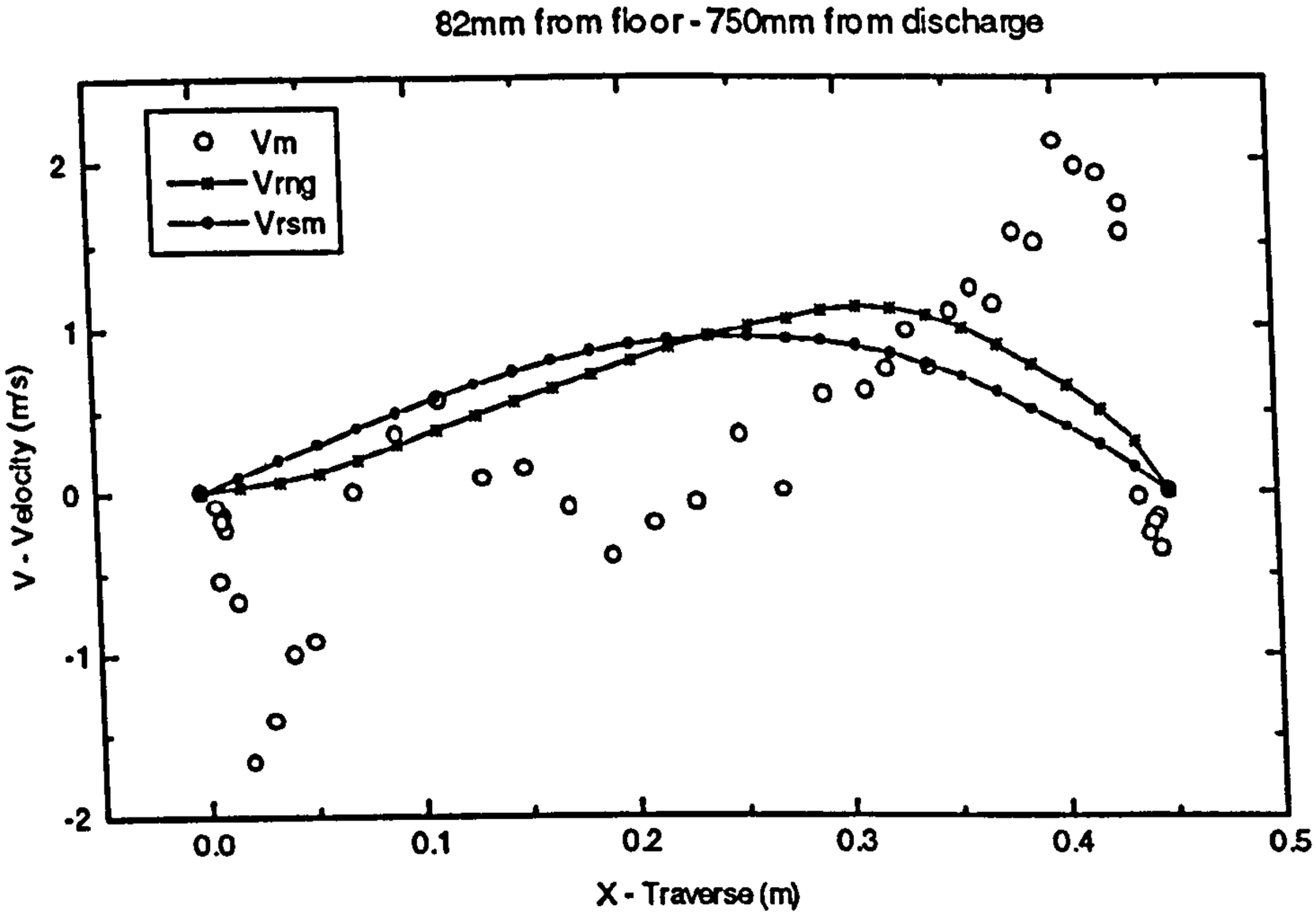

Figure 8-29 82 mm from the floor and 750 mm from discharge (V-velocity)

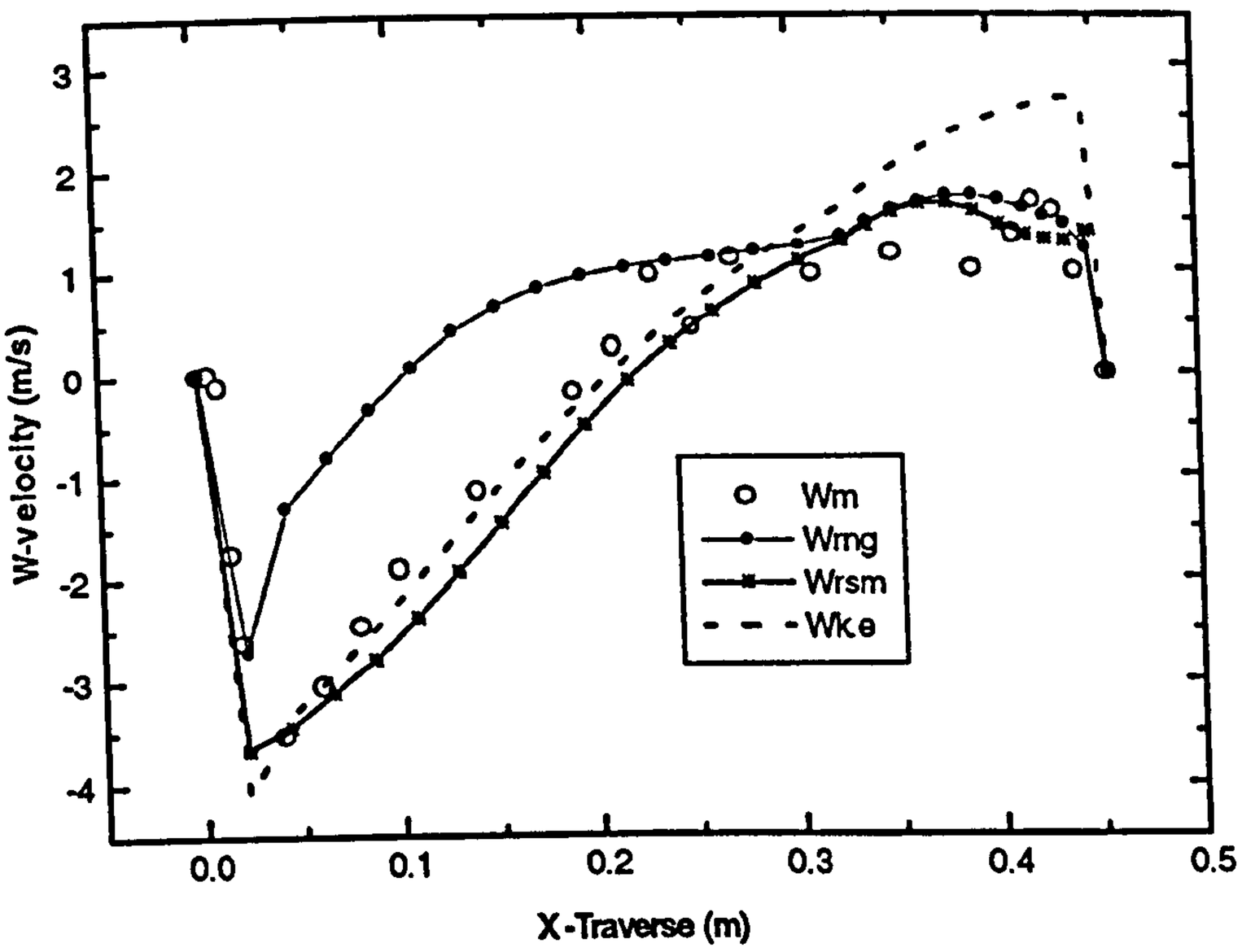

Figure 8-30 82 mm from the floor and 52 mm behind the discharge (W-velocity)

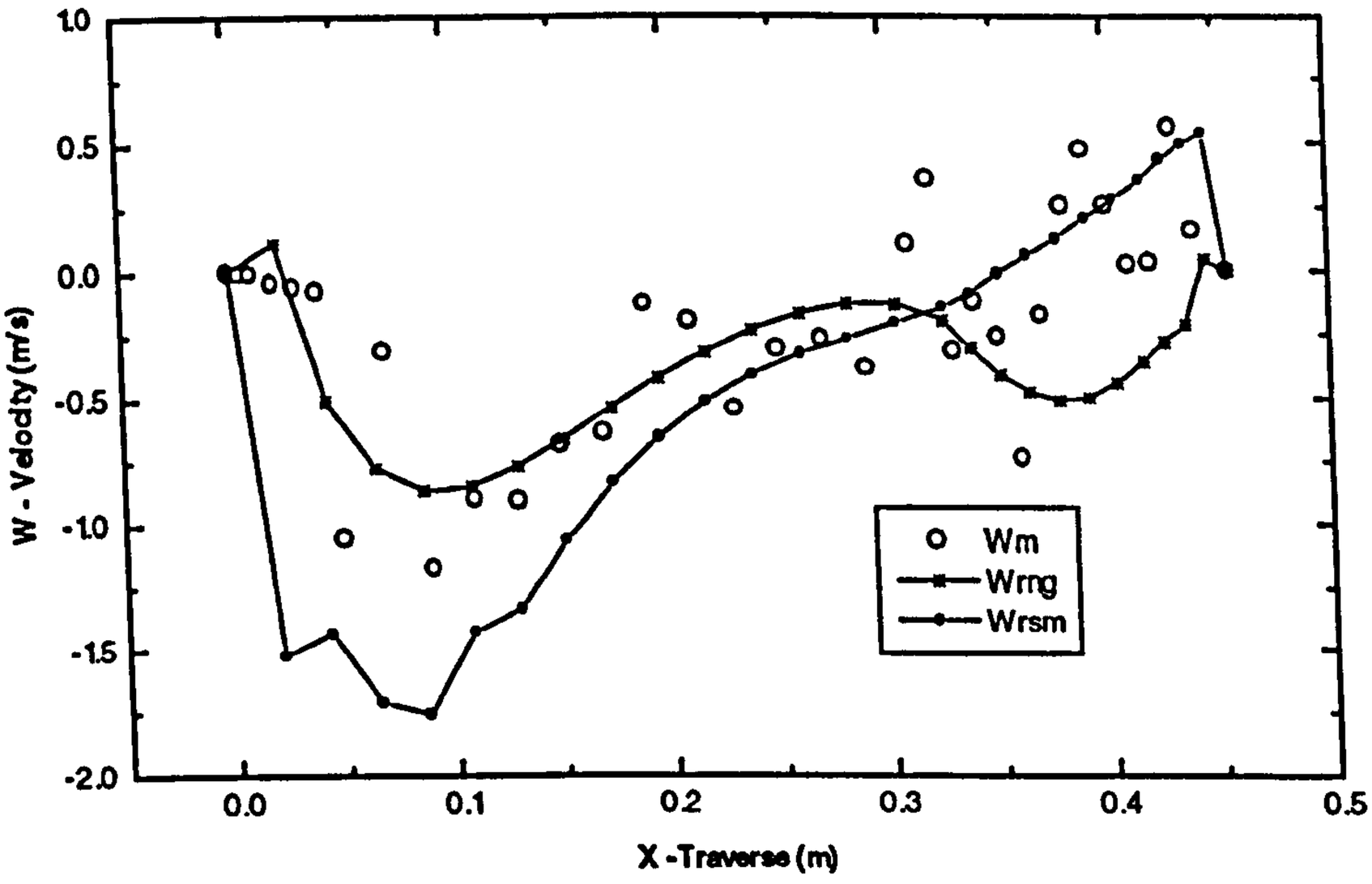

Figure 8-31 82 mm from the floor and 250 mm behind the discharge (W-velocity)

Table 8 -1 - Summary of CFD comparisons with LDA results.

Figure numb-er	standard k-ε	k-ε RNG	RSM	Comments
8-14(W)	Good	Good	Good	All models predict flow quite well with a sight over prediction for k-ε and the RNG models. However the RSM does not pick up the entrainment as well as the RNG
8-15 (V)	poor	Poor	Poor	Models predict general Ch . It should be noted that the RMS. in this region is between 1.5-2.5 indicating frantic oscillating of the air since actual values are between 0 -1.5. Both models over predict.
8-16 (W)	good	Very Good	Satisfactory (Sat)	RNG clearly giving the best prediction. RSM under predicts.
8-17 (V)	poor	Satisfactory	Poor	RNG best but fails to predict a bias toward wall on the right hand side.
8-18 (W)	Sat	Sat	Sat	RNG over predicts at jet centre while RSM under predicts.
8-19 (V)	poor	Poor	Poor	In most cases RMS. values higher than actual value indicating a very turbulent region.
8-20 (W)	Poor	Very Good	Very Poor	Gradient on RNG model a little steep otherwise very good - possible due to wall function.
8-21 (V)	poor	Sat	Sat	Good predictions for high RMS. values
8-22 (W)	very Poor	Sat	Very Poor	All models predict air leave via the left hand side when in fact it tends to move to the right hand side of the roadway.
8-23 (V)	poor	very poor	Poor	
8-24 (W)	Poor	Good	Poor	RNG predicts the phenomena quite well.
8-25 (V)	poor	Sat	poor	High RMS. in relation to small values.
8-26 (W)	Sat	poor	Good	RNG over predicts in Jet region where air is very turbulent
8-27	poor	Poor	Poor	Very turbulent region with high RMS. values.

(V)				
8-28 (W)	Good	Good	Good	RNG slight over prediction with RSM under predicting
8-29 (V)	poor	Poor	Poor	Does not predict features such as the bias of the flow toward the walls.
8-30	Sat	Very Poor	Good	RSM clearly producing the best prediction.
8-31	Very poor	Sat	Sat	RSM predicts the entrainment where the RNG does not. However RNG better in other region.

8.4.2.2 *Discussion of 5m configuration.*

The standard k-ε turbulence model was not used to for this configuration because the previous set and the literature suggest it cannot model three dimensionality very well. The k-ε RNG model predicted the general characteristics for most of the cases (figure 8-32 to 8-36). However, the actual predicted velocity values were not as accurate as the previous set of simulations obtained from the 10m configuration. This is probably due to high turbulence levels caused by the jet bouncing off the face. It should be noted that a large percentage of the measured values on the left hover around zero (figures 8-32 -8-34) with typical RMS values of 2.5.

The maximum velocity in the jet region was modelled by the k-ε RNG model to within fifteen percent (figure 8-32 to 8-34) for all cases. The RSM model did not predict the flow as well as the RNG model.

The LDA measurements indicated very high turbulence intensity from 0 metres to 0.25m from the left edge. Almost all the measured velocities in this region for 8-32 to 8-34 were +/- 1 m/s and in most cases were less than 0.5 m/s with RMS in the range of 1.3 - 2.2. This indicates that the turbulence intensity of this region is very high (100-300%). Hence as demonstrated earlier the model has difficulty in modelling flow with excessive turbulence intensity.

The predictions for the area behind the duct do not predict the actual characteristic very well (figures 8-35, 8-36). The model predicts that the majority of the air leaves via the top. This is demonstrated by the high negative values in figure 8-35 whereas the experimental results suggest that the majority of air leaves via the bottom of the roadway (figure 8-36).

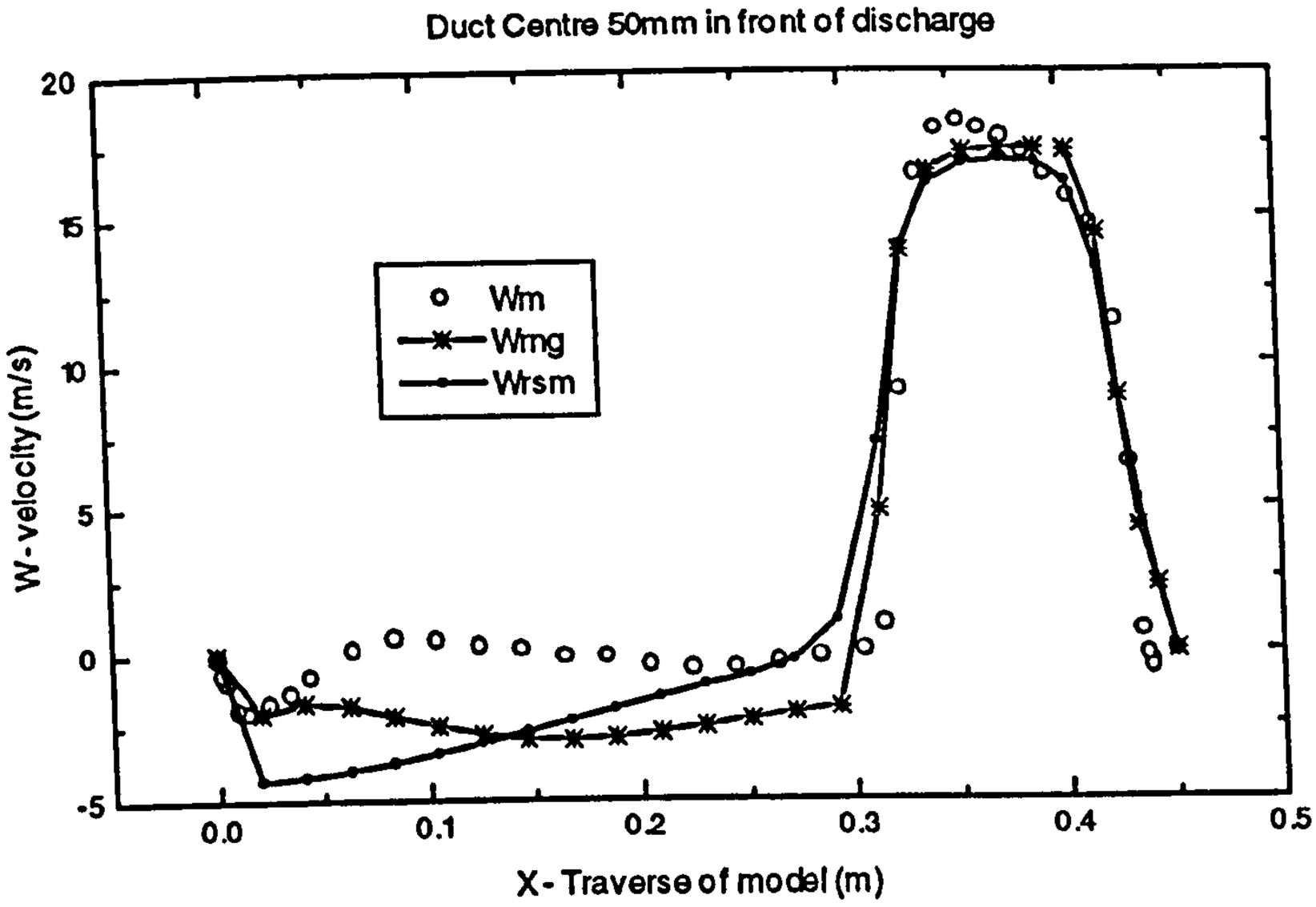

Figure 8-32 Duct centre at 50 mm form discharge (W-velocity)

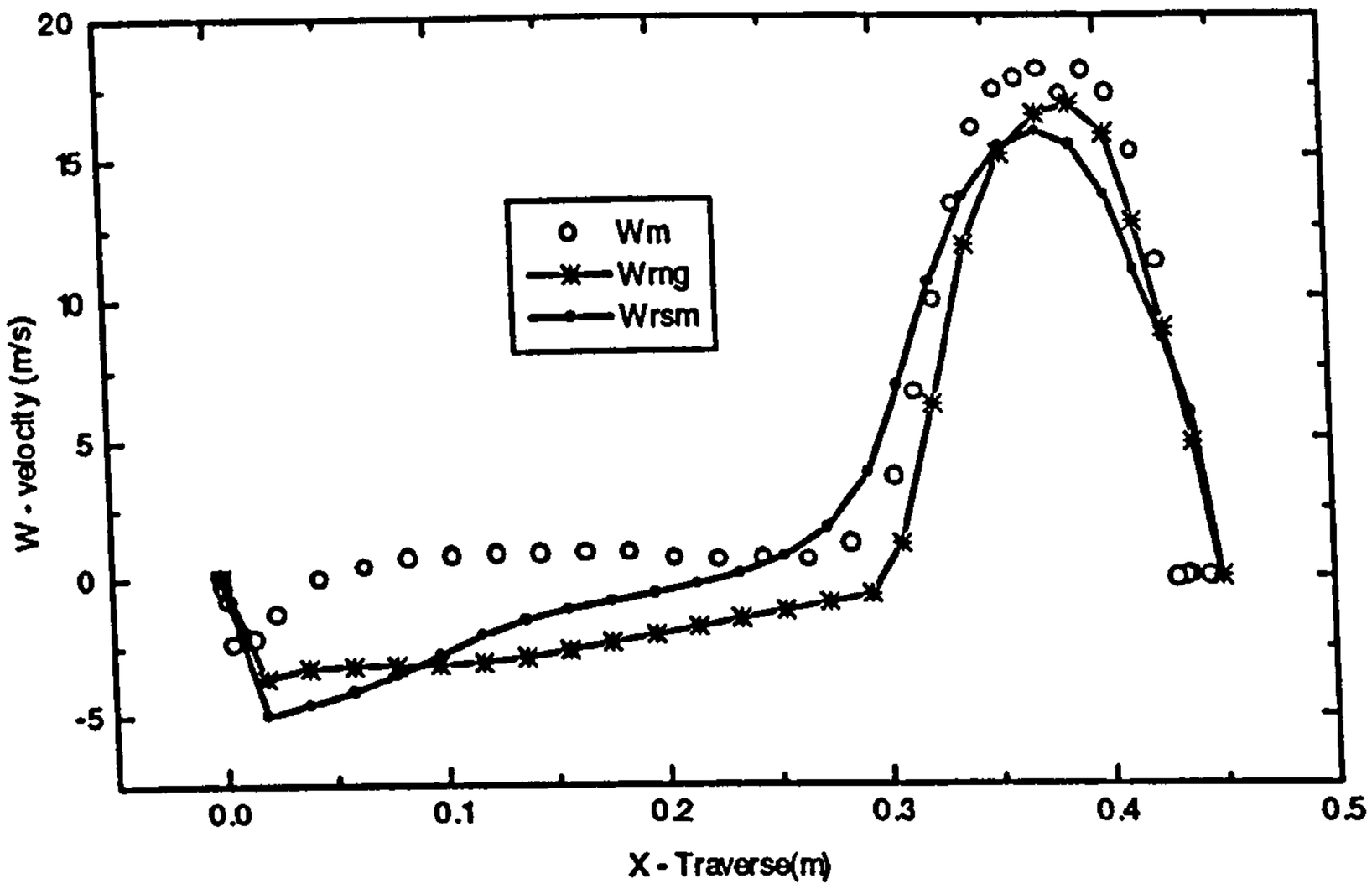

Figure 8-33 Duct centre at 250 mm from duct discharge (W- velocity)

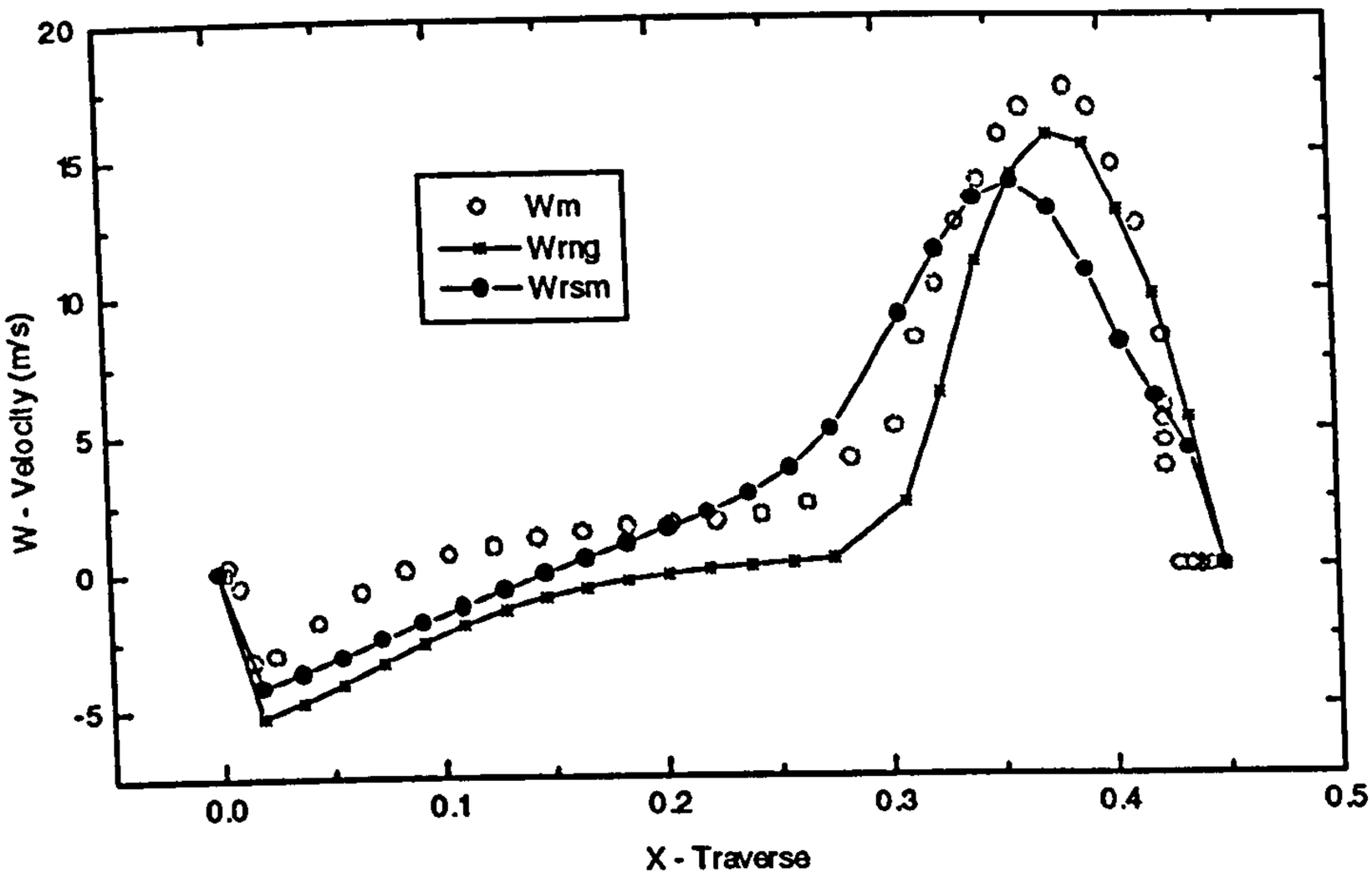

Figure 8-34 Duct centre at 350 mm from duct discharge (W- velocity)

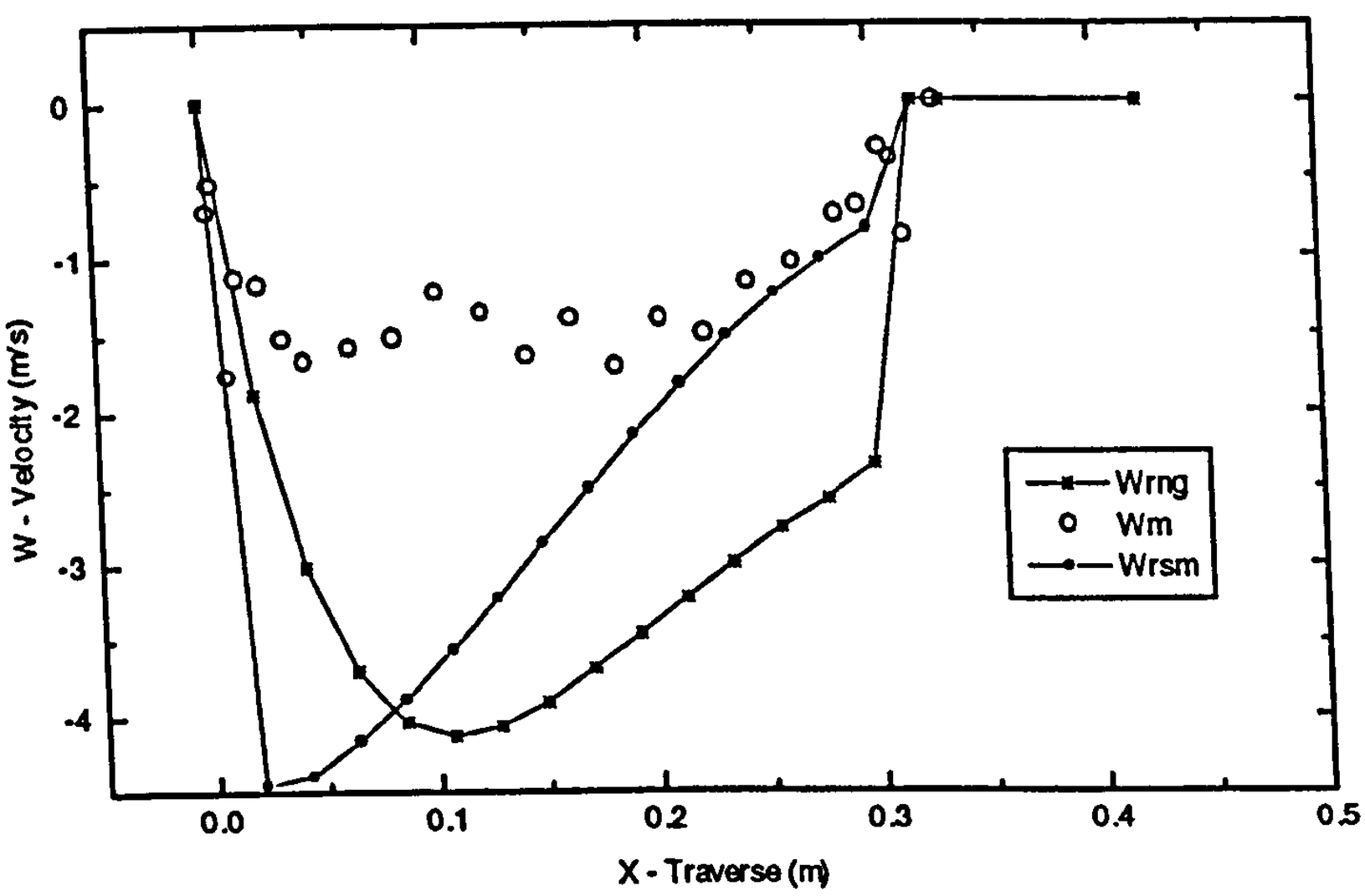

Figure 8-35 Duct centre 100 mm behind the discharge (W- velocity)

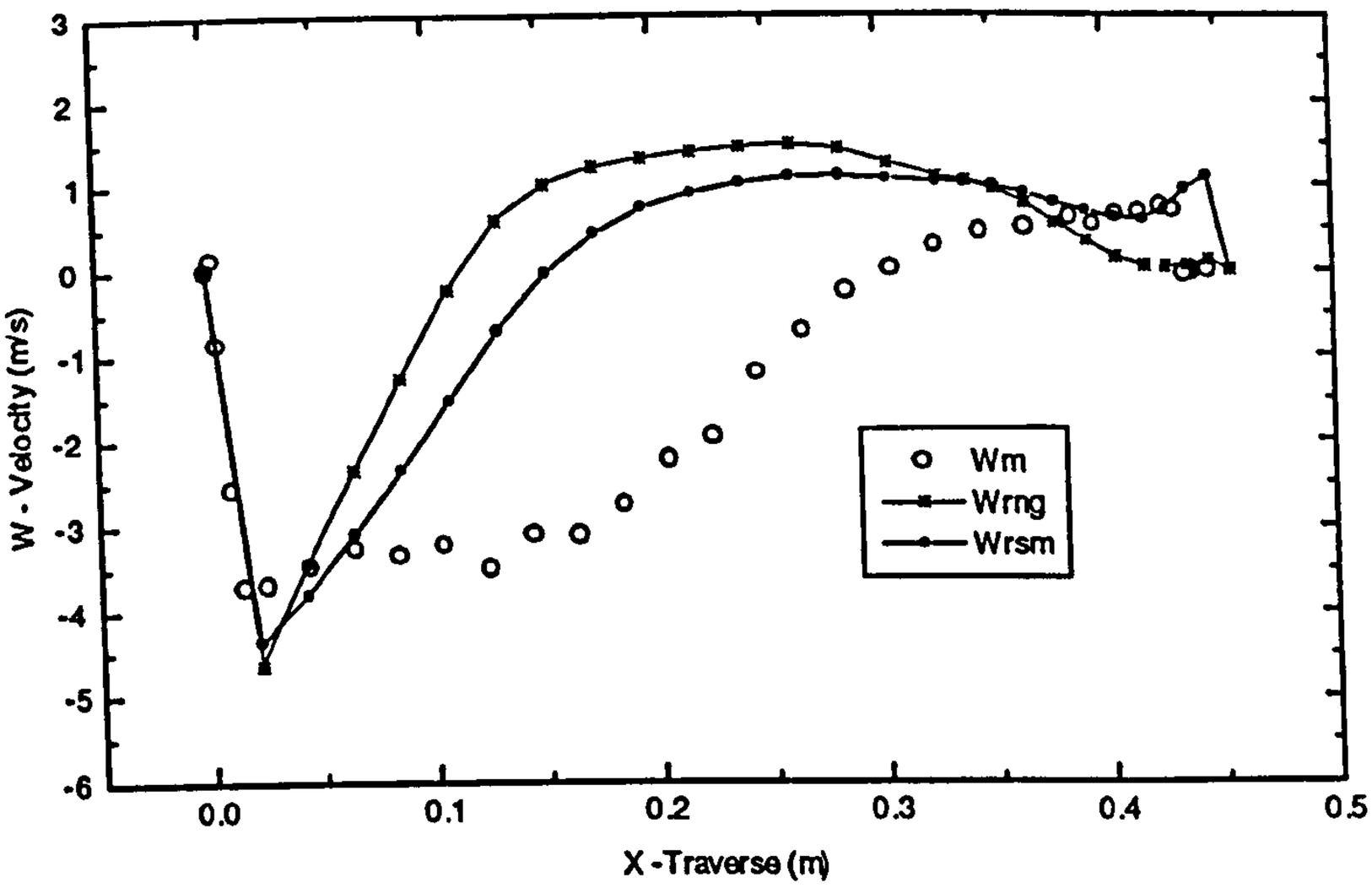

Figure 8-36 82 mm from the floor at 100 mm behind the duct. (W- velocity)

8.5 CONCLUSIONS

The CFD predictions obtained from the model generally agree with the flow patterns attained from the flow visualisation study.

The LDA has produced quantitative measurements for comparative purpose with CFD. The predictions obtained for the k-ε RNG model are much better in the central jet region than any other model tested. The RSM model produced slightly better predictions for the lower region when compared with the RNG model. Overall the k-ε RNG returns the superlative forecast for the five and ten-metre configuration. Woodburn (1996) also demonstrated that the modified k-ε model produced better results than the standard k-ε model. It has now been shown that the k-ε RNG produces better results for the two configurations discussed.

It is clear that the CFD models produce superior predictions for flows with reasonable turbulence values such as that in the jet region. The higher the turbulence intensity the more inaccurate the results become. It has also been demonstrated that as one approaches zero it is harder to accurately predict.

8.6 ACCURACY OF EXPERIMENTAL CFD SIMULATIONS - A SENSITIVITY ANALYSIS.

8.6.1 EFFECT OF ROUGHNESS ON JET PENETRATION.

Two identical grids containing sixty two thousand cells were constructed in the usual manner. The duct was positioned 20m from the face delivering $5m^3/s$. The k-ε RNG turbulence model, the power law discretisation scheme and the SIMPLEC algorithm were used to obtain a solution. The Elog value was set to 9.79 for a smooth wall and 0.064 for a rough wall. (The calculation process can be found in the appendix 5.)

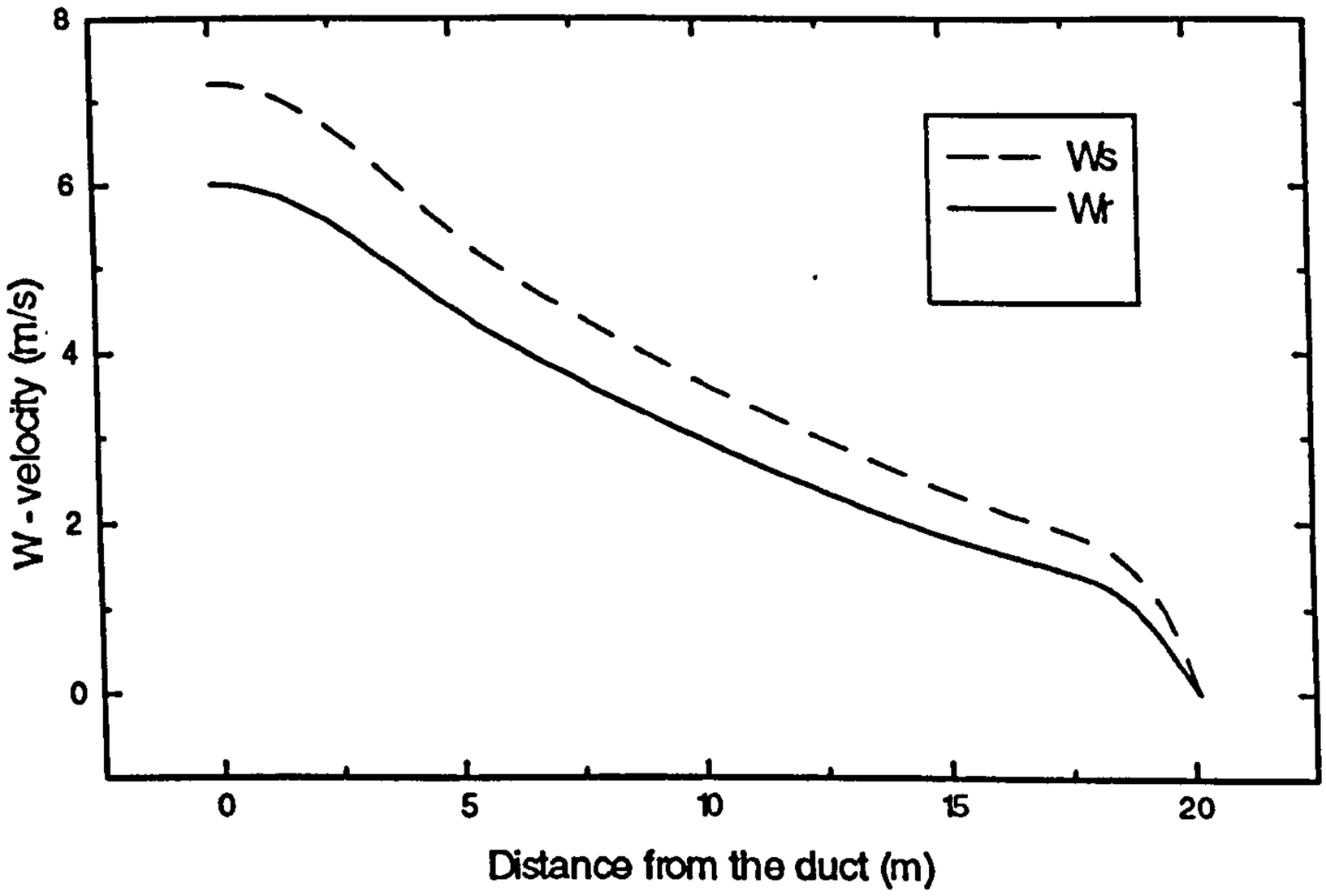

Figure 8-37 - Comparison of rough wall and smooth wall using k-ε RNG turbulence model.

Figure 8-37 illustrates a plot of maximum centreline velocity against distance. It shows how the roughness of the wall affects the penetration of the jet. Therefore, it is paramount that a roughness factor be included to represent a given situation fully.

8.6.2 EFFECT OF VARYING THE DENSITY/VISCOSITY.

The experimental results were obtained in an environment that varied in temperature thus the density and viscosity altered. The initial CFD prediction was conducted using standard air density and a viscosity based on a room at twenty degrees Celsius. Therefore, the density and viscosity were altered in the CFD model.

The resultant values were plotted against the previous set of predictions and experimental results. There was no significant difference between results obtained from the two simulations.

8.6.3 GRID SPACING

It has been demonstrated that a grid independent solution has been obtained for the general case. However the steep gradient near the wall may be due to an inadequate number of cells near the wall. It was decided to increase the grid density close to the wall to see if this steep gradient on the left-hand side was eliminated (figure 8-22).

The increase resulted in a smoothing of the gradient and the central region. However the overall result did not alter significantly. It is possible that a large increase of cells is required to fully represent the flow regime behind the duct. However, there are not adequate computer resources available to increase the grid beyond 120k cells at present.

8.6.4 DISCRETISATION SCHEME

The accuracy of the Power law scheme (default scheme in Fluent) is first order in terms of Taylor series truncation error. This scheme is the most widely used and is the scheme recommend. It was decided to test the QUICK discretisation scheme to asses its accuracy when compared to the Power law scheme. It uses a three point upstream weighted quadratic interpolation for the cell face values. Since the scheme is based on a quadratic function it has a third order accuracy in terms of Taylor series truncation error on a uniform mesh.

The QUICK scheme was switched on and the model sent for processing. The solution did not converge to the required degree of accuracy because the pressure value oscillated. Hence it was decided to employ the QUICK scheme on the velocity and the power law scheme on the pressure. Although the residual error did decrease it was not sufficient to eliminate the uncertainty.

In an attempt to identify areas where the scheme was failing, the partly converged solution was compared with the experimental results. The predicted values utilising QUICK were close to the predictions obtained using the power law scheme in the jet region. However, the region behind the duct where flow oscillated between positive and negative the QUICK prediction was totally inaccurate. It has been reported that the QUICK scheme is unstable in reversing flows (Versteeg & Malalasekera, 1995). This exercise has demonstrated that where there the flow regime exhibits high curvature and rotation the scheme is very unstable.

Total Variation Diminishing schemes are currently being developed to achieve oscillation free solutions and initial testing of these schemes have proved useful.

8.6.5 PRESSURE/VELOCITY COUPLING

The SIMPLEC algorithm resulted in a reduction in CPU time for the same model to converge with no significant differences in the overall prediction.

8.6.6 WALL FUNCTIONS

The standard wall function was used for the majority of the simulations and proved to be quite robust. When the non-equilibrium wall function was utilised it caused stability problems. In other words it is very difficult to achieve convergence.

8.6.7 CONCLUSIONS

1) A roughness factor needs to be built into the model to represent the situation fully.

2) The grid spacing behind the duct needs to be increased dramatically.

3) The QUICK discretisation scheme is unstable in this type of flow.

4) The non-equilibrium wall function leads to instability.

8.7 SUMMARY.

Comparisons of the flow visualisation, LDA and CFD predictions have been presented together with a discussion and conclusions. A sensitivity analysis on some of the parameters was also conducted and conclusions drawn.

The following chapter reports on the underground measurement programme conducted at Wistow Colliery in North Yorkshire.

9. CASE STUDY - WISTOW COLLIERY, NORTH YORKSHIRE.

9.1 INTRODUCTION.

Wistow Colliery is situated nineteen miles South West of York City (Figure 9-1). The mine forms an integral part of the Selby complex, which also includes the Stillingfleet, Riccall, Whitemoor and North Selby mines. Environmental concerns raised during the planning stage lead to the concept of the five satellite mine delivering coal by conveyors to the surface via a drift at the Gascoigne wood complex (see Plan in Appendix 7). The coal is then washed and brought by rail to the power stations in the Aire valley.

Wistow Colliery commenced production in the Barnsley seam in 1983. The seam varies in thickness from 2 - 3.25 m. At Wistow the coal seam is 350 metres below the surface and dips steeply to the North East where it is 1044 metres below the surface at North Selby. Wistow is unique in that it has to date used four mining techniques to produce coal. These include longwall (retreat), single entry shortwall (120m), microfaces (40m) and room and pillar. The later techniques are utilised because the Western edge of the pit is close to the water table. Therefore, large-scale caving of the strata is not possible and it must be left supported. On the Eastern side of the mine where the coal is further away from the Permian strata, coal faces are being worked on the longwall principle. Riccall, Stillingfleet and Whitemoor followed Wistow when they began producing coal in 1988. Wistow currently holds European underground output record with 108,700 tonnes in one week.

During this project a series of ventilation surveys were conducted within drivage headings at the colliery. Two of these heading were advance developments for retreat shortwall faces and were ventilated using a conventional auxiliary overlap system. The third heading was within a room and pillar operation. The general flow characteristics observed during these surveys are introduced and the results are compared with CFD models of each heading.

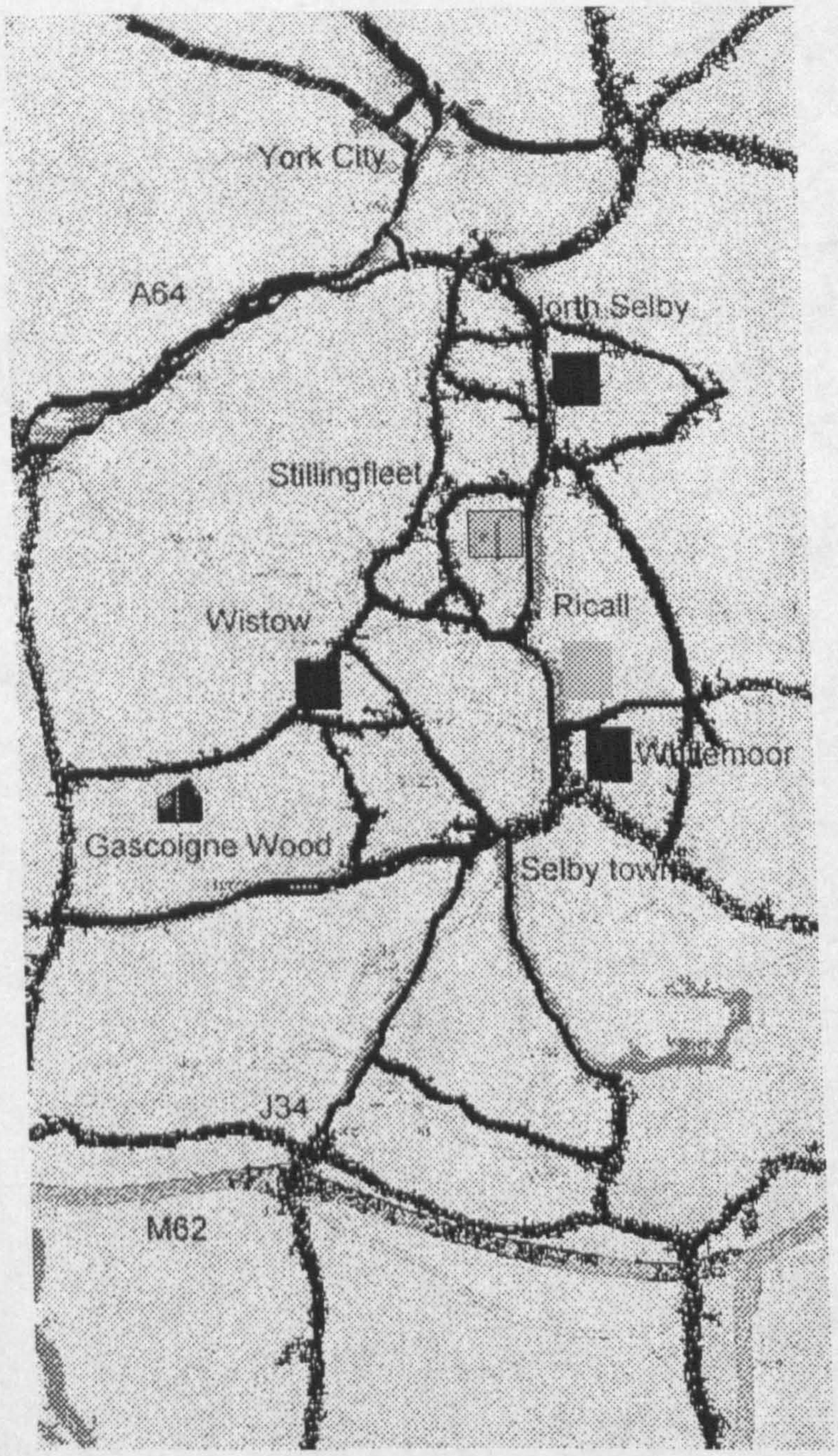

Figure 9-1 - Map of Wistow/Selby complex.

9.2 CASE 1 - 143'S HEADING CONVENTIONAL OVERLAP.

9.2.1 Description of the heading

This heading is located in the Southern section of the mine (Appendix 7 - Mine plan) and employs a conventional overlap system to ventilate the face. The forcing duct (760mm) was positioned 35m from the face in the top left corner. The reinforced exhaust duct (not operational) was situated 3m from the face. The drivage was 300m inbye with a projected drivage length of 800m. The managers minimum at this type of heading was set to 4.5m^3/s.

The Figure 9-2 illustrates the position of the conveyor, continuous miner, cables and ducting. The heading was not operational because the team was waiting for a length of flatlay ducting to arrive from the pit bottom. The additional length of ducting was necessary for the heading to proceed cutting.

9.2.2 Measurement methodology.

There was a range of pressure and velocity measurements taken during the course of the ventilation survey. The centreline velocity in the duct was attained using a pitot static tube inserted into the duct a few metres behind the outlet. The pitot was connected with tubing to a magnehelic gauge, which displayed a differential pressure measurement. The velocity was calculated from this velocity pressure reading using equation 3.1. The duct air quantity was calculated by multiplying the velocity by the cross sectional area (Q = V*A). Point velocity measurements were also recorded within the initial part of the jet using a pitot static tube.

Fixed point anemometer measurements using a LCA 30 IS digital vane anemometer (figure 2-9) were taken in sections of the roadway at intervals illustrated in figure two and along the duct centreline. The measurement traverse sections represent the distance from the duct outlet with zero metres datum taken to be level with the duct outlet. The measurement points have been labelled (i) - (viii) and will be referred to in this manner

in the discussion. The mean velocity was calculated from a series of three consecutive anemometer measurements taken at fixed points over a period of sixty seconds.

In areas of fluctuating low velocities, measurements were not possible. Therefore in these regions the flow regime was mapped using a combination of smoke tubes and ribbons suspended from the ceiling. The general flow characteristics of the region behind the duct and >27m in front of the duct were compared with the CFD predictions in a more general manner. Moving traverses were conducted utilising an anemometer to ascertain the quantity leaving the roadway. These moving traverses were conducted until three readings agreed to within five percent.

The following case studies outlined in this chapter used a similar measurement methodology to obtain point anemometer measurements, duct quantities and the general body quantity. Where measurements were not possible qualitative flow visualisation studies were employed using smoke tubes and ribbons suspended from the ceiling.

9.2.3 Development of the CFD model.

The mesh represented the underground heading geometrically. Initially the solution was solved with no obstructions in the roadway and utilising the k-ε RNG turbulence model. The results of this prediction were then compared to the field measurements, which showed reasonable correlation. However, obstructions had to be included in order to model the given situation with a greater degree of certainty. The scaled block models representing the conveyor and CM were then added. Once the solution had converged the prediction were compared with the range of field readings described in the previous section.

It was noticed that velocities in some regions of the jet were excessive when compared to actual results. A probable explanation for this discrepancy was the conveyor had been modelled as a solid block whereas in reality it had free surface underneath. This results in a channelling effect and a reduction in area resulting in higher velocities.

Other factors which were subsequently identified as producing inaccuracies in the predicted results in this region was the omission of a stage loader, trailing cables and a roughness factor. Therefore in an attempt to achieve closer correlation with the model, the conveyor was reduced in size, a stage loader and trailing cables added. Finally a roughness factor was included in the model and the resultant prediction compared with field results. These predictions yielded better results than the previous simulations. Hence they were employed for comparative purposes. The RSM turbulence model was then initiated and the ensuing predictions contrasted with the field measurements and the k-ε RNG turbulence model. (Figure 9-4 - 9-10).

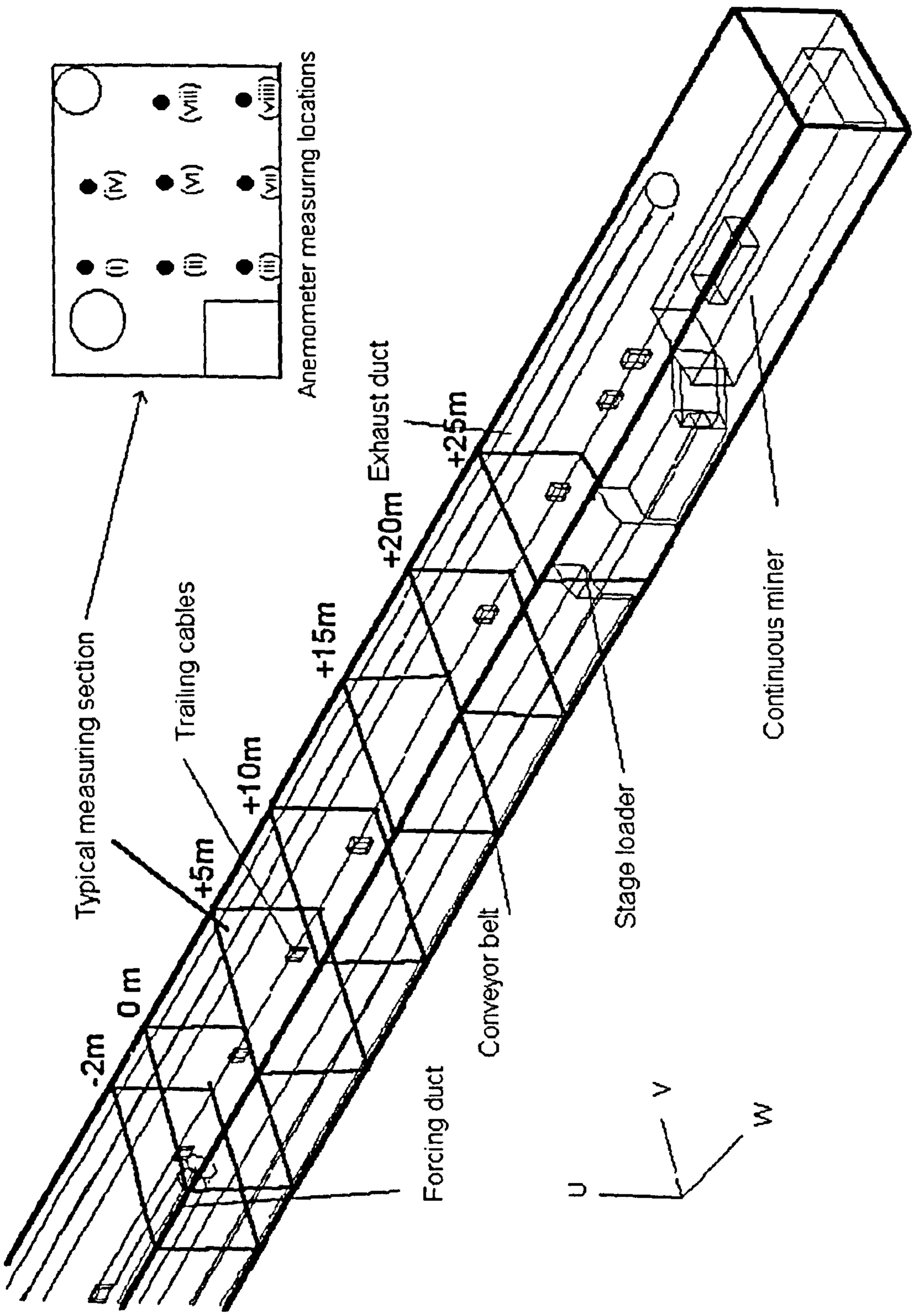

Figure 9-2 - 143's heading layout

9.2.4 Presentation and discussion of results.

Figure 9-3 illustrates a dimensionless plot of velocity against distance as a function of duct area. The k-ε RNG and the RSM turbulence models are represented by Wrng and Wrsm respectively. The experimental values are represented by exp.

The RSM model underpredicts the measured (figure 9-3) values slightly whereas the RNG turbulence model over predicts the jet velocities. Both turbulence models predict that the jet penetrates a greater distance than the measurements suggest. Beyond a dimensionless distance of 30 x/d the predicted values do not compare favourably with measured results. One possible reason for this discrepancy could be the turbulent nature of the air. This may have precluded accurate measurement of the flow patterns.

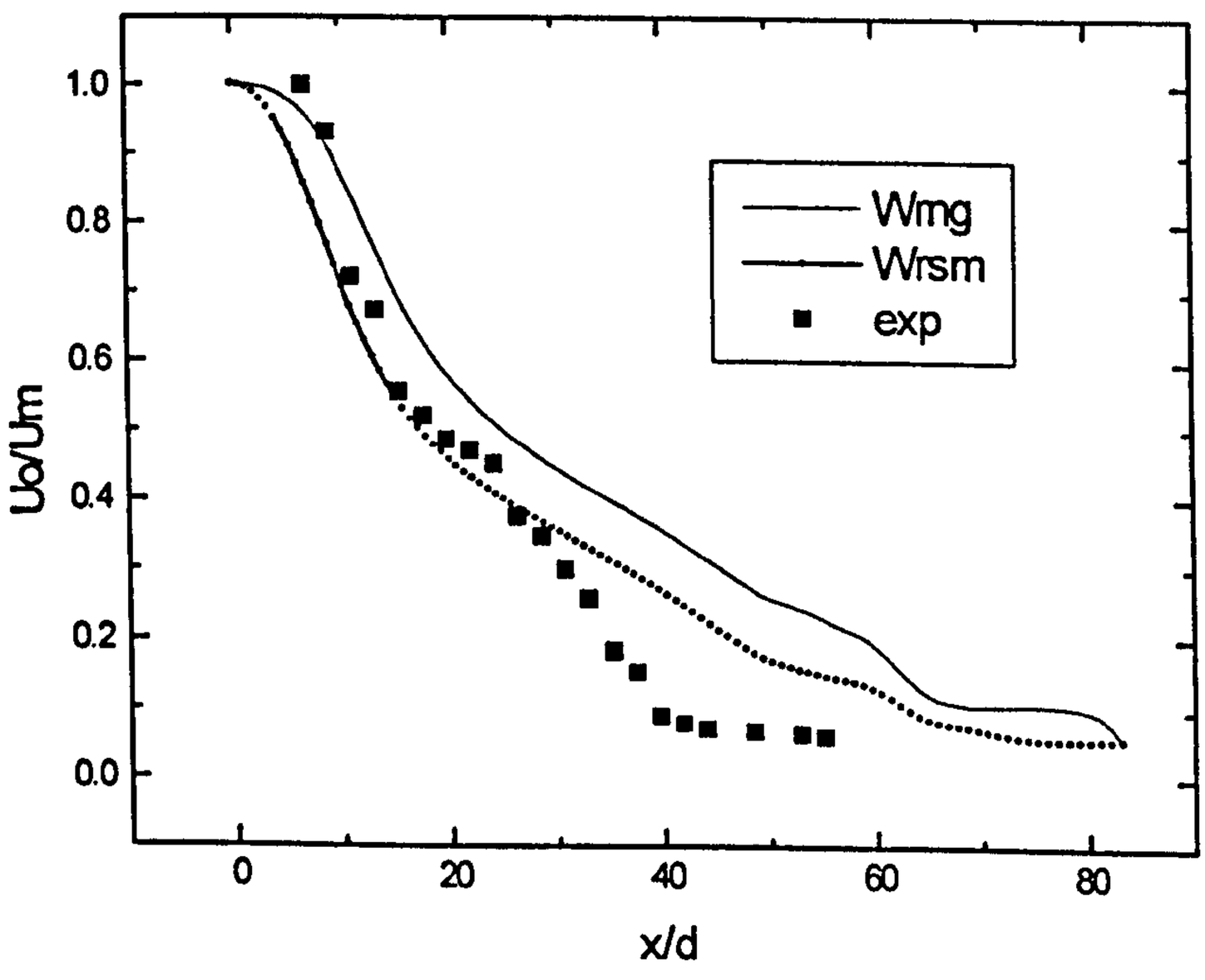

Figure 9-3 - Dimensionless plot of velocity against distance from a duct with a certain area.

Where; U_0 = Exit velocity from outlet, U_m = Maximum velocity at a certain distance from duct outlet, X = distance from duct outlet, d = area of duct outlet.

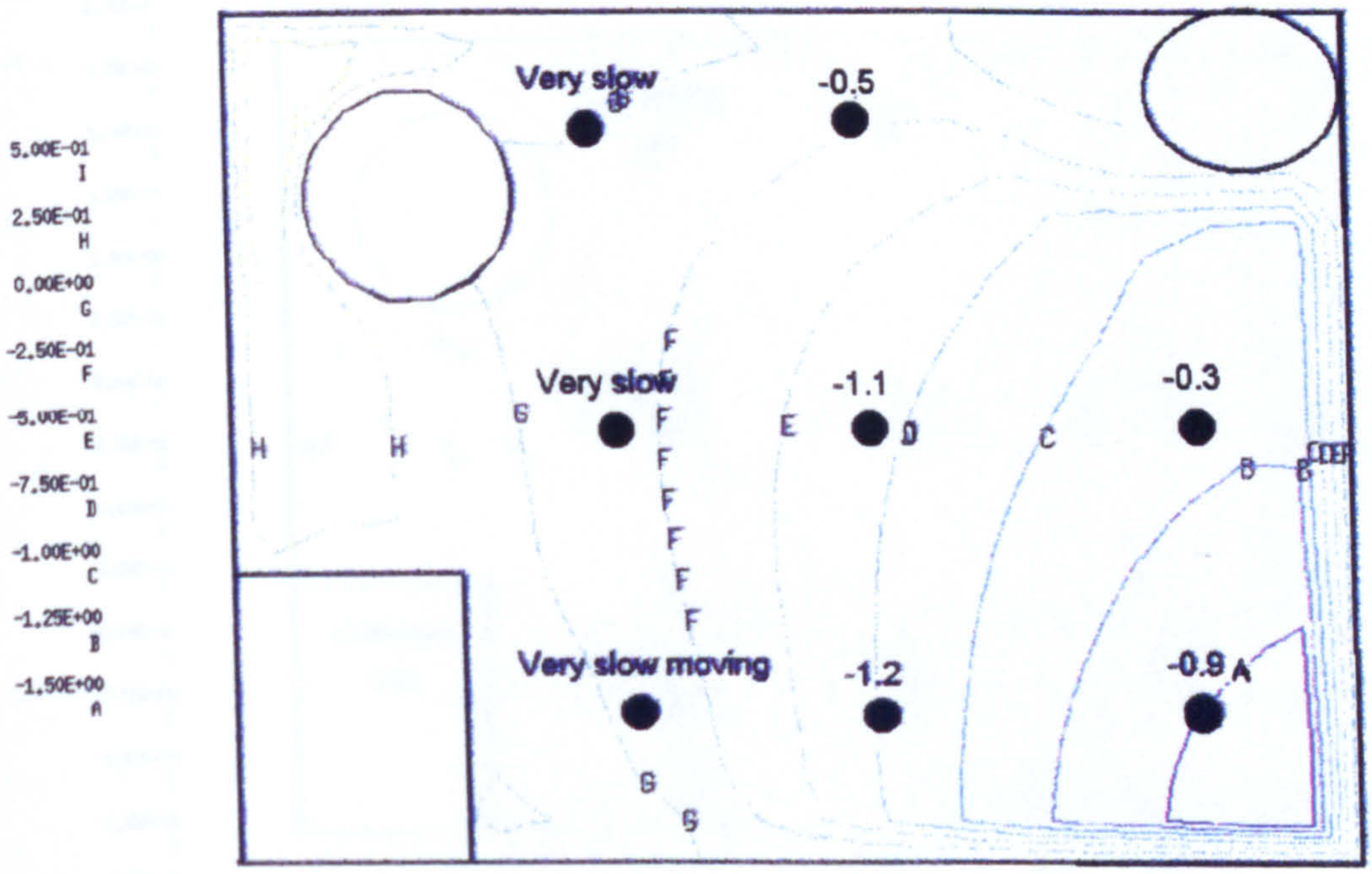

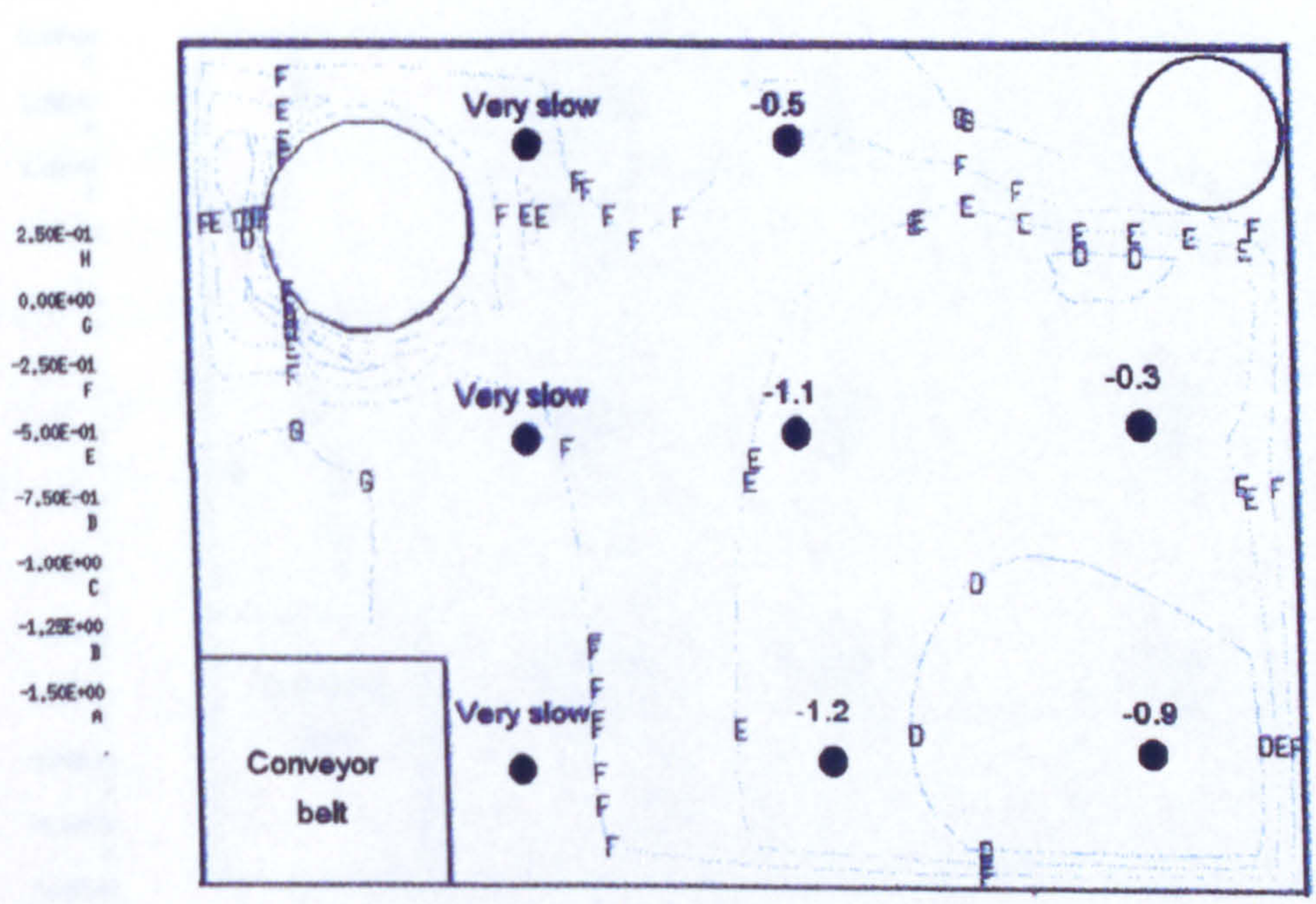

Figure 9-4 - Section -2m - RNG (top) and RSM (bottom) turbulence models.

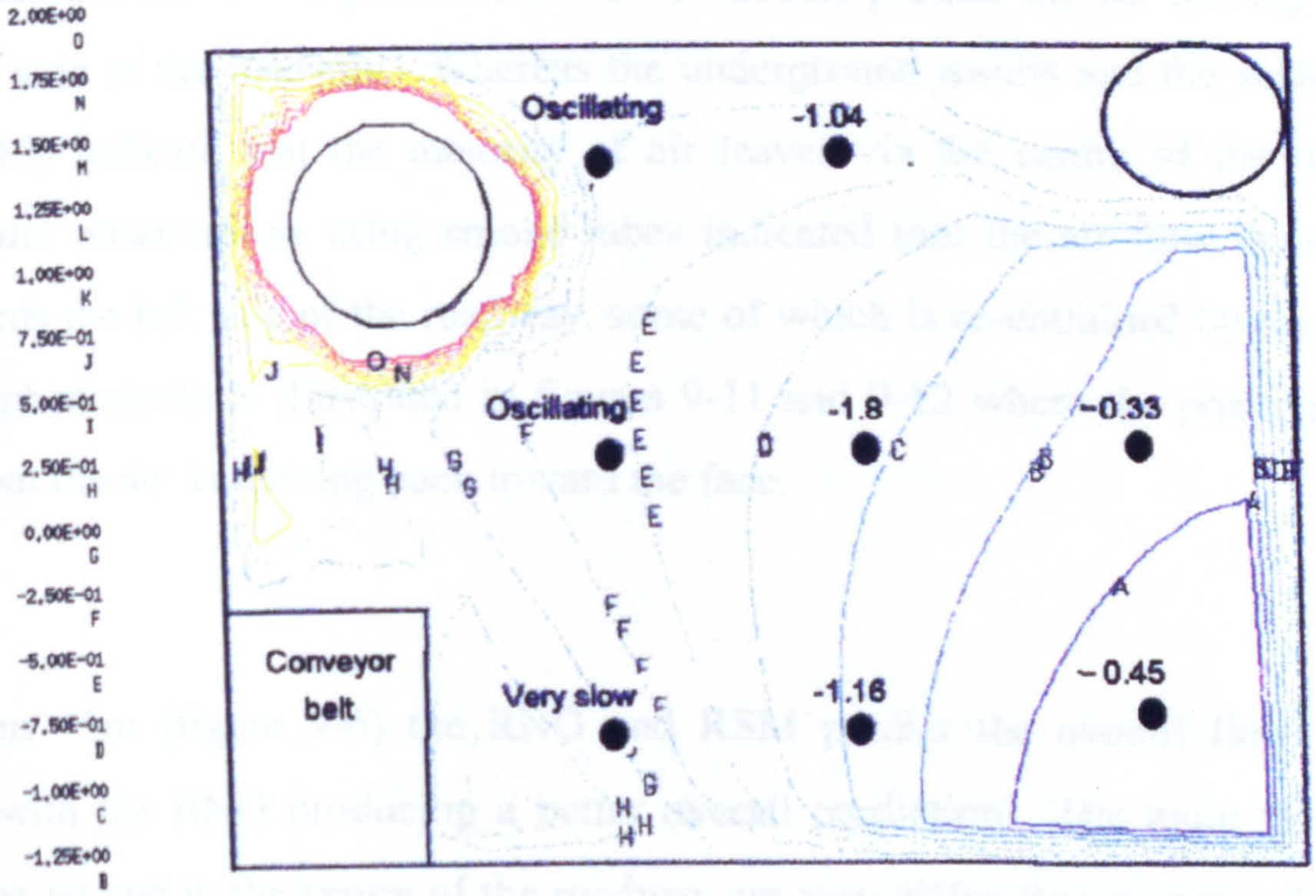

Figure 9-5 - Section 0m - RNG (top) and RSM (bottom) turbulence models.

Across the traverse sections -2m and 0m (figure 9-4, 9-5) the RNG and RSM TM produced similar erroneous predictions. Both models predict the air leaving via the right hand side of the roadway. Whereas the underground results and the scale model (figure 8-19) indicate that the majority of air leaves via the centre of the roadway. Underground observations using smoke tubes indicated that the air flow does in fact drift towards the left side of the roadway, some of which is re-entrained by the forcing jet. This phenomena is illustrated in figures 9-11 and 9-12 where the positive values indicate that the air is moving back toward the face.

For section +5m (figure 9-6) the RNG and RSM predict the overall flow features correctly with the RNG producing a better overall prediction. The main flow fields close to the jet and in the centre of the roadway are very difficult to measure due to the pulsating nature of the jet. It has been shown previously in the scale studies that these regions produces a high degree of variance and are time dependent. Therefore one might expect inaccuracies in the CFD since it is based on an average value at a particular time.

The RNG model produces slightly better predictions in the developed regions of the flow in section +10m (figure 9-7) whereas the RSM model under predicts velocity measurements. Section +15m (figure 9-8) shows that the RNG model predicts more accurately in areas where the flow is more developed and RSM better in the jet region with its high degree of turbulence. For the remaining sections (figure 9-9 & 9-10) the RNG over predicts while the RSM under predicts.

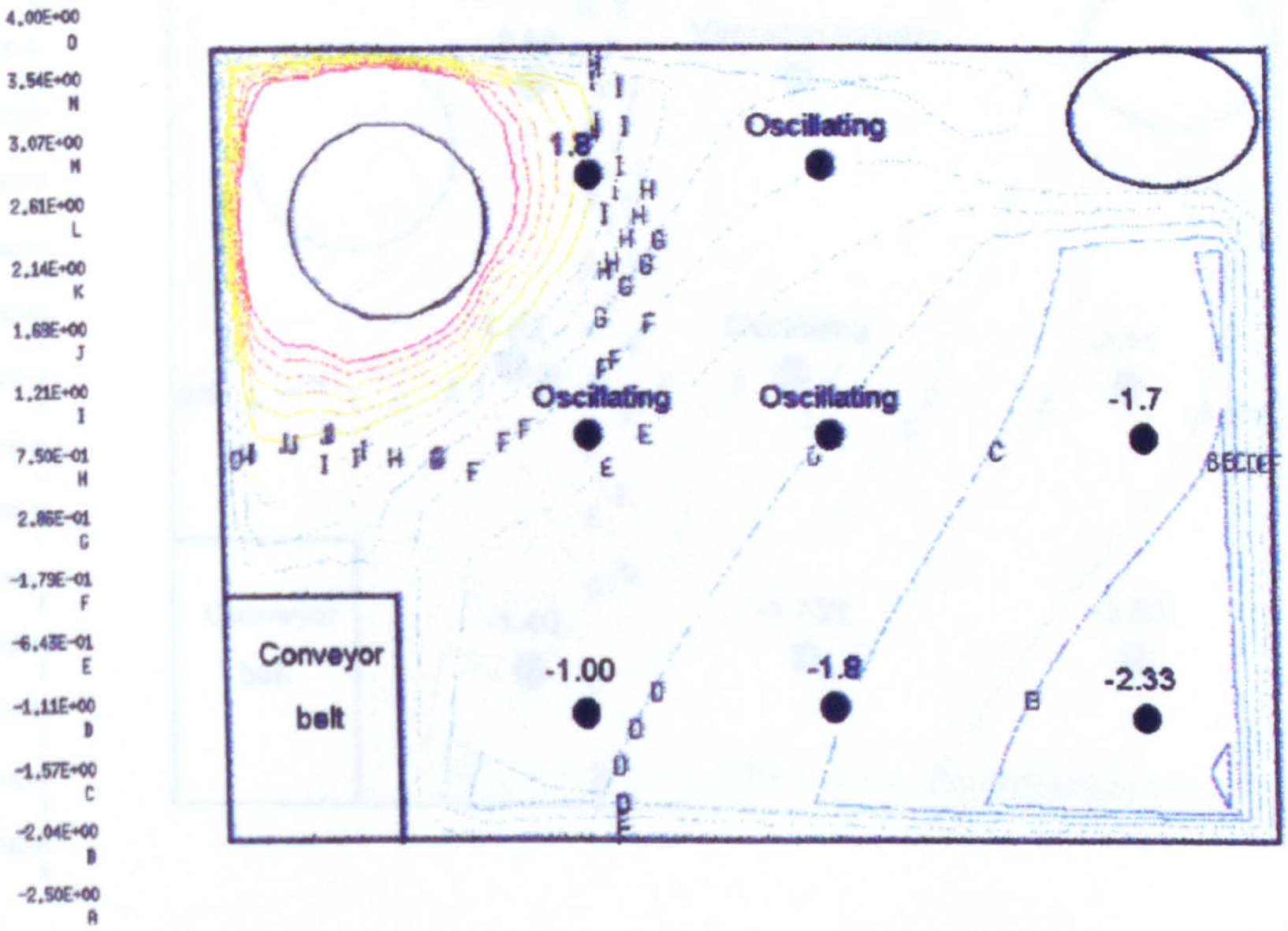

Figure 9-6 - Section 05m - RNG (top) and RSM (bottom) turbulence models.

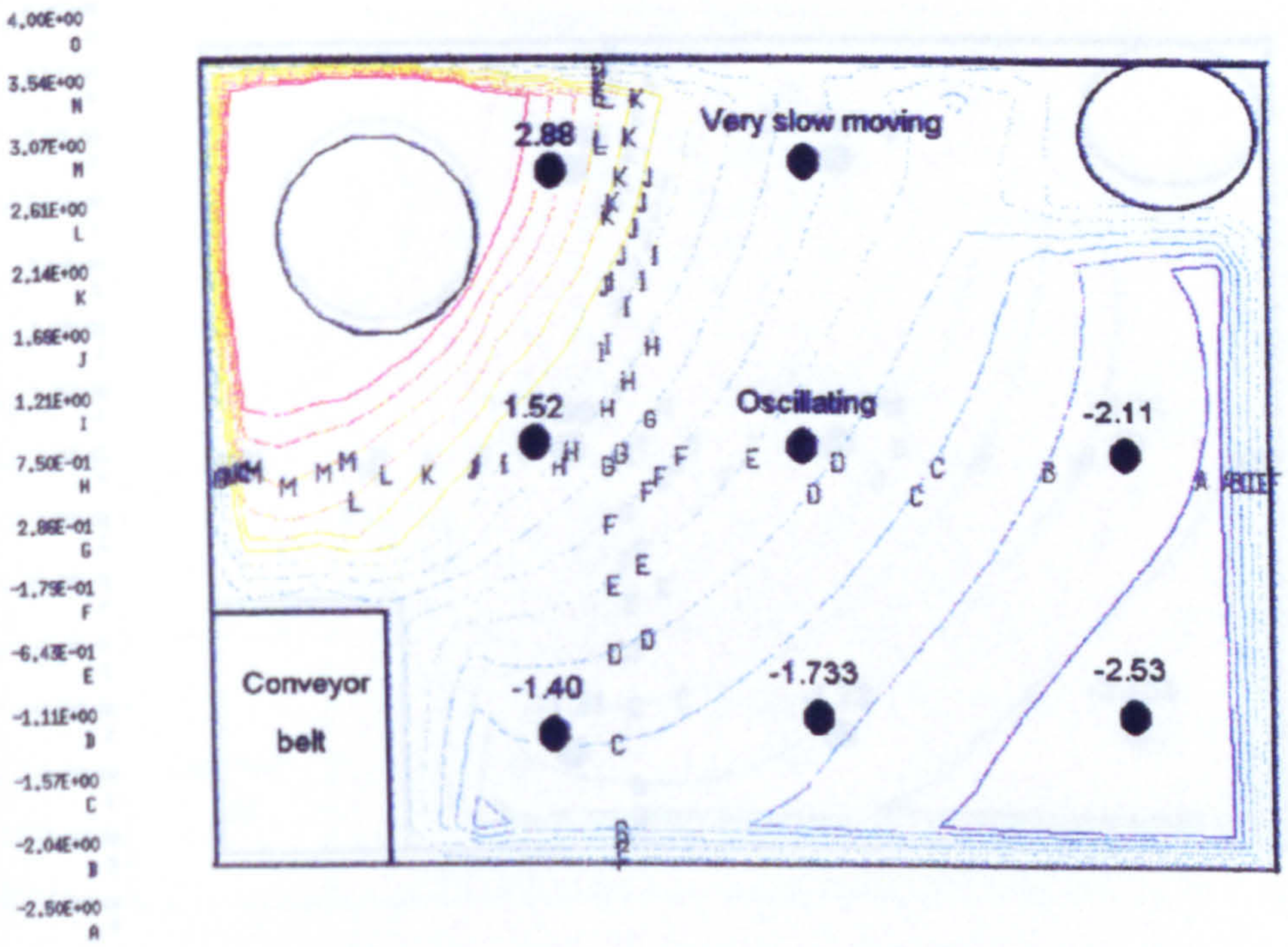

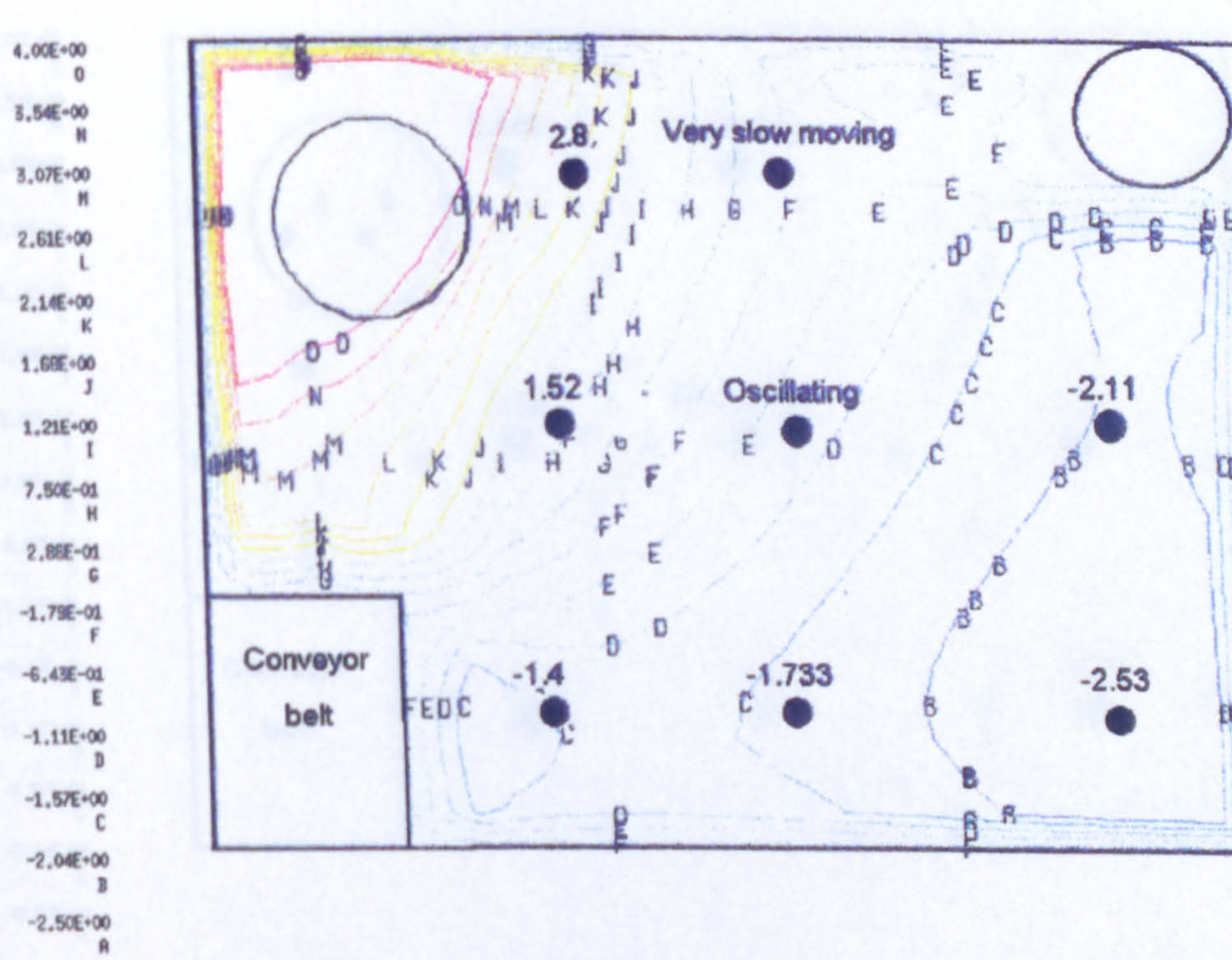

Figure 9-7 - Section +10m - RNG (top) and RSM (bottom) turbulence models.

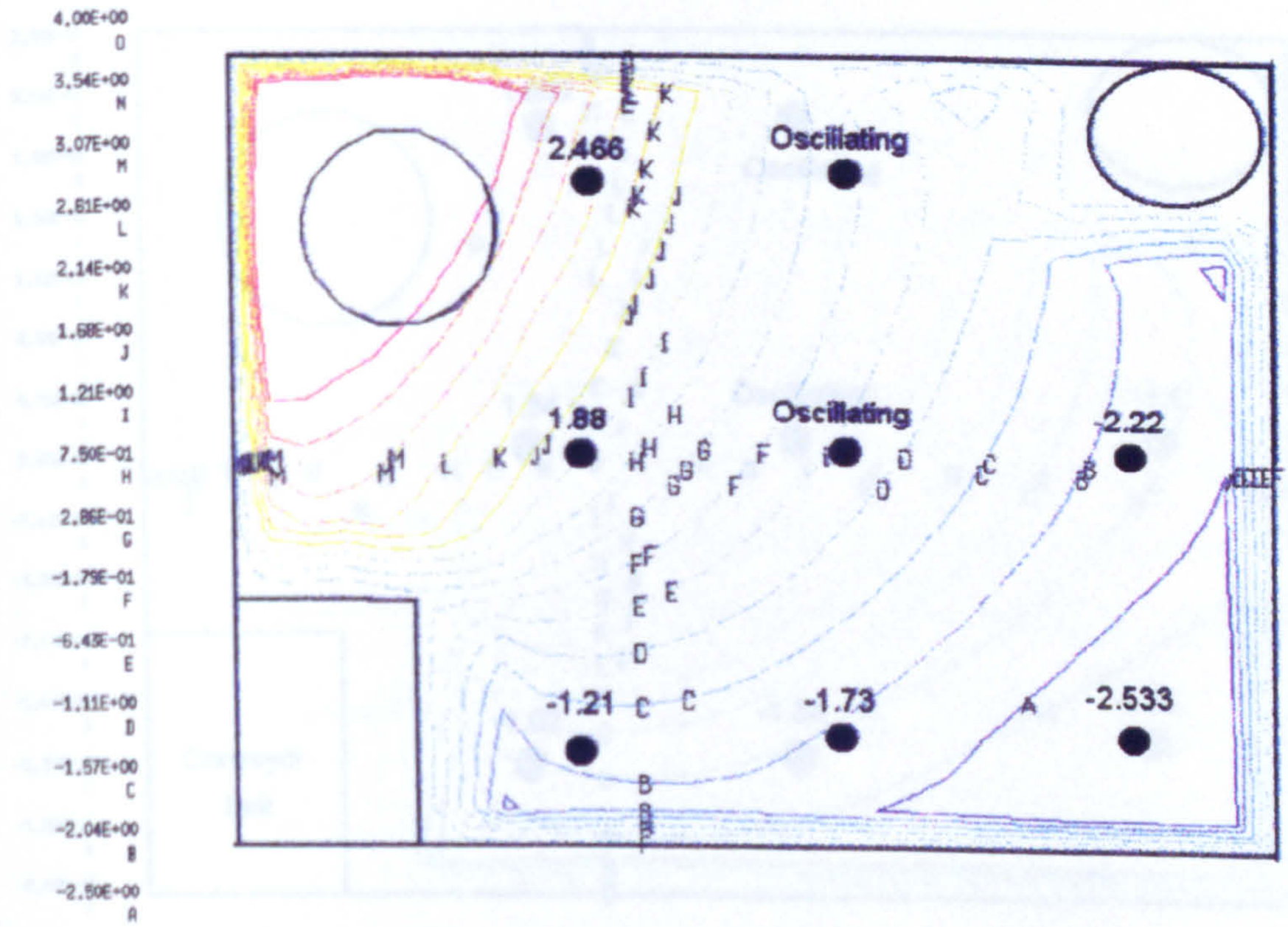

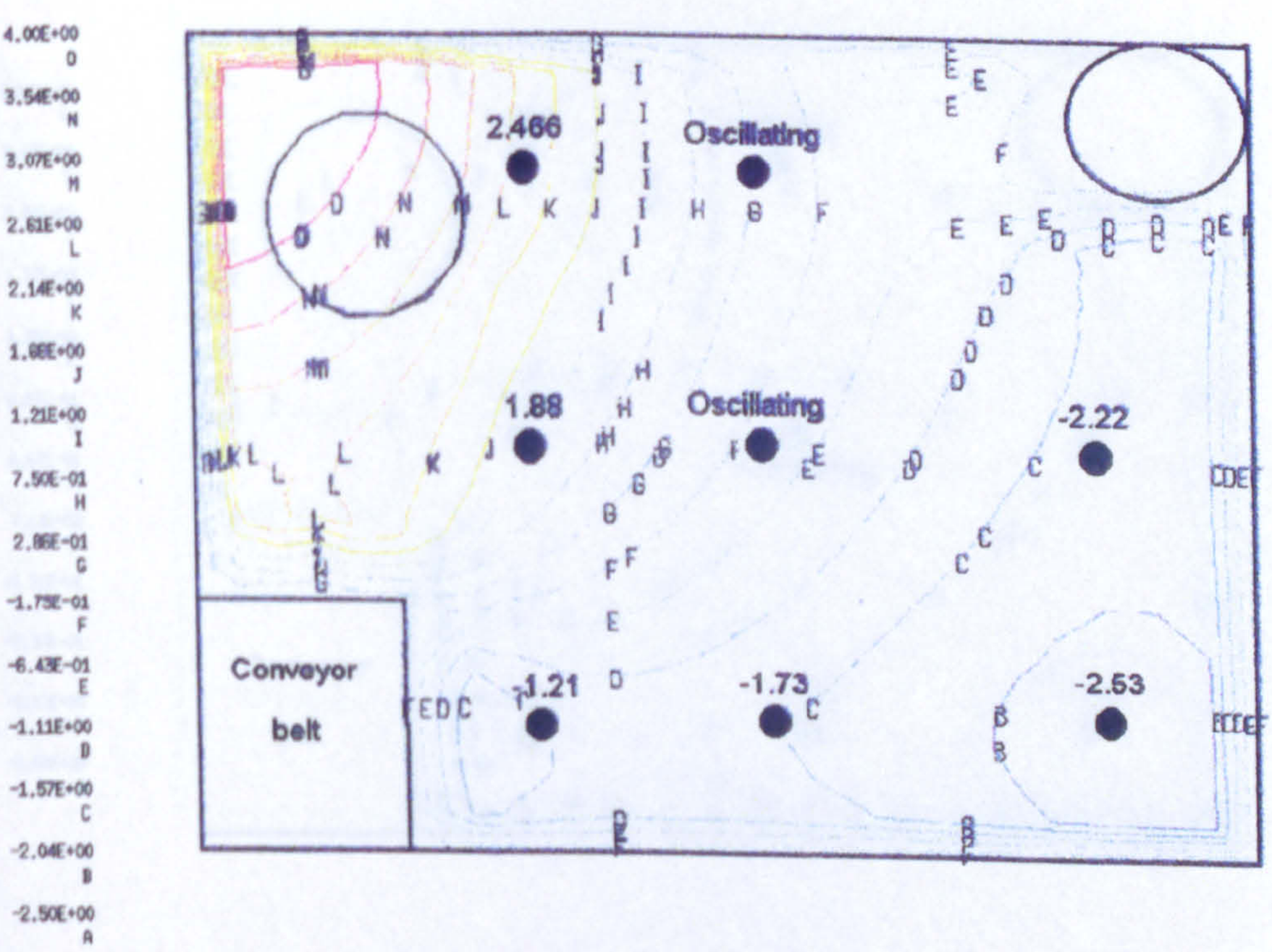

Figure 9-8 - Section +15m - RNG (top) and RSM (bottom) turbulence models.

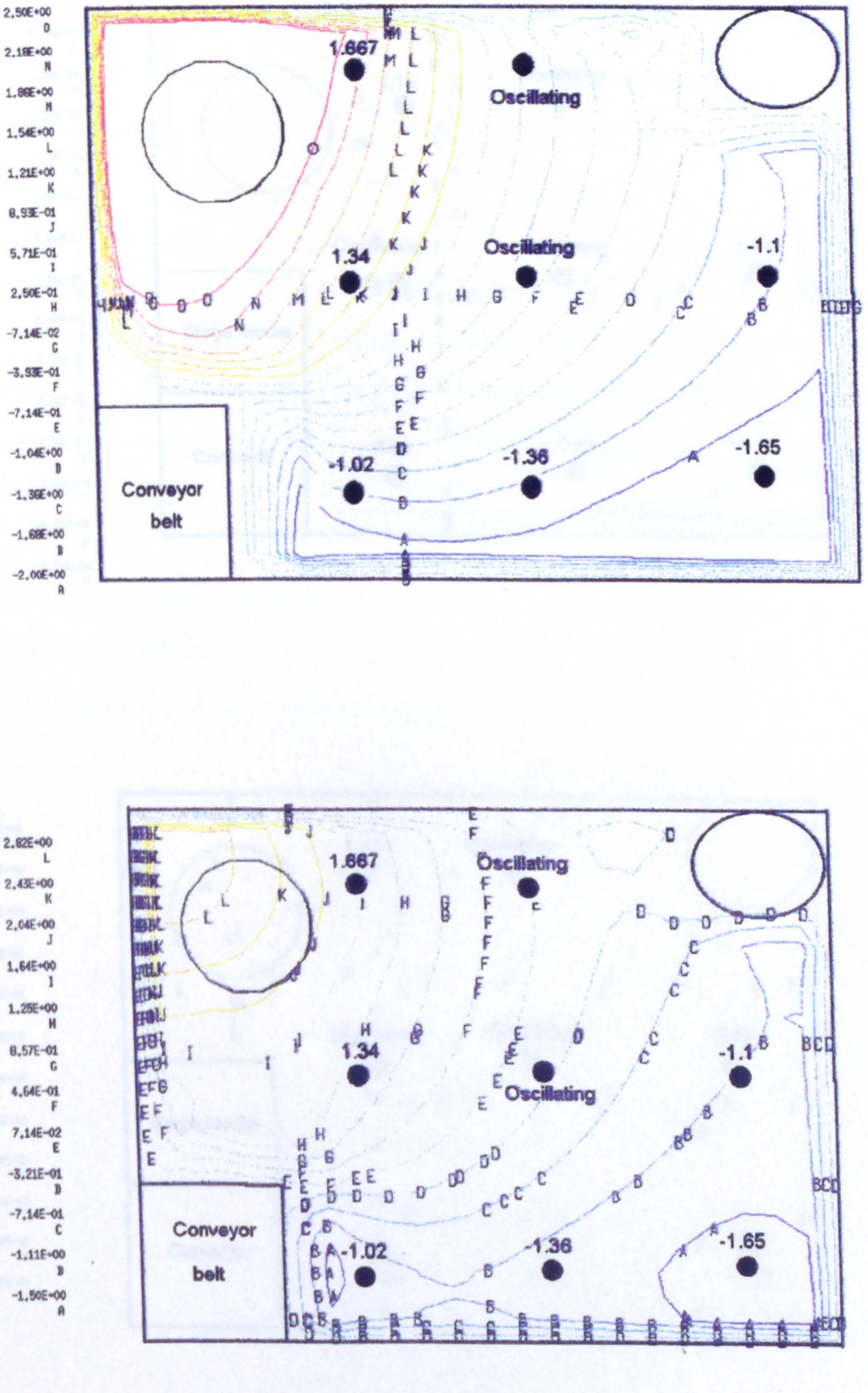

Figure 9-9 - Section +20m - RNG (top) and RSM (bottom) turbulence models.

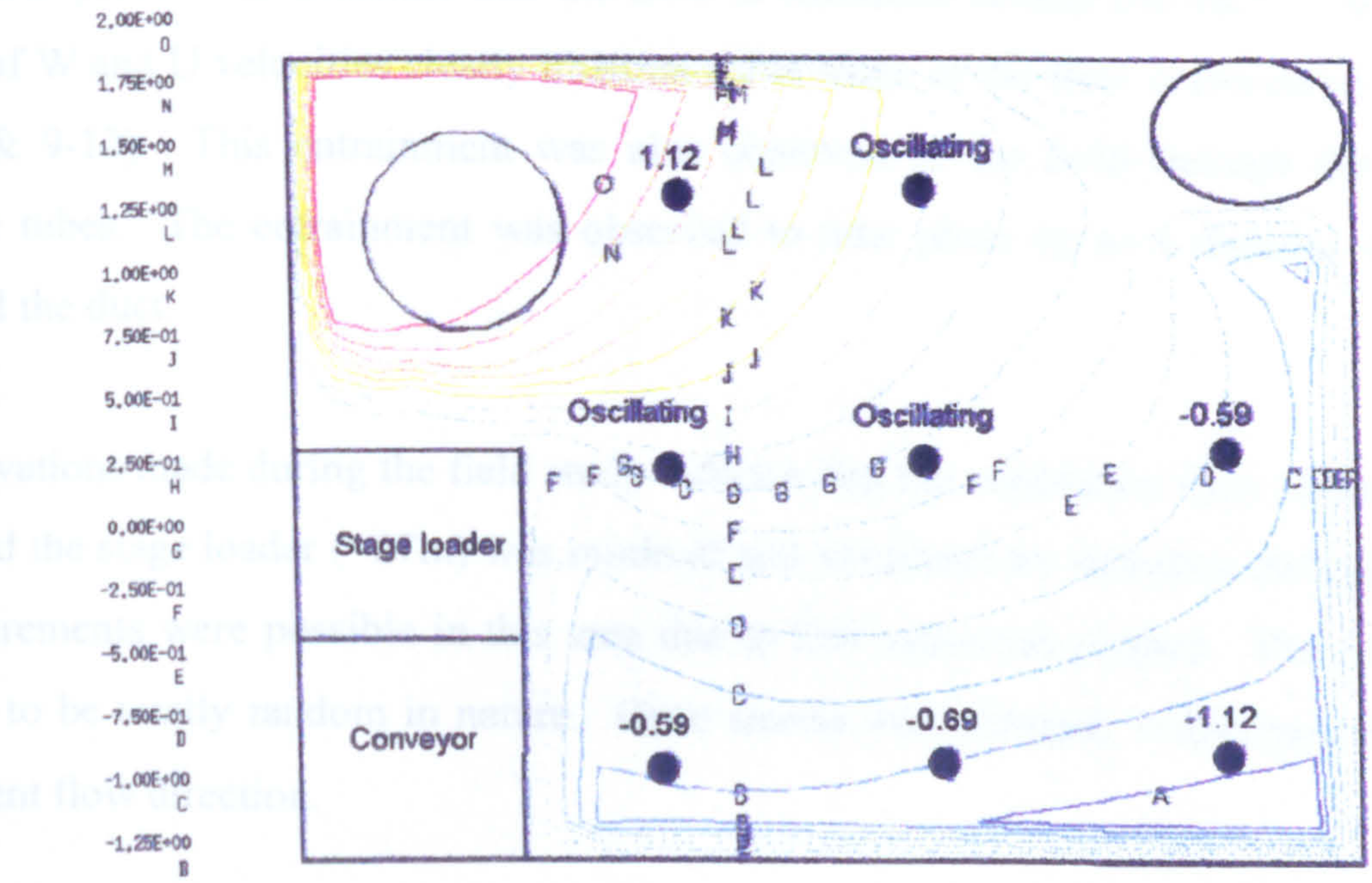

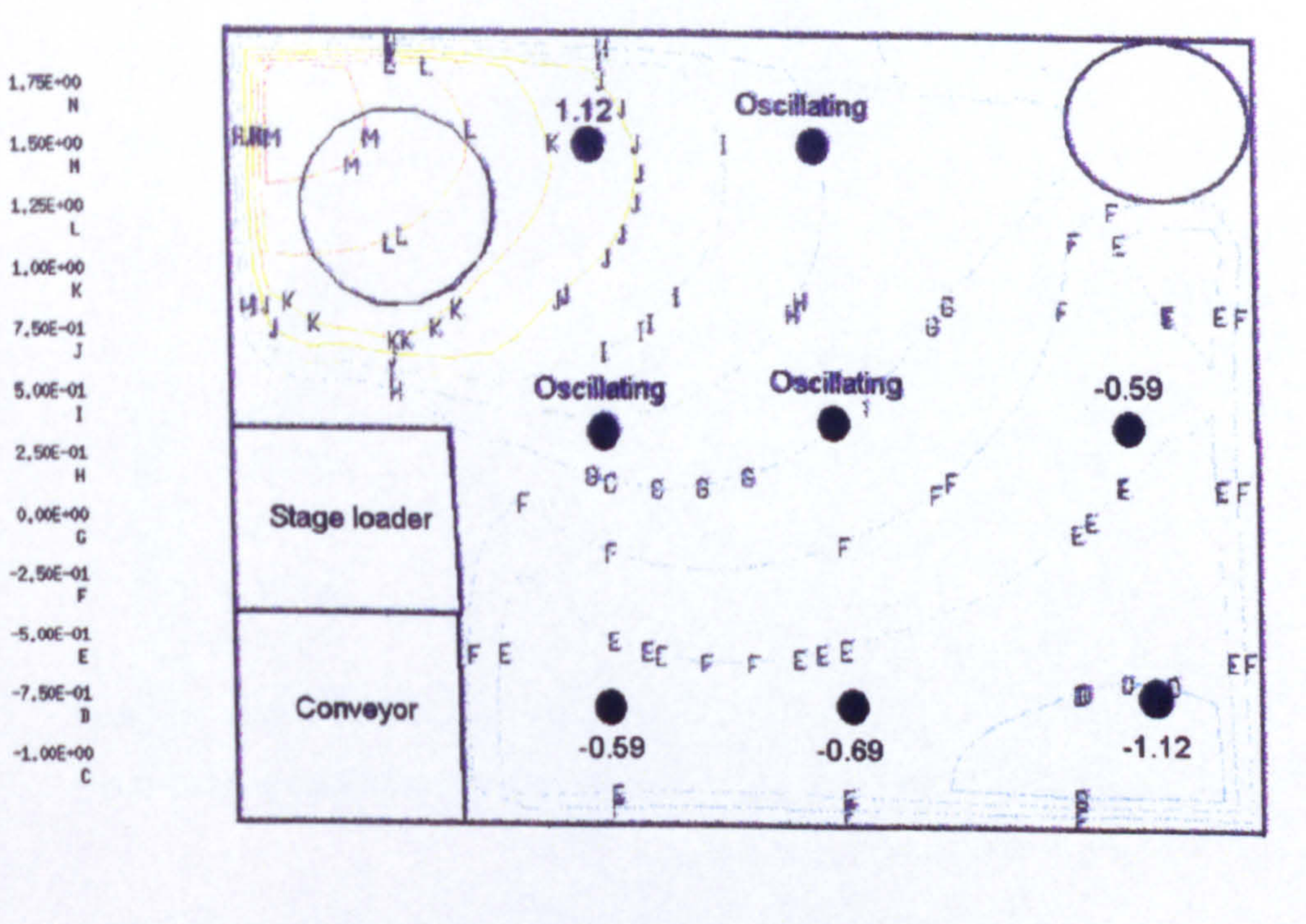

Figure 9-10 - Section +25m - RNG (top) and RSM (bottom) turbulence models.

The CFD predictions illustrate that the flow is entrained behind the duct. The vector plots of W and U velocities clearly illustrates that some of the flow is entrained. (figure 9-11 & 9-12). This entrainment was also observed in the field through the use of smoke tubes. The entrainment was observed to take place up to a distance of 3.5m behind the duct.

Observations made during the field study indicate that the ventilation flow in the region beyond the stage loader (<27m) was minimal and ventilated by turbulent diffusion. No measurements were possible in this area due to low velocities present. The flow was found to be totally random in nature. Once smoke was released, it dispersed with no apparent flow direction.

The prediction shows the main flow being deflected by the stage loader and then moves outbye while the remaining air diffuses into the opening. This is indicated by the very low velocity magnitudes evident (figure 9-13).

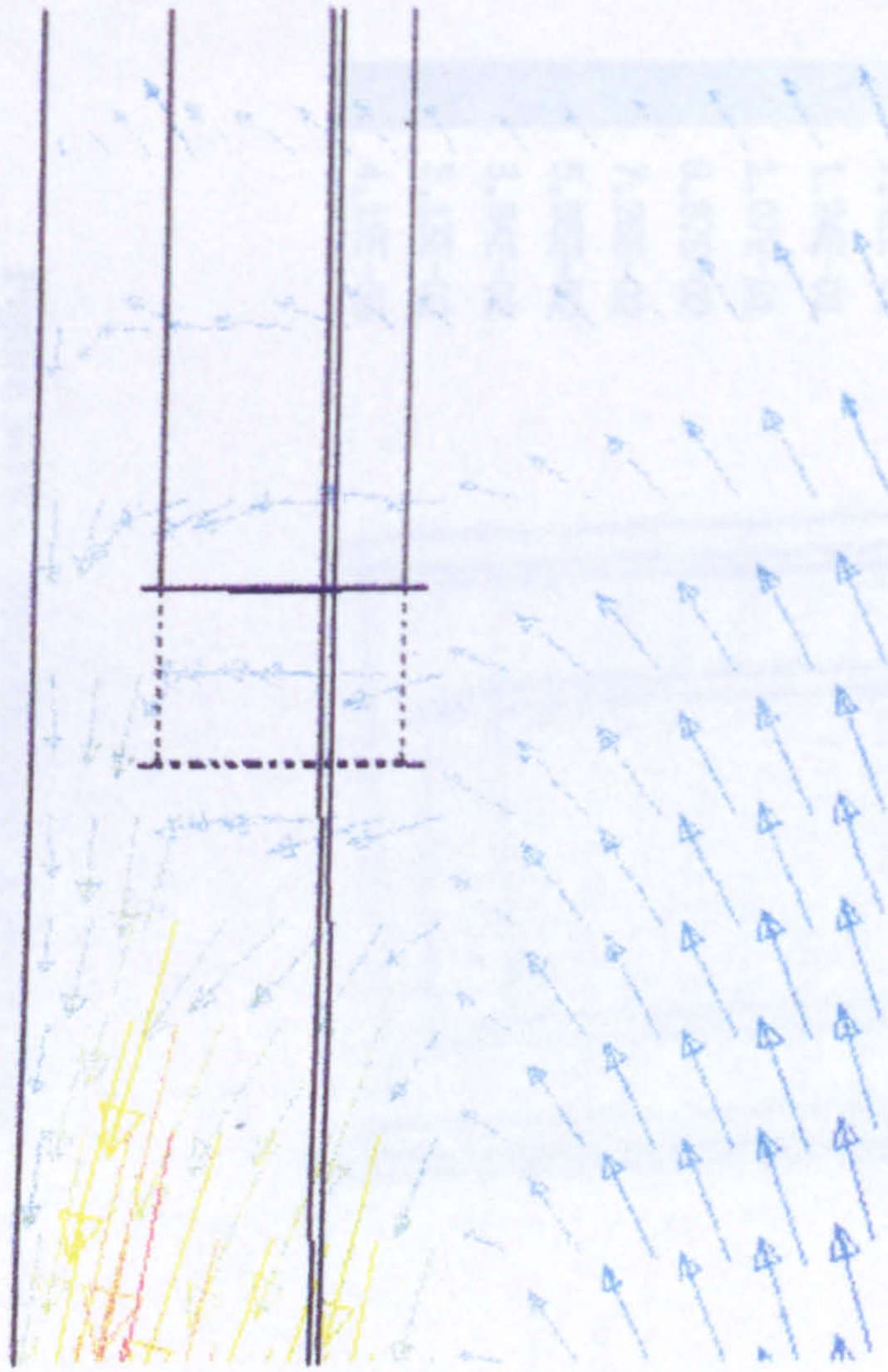

Figure 9-11 - Entrainment of air around duct region using U-Velocity vector plots.

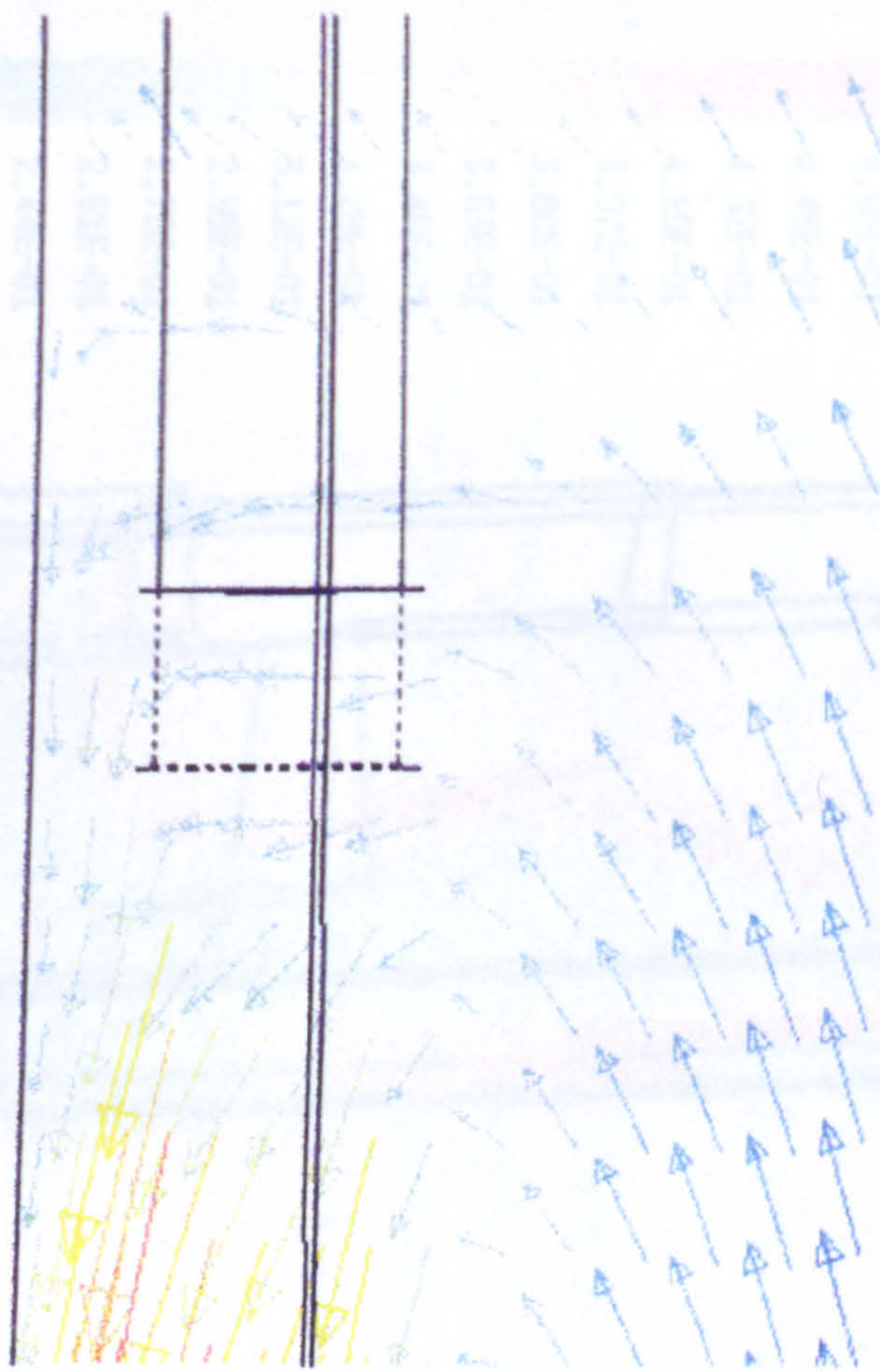

Figure 9-12 Entrainment of air around duct region using W-Velocity vector plots.

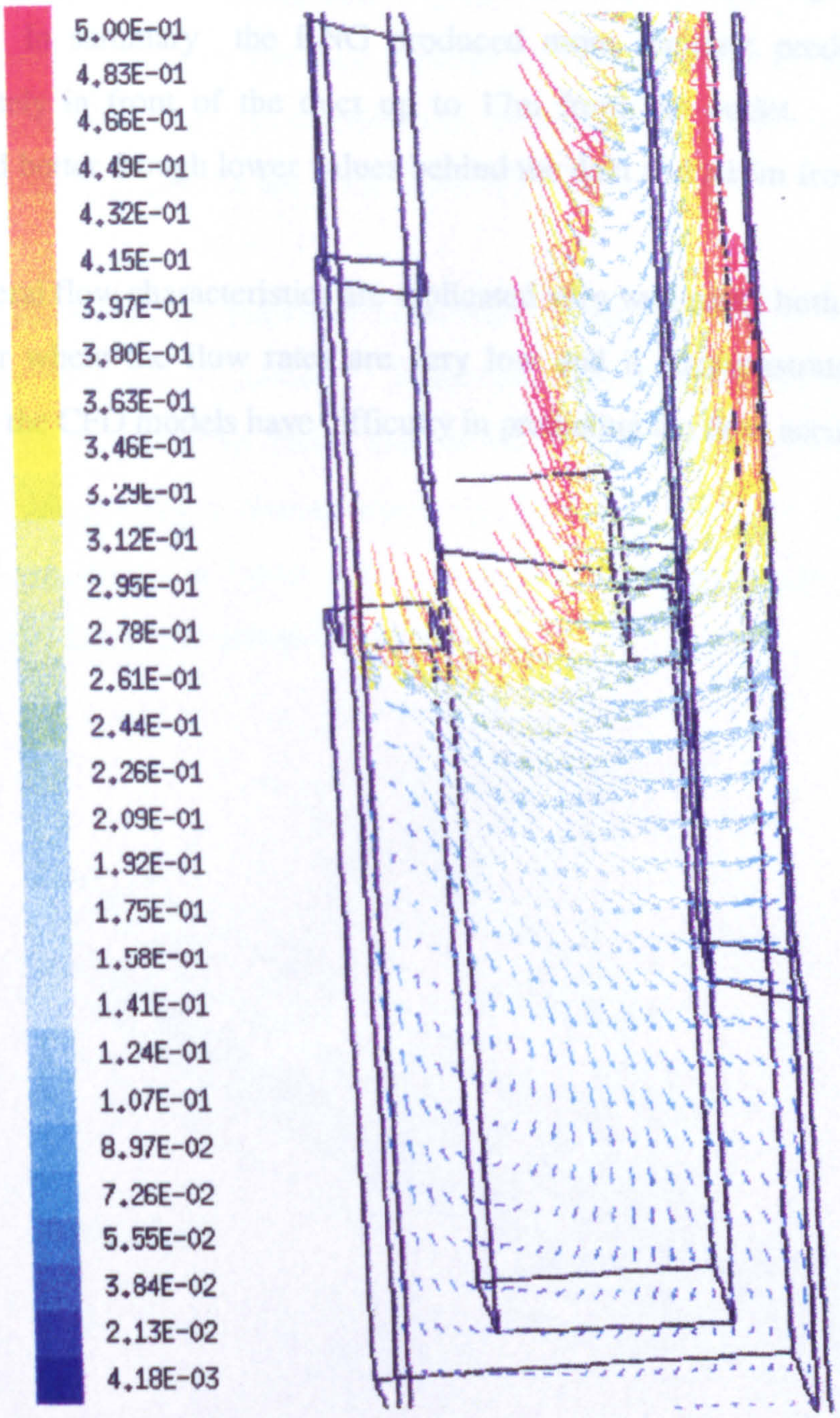

Figure 9-13 - Slice through centre of duct.

9.2.5 Conclusions

A comparison between the series of underground measurements and CFD predictions indicate that in regions of developed flow the RNG produces better results. The RSM under predicts actual velocities but is better where a high degree of uncertainty is evident. In summary the RNG produced more accurate predictions in the areas immediately in front of the duct up to 17m from the outlet. Whereas the RSM predicted better though lower values behind the duct and >15m from the duct outlet.

The general flow characteristics are replicated very well using both turbulence models. However where the flow rates are very low and it demonstrates a high degree of variance the CFD models have difficulty in predicting the flow accurately.

9.3 CASE 2 - 75'S HEADING CONVENTIONAL OVERLAP.

This experiment was conducted in 75's heading which is located in the North of the mine (Plan 1 - Appendix 7). The heading is 4.1m wide by 3.1m high and is ventilated using a conventional overlap system. (figure 9-14) An exhaust duct 600mm in diameter was maintained 3m from the face through the use of a mono-rail. A forcing duct 900mm in diameter, was positioned 15m from the face. The exhaust duct extracted 56% of the air delivered by the forcing duct (2.5m^3/s).

Forcing and exhaust air quantities were ascertained using a pitot inserted into the duct detailed in the previous section. Point anemometer measurements were also taken along the jet centreline to within four metres of the face. These are compared with predicted values using a dimensionless plot (figure 9-15). The overall predicted flow pattern is illustrated in figure 9-16. A representative longitudinal slice through the centre of the duct is illustrated in figure 9-17.

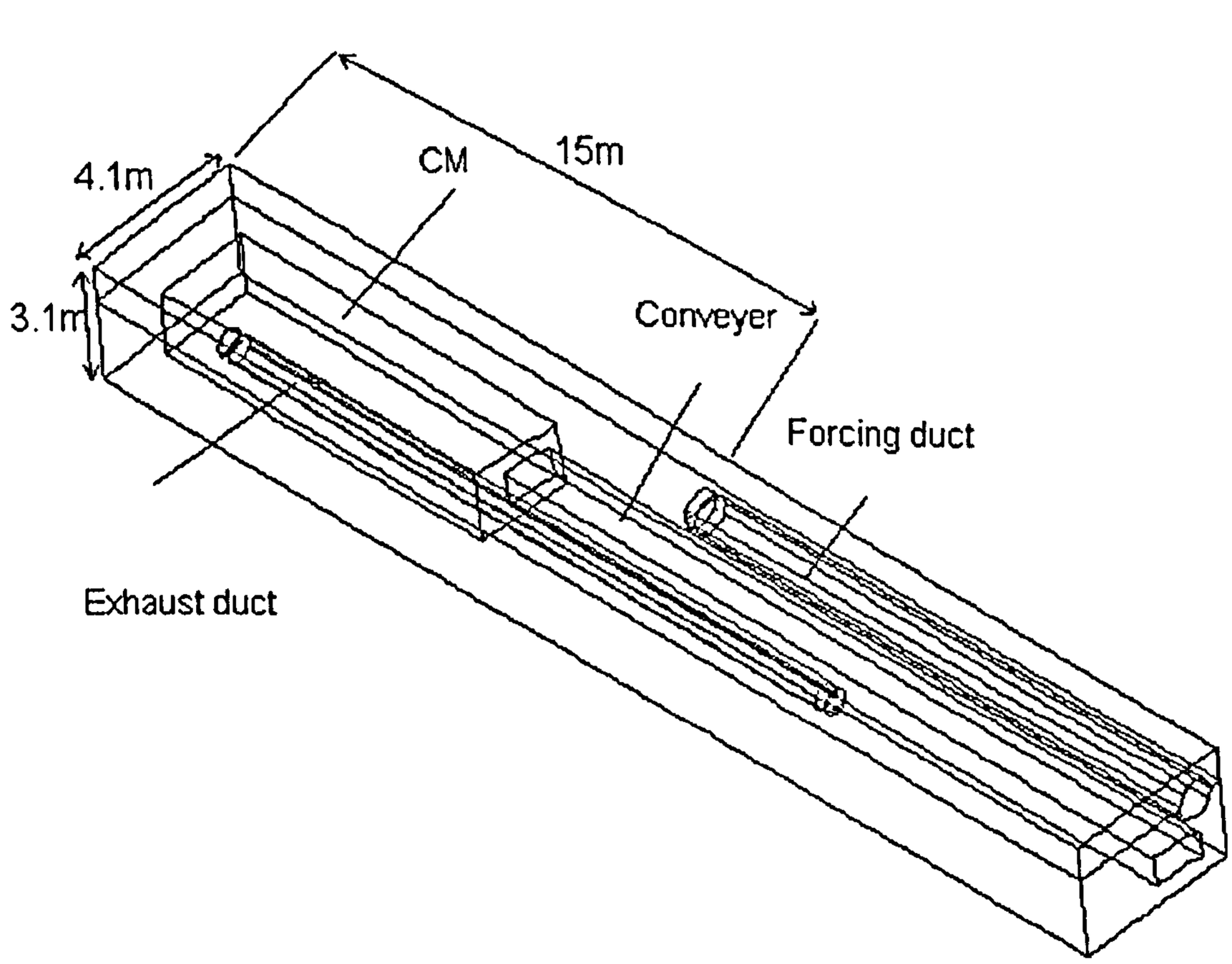

Figure 9-14 - 75's heading employing a conventional overlap auxiliary ventilation system

9.3.1 The Construction of the CFD model.

Initially the geometry was constructed in DDN in the usual manner. The grid was constructed by splitting the domain into separate blocks. The node densities were then specified along the edges of each sub block and the resultant mesh created. The resultant mesh was analysed in Leo and any alterations required were undertaken. The grid was imported into the Fluent package and the physical constant specified. The k-ε RNG turbulence model initiated and the solution sent for processing. This particular scenario was difficult to converge to the required degree of accuracy. Some subsequent under-relaxation on some of the parameters was required to help satisfy the convergence criteria.

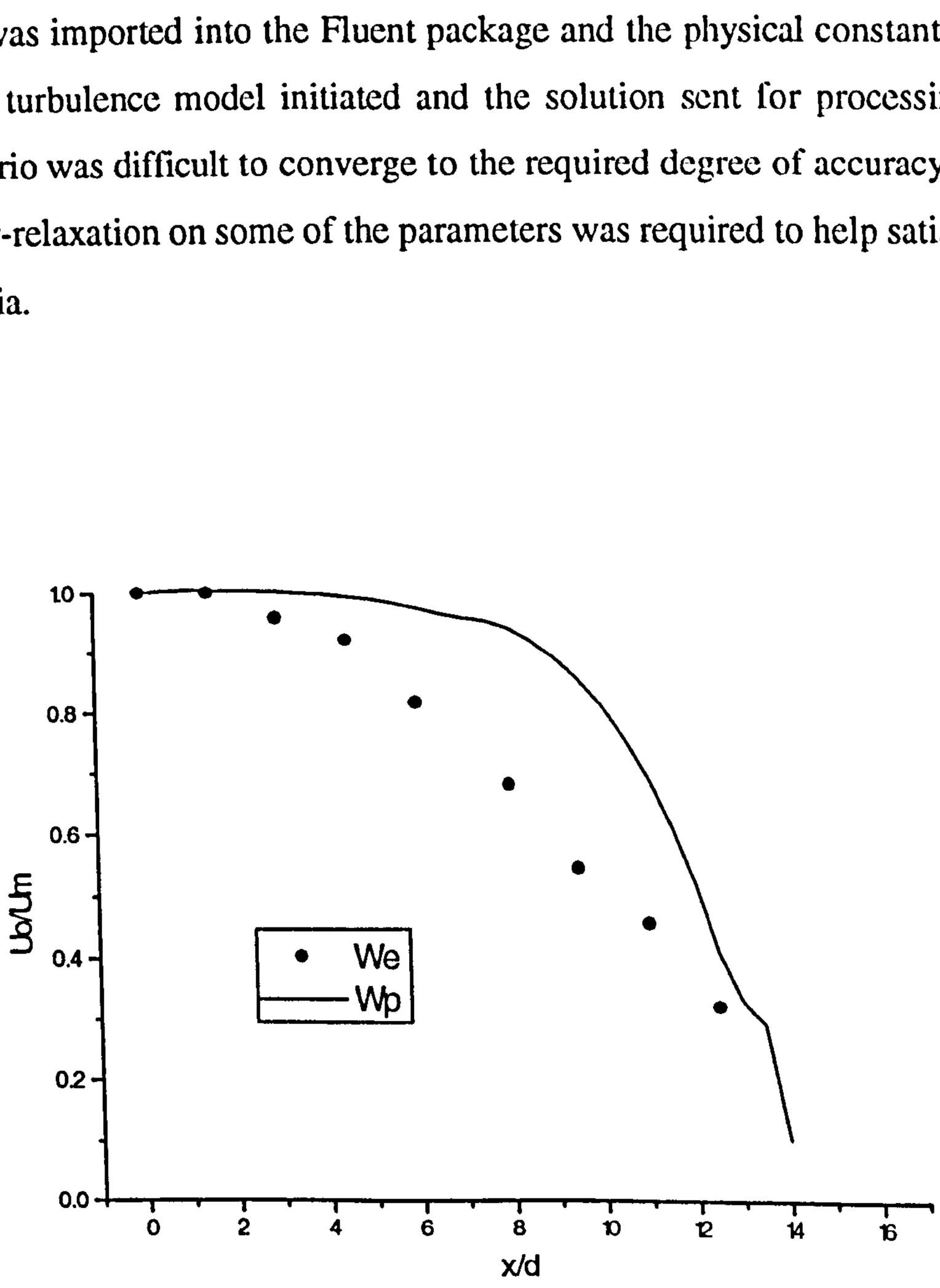

Figure 9-15 - Dimensionless plot of W-velocities measurements versus predictions in jet region.

9.3.2 Presentation and discussion of results

The dimensionless plot (figure 9-15) illustrates the predicted and experimental jet centreline velocities. The experimental and predicted results compare quite well in the initial region of the jet. The velocities in the middle of the jet are over predicted by the k-ε RNG turbulence model. The latter experimental readings compare quite well with the model prediction. This clearly illustrates that the dispersion of the jet is been under predicted.

Figure 9-16 illustrates predicted W-velocity vector plotted on a number of vertical planes. The velocity vector representing the forcing jet can be seen to drift towards the exhaust duct with a secondary re-circulation zone forming on the right-hand side of the roadway. These features are more clearly identified on the longnitudal section taken through the centre of the forcing jet. (figure 9-17) The air flow can be seen to leave the roadway via the lower region of the roadway on both the right and left sides (figure 9-17). However, in reality when the CM is cutting water sprays mounted on the boom will direct the air around the face. Other sprays used for dust control will also distort the flow features. Venturi airmovers are also present in some headings. Thus caution should be taken when interpreting the results obtained from these initial CFD simulations.

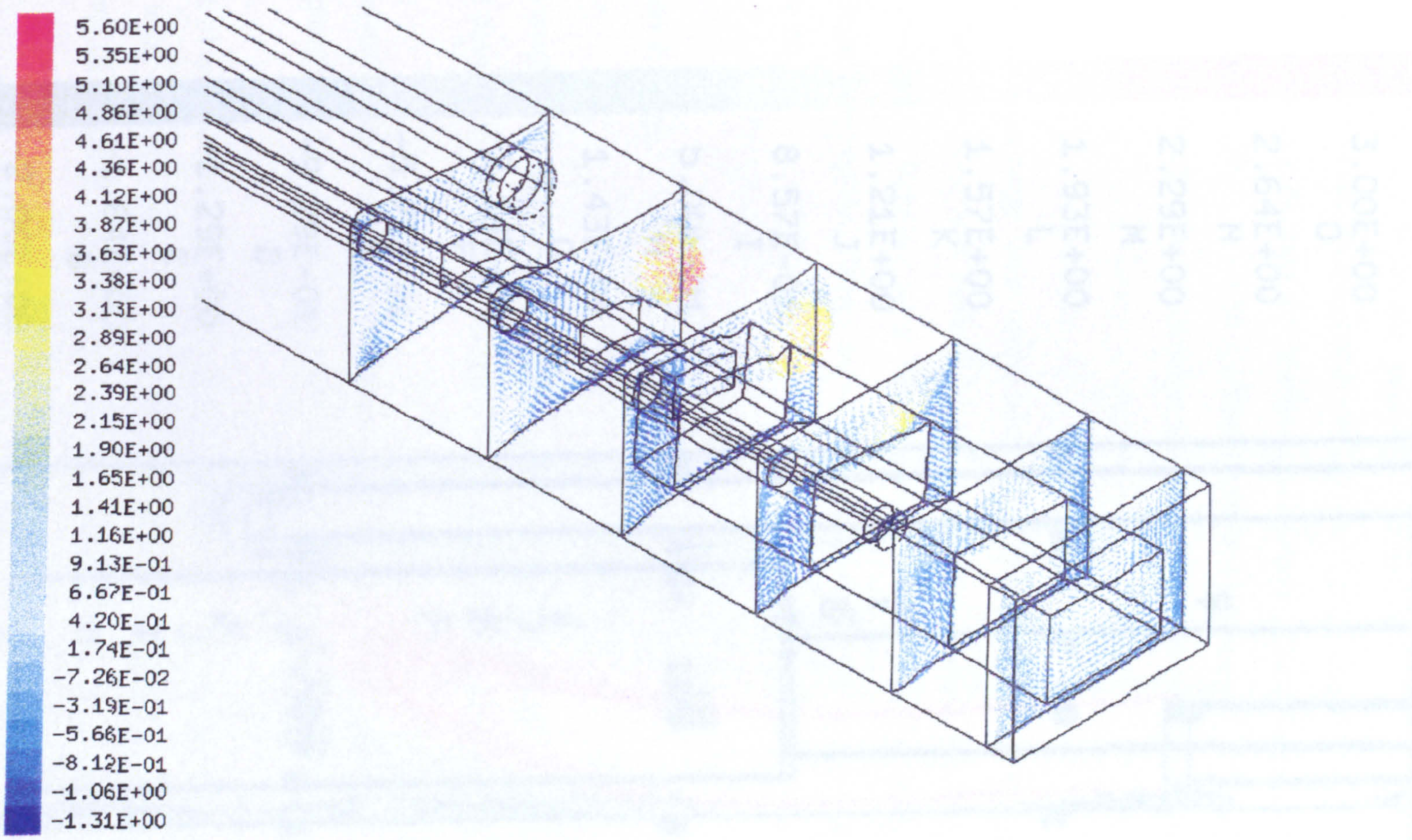

Figure 9-16 - W -velocity vectors illustrating flow patterns

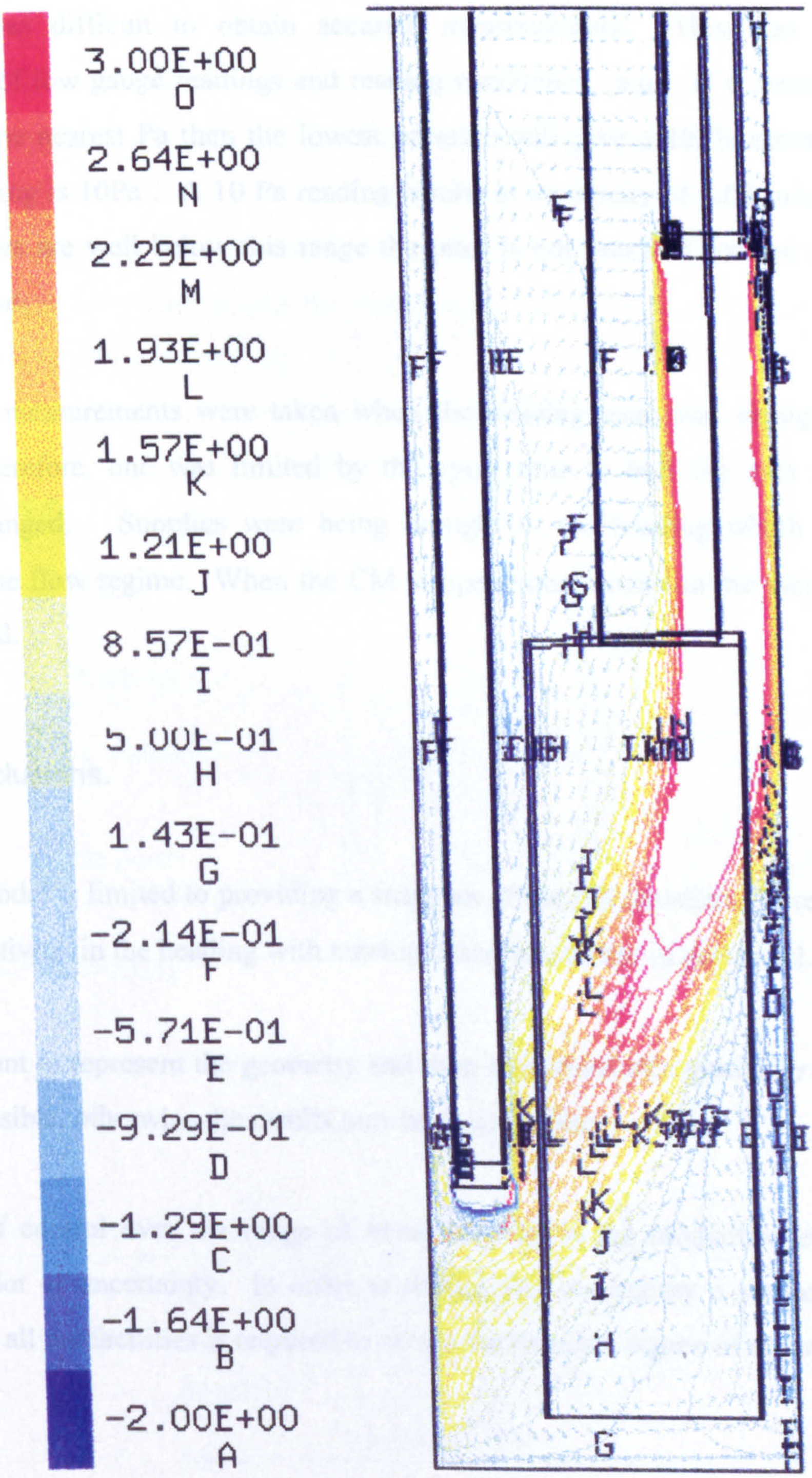

Figure 9-17 - Overlay of Velocity vectors and contours

9.3.2.1 Problems encountered in 75's.

Due to problems with low and fluctuating velocities experienced within the face of the heading it was difficult to obtain accurate measurements. This was due to a combination of low gauge readings and reading oscillation. e.g. If a pressure gauge can read to the nearest Pa then the lowest pressure will give a 10 % accuracy if the pressure reading is 10Pa . A 10 Pa reading results in a velocity of 4.08 m/s and since most velocities are well below this range the pitot is not practical for use in the low velocity region.

Air velocity measurements were taken when the heading team was engaged in roof bolting. Therefore, one was limited by the cycle time to bolt the area before the situation changed. Supplies were being brought to the heading which may have influenced the flow regime. When the CM is operational access to the vicinity of the face is denied.

9.3.3 Conclusions.

The CFD model is limited to providing a snapshot of the full situation. In reality, there is a lot of activity in the heading with machines and movement of personnel.

It is important to represent the geometry and inlet conditions of a particular scenario as close as possible, otherwise the results may be meaningless.

The lack of control over the range of measurements in the production environment leads to a lot of uncertainty. In order to reduce this uncertainty a surface full-scale model with all the facilities is required to obtain the required degree of accuracy.

9.4 CASE 3 - ROOM AND PILLAR OPERATIONS.

9.4.1 Heading details

The room and pillar operations are situated in the southern section of the mine to the west of 143's. (Plan - appendix 7) The room and pillar operation is cyclic in nature. Consequently while the CM is cutting in one heading an adjacent drivage is being rock bolted. This increases the utilisation of the CM and normally results in greater production. Figure 9-18 illustrates the ventilation system employed in the room and pillar operations at Wistow Colliery.

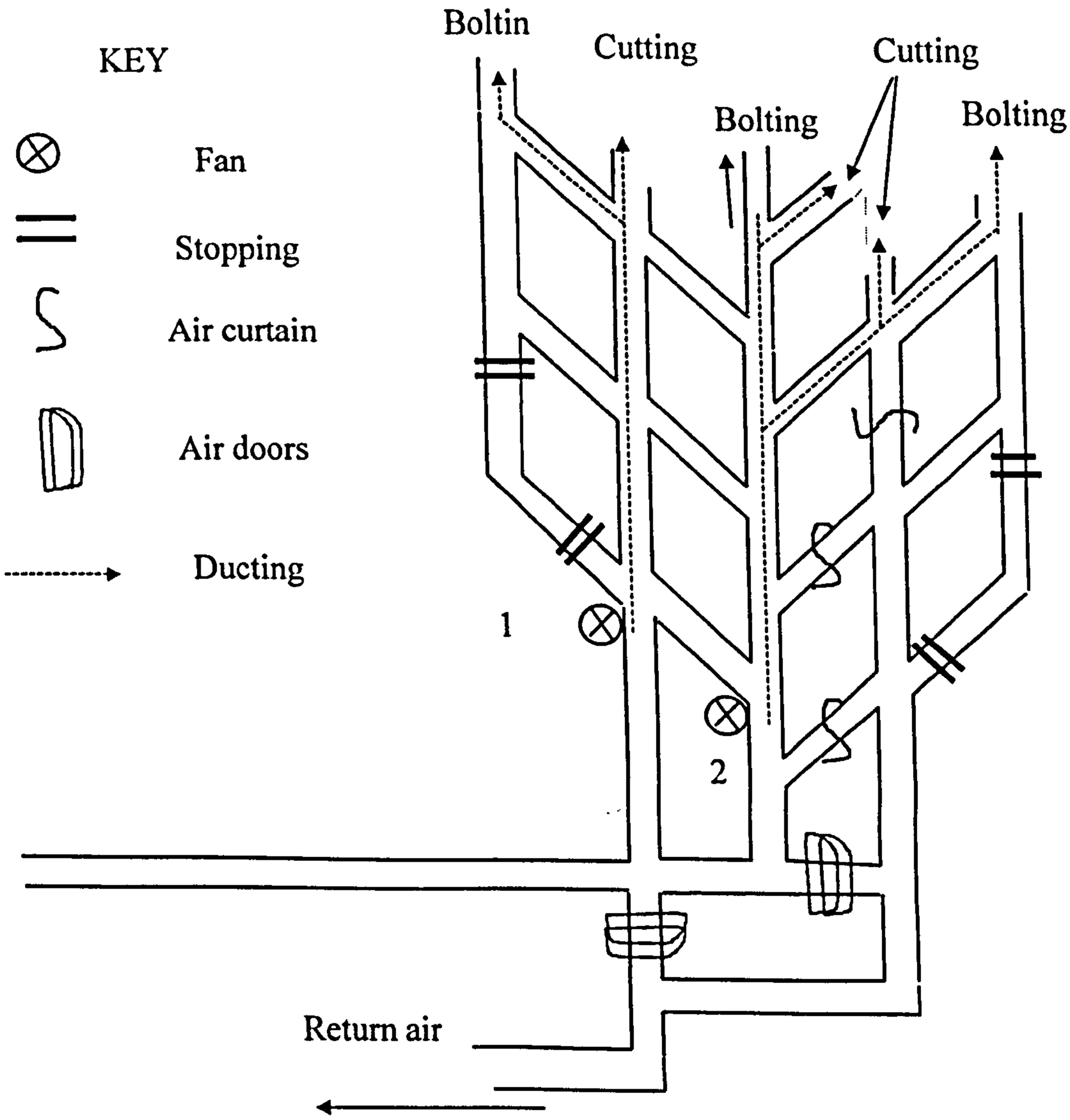

Figure 9-18 - Room and pillar operations at Wistow Colliery.

The system consists of two forcing auxiliary fans. The two fans supply air to the headings via flatlay ducting. The return air circuit is controlled by stoppings and bratttice cloth strategically placed to course the air around and out of the district. As the district extends further away from the main roadway a booster fan will be installed.

9.4.2 Measurement locations

It was not possible to attain accurate measurements in the production zones because of the busy and congested environment. Therefore, a measurement programme was under taken in the heading that had just been roof bolted (figure 9-19). The rooms had a width of 5.5 metre and were 3.5 m in height. A 760mm forcing duct situated 7 m from the face delivered 3.5 m^3/s to the heading. This forcing duct is normally fitted with a winsock but was removed during the experimental measurements. The peak velocities were recorded in the region of the jet and compared to CFD predictions using a dimensionless plot (figure 9-20). Point measurements with the LCA 30IS (figure 2.9) anemometer were taken at various sections in the heading (figure 9-20 to 9-24).

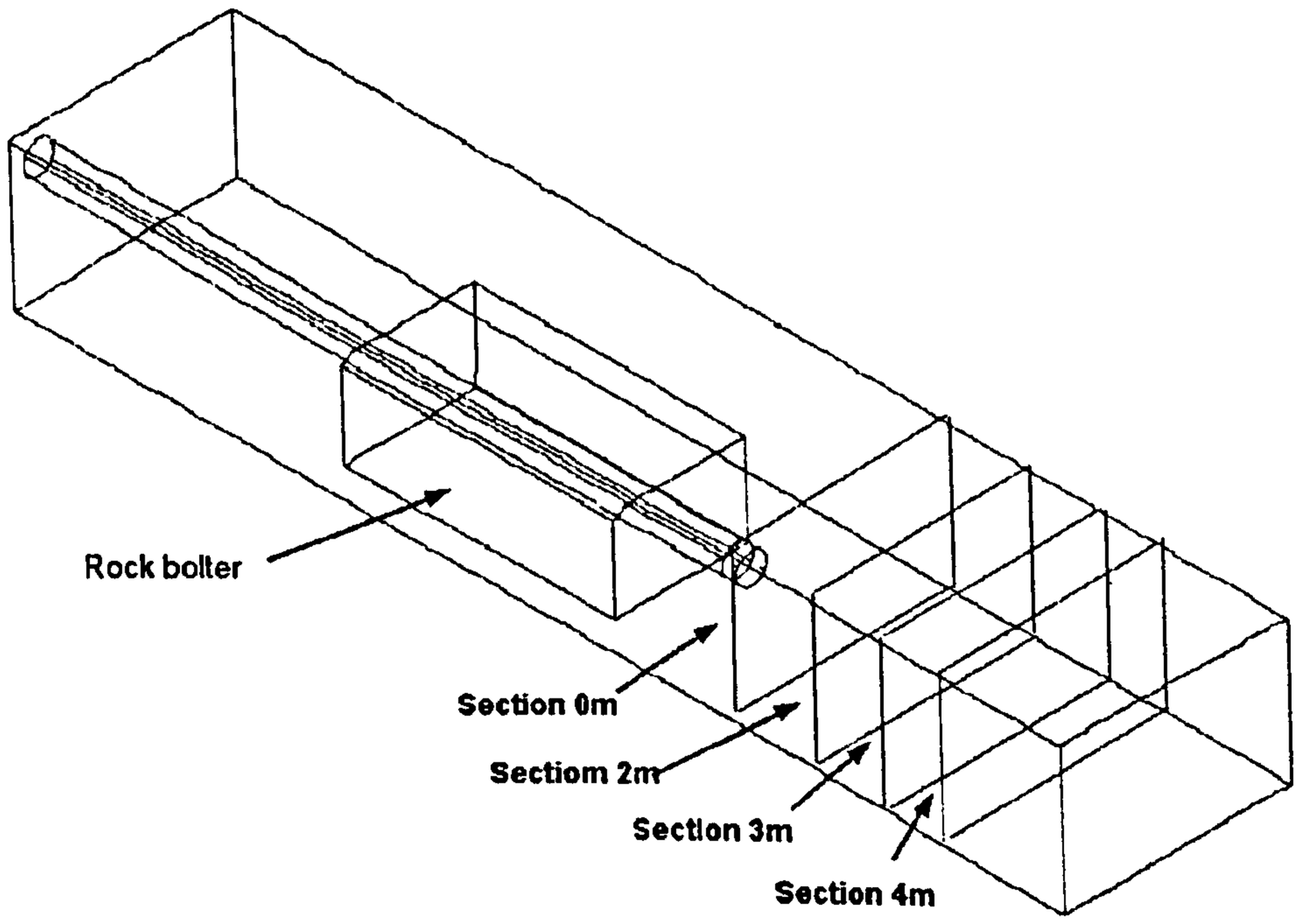

Figure 9-19 Sketch of measuring locations in room and pillar operation.

9.4.3 The construction of the CFD model

The mesh was constructed in a similar manner to that described in the previous sections. The grid had eighty one thousand cells in total with more cells inserted in the region from the duct to the face. This was performed in an attempt to capture the effects of the jet in the roadway. The k-ε RNG model was used to model the turbulent fluctuations in the flow regime. This model was utilised because of the observed improvement of accuracy in predicting flows within this region.

9.4.4 Presentation and discussion of results.

From an analysis of the results plotted on figure 9-20 the predicted jet centreline velocities slightly overpredict the experimental results. However the results from this heading show a closer correlation to those obtained for the previous heading described in section 9.3. This is probably because more control was possible over the period of experimental measurement programme. It has also been shown in figure 9-3 and the scale experimental work described in chapter 8 that the predictions in this region are very good. (i.e x/d values of 9-20)

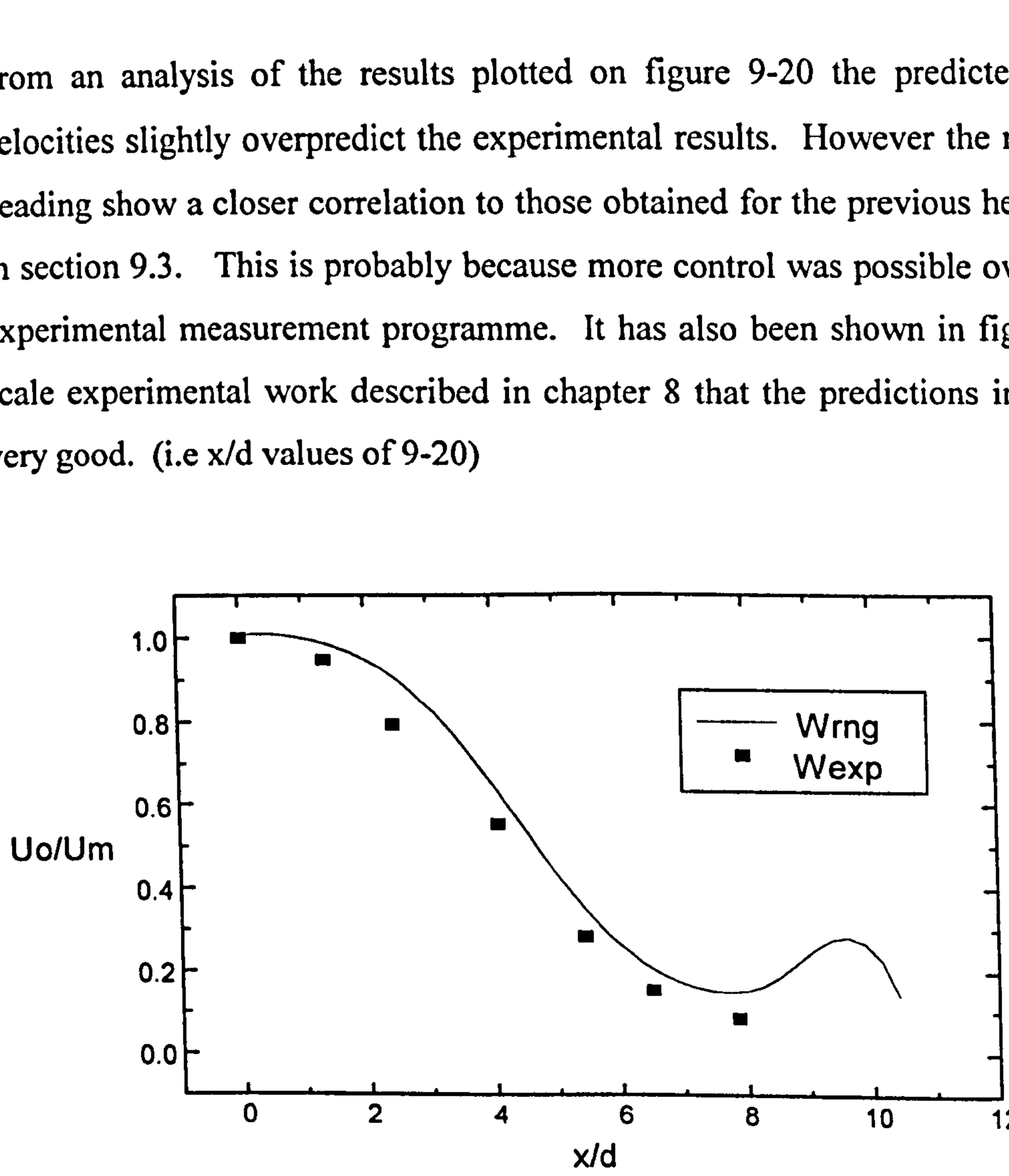

Figure 9-20 - Comparison of predicted (Wrng) and measured (Wexp) W - velocities from duct outlet to face.

The CFD models have successfully reproduced the general characteristics and flow directions very well for all cases studied. All of the simulations replicate the Coanda effect. The air then scours the face and leaves via the right side of the roadway. The predictions and measurements compared favourably considering the hostile conditions encountered underground.

The CFD model replicated the re-entrainment (indicated by the positive velocity values) occurring behind and below the duct (figure 9-22). This phenomena occurs in the field and was mapped using smoke tubes. The zone of en-trainment extends a little too far to the right of the roadway. This trend was also evident in the scale model study (chapter eight). The majority of the air leaves the drivage via the top of the roadway and is predicted very well by the model.

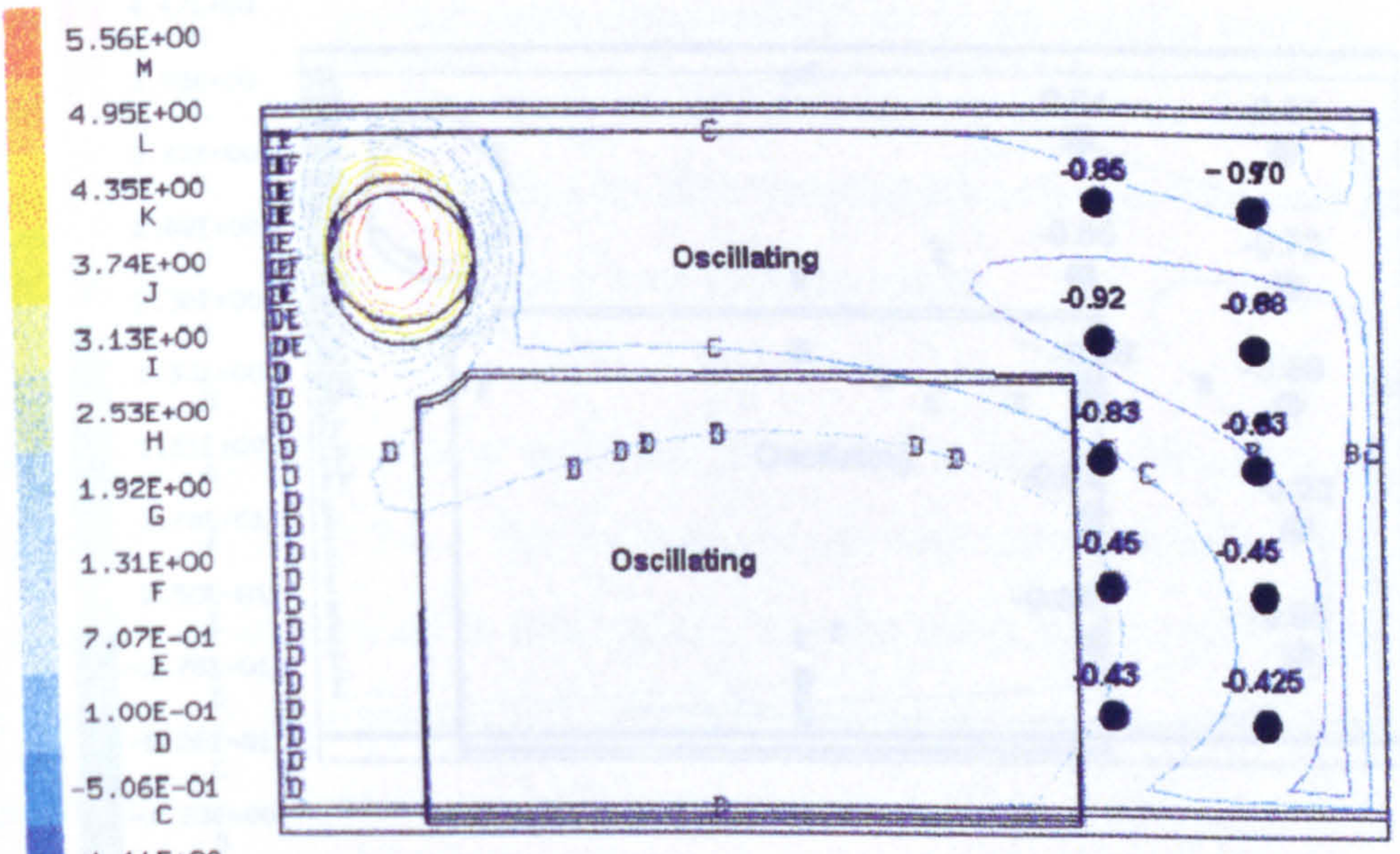

Figure 9-21 - 0m at duct outlet

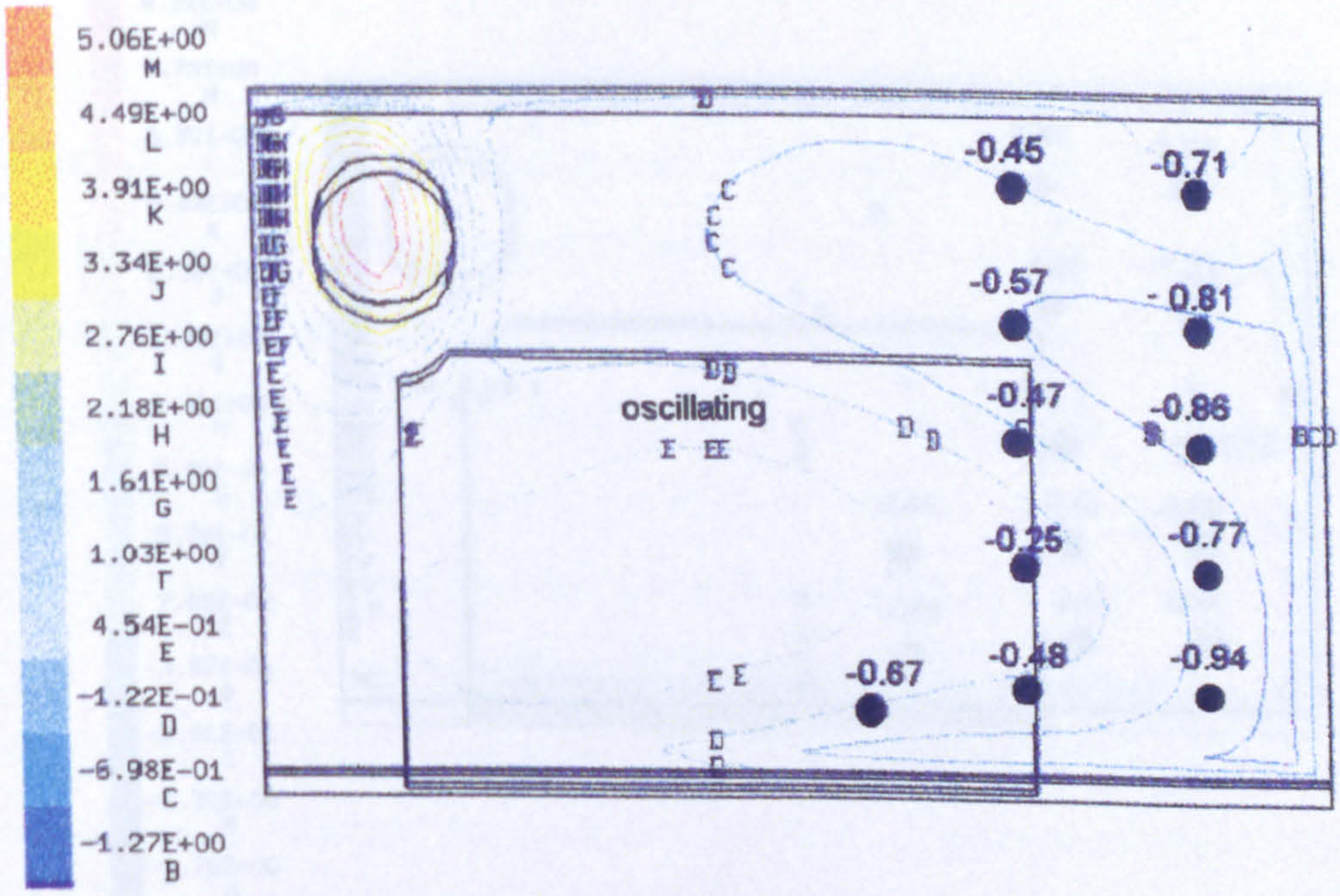

Figure 9-22 - 2m from duct outlet

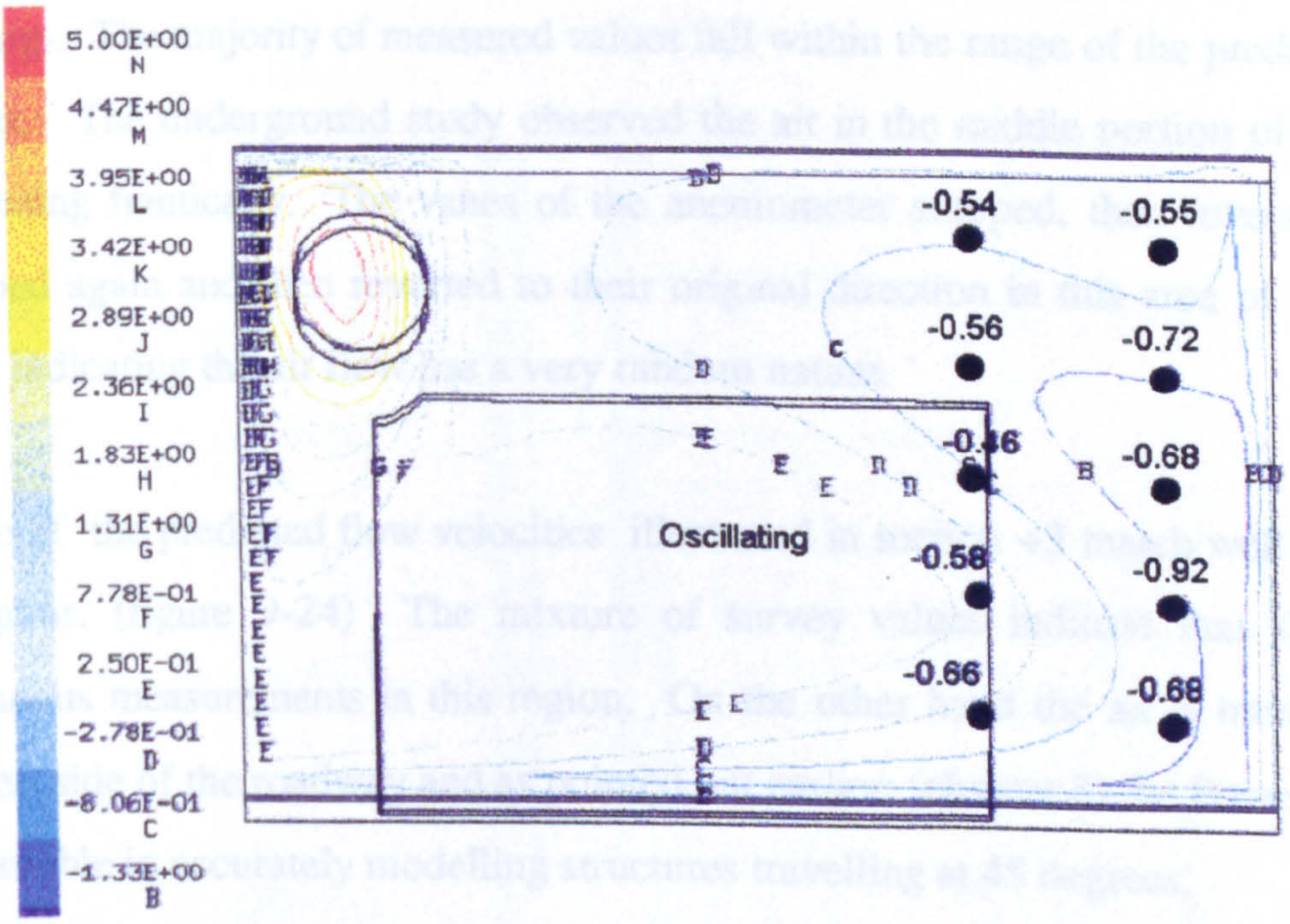

Figure 9-23 - 3m from duct outlet

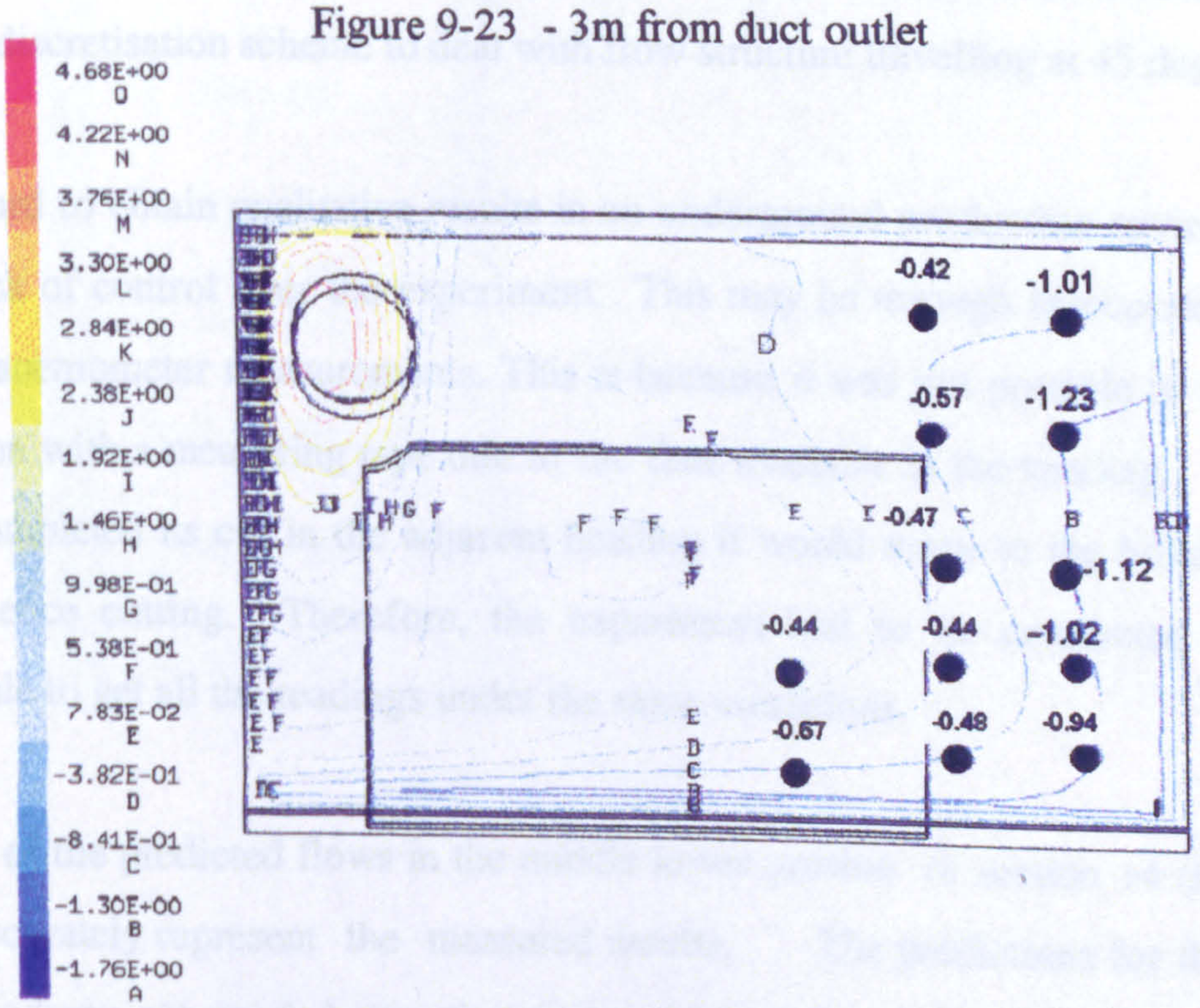

Figure 9-24 - 4m from duct outlet

In section +2 (figure 9-23) the predictions compare favourably with the measured readings. The majority of measured values fall within the range of the predicted contour values. The underground study observed the air in the middle portion of the roadway oscillating frantically. The vanes of the anemometer stopped, then reversed direction, stopped again and then reverted to their original direction in this area of the roadway. Thus indicating the air flow has a very random nature.

Some of the predicted flow velocities illustrated in section +3 match well whilst others are poor. (figure 9-24) The mixture of survey values indicate that there may be erroneous measurements in this region. On the other hand the air is travelling toward the left side of the roadway and as pointed out earlier; (chapter 8) the Power law scheme has trouble in accurately modelling structures travelling at 45 degrees.

This variation between measured and predicted values may be attributed to one or a combination of the following; 1) an inherent error in the measured values, 2) the ability of the discretisation scheme to deal with flow structure travelling at 45 degrees.

It is hard to obtain qualitative results in an underground production environment due to the lack of control over the experiment. This may be through inaccurate placement of point anemometer measurements. This is because it was not possible to measure every position with a measuring tape due to the time available in the heading. Once the CM has completed its cut in the adjacent heading it would move to the bolted heading and commence cutting. Therefore, the experiment had to be conducted as quickly as possible to get all the readings under the same conditions.

Some of the predicted flows in the middle lower portion of section +4 (figure 9-25) do not accurately represent the measured results. The predictions for the right side of the roadway are much better that those obtained for the section +3. This may also indicate that some of the measurements acquired for section +3 are inaccurate.

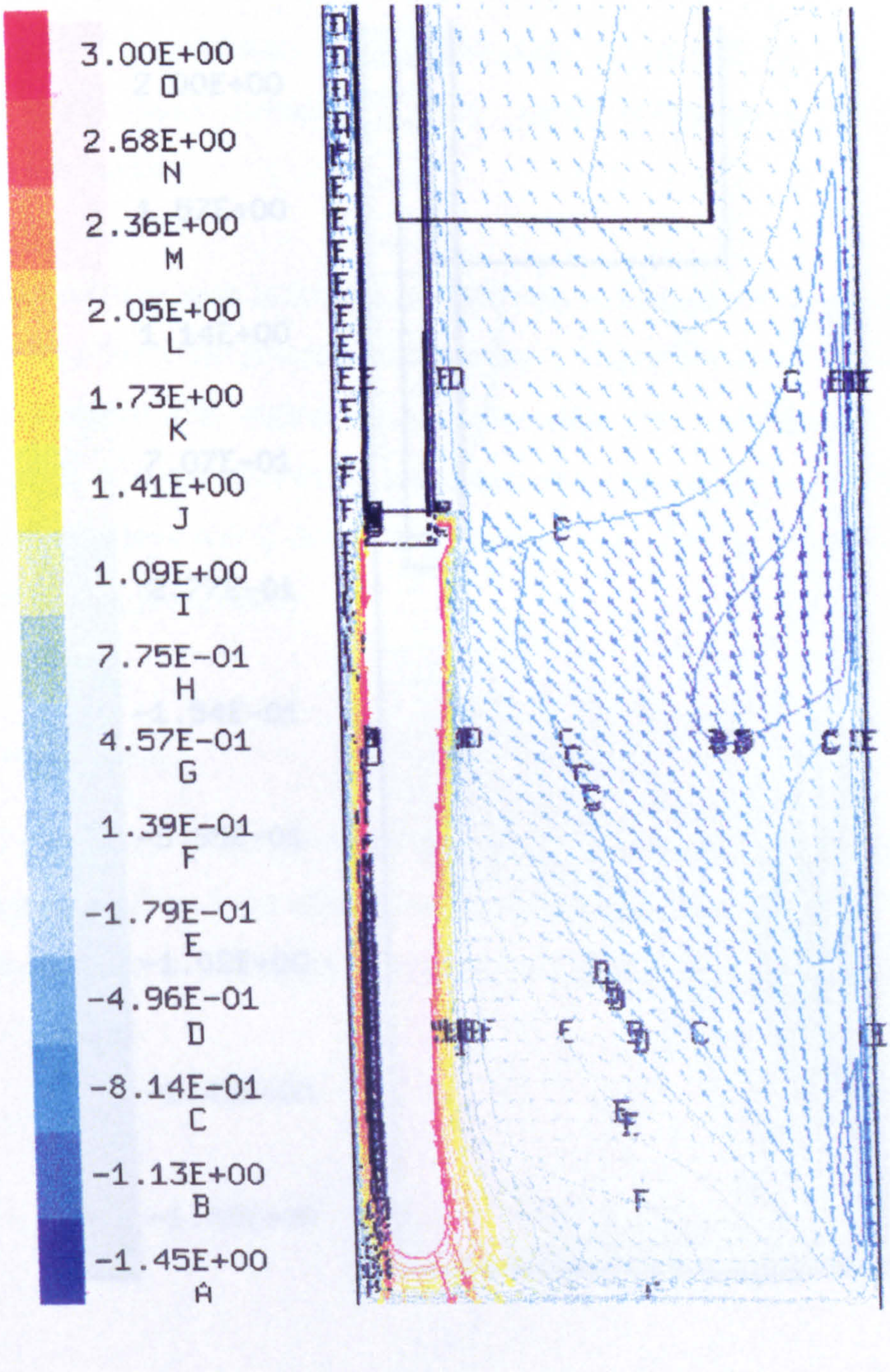

Figure 9-25 - Slice through centre of the duct with vectors overlayed on velocity vectors.

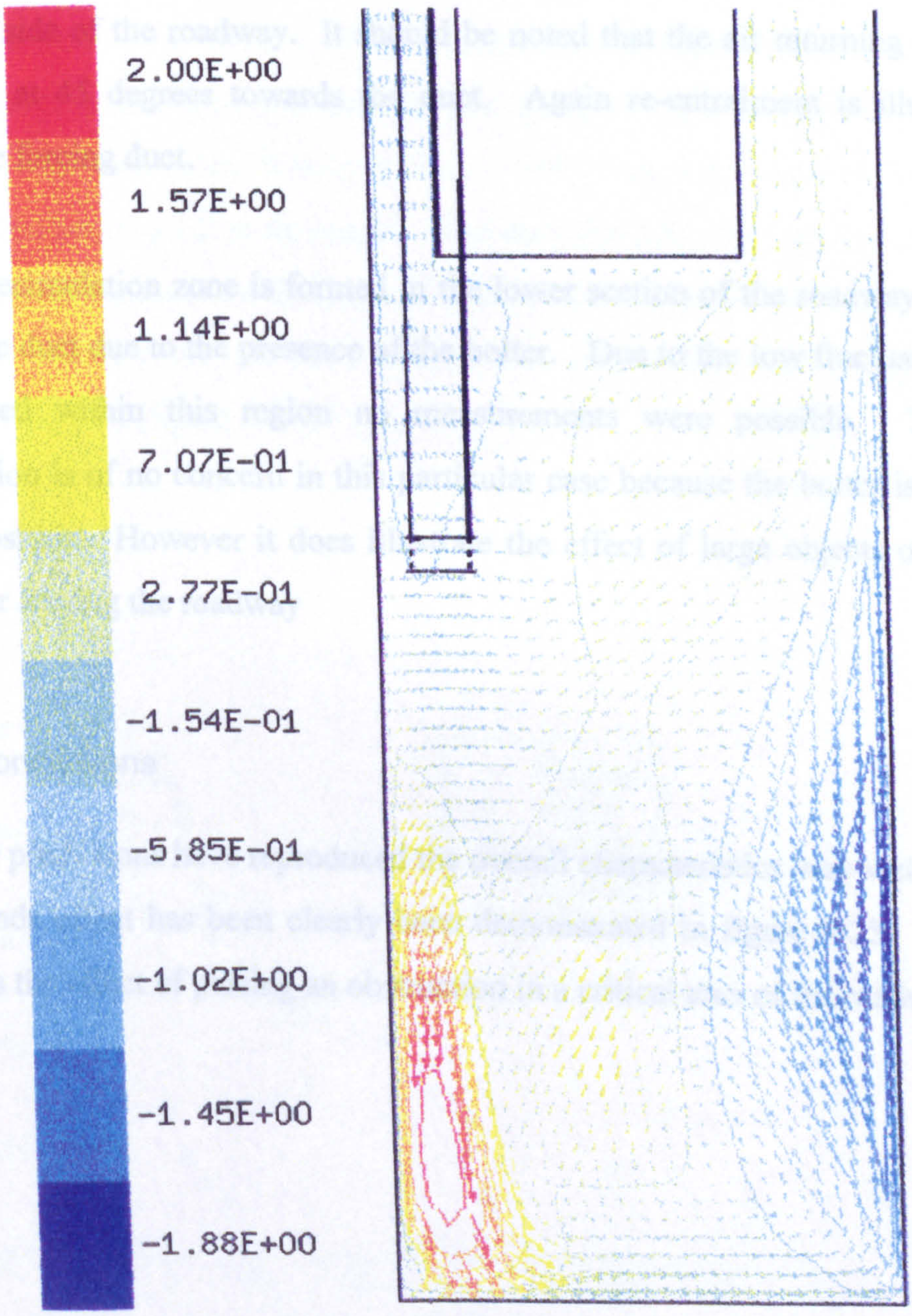

Figure 9-26 - Slice through middle of the roadway with a W-velocity vectors on a contour plot.

Figure 9-25 illustrates a longitudinal slice through the centre of the duct with the predicted velocity vectors overlaid on contours. It illustrates the jet clinging to the wall, scouring the face and leaving the roadway. The interaction between the jet and the returning air causes the air to oscillate randomly whilst the majority of air leaves via the rights side of the roadway. It should be noted that the air returning from the face does drift at 45 degrees towards the duct. Again re-entraiment is illustrate at and behind the forcing duct.

A small recirculation zone is formed in the lower section of the roadway (figure 9-26) behind the duct due to the presence of the bolter. Due to the low fluctuating velocities experienced within this region no measurements were possible. This zone of recirculation is of no concern in this particular case because the bolter is not normally in this position. However it does illustrate the effect of large objects obstructing the path of air leaving the roadway

9.4.5 Conclusions

The CFD predictions have reproduced the overall characteristics very well for this case. The Coanda effect has been clearly been demonstrated in figure 9-25. Figure 9-26 illustrates the effect of placing an obstruction in a critical area of the roadway.

9.5 VALIDITY OF MEASUREMENTS.

9.5.1 Comparison of experimental and CFD data with previous data.

In order to assess the validity of the measurement programme it was necessary to compare them to previous data in a similar scenario. The experimental results were compared with data from Wesley (1984). This data was obtained from an arched roadway section of a 1/2 scale model. The duct diameter was not specified, therefore an assumption was made on the basis of typical duct diameters employed in Germany at that time. The data for the three case studies and Wesley data is represented on a dimensionless plot (figure 9-28)

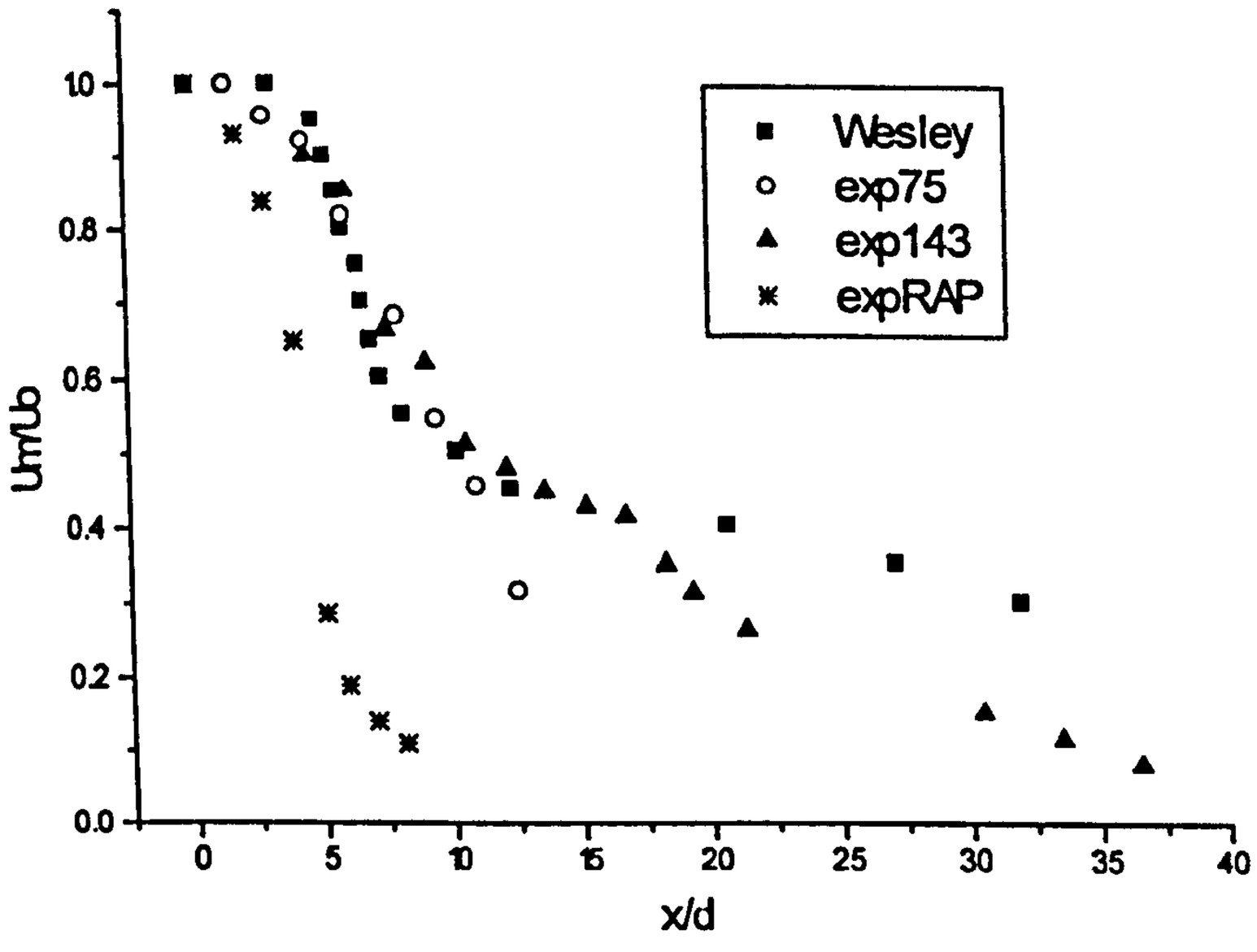

Figure 9-27 - Comparison of experimental studies and previous data

The experimental results obtained from 75's headings (exp75's) and 143's (exp143) compare favourably with Wesley's data. The latter measurement points for headings 75's and RAP tail off because the close proximity of the face (7m and 15m respectively). Thus the jet's penetration is ended prematurely. In the case of 143's the effect of the stage loader probably accounts for the discrepancy.

Considering the conditions in the underground environment and the instrumentation utilised the results obtained are quite satisfactory.

Figure 10-29 illustrates the predicted values against Wesley's data. This clearly shows the k-ε RNG model over predicting for the 75's heading case. The prediction obtained for 143's heading takes the stage loader into account and thus predicts lower values for x/d values in excess of 15-20.

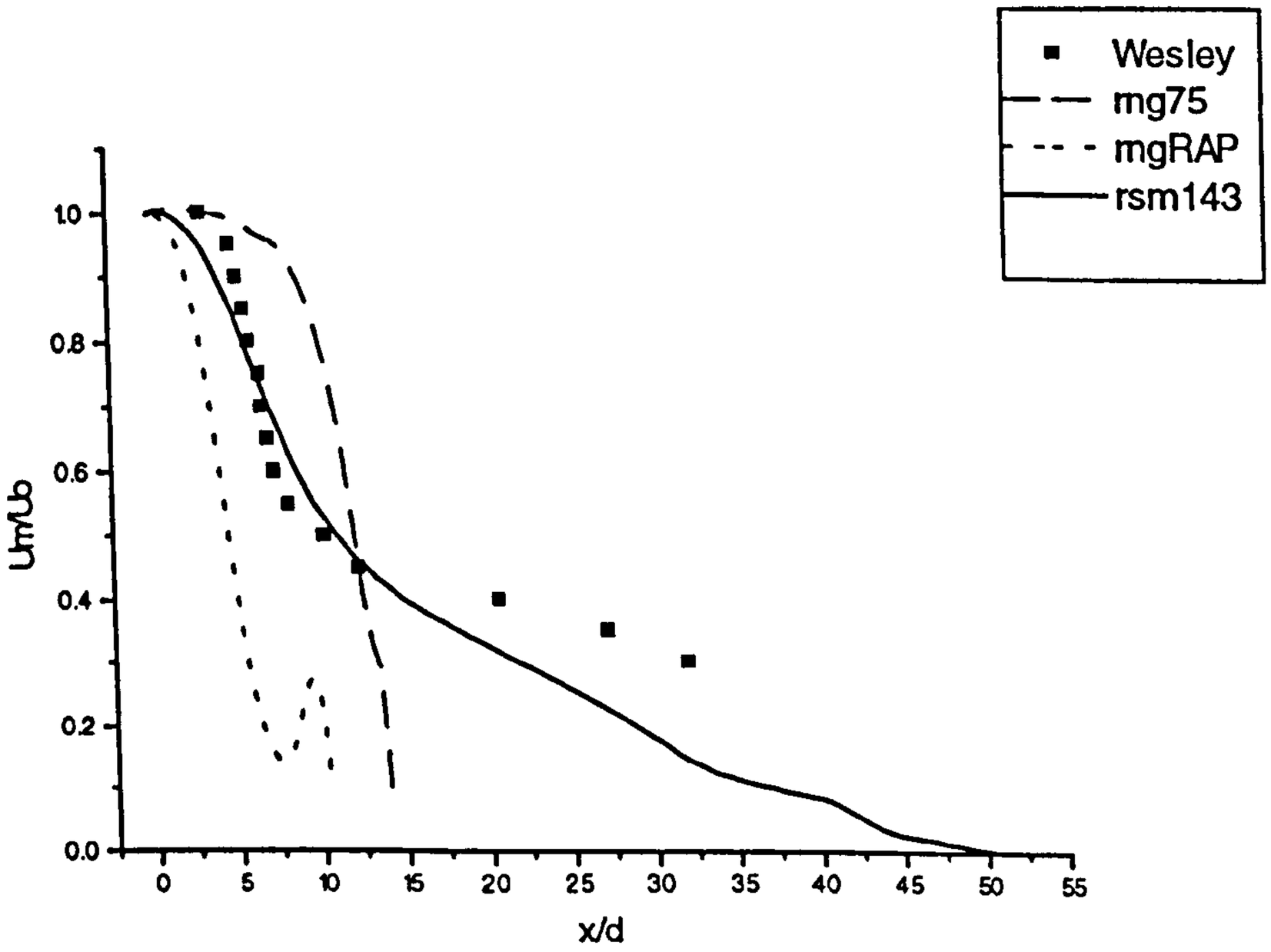

Figure 9-28 - Comparison of Wesley's data against experimental predictions.

9.5.2 Conclusion.

The data obtained in the jet region from the underground environment is reasonably accurate when compared with experiments conducted in a controlled environment. Therefore it could be surmised that the data obtained in the remaining section of the roadway is reasonably accurate.

9.6 SUMMARY.

The results of the measurement programme conducted in the underground headings have been presented. The resultant CFD predictions have showed reasonable correlation.

The underground measurements in the jet region have been validated against data obtained by Wesely (1984).

The following chapter reviews the conclusions obtained throughout this thesis.

10. CONCLUSIONS AND FURTHER WORK.

10.1 SUMMARY OF CONCLUSIONS

Previous research introduced in chapter five indicated that a jet emanating from a circular orifice has a penetration distance of approximately twenty metres. This has been reinforced by the underground experiments conducted in heading 143's at Wistow colliery.

In order to have any confidence in the predicted values one must demonstrate that the final solution achieved is independent of the node density. This reduces the uncertainty associated with computational grids.

The CFD models of full scale gallery trials (chapter 5) have predicted the general flow characteristics qualitatively. However, in order to have more confidence in the model predictions one must demonstrate that the values obtained are reasonably accurate. This lead to a series of physical scale model tests using laser light and Laser Doppler Anemometry (LDA) to obtain quantitative data in a controlled environment.

The CFD predictions obtained from the model discussed in chapter eight generally agree with the flow patterns attained from the flow visualisation study.

The LDA study detailed in chapter eight has produced quantitative measurements for comparative purpose with CFD. The predictions obtained for the k-ε RNG model are much better in the central jet region than any other model tested. The RSM model produced slightly better predictions for the lower region when compared with the RNG model. Overall the k-ε RNG returns the superlative forecast for the five and ten metre configuration. Woodburn also demonstrated that the modified k-ε model produced better results than the standard k-ε model.

The sensitivity analysis conducted in the latter part of Chapter Eight illustrated a number of important points;

1) wall roughness is an important part of the modelling process.
2) varying the density and viscosity does not alter the overall prediction significantly.
3) the grid spacing behind the duct needs to be increased dramatically.
4) higher order discretisation schemes tend to be unstable for this type of flow.
5) the standard wall function was the most stable scheme employed.

It is clear that the CFD models produce superior predictions for flows with reasonable turbulence intensity values, for example, the jet region. The higher the turbulence intensity the more inaccurate the results become. It has also been demonstrated that the closer one approachs zero the harder it is to predict.

The 143's heading case study detailed in Chapter Nine found that the RNG prediction compared favourably with measured results in the areas immediately in from of the duct up to 17m from the outlet. Whereas the RSM produced better comparisons for the low fluctuating velocities behind the duct and >15m from the duct outlet.

The general flow characteristics are predicted very well using both models. However where the flow rate is very low and it demonstrates a high degree of variance both CFD turbulence models have difficulty in predicting the flow accurately.

It is important to represent the geometry and inlet conditions of a particular scenario as close as possible, otherwise the results may be meaningless.

The lack of control over the range, repeatability and accuracy of measurements in the production environment leads to a lot of uncertainty. In order to reduce this uncertainty a surface full-scale model with all the facilities is required to obtain quantitative measurements in a controlled environment.

The CFD model is limited to a snapshot of the full situation. In reality there is a lot of activity in the heading with machines and personnel moving around. Therefore it is important to represent the situation as closely as possible

This thesis had fulfilled its objectives; it has demonstrated that CFD can provide a useful predictive tool in the investigation of the flow patterns within drivages. The user should always be aware of the physical and numerical limitations of the models employed particularly the turbulence models. The CFD model is a useful tool when used in conjunction with physical models and field measurement where possible.

10.2 FURTHER WORK.

The lack of control in the production environment leads to a lot of uncertainty. In order to reduce this uncertainty a surface full-scale model with all the facilities is required to obtain the required degree of accuracy.

Further underground work in an old working district with all the equipment would also be beneficial.

It is necessary to attain superior computer resources to undertake sensitivity analysis on the grid behind the duct in the CFD model.

The CFD models may be employed to assist in the design a new auxiliary ventilation system. This may involve simple changes like the position of the duct or the quantities delivered. Finally, a novel auxiliary system could be designed using CFD models before full scale testing.

Predicted values in classic flows such as an impinging wall jet in flows with low turbulence intensity are quite good. The most likely reason for this is that; constants utilised in some of the equations are *"fixed"* to predict this well know type of flow regimes. Hence, it may be useful to alter these constants and then compare the resultant predictions. This is beyond the scope of this thesis and will be conducted at a later stage.

REFERENCES

Abramovich, G.N, (1963) *The Theory of turbulent jets* MIT , Cambridge Massachusetts.

Apte, V.B, Green, A.R, and Kent, J.H, (1991) *Pool fire plume flow in a large-scale wind tunnel.* In Fire Safety Science - Proceedings of the thirs international symposium, 1991

Aziz, N , Srinivasa Rao B, Baafi E. (1993) *Application of Computational Fluid Dynamics codes to develop effective gas/dust control measures in underground coal mines.* Australian Coal Journal, No 42, 1993. pp 19-27

Bachlin, W., Theurer, W. and Plate, E. J. 1991, *Wind Field and dispersion in a built up area - A comparision between field measurements and wind tunnel data.* Atmospheric Environment, Vol.25A, No 7, pp 1135-1142.

Baker, R.C (1992) *An Introductory guide to Flow Measurement.* MEP, London.

Bakke, P. & Leach, S.J. (1962) *Principles of formulation and dispersion of methane roof layers and some remedial measures.* Min Eng 121(22) 645-58

Barker, A.H. & Highton, W. (1981) *Auxiliary ventilation in its wider aspects.* The Mining Engineer, February 1981.

Beard, A (1992) *Limitations of computers models.* Fire Safety Journal 18:375-391, 1992.

Bettis et al, (1994) *The Use of physical and mathematical modelling to assess the hazards of tunnel fires.* 8th International symposium on Aerodynamics of Vehicle Tunnels, 6-8 July, 1994 in Liverpool, UK.

Brandeis, J and Bergmann, D.J (1983) *A numerical study of tunnel fires.* Combustion Science and Technology, 35: pp 133-155

Brodke, R.S (1967) *The Phenomena of fluid motion* Addison-wesley, London

Browning, E.J (1983) *An approximate Method for Auxiliary Ventilated Calculations,* Min Engr, Vol 143, No 264, September pp129-34.

Browning E J, Warwick J S. (1993) *Ignition Prevention.* Min Eng, Jan 93, Vol. 152, No 376, p 204-212.

Brunner et al, (1995) *Examples of the application of CFD simulation to mine and tunnel ventilation,* Proc of the 7th Us mine Ventilation Symposium, SME Littleton, Colorado. pp479-484

Campbell, C.P. and Dupree, A.W. (1987) *Evaluation of methane dilution capacity of ablowing face ventilation system using a water sprayfan and dust scrubber.* MSHA 5th US Mine ventilation Symposium. 1987

Cantrell, B.K. et al, (1991) *Pollutant levels in underground Coal mines using Diesel equipment* The 1991 SME annual meeting, Denver, CO, pp25-28.

CEC. (1982) *Application of computer-based environmental monitoring.* Report by Directorate general (Energy).

Cermak, J.E, (1974) *Application of Fluid Mechanics to Wind Engineering,* A freeman Scholar Lecture, The American Society of Mechanical Engineers, New York, pp30.

Chan, L, Carlson, D.H., Johnson, J.H. (1993) *Apparatus and methodology for controlling mine ambient air quality based on Tailpipe and ambient Air pollution Measurements.* Proc. 6th US Mine Ventilation Symposium. SME 1993. Ed: Bhaskar R. pp 77-82.

Chasse, P. (1993) *Sentitivity study of different modelling techniques for the computer simulation of tunnel fires comparison with experimental measures.* In C.F.D.S. International Users Conference, 1993.

Cluett A. (1987) *Ventilation systems for mechanised drivages.* Engart Fans Ltd.

Cooke, W.E. (1926) *Experiments on the flow in ducts.* Trans IMineE 1937-8 73 p78.

Davis, M.R. & Winarto, H (1980) *Jet diffusion from a circular nozzle above a solid plane.* Journal of fluid Mechanics, Vol 101 part 1 pp201-221.

De Kock R D and Smith J G. (1988) *A new and effective approach to colliery heading ventilation using hydraulically driven fans*. Proc. 4th Int. Mine vent congress, Brisbane Queensland July 1988 p 105-112.

Durst, F., Melling, A, and Whitelaw, J.H. (1981) *"Principles and practice of laser-Doppler Anemometry"* Academic Press, London.

ECSC (1986) *Further work on dust control in drivages* project No 7260-02/004/08, British Coal, 1986

ECSC (1992) *Control of Respirable Dust and Methane at high ouput sites*, Project No. 7263-01/070/08, 1992

English W (1994) *Development of Ventilation, Monitoring and Control*, ECSC Project 7220-AC/843 Final Report, Transmitton.

Fennell, D (1988) *Investigation into the King's Cross Underground Fire* HMSO, London

Ferziger, J H (1993) A computational fluid dynamicist's view of computational wind engineering. Journal of Wind engineering and industrial Aerodynamics, 46-47: 879-880.

Fluent User guide Version 4.3 vol 1-4 1995.

Forrester, D. (1996) *Underground Continuous mining - An overview* CIM Bulletin, Vol 89 No 1000.

Freitas, C. J (1995) *Perspective: Selected Benchmarks from Commercial CFD Codes.* Trans ASME Vol, 117, June 1995 pp 208-218

Galea, E.R. and Markatos, N.C. (1987) *The mathematical modelling and computer simulation of fire in aircraft.* International journal of heat and mass transfer, 34 pp181-197.

Gilles, A.D.S, (1982) *Improved coal Face Ventilation Through use of Dust Scrubber Systems leads to greater production efficiency* Proc. 1st US Mine Ventilation Symposium. SME 1982. Ed: Hartman, H.. pp 43-53.

Glauert, M.B. (1956) *The Wall Jet Journal of Fluid Mechanics*, Vol 1 pp 625-643.

Gong, R. and Jankowski, R.A, (1991), *Studies on underboom dust control to reduce operator exposure to dust.* Proc of the 5th US Mine Ventilation Symosium, SME Ed Wang, pp 197-206.

Goodman G V R. and Taylor C D. (1993) *A technique for evaluating scrubber recirculaton during deep cut mining.* Proc. 6th US Mine Ventilation Symposium. SME 1993. Ed: Bhaskar R. p 19-24.

Graumann, K (1978) *Ventilation around roadway heading machines with de-dusting equipment.* Bergbam 6/1978 pp266-272.

Hazardous gases underground. *Notes for guidance NG/9.* British Coal Technical department.

Houghton A. (1993). *Development is the key* Min. Eng., Vol. 153, No 384, p73-83.

HSE. (1978) *A review of auxiliary and booster fan ventilation practice in mines.* HMSO 1978.

Hunt, J.C. and Fernholz, H, (1975) *Wind tunnel simulation of the atmospheric Boundary Layer*: A report on Euromech 50, Journal of Fluid Mechanics, Vol 70, part 3, pp 543-559.

Jankowski R A, Jayaraman N I, and Babbitt C A. (1987) *Water spray systems for reducing the quartz dust exposure of the continuous miner operation.* Proc 3rd Mine Ventilation Symposium. SME 1987. Ed Mutmansky J M p605-611

Jayaraman., N.I., Jankowski, and Babbit, C.A. (1989) *High Pressure Water powered Scrubbers For Continuous Miner Dust Control.* Proc 4th US Mine Ventilation Symposium. Ed Malcolm Mc Pherson pp 437-443.

Konduri, I.M, Mc Pherson, and M.J, Topuz, E (1997) *Experimental and Numerical Modeling of Jet Fans for Auxiliary Ventilation* in Mines Proc. 6th International Mine Ventilation Congress. May 17-22, 1997, Pittsburgh, Pennsylvania.

Konig-Langlo, G. and Schatzmann, M.1991, *Wind Tunnel Modelling of heavy gas dispersion.* Atmospheric environmet, Vol 25A, pp 1189-1198.

Lakshminarayana, B, 1991 *An Assessment of Computaional Fluid Dynamics Techniques in the Analysis and Design of Turbo machanery - The 1990 Freeman Scholar Lecture.* Trans of ASME Journal of Fluids Engineering. September 1991, Vol 113 p320

Lea C, (1994) *Computational modelling of mine fires.* The Mining Engineer, July,, pp17-21

Lippman, M. & Schlesinger, R.B (1979) *Chemical contamination in the human Environment.* Oxford university press, New York.

Lowndes, I.S and Moloney, K.W, (1996) *A Review of Diesel Exhaust Emission Monitoring and Control Technology,* Trans of IMinE, Mining Technology, Sept 1996

Lowndes, I.S, Roberts, B.H, Moloney, K.W, (1994) *Environmental monitoring and control in headings* ECSC research Project 7220-AC/847, October 1994.

Lowndes and Tuck, (1996) *Review of mine ventilation system optimization* Trans IMM Vol 105, A81-136. pp A114

McCready, D.I. (1986) *Wind Tunnel Modelling of small particle deposition.* Aerosol Science and Technology, Vol.5 pp 301-312.

McFarland, A.R., Ortiz, C.A. Cermak, J.E., Peterka, J.A. and LI, W, W. 1990 *Wind tunnel evaluationof a rotating element large-particle sampler* Aerosol Science and Technology Vol 12, pp 422-430.

M^{C}Kinney and Brunner (1994) *Critical velocity of air verus detailed modelling using CFD techniques in tunnel fires.* American Public Transit Conference, Sacramento, 1994.

Mc Pherson M J. (1993) *Subsurface Ventilation and Environmental Engineering.* Chapman and Hall.

Meetz E J, and Meyer C F. (1993) *Some applications of ductless fans in bord and pillar headings in South African coal mines.* Proc. 6th US Mine Ventilation Symposium. SME 1993. Ed: Bhaskar R. p 475-481.

Metha, U.B. (*1991) *Some Aspects of Uncertainty in Computational Fluid Dynamics Results* Trans of ASME Journal of Fluid Engineering, December 1991, Vol 113 pp538-543.

Meyeroltmanns, W et al (1986) *Ventilation systems for tunnel construction sites and their use in dust extraction.* HSE Translation 11889.

Millar, W. and Bryan, A.M(1938). *The effect of standing tubs on the resistance of mine airways by tests on models.* Trans IMinE 1937-38 95 p413.

Mining and Minerals Engineering. (1968) *New anemometer.* Min. and Min. Eng., Vol 4, No 5, pg 75.

Mogan, J.P. & Dainty, E.D. (1994) *Polynuclear aromatic hydrocarbons in Canadian underground mines.* CIM Bulletin, May 1994. Pp46-48.

Moloney, K.W., Lowndes, I.S., Stokes, M.R. (1996) *Computational Fluid Dynamics (CFD) Simulations of full scale gallery trials.* The First International Symposium on Mine Environmental Engineering. 29-31 1996 Kutahya, Turkey.

Morton, G.S. (1993) *Technical measures to control diesel exhaust particulate emissions in coal mines.* ECSC Project No. 7263-02/088. HSEC and BC

Mutama, K & Hall, A.E (1995) *The entrainment, pressure and flow process of a jet fan modelled in a square section tunnel.* Proceedings of the 7th US Mine Ventilation Symposium Ed Wala, A.M. pp379-384.

Nakayama, S, Inque, and M. Uchino, K (1993) *Airflow Analysis by computational fluid dynamics with auxilary ventilation at the heading face.Personal communication.*

Oberholzer, J.W. & Meyer, C.F.(1995) *Computer Modelling in the Solution of Continuous Miner Heading Ventilation Problems.* APCOM XXV 1995 Conference. Brisbane 9-14 July 1995.

Padmanabham, G. & Lakshmana, B.H (1991) Mean and Turbulence Characteristics of a Class of Three-Dimensional Wall Jets. Trans of ASME. Vol 113, December pp620-634.

Patankar, S.V. (1980) *Numerical heat transfer and fluid flow*, Hemisphere Publishing Corporation, Taylor & Francis group, New York.

Raine, E.J. (1960) *Layering of firedamp in longwall workings* Min. Eng. 119 579-91.

Rajaratnam, N and Pani, B.S (1974) *Three dimesional turbulent wall jets.* Journal of hydraulic Division Vol 100, No1 pp69-83.

Ramani, R.V. (1992) *Mine Ventilation* in SME Mining Engineering Handbook, 2nd Edition, Vol 1 (Ed Hartman, H.L.). Littleton, Colorado.

Ruggieri, S.K., Volkwein, J.C., Kissell, F.N., McGlothlin, C. (1985) *Extended advance face ventilation systems,* Proc 2nd US Mine Ventilation Symposium. Ed Mousset-Jones P. P543-549.

Sales, T.J.R and Hinsley, F.B. (1952) *The use of models in the study of airflow in mines.* Trans IMineE Vol 111 p

Samanta A, Bhaskar R, and Gong R. (1993) *Studies on the use of scrubbers in continuous miner faces.* Proc. 6th US Mine Ventilation Symposium. SME 1993. Ed: Bhaskar R p51-56.

Shuttleworth, S.E.H. (1963) *Ventilation at the face of a heading, studies in the laboratory and underground.* Journal of Rock Mechanics, Mining Science, Vol 1 pp79-92 Pergamon Press

Sieger. (1988) *Technical Literature.*

Srinivasa Rao, B et al, (1993) *Three dimensional modelling of air velocities and dust control techniques in a longwall face.* . Proc. 6th US Mine Ventilation Symposium. SME 1993. Ed: Bhaskar, R. Littleton, Colorado pp287-292.

Stewart, D.B., Dainty, E.D., Mogan, J.P. (1976) *Diesel emissions with respect to mine environment.* CIM Bulletin, 69, 765, pp 85-89, Janurary 1976.

Sullivan, P & Heerden, V.N. J, (1993) *The Simulation of Environmental Conditions in Continuous Miner Developments Using CFD.* Journal of the mine Ventilation of South Africa, Jan 1993 pp2-11

Sykes G. (1989) *The drivage and support of retreat faces.* Min. Eng. December 1989. Vol. 149. No 339. P240-248.

Tagaki, E, (1978) *Ventilation in tunnels and in tunnelling operations* Saiko to Hoan (Mining and Safety, Japan, April 1978 Vol 24, No 4 206-217.

Tanius, A (1987) *Aboveground testing of three coal mine ventilation systems.* 3rd US Mine Ventilation Symposium 1987.

Terblanche, A.P.S., (1992) *Health aspects of diesel emissions in trackless mining.* in the 5th International Mine Ventilation Congress, Ed Yang, Y.J., pp57-59.

Tong, H.Y. & Karasek, F.W. (1984) *Quantification of PAH's in diesel exhaust particulate matter by high performance liquid chromatography fractionation and high -resolution gas chromatography.* Anal. Chem.56 2129

Uchino, K & Inoue, M (1997) *Auxiliary ventilation at a heading face by a fan.* 6th International Mine Ventilation Congress. SME Littleton, Colorado.

Van de Leur, P,H,E., Kleijn, C.R and Hoogendoorn, C.J (1989) *Numerical study of stratifed smoke flow in a corrridor.* Fire safety journal, 14: pp 287-302

Van Doormal, J. P amd Raithby, G.D. (1984) *Enhancements of the SIMPLE method for predicting Incompressible Fluid Flows*, Numerical Heat transfer, Vol 7, pp147-163.

Versteeg, H.K, & Malalasekers, W, (1995) *An introduction to computational fluid dynamics - The finite volume method.* Longman Scientific and technical.

Volkwein J C, Thimons E D, Halfinger, G. (1985) *Extended advance of continuous miner successfully ventilated with a scrubber in a blowing section.* Proc 2nd US Mine Ventilation Symposium. Ed Mousset-Jones P. P741-745.

Vutukuri, V.S (1983) *Air leakage in ventilation ducting and the design of Auxiliary ventilation systems*, Min Engr, Vol 143, No 262, July, pp 37-43

Vutukuri, V.S. & Lama, R.D (1986) *Environmental Engineering in mines, OUP,1986*

Vutukuri, V.S (1993) *An Appraisal Of Accuracy of Various Formulas For the design of a Simple Auxiliary Ventilation System.* Proc of the 6th US Mine Ventilation Symposium SME Ed Bhaskar, Salt Lake City.

Wala et al (1997) *Validation study of CFD as a tool for Mive Ventilation Design* 6th International Mine Ventilation Congress. SME Littleton, Colorado.

Wang, Y.P., Tien, J.C, Wilson, J.W., Erten, M.H, (1991) *Use of surfactants for dust control in mines - A laboratory study*. Proc of the 5th US Mine Ventilation Symosium, SME Ed Wang, pp 197-206.

Waytulonis, R.A. (1992) *Diesel exhaust control* in SME Mining Engineering Handbook, 2nd Edition, Vol 1, (Ed by Hartman, H.L.), Littleton, Colorado, US.

Wesely R. (1984) *Airflow at heading faces with forcing auxiliary ventilation.* Proc 3rd International Mine Vent Congress. IMM p73-81.

White , F.M. (1986) *Fluid Mechanics* 2nd edition McGraw-Hill International editions. Mechanical Engineering Series.

Williams G. (1993) *Simply the best.* Mine Eng. Jan 1993, Vol. 152, No 376, p 199-202.

Woodburn, P. (1996) *Computational fluid dynamics simulation of fire-generated flows in tunnels and corridors.* Cambridge, PhD Theses.

Yates, C. Lowndes, I.S. Moloney. K.W. and Roberts, B.H.(1996) *Drivage Ventilation System at Welbeck Colliery.* Trans IMineE. Mining Technology December 1996 pp319-323.

APPENDIX ONE - Typical relationships of fuel-air ratio and relative concentrations of diesel exhaust components

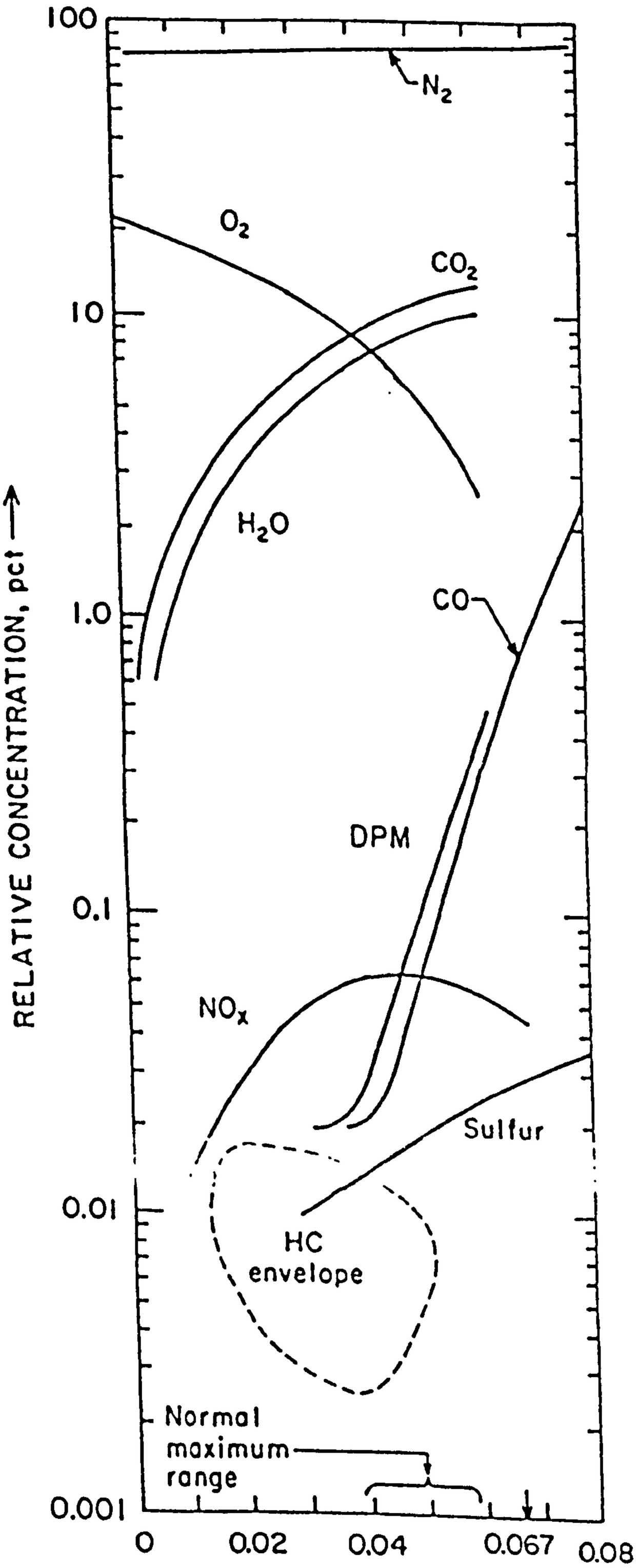

APPENDIX TWO - Fortran program to calculate duct leakage.

```
C234567
      REAL QI,QO,PI,PO,LD,RD,CR,X,Q1,Q2,L


      OPEN(7,FILE='DEFAULT7.DAT')
      READ(7,*) QI,QO,PI,PO,LD
      CLOSE(7)

 1    CALL CLS
      WRITE(6,10)
 10   FORMAT(36('*'),2X,'MENU',36('*'))
      WRITE(6,20)
 20   FORMAT(2X,'1   CHANGE PARAMETERS',18X,'2   RUN')
      WRITE(6,30)
 30   FORMAT(2X,'3   DESIGN',29X,'4   EXIT')
      WRITE(6,40)
 40   FORMAT(79('*'))

      WRITE(6,50)PI
 50   FORMAT(10X,'1  PRESSURE AT INLET=',F8.3)
      WRITE(6,60)PO
 60   FORMAT(10X,'2  PRESSURE AT OUTLET=',F8.3)
      WRITE(6,70)QI
 70   FORMAT(10X,'3  QUANTITY OF AI AT INLET=',F6.2)
      WRITE(6,80)QO
 80   FORMAT(10X,'4  QUANTITY OF AIR AT OUTLET=',F6.2)
      WRITE(6,90)LD
 90   FORMAT(10X,'5  LENGTH OF DUCT=',F6.0)
      WRITE(6,40)
      WRITE(6,*)' '
      WRITE(6,*)'ENTER OPTION REQUIRED'
      READ(5,*) IOPT

      IF(IOPT.EQ.1) CALL DEFAULTS(QI,QO,PI,PO,LD)
      IF(IOPT.EQ.2) THEN
      CALL CLS

      RD=((PI-PO)/LD)*(((5/((2*QI)+(3*QO)))**2))
      RD=RD*100

      CR=((3*(QI-QO))*(PI-PO))/(((PI**1.5)-(PO**1.5))*2*LD)
      CR=CR*100*(1000**0.5)
      WRITE(6,100)RD
100   FORMAT(10X,'RESISTANCE COEFFICIENT OF LEAKLESS DUCT=',F10.6)
      WRITE(6,200)CR
200   FORMAT(10X,'LEAKAGE COEFFICIENT=',F10.6)
      READ(5,*)
      ENDIF

      IF(IOPT.EQ.3) THEN
      CALL CLS
      WRITE(6,150)
150   FORMAT(2X,'VALUE FOR REQUIRED QUANTITY AT FACE=')
```

```
   READ(5,*)Q2
   WRITE(6,152)
152  FORMAT(2X,'LENGTH OF DUCT=')
   READ(5,*)L

   WRITE(6,153)
153  FORMAT(2X,'RESISTANCE COEFFICIENT OF LEAKLESS DUCT=')
   READ(5,*)RD
   WRITE(6,154)
154  FORMAT(2X,'LEAKAGE COEFFICIENT=')
   READ(5,*)CR

   CR=CR*L/100
   RD=RD*L/100

   X=1.02+(0.0185*CR*(RD**0.5))+(0.00015*(CR**2)*RD)


   Q1=Q2*X


   WRITE(6,151)Q1
151  FORMAT(2X,'QUANTITY REQUIRED TO BE TAKEN IN BY FAN=',F7.3,
   &",1X,'M3/S')
   READ(5,*)

   ENDIF

   IF(IOPT.EQ.4) THEN
   CALL CLS
   STOP
   ENDIF
   GOTO 1
   END

C****************** SUBROUTINE FOR FILE **************C
   SUBROUTINE DEFAULTS(QI,QO,PI,PO,LD)
   REAL QI,QO,PI,PO,LD

 1  CALL CLS
   WRITE(6,40)
 40  FORMAT(79('*'))
   WRITE(6,111)
 111  FORMAT(30X,'EDIT PARAMETERS')
   WRITE(6,40)
   WRITE(6,50)PI
 50  FORMAT(10X,'1  PRESSURE AT INLET=',F8.3)
   WRITE(6,60)PO
 60  FORMAT(10X,'2  PRESSURE AT OUTLET=',F8.3)
   WRITE(6,70)QI
 70  FORMAT(10X,'3  QUANTITY OF AI AT INLET=',F6.2)
   WRITE(6,80)QO
 80  FORMAT(10X,'4  QUANTITY OF AIR AT OUTLET=',F6.2)
   WRITE(6,90)LD
 90  FORMAT(10X,'5  LENGTH OF DUCT=',F6.0)
   WRITE(6,40)
```

```
WRITE(6,*)' '


WRITE(6,*)' '
WRITE(6,*)' '
WRITE(6,*)' '
WRITE(6,*)'SELECT PARAMETER TO BE CHANGED(ENTER 10 TO EXIT)'
READ(5,*)IOPT

IF(IOPT.EQ.10) THEN
OPEN(7,FILE='DEFAULT7.DAT')
 WRITE(7,*) QI,QO,PI,PO,LD
   CLOSE(7)
   RETURN
   ENDIF

   IF(IOPT.EQ.1) THEN
   WRITE(6,121)
   READ(5,*)PI
   ENDIF
121  FORMAT(1X,'ENTER PRESSURE AT INLET')

   IF(IOPT.EQ.2) THEN
   WRITE(6,122)
   READ(5,*)PO
   ENDIF
122  FORMAT(1X,'ENTER PRESSURE AT OUTLET')

   IF(IOPT.EQ.3) THEN
   WRITE(6,123)
   READ(5,*)QI
   ENDIF
123  FORMAT(1X,'ENTER QUANTITY AT INLET')

   IF(IOPT.EQ.4) THEN
   WRITE(6,124)
   READ(5,*)QO
   ENDIF
124  FORMAT(1X,'ENTER QUANTITY AT OUTLET')

   IF(IOPT.EQ.5) THEN
   WRITE(6,125)
   READ(5,*)LD
   ENDIF
125  FORMAT(1X,'ENTER LENGTH OF DUCT')
   GOTO 1
   END


   SUBROUTINE CLS
   DO 2 I=1,24
   WRITE(6,*)' '
  2 CONTINUE
   RETURN
   END
```

APPENDIX THREE - Venturimeter and its calibration.

Venturi meter.

The venturi differential pressure devive was invented by Clemens Herschell (1842-1930). For this experiment the venturi was fabricated from Aluminium in accordance with BS 1042. (Figure X.5) It has a tapered convergent section from 1-2 thus pressure losses are small and equation 1 gives a good estimate of the velocity in the main pipe based on the preesure difference Δp.

$$V_1 = \frac{m}{\sqrt{1-m^2}}\sqrt{\frac{2\Delta p}{\rho}} \qquad \text{Equation A.1}$$

Where m = d2/D2 and D = main pipe diameter, d = throat diameter.

It is also necessary to introduce a discharge coefficient C (0.995) this equates to 1% uncertainty. If a lower value of uncertainty is required then Calibration is necessary. It is necessary to have five diameters of straight pipe upstream of the venturi to eliminate

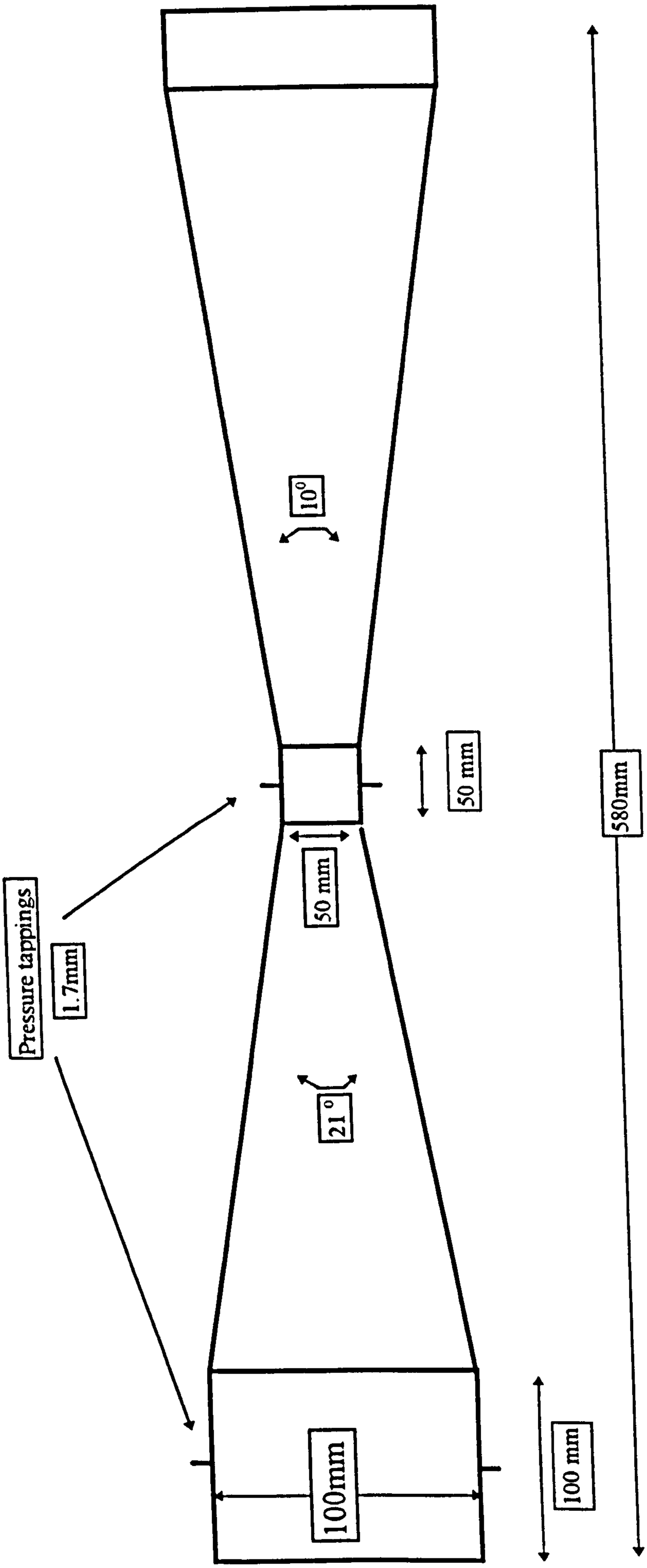

Venturi Meter (not to scale) constructed in accordence with BS 1042.

APPENDIX FOUR - Improving Grid quality.

Adjacent cell size ratio and Aspect ratio.

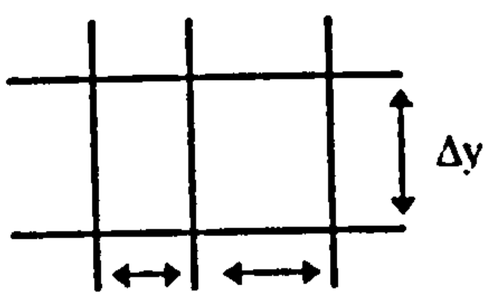

Adjacent Cell size Ratio $\Delta x2/\Delta x1 < 2.$

Aspect ratio $\Delta y/\Delta x < 5.$

Skewness in 2-D

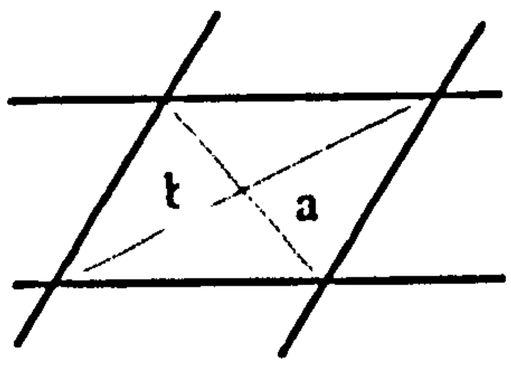

Skewness = 1- a/b

Skewness in 3-D

For a given element, the normals of each face are normalised with respect to the largest normal. The skewness of the element is defined as the maximum dot product of a normal of a face with the normal of an adjacent face.

The maximum skewness of a hex grid should be less than 0.95

Improving the grid further

There are three options that can improve the quality of a grid

Smoothing

Smoothness

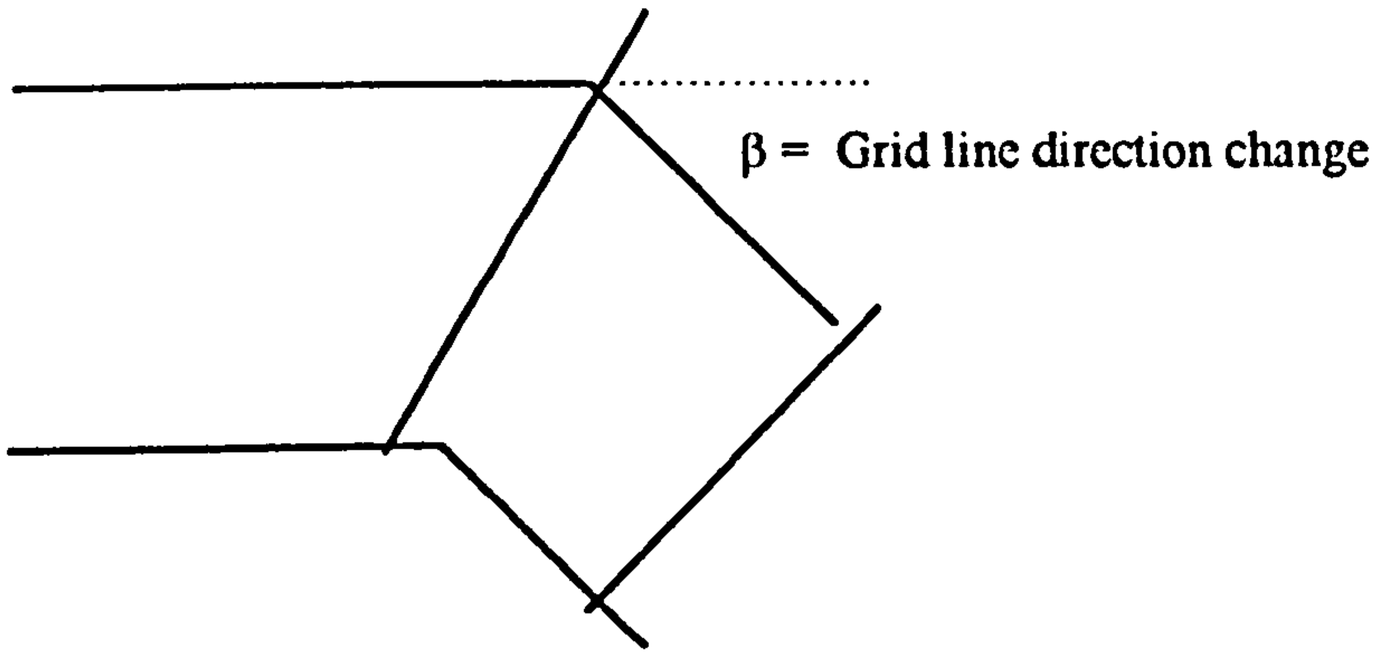

There are two smoothing algorithms available:

-Laplace

-Thomas-Middlecoff ("etm")

Orthogonal interpolation at the boundary

There are two interpolation method available to reduce skewness near the boundary:

- Eriksson("tie)
- Hermite-Orthogonal("tio")

Deactivate control volumes with very bad skewness

If one is unable to reduce the skewness at the boundary change the live cells to wall cells. This is recommended if severe instability problems are encountered.

APPENDIX FIVE - Calculation of roughness.

The Fluent system models the boundary layer close to the wall using various so called wall functions. These functions are based upon the log-wall law of the wall, which is described in the various texts. The standard form of the wall functions assume that the wall is smooth, non smooth walls may be modelled by modification of the constant E to form E' which occurs in the log-wall function below:

$$\frac{u_p}{u^*} = \frac{1}{\kappa} \ln (Ey^+) - \Delta B(K_s^+)$$

1) Given the hydraulic diameter, the Reynolds number based on the hydraulic diameter and the average velocity u, assess the type of surface a friction factor can be selected from published data.

2) the e/d ratio may then be found from a moody diagram.

3) Calculate K_s^+ from

$$K_s^+ = e/d \, Re_d \sqrt{\frac{f}{8}}$$

4) Calculate E' from

$$E' = \frac{E}{1 + 0.3K_s^+}$$

Where E = 9.76 (Von Karman constant.

Atkinson friction factors K, must be first converted to a Darcy type dimensionless friction factors f.

APPENDIX 6 - Data Processing Algorithms.

Untransformed Velocity Component.

$$U_x = f_{d1}\frac{\lambda}{2\sin\theta/2}$$

Where λ is the laser wavelength, θ is the half the angle between the laser beams and f is the doppler frequency for channel one.

The direction of U_x is in the plane of the beams, perpendicular to the angular bisector of θ. Similar results hold for U_y and U_w.

Transformed velocity component.

$$\begin{pmatrix} Ux \\ Uy \\ Uz \end{pmatrix} = \cos\gamma_{ij}\begin{pmatrix} U \\ V \\ W \end{pmatrix}$$

Where γij is the solid angle subtended by the unit vectors (ii. ij) I=1, 2, 3, j=x, y, z.
For a 3D LDA system with axis y and 2 in the vertical plane and axes 1, 3, x and z in the horizontal plane (axes 1 and 3 are perpendicular to optical axis 1 and 3 respectively) and the z axis bisects optical axis 1 and 3, use the flowing values for transformation matrix;

$$\begin{matrix} U \\ V \\ W \end{matrix} = \begin{matrix} \frac{1}{2\cos\psi/2} & 0 & \frac{1}{2\cos\psi/2} \\ 0 & 1 & 0 \\ \frac{1}{2\sin\psi/2} & 0 & -\frac{1}{2\sin\psi/2} \end{matrix} \begin{matrix} U_x \\ U_y \\ U_z \end{matrix}$$

Where U,V,W are the transformed components, Ux, Uy and Uz are the measured components and ψ/2 is the angle between the z axis and the 1 axis.

Mean value

$$\overline{U}_{unweighted} = \frac{\Sigma U_i}{\Sigma N}$$

I = 1,2, 3....N

PAGE
MISSING
IN
ORIGINAL

APPENDIX 7

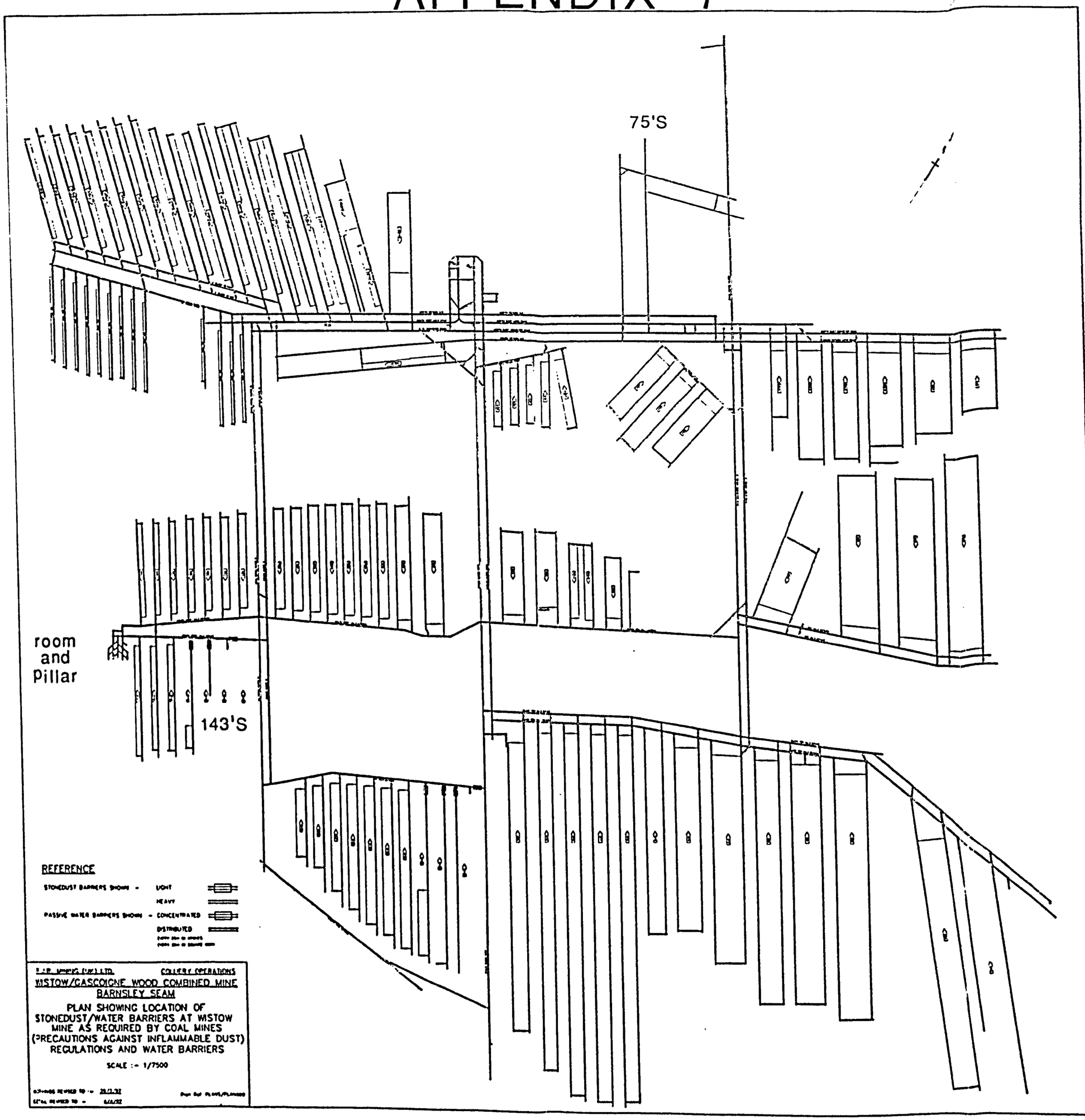
75'S
room
and
Pillar
143'S
REFERENCE
STONEDUST BARRIERS SHOWN - LIGHT
HEAVY
PASSIVE WATER BARRIERS SHOWN - CONCENTRATED
DISTRIBUTED
COLLIERY OPERATIONS
WISTOW/GASCOIGNE WOOD COMBINED MINE
BARNSLEY SEAM
PLAN SHOWING LOCATION OF STONEDUST/WATER BARRIERS AT WISTOW MINE AS REQUIRED BY COAL MINES (PRECAUTIONS AGAINST INFLAMMABLE DUST) REGULATIONS AND WATER BARRIERS
SCALE :- 1/7500